

ISOTOPE AND HYDROCHEMICAL INVESTIGATION ON URANIUM IN GROUNDWATER OF SOUTH-WEST PUNJAB AND CENTRAL RAJASTHAN

By

**DIKSHA PANT
CHEM01201404022**

BHABHA ATOMIC RESEARCH CENTRE, MUMBAI

*A thesis submitted to the
Board of Studies in Chemical Sciences*

*In partial fulfillment of requirements
for the Degree of*

**DOCTOR OF PHILOSOPHY
of
HOMI BHABHA NATIONAL INSTITUTE**

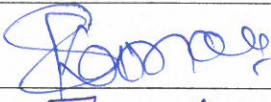


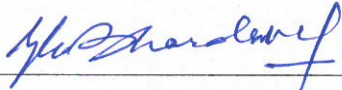
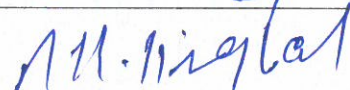
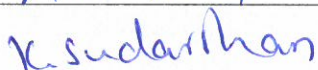


JANUARY, 2021

Homi Bhabha National Institute

Recommendations of the Viva Voce Committee

As members of the Viva Voce Committee, we certify that we have read the dissertation prepared by Mrs. Diksha Pant entitled "Isotope and hydrochemical investigation on uranium in groundwater of south-west Punjab and central Rajasthan" and recommend that it may be accepted as fulfilling the thesis requirement for the award of Degree of Doctor of Philosophy.

Chairman – Dr. S. Kannan		13/03/2021
Guide / Convener – Dr. K. Tirumalesh		13/03/2021
Examiner - Dr. Manish Kumar Goyal		13/03/2021
Member 1- Dr. Y.K. Bhardwaj		13/03/2021
Member 2- Dr. R.K. Singhal		13/03/2021
Member 3- Dr. K. Sudarshan		13/03/2021

Final approval and acceptance of this thesis is contingent upon the candidate's submission of the final copies of the thesis to HBNI.

I hereby certify that I have read this thesis prepared under my direction and recommend that it may be accepted as fulfilling the thesis requirement.

Date: 13/03/2021

Place: Mumbai


Signature

(Dr. K. Tirumalesh)

Guide

STATEMENT BY AUTHOR

This dissertation has been submitted in partial fulfillment of requirements for an advanced degree at Homi Bhabha National Institute (HBNI) and is deposited in the Library to be made available to borrowers under rules of the HBNI.

Brief quotations from this dissertation are allowable without special permission, provided that accurate acknowledgement of source is made. Requests for permission for extended quotation from or reproduction of this manuscript in whole or in part may be granted by the Competent Authority of HBNI when in his or her judgment the proposed use of the material is in the interests of scholarship. In all other instances, however, permission must be obtained from the author.



Diksha Pant

DECLARATION

I, hereby declare that the investigation presented in the thesis has been carried out by me. The work is original and has not been submitted earlier as a whole or in part for a degree / diploma at this or any other Institution / University.



Diksha Pant

1. **Name of the Student: Mrs. Diksha Pant**
2. **Name of the Constituent Institution: Bhabha Atomic Research Centre, Mumbai**
3. **Enrolment Number: CHEM01201404022**
4. **Board of Studies: Chemical Sciences**
5. **Thesis title: Isotope and hydrochemical investigation on uranium in groundwater of south-west Punjab and central Rajasthan**

List of Publications arising from the thesis

Journal (05):

1. "Study on uranium contamination in groundwater of Faridkot and Muktsar districts of Punjab using stable isotopes of water", **Diksha Pant**, Tirumalesh Keesari, Diana Sharma, Madhuri Rishi, Gagandeep Singh, Ajay Kumar, U. K. Sinha, A. Dash, R. M. Tripathi(2017),*Journal of Radioanalytical and Nuclear Chemistry*DOI 10.1007/s10967-017-5284-0
2. "Study on groundwater quality in parts of Rajasthan with special reference to uranium contamination", **Diksha Pant**, Tirumalesh Keesari, A. Roy, U.K. Sinha, Manveer Singh, S.K. Jain, R.M. Tripathi (2019), *Journal of Radioanalytical and Nuclear Chemistry*DOI 10.1007/s10967-019-06525-6
3. "Spatial and temporal distribution of dissolved radon in uranium impacted aquifers of southwest Punjab", **Diksha Pant**, Tirumalesh Keesari, Madhuri Rishi, Diana Sharma, Nandini Thakur, Gagandeep Singh, Priyanka Sangwan, Ajay Jaryal, U.K. Sinha, R.M. Tripathi (2019),*Journal of Radioanalytical and Nuclear Chemistry*DOI: 10.1007/s10967-019-06656-w
4. "Quality and Quantity of Groundwater in Highly Exploited Aquifers of Northwest India", **Diksha Pant**, Tirumalesh Keesari, Madhuri Rishi, Ajay Jaryal, Diana A. Sharma, Nandini Thakur, Gagandeep Singh, S. N. Kamble, Priyanka Sangwan, U. K.

Sinha, R. M. Tripathi (2020), *Journal of Hazardous, Toxic, and Radioactive Waste* DOI: 10.1061/(ASCE)HZ.2153-5515.0000483

5. "Hydrochemical evolution of groundwater in the waterlogged area of southwest Punjab", **Diksha Pant**, Tirumalesh Keesari, Madhuri S. Rishi, Diana Anoubam Sharma, Ajay Jaryal, Suryakant Namdev Kamble, Uday Kumar Sinha (2020), *Arabian Journal of Geoscience* DOI: 10.1007/s12517-020-05795-9

Conference/Symposium (07)

1. "Canal water and groundwater interactions in Malwa region of Punjab – an isotope perspective", **Diksha Pant**, Tirumalesh Keesari, U.K. Sinha, Hemant Mohokar, Ajay Jaryal, G.N. Mendhekar, Madhuri Rishi and Diana Sharma Proceedings of **ISMAS 2015**, February 2-6, Jodhpur, page 124-125.
2. "Geochemical investigation on groundwater of Southwestern Punjab with special reference to Uranium", Tirumalesh Keesari, Madhuri Rishi, **Diksha Pant**, U.K. Sinha, Ajay Kumar DAE-BRNS 12th National Symposium on Nuclear Chemistry and Radiochemistry (**NUCAR 2015**) February 9-13, 2015, page 611.
3. "Environmental isotopic study on uranium contamination in groundwater of Faridkot and Muktsar districts of Punjab", **Diksha Pant**, Tirumalesh Keesari, Madhuri Rishi, Diana Sharma, Gagandeep Singh, Ajay Kumar, U.K. Sinha, A. Dash, R.M. Tripathi 13th DAE-BRNS National Symposium on Nuclear Chemistry and Radiochemistry (**NUCAR 2017**) February 6th-10th, 2017, page 632-633.
4. "Identification of recharge sources to shallow and deep groundwater of Faridkot and Muktsar Districts, Punjab, India", **Diksha Pant**, Ajay Jaryal, K. Tirumalesh, Diana Sharma, Madhuri Rishi, U.K. Sinha, R.M. Tripathi Proceedings of **ISMAS 2017**, March 23rd -25th 2017, BARC, Mumbai, page 158-160

5. "Study on groundwater quality in parts of Rajasthan with special reference to uranium contamination" **Diksha Pant**, Tirumalesh Keesari, A. Roy, U.K. Sinha, Manveer Singh, S.K. Jain, R.M. Tripathi **ARCEBS- 2018** conference in Kolkata.
6. "Spatiotemporal distribution of dissolved radon in uranium impacted aquifers of southwest Punjab" **Diksha Pant**, Tirumalesh Keesari, Madhuri Rishi, Diana Sharma, Nandini Thakur, Gagandeep Singh, Priyanka Sangwan, Ajay Jaryal, U.K. Sinha, R.M. Tripathi **NUCAR-2019**
7. "Assessment of groundwater quality of Muktsar district, Punjab with special reference to nitrate contamination. National conference on groundwater sustainability", **Diksha pant**, Tirumalesh Keesari, Diana Sharma, Madhuri Rishi, Ajay Jaryal, U.K. Sinha and R.M. Tripathi, Manav Rachna Institute, Faridabad, 28th March **2019** page no 13.

Diksha

Diksha Pant

Dedicated to My Family

Acknowledgements

The realization of the thesis was accompanied with the support and encouragement of numerous people including my family, friends and colleagues to whom I would like to pass my greatest appreciation. First and foremost, I would like to thank my guide **Dr. K. Tirumalesh** for his patience, support and encouragement that he has rendered me throughout my work. His knowledge and experience have helped me throughout my Ph.D. I am indebted to him for the time he has devoted on me. I would like to acknowledge the chairman of my Ph.D. doctoral committee **Dr. S. Kannan** and other committee members **Dr. R.K. Singhal**, **Dr. Y.K. Bhardwaj** and **Dr. Kathi Sudarshan** for their constructive remarks, guidance, encouragement and time.

I am thankful to **Dr. P.K. Pujari**, Group Director, Radiochemistry and Isotope (RC&I) Group and **Dr. H.J. Pant**, Head, Isotope and radiation application Division for their constant support and motivation. I would like to extend my sincere gratitude to **Dr. U.K. Sinha**, Head, Isotope Hydrology section for his constructive remarks and fruitful discussion that has help me sail through course of my Ph.D. smoothly. I would also like to pass my sincere gratitude to **Dr. Madhuri Rishi and her team**, Department of Environment science, Panjab University, Chandigarh and **Dr. S.K. Jain** and **Dr. Manveer Singh** from Central Groundwater Board for their support in the sampling. I would like to extend my sincere gratitude to **Dr. R.M. Tripathi** and **Mr. S.K. Sahoo** of Health Physics Division for their encouragements and scientific discussions.

I would like to pass my sincere thanks to all my colleagues for their support throughout. I would especially like to acknowledge the help that **Mr. Annadasankar Roy**, **Dr. Diana A. Sharma**, **Mr. H.V. Mohokar**, **Mr. Ajay Kumar Jaryal** **Mr. S.N. Kamble** and **Mr. Sitangshu**

Chatterjee have extended to me throughout my Ph.D. work, they all have been the life saviors. I would like to pass my sincere thanks to Analytical Chemistry Division especially **Dr. K.K. Swain** for his support in analysis of few samples. I wish to express my sincere thanks to my teachers since childhood for making me the person I am and for always been motivating and encouraging at every step of life. I would like to thank my friends, especially **Mr. Vikram Singh** for his help with the geological information of the study area and **Dr. Praveen Kumar Verma** with thermodynamic information of uranium complexes

I am eternally grateful to my Late Grandparents for their blessings, love, support and the values they have embedded in me. I would like to extend my sincere gratitude to **Mr. Chander Prakash Chawla** (my Father) and **Mrs. Sneh Lata** (my Mother) for their blessings, love support and care which they have rendered me at each step of my life. Without their constant support and push, I would not have achieved so much in my life; they have been the driving force of my life. I would like to pass my sincere thanks to my younger but more mature brother of mine (**Mr. Hinish Chawla**) for his trust, motivation and encouragement that always keep me on toes to do something better. I would also like to thank my Husband (**Mr. Amar Dutt Pant**) for being the supportive life partner that one could ask for. I am also grateful to My in laws for their blessing. Last but not the least I would like to pass my thanks to the most important person of my life, my son **Master Reyansh Pant**, for his love and support.

Table of Contents

	Description	Page No.
	SYNOPSIS	I
	List of Abbreviations	xii
	List of Figures	xiii
	List of Table	Xviii
CHAPTER 1	Introduction	1
1.1	Groundwater Scenario in the world and India	2
1.2	Groundwater contamination	5
1.3	Uranium Contamination	10
1.3.1	Health effects	12
1.3.2	Uranium Mobilization:	15
1.3.3	Uranium contamination in groundwater	17
1.3.3.1	World scenario	17
1.3.3.1	Indian scenario	18
1.4	Limitations and motivation for the study	25
1.5	Objectives	29
1.6	Thesis outline	30
CHAPTER 2	Methodology	33
2.1	In situ analysis	33
2.2	Major ion chemistry	34
2.2.1	Working principle	35
2.2.2	Applications	37
2.2.2.1	Suitability of water	37
A)	Drinking:	37
B)	Irrigation	37
C)	Composite water quality index	38
2.2.2.2	Geochemical processes	39
2.3	Uranium and its isotopes	40
2.3.1	Total Uranium determination	40
2.3.1.1	Measurement	41
2.3.1.2	Working principle	41
2.3.2	Uranium isotope determination	42
2.3.2.1	Measurement	42
2.3.2.2	Working principle	44
2.3.3	Applications	46
2.4	Environmental isotopes of water ($\delta^2\text{H}$ and $\delta^{18}\text{O}$)	48
2.4.1	Stable Isotopes ($\delta^{18}\text{O}$ and $\delta^2\text{H}$)	51
2.4.1.1	Measurement	51
2.4.1.2	Working principle	53

2.4.2	Radioisotope (Tritium (^3H))	54
2.4.2.1	Measurement	54
2.4.2.2	Working principle	56
2.4.3	Applications	56
2.5	Spatial, geochemical and statistical Methods	57
2.5.1	Geographic Information System (GIS)	57
2.5.2	Aquachem	57
2.5.3	Origin	57
2.5.4	WATEQ4F	57
2.5.5	Multivariate analysis	59
2.5.5.1	Pearson's correlation	59
2.5.5.2	Principle Component Analysis (PCA)	60
	Source and mobilization of uranium in groundwater of	
CHAPTER 3	Southwest Punjab	62
3.1	Study area description	62
3.2	Sampling	65
3.3	Results and discussion	67
3.3.1	General water quality	67
3.3.1.1	Physicochemical parameters	67
3.3.1.2	Chemical parameters	71
3.3.2	Suitability of water	76
3.3.2.1	Suitability for drinking	76
3.3.2.2	Suitability for irrigation	81
A)	Sodium absorption ratio (SAR)	82
B)	Sodium percentage (Na%)	85
C)	Residual sodium carbonate (RSC)	86
D)	Permeability index (PI)	87
E)	Magnesium Hazard (MH)	88
F)	Kelley's ratio (KR)	88
G)	Corrosive Ratio (CR)	89
3.3.2.3	Composite water quality index	89
3.3.3	Geochemical evolution	90
3.3.3.1	Ion Exchange	95
3.3.3.2	Carbonate Weathering	97
3.3.3.3	Silicate Weathering	98
3.3.4	Source and recharge mechanism of groundwater	100
3.3.5	Factors impacting uranium distribution in groundwater	108
3.3.5.1	Uranium distribution: Spatial and Temporal	108
A)	Uranium distribution and seasonal variation	108
B)	Spatial distribution	110
C)	Depth profile	112

3.3.5.2	Correlations of uranium	115
3.3.5.3	Factor analysis or Principal Component Analysis	117
A)	Shallow zone	117
B)	Deep zone	118
3.3.5.4	Uranium Speciation	122
3.3.5.5	Saturation Index	123
3.3.5.6	Uranium isotopes	125
3.4	Conclusions	127
	Source and mobilization of uranium in groundwater of Central	
CHAPTER 4	Rajasthan	130
4.1	Study area description	130
4.2	Sampling	136
4.3	Results and discussion	137
4.3.1	General water quality	137
4.3.1.1	Physicochemical parameters	137
4.3.1.2	Chemical parameters	141
4.3.2	Suitability of water	145
4.3.2.1	Suitability for drinking	145
4.3.2.2	Suitability for irrigation	150
A)	Sodium absorption ratio (SAR)	151
B)	Sodium percent (Na%)	154
C)	Residual sodium carbonate (RSC)	155
D)	Permeability index (PI)	156
E)	Magnesium Hazard (MH)	156
F)	Kelley's ratio (KR)	157
G)	Corrosive Ratio (CR)	157
4.3.2.3	Composite water quality index	158
4.3.3	Geochemical evolution	159
4.3.3.1	Ion Exchange	164
4.3.3.2	Carbonate Weathering	165
4.3.3.3	Silicate Weathering	166
4.3.4	Source and recharge mechanism of groundwater	166
4.3.5	Factors impacting uranium distribution in groundwater	172
4.3.5.1	Uranium distribution	172
A)	Uranium distribution: seasonal variation in both formation	172
B)	Spatial distribution	174
C)	Depth profile	178
4.3.5.2	Correlations of uranium	178
4.3.5.3	Factor analysis or Principal Component Analysis	181
A)	Alluvial formation	181
B)	Hard rock formation	185

4.3.5.4	Uranium Speciation	186
4.3.5.5	Saturation Index	186
4.3.5.6	Uranium isotope	188
4.4	Conclusions	189
CHAPTER 5	Comparative Analyses	192
5.1	Hydrochemical drivers	192
5.2	Uranium distribution	194
5.2.2	Seasonal variation	194
5.2.2	Depth variation	197
5.3	Groundwater recharge and dynamics	199
5.4	Uranium isotope variations	200
5.5	Conceptual diagram of uranium release in groundwater in alluvial formations	204
5.6	Conceptual diagram of uranium release in groundwater in hard rock formations	205
Chapter 6	Summary, Remediation Measures and Future scope	208
	References	219

List of Abbreviations

Abbreviation	Full Form	Abbreviation	Full Form
AERB	Atomic Energy Regulatory Board	LED	Light Emitting Diode
AR	Activity Ratio	LSC	Liquid Scintillation Counter
ASTDR	Agency for Toxic Substances and Disease Registry	LMWL	Local Meteoric Water Line
AH	Ampere Hour	MH	Magnesium Hazard
amu	Atomic Mass Unit	PIPS	Passivated Ion-Implanted Planar Semiconductor Detector
amsl	Above Mean Sea Level	%Na	Percent Sodium
BIS	Bureau of Indian Standards	PI	Permeability Index
bgl	Below Ground Level	PMT	Photo Multiplier Tube
BFT	Best Fit Line	PTFE	Polytetrafluoroethylene
CGWB	Central Ground Water Board	Post	Postmonsoon
CBE	Charge Balance Error	psi	Pound-force per square inch
CR	Corrosive Ratio	Pre	Premonsoon
CPS	Counts per second	PC	Principle Component
DNA	Deoxyribo Nucleic Acid	PCA	Principle Component Analysis
DPS	Disintegration per Second	PHED	Public Health Engineering Department
DWQI	Drinking Water Quality Index	RSC	Residual sodium carbonate
EC	Electrical Conductivity	SVD	singular value decomposition
ED	Electrochemical Detector	SAR	Sodium Absorption Ratio
EDTA	Ethylene Diamine Tetra Acetate	K _{sp}	Solubility Product
GIS	Geographic Information System	SPSS	Statistical Package for the Social Sciences
GMWL	Global Meteoric Water Line	TDS	Total Dissolved Solids
GPS	Global Positioning System	TH	Total Hardness
ICP-OES	Inductively Coupled Plasma Optical Emission Spectroscopy	TU	Tritium Unit
IAEA	International Atomic Energy Agency	UV	Ultra Violet
IC	Ion Chromatography	USA	United States of America
IAP	Ionic Activity Product	UNSCEAR	United Nations Scientific Committee on the Effects of Atomic Radiation
IWQI	Irrigation Water Quality Index	USSL	United States Salinity Laboratory plot
IRMS	Isotope Ratio Mass Spectrometer	VSMOW	Vienna Standard Mean Oceanic Water
KR	Kelly's Ratio	WHO	World Health Organisation

List of Figures

	Description	Page. No.
Chapter 1		
Fig. 1.1	Distribution of water on Earth	1
Fig. 1.2	Map of India indicating the stage of development	5
Fig. 1.3	Different aquifer of India showing uranium concentration	19
CHAPTER 2		
Fig. 2. 1	Field sampling along with in-situ field parameter measurement	34
Fig. 2.2	Dionex ion chromatography system	35
Fig. 2.3	A typical ion chromatograph for a) anions and b) cations	36
Fig. 2.4	LED fluorimeter i.e. UA1, Quantalase	41
Fig. 2.5	Stages of column preparation and uranium stripping	43
Fig. 2.6	Flow diagram showing step involved in preparation of electroplating solution	43
Fig. 2.7	Electroplating setup and alpha spectrometer	44
Fig. 2.8	Variation in uranium concentration and AR ($^{234}\text{U}/^{238}\text{U}$) with distance from recharge	47
Fig. 2.9	Uranium mobilization processes	48
Fig. 2.10	The scatter plot of $\delta^{18}\text{O}$ and $\delta^2\text{H}$ indicating phenomenon leading to change in isotopic values.	50
Fig. 2.11	Multiflow-IRMS-Isoprime100 system	52
Fig. 2.12	Tritium electrolytic enrichment setup	55
CHAPTER 3		
Fig. 3 1	Lithological cross-section of Faridkot district a) transect A-A' and b) transect B-B'	64
Fig. 3.2	Lithological cross-section of Muktsar district a) transect A-A' and b) transect B-B'	65
Fig. 3.3	Sample location map for Muktsar and Faridkot districts	66
Fig. 3.4	Box plot for physiochemical parameters a) premonsoon of the shallow zone, b) premonsoon of deep zone c) postmonsoon of the shallow zone and d) postmonsoon of the deep zone.	68
Fig. 3.5	Depth profile for physicochemical parameters a) EC, b) alkalinity and c) pH for premonsoon season and d) EC, e) alkalinity and f) pH for postmonsoon season of both the zones	71
Fig. 3.6	Box plot for major ions present in groundwater from shallow and deep zone in both the seasons	73
Fig. 3.7	Depth profile for a) NO_3^- ion concentration in premonsoon b) F^- ion concentration in premonsoon c) NO_3^- ion concentration in postmonsoon and d) F^- ion concentration in postmonsoon season	76
Fig. 3.8	TDS vs TH plot to understand water type.	81
Fig. 3.9	USSL plot of groundwater from a) shallow and b) deep zones for premonsoon and postmonsoon seasons	82

Fig. 3.10	Wilcox plot of groundwater from a) shallow and b) deep zone for premonsoon and postmonsoon seasons	86
Fig. 3.11	Permeability index of groundwater from a) shallow and b) deep zones for premonsoon and postmonsoon seasons	88
Fig. 3.12	Piper trilinear plot showing water facies for a) shallow and b) deep zones during both the seasons	91
Fig. 3.13	Gibbs plot a) cationic and b) anionic for both the seasons in the shallow zone	92
Fig. 3.14	Gibbs plot a) cationic and b) anionic for both the seasons in the deep zone	92
Fig. 3.15	Bivariate plots a) Shallow: Na^+ -normalized Ca^{2+} versus Na^+ normalized HCO_3^- , b) Deep: Na^+ -normalized Ca^{2+} versus Na^+ normalized HCO_3^- , c) Shallow: Na^+ -normalized Ca^{2+} versus Na^+ normalized Mg^{2+} and d) Deep: Na^+ -normalized Ca^{2+} versus Na^+ normalized Mg^{2+}	93
Fig. 3.16	Plot of $\text{Ca}^{2+} + \text{Mg}^{2+}$ vs $\text{Na}^+ + \text{K}^+$ of groundwater samples from the study area	95
Fig. 3.17	Plot of $(\text{Na}^+ - \text{Cl}^-)$ vs. $(\text{Mg}^{2+} + \text{Ca}^{2+}) - (\text{HCO}_3^- - \text{SO}_4^{2-})$ illustrating reverse ion exchange	96
Fig. 3.18	Plot of $(\text{Ca}^{2+} + \text{Mg}^{2+})$ vs. $(\text{SO}_4^{2-} + \text{HCO}_3^-)$ of groundwater samples from the study area	97
Fig. 3.19	Plot of $(\text{Na}^+ + \text{K}^+)$ vs $(\text{Ca}^{2+} + \text{Mg}^{2+})$ for groundwater samples from the study area	99
Fig. 3.20	Plot of TZ^+ vs $\text{Na}^+ + \text{K}^+$ of groundwater samples from the study area	100
Fig. 3.21	Box plot for a) Deuterium and b) Oxygen-18 for both the seasons and both the zones	101
Fig. 3.22	Dexcess vs $\delta^{18}\text{O}$ plot for both the seasons from the shallow and deep zones	102
Fig. 3.23	Stable isotope plot for a) shallow and b) deep zone for both the seasons	103
Fig. 3.24	Stable isotope plots for a) shallow and b) deep zones for both the seasons	106
Fig. 3.25	Depth profile for tritium for shallow and deep zones	107
Fig. 3.26	Schematic diagram for groundwater recharge and flow	108
Fig. 3.27	Box plot of uranium in both the zones and both the seasons	109
Fig. 3.28	Percent samples above a) WHO and b) AERB limits	110
Fig. 3.29	Spatial distribution of dissolved uranium a) premonsoon and b) postmonsoon	110
Fig. 3.30	Spatial distribution of HCO_3^- in a) premonsoon and b) postmonsoon seasons	111
Fig. 3.31	Spatial distribution of NO_3^- in a) premonsoon and b) postmonsoon seasons	112
Fig. 3.32	Depth profile of uranium for a) shallow and b) deep zone for both the seasons	113

Fig. 3.33	Correlation of uranium with HCO_3^- ions in a) premonsoon and b) postmonsoon seasons for both the zones	113
Fig. 3.34	Correlation of uranium with NO_3^- ions in a) premonsoon and b) postmonsoon seasons for both the zones	114
Fig. 3.35	Correlation of uranium with EC in a) premonsoon and b) postmonsoon season.	114
Fig. 3.36	Correlation of physicochemical parameters and major ions with uranium for a) shallow and b) deep zones for both the seasons	116
Fig. 3.37	Box plot of saturation indices for common uranium minerals for a) shallow and b) deep zones for both the seasons	124
Fig. 3.38	Depth profile for AR ($^{234}\text{U}/^{238}\text{U}$)	125
Fig. 3.39	Activity ratio vs. inverse concentration plot to identify the process for uranium mobilization for both the zones	126
CHAPTER 4		
Fig. 4.1	Aquifer map of Jaipur district showing the area covered under various formations	133
Fig. 4.2	Aquifer map of Dausa district showing the area covered under various formation	135
Fig. 4.3	Sample location map	137
Fig. 4.4	Box plot for physiochemical parameters a) premonsoon of alluvial formation, b) premonsoon of hard rock formation c) postmonsoon of alluvial formation and d) postmonsoon of hard rock formation.	140
Fig. 4.5	Depth profile for physicochemical parameters a) EC, b) alkalinity and c) pH for alluvial formation and d) EC, e) alkalinity and f) pH for hard rock formation of both the seasons.	141
Fig. 4.6	Box plot for major ions present in groundwater from a) premonsoon alluvial, b) premonsoon hard rock, c) postmonsoon alluvial and d) postmonsoon hard rock formations	142
Fig. 4.7	Depth profile for a) NO_3^- ions in alluvial formation, b) F^- ions in alluvial formation c) NO_3^- ions in hard rock formation and d) F^- ions in hard rock formation in both the seasons	145
Fig. 4.8	TDS vs TH plot to understand water type for pre and postmonsoon seasons for both the formations.	150
Fig. 4.9	USSL plot of groundwater from a) alluvial and b) hard rock formation for premonsoon and postmonsoon seasons	154
Fig. 4.10	Wilcox plot for a) alluvial formation and b) hard rock formation for premonsoon and postmonsoon seasons	155
Fig. 4.11	Permeability index of groundwater from a) alluvial and b) hard rock formation for premonsoon and postmonsoon seasons	156
Fig. 4.12	Piper trilinear plot showing water facies for a) alluvial and b) hard rock formations	159
Fig. 4.13	Gibbs plot a) cationic and b) anionic in the premonsoon and postmonsoon seasons for the alluvial formation	160
Fig. 4.14	Gibbs plot a) cationic and b) anionic in the premonsoon and postmonsoon seasons for the hard rock formation	161

Fig. 4.15	Bivariate plots a) Alluvial: Na^+ -normalized Ca^{2+} versus Na^+ normalized HCO_3^- , b) Hard rock: Na^+ -normalized Ca^{2+} versus Na^+ normalized HCO_3^- , c) Alluvial: Na^+ -normalized Ca^{2+} versus Na^+ normalized Mg^{2+} and d) Hard rock: Na^+ -normalized Ca^{2+} versus Na^+ normalized Mg^{2+}	162
Fig. 4.16	Plot of $\text{Ca}^{2+} + \text{Mg}^{2+}$ vs $\text{Na}^+ + \text{K}^+$ of groundwater samples from the study area	163
Fig. 4.17	Plot of $(\text{Na}^+ - \text{Cl}^-)$ vs. $(\text{Mg}^{2+} + \text{Ca}^{2+}) - (\text{HCO}_3^- - \text{SO}_4^{2-})$ illustrating reverse ion exchange	164
Fig. 4.18	Plot of $(\text{Ca}^{2+} + \text{Mg}^{2+})$ vs. $(\text{SO}_4^{2-} + \text{HCO}_3^-)$ of groundwater samples from the study area	165
Fig. 4.19	Plot of TZ^+ vs $\text{Na}^+ + \text{K}^+$ of groundwater samples from the study area	166
Fig. 4. 20	Box plot for a) Deuterium and b) Oxygen-18 for both season of both formation	167
Fig. 4.21	Dexcess vs $\delta^{18}\text{O}$ plot for both seasons from the alluvial and hard rock formations for both the seasons	168
Fig. 4.22	Stable isotope plots for a) alluvium and b) hard rock formations for both the seasons	169
Fig. 4.23	Stable isotope plots for a) alluvium and b) hard rock formations for both the seasons	171
Fig. 4.24	Depth profile for tritium for alluvium and hard rock formation	171
Fig. 4.25	Schematic diagram for groundwater recharge and flow	172
Fig. 4.26	Box plot of uranium in both the formations and both the seasons	173
Fig. 4. 27	Percent samples above a) WHO and b) AERB limits for both the formations and both the seasons	174
Fig. 4.28	Spatial distribution of dissolved uranium a) premonsoon and b) postmonsoon	175
Fig. 4. 29	Spatial distribution of HCO_3^- in a) premonsoon and b) postmonsoon seasons	175
Fig. 4. 30	Spatial distribution of NO_3^- in a) premonsoon and b) postmonsoon seasons	176
Fig. 4. 31	Correlation of uranium with HCO_3^- ions in a) premonsoon and b) postmonsoon seasons	177
Fig. 4. 32	Correlation of uranium with NO_3^- ions in a) premonsoon and b) postmonsoon seasons	177
Fig. 4.33	Depth profile of uranium for a) alluvium and b) hard rock formations	178
Fig. 4.34	Correlation of physicochemical parameters and major ions with uranium for a) alluvium and b) hard rock formations in both the seasons	179
Fig. 4.35	Correlation of uranium with EC in a) premonsoon and b) postmonsoon season.	180
Fig. 4.36	Box plot of saturation indices for common uranium minerals for a) alluvial and b) hard rock formations for both the seasons	187
Fig. 4. 37	Depth profile for AR ($^{234}\text{U}/^{238}\text{U}$)	188

Fig. 4.38	Activity ratio vs. inverse concentration plot to identify the process for uranium mobilization for both the formations	189
CHAPTER 5		
Fig. 5.1	Box plot of uranium in pre and postmonsoon season of Punjab	195
Fig. 5.2	Box plot of uranium in pre and postmonsoon seasons of Rajasthan	197
Fig. 5.3	Correlation between nitrate and $\delta^{18}\text{O}$ for samples from study area under Punjab	198
Fig. 5.4	Correlation between nitrate and $\delta^{18}\text{O}$ for samples from study area under Rajasthan	199
Fig. 5.5	Stable isotope distributions of districts of Punjab and Rajasthan	200
Fig. 5.6	Schematic diagram of alpha recoil phenomenon	201
Fig. 5.7	Box plot of AR ($^{234}\text{U}/^{238}\text{U}$) for Punjab	202
Fig. 5.8	Box plot of AR ($^{234}\text{U}/^{238}\text{U}$) for Rajasthan	203
Fig. 5.9	Uranium release mechanism in alluvial formations of Punjab	205
Fig. 5.10	Uranium release mechanism in hard rock formation of Rajasthan	207
CHAPTER 6		
Fig. 6.1	Plausible scenarios based on AR and uranium concentration	217

List of Table

	Description	Page No.
CHAPTER 1		
Table 1.1	Categorization based on the stage of development	4
Table 1.2	Chemical contaminants with their permissible limits, source and health effects on human	8
Table 1.3	Isotopes of uranium with their half-life and abundances	11
Table 1.4	Uranium concentrations in various rocks	11
Table 1.5	Concentration of uranium in groundwater around the World	18
Table 1.6	Concentration of uranium in groundwater in India	20
Table 1.7	Principle aquifer system with dissolved uranium concentrations and percent samples exceeding the WHO permissible limits	27
Table 1.8	Characteristics of the study area	28
Chapter 2		
Table 2.1	Irrigation quality parameters calculation formulas	38
Table 2.2	Parameters and standards for DWQI	39
Table 2.3	Parameters with their weighting factor and standards for IWQI	39
Chapter 3		
Table 3. 1	Percentage of samples from the different depths	65
Table 3.2	Summary of physicochemical and chemical parameters for both the seasons of shallow and deep zones.	69
Table 3.3	Compiled water quality data for shallow and deep zones of the study area for both the seasons	79
Table 3.4	Suitability of water for drinking and irrigation on basis of TDS, TH and EC	80
Table 3.5	Compiled irrigation water quality data for shallow and deep zones of the study area for both the seasons	83
Table 3.6	Suitability of water for irrigation on basis of SAR, Na% and RSC	84
Table 3.7	PCA output Varimax rotated for the shallow and deep zones for both the seasons.	120
Table 3.8	The correlation of components with the various variables in both shallow and deep zones for both the seasons.	121
Table 3.9	Various species formed by uranyl ion in groundwater from both the zones	123
Chapter 4		
Table 4.1	Geological succession of Jaipur district, Rajasthan.	131
Table 4.2	Hydrogeology of Jaipur district, Rajasthan	132
Table 4.3	Geological succession of Dausa district, Rajasthan.	134
Table 4.4	Hydrogeology of Dausa district, Rajasthan	135
Table 4.5	Percentage of samples from the different formations	136

Table 4.6	Summary of physicochemical and chemical parameters for both the seasons of alluvium and hard rock formations	139
Table 4.7	Compiled water quality data for alluvium and hard rock formations of the study area for both the seasons	147
Table 4.8	Suitability of water for drinking and irrigation on basis of TDS, TH and EC	149
Table 4.9	Compiled irrigation water quality data for alluvium and hard rock formations of the study area for both the seasons	152
Table 4.10	Suitability of water for irrigation on basis of SAR, sodium percent and residual sodium carbonate	153
Table 4.11	PCA output Varimax rotated for the alluvial and hard rock formations	183
Table 4.12	The correlation of components with the various variable in both alluvial and hard rock formations.	184
Table 4.13	Various species formed by uranyl ion in groundwater from both the formations	186
Chapter 5		
Table 5.1	Comparative table for Punjab and Rajasthan	196

Chapter 6 Summary and Future scope

Summary

Water being an integral part of human body, it is of prime importance. This necessitates the sustainable management of water resource in terms of quantity and quality. Declining groundwater levels and increasing contaminants in groundwater are reports by many researchers in India, one of which is uranium. With the health implications related to uranium, it is of utmost importance to understand the sources and release mechanism of uranium into the groundwater. Studies suggest an increasing uranium contamination in groundwater and provide some conclusions on the likely controls, but none of them relates the aquifer characteristics, aquifer dynamics and the hydrochemical drivers which are very vital in controlling the uranium mobilization. With an objective, to understand the role of aquifer dynamics, aquifer characteristics, hydrochemistry (rock-water interactions) etc on uranium mobilization this research work was undertaken choosing in two geologically different terrains namely i) Muktsar and Faridkot districts of Punjab having alluvial formation and ii) Jaipur and Dausa districts of Rajasthan having alluvial and hard rock mixed formations. The results obtained in this study helps in evolving a holistic mechanism for uranium mobilization considering the different geological terrains of the India. These inferences and conclusions would also be applicable to similar geological formations in other countries as well. The similarities between the study areas include semi-arid climate, rainfall distribution and cropping intensity while dissimilarity pertains to geology, Punjab is alluvial formation while Rajasthan is both alluvial and hard rock formations.

In the shallow zone groundwater from study area under Punjab, 43% of samples were unsuitable for consumption in premonsoon which decreased to 29% in postmonsoon season while, for deep zone 30% of the samples were unsuitable for drinking which decreased to 12% in postmonsoon season. The groundwater from the study area of Rajasthan shows 25%

of samples are unsuitable for drinking in premonsoon season which increased to 71% in postmonsoon for alluvial formation. For hard rock formation, 60% of the samples from both seasons were unsuitable for their use. 100% of the groundwater from both Punjab (Muktsar and Faridkot) and Rajasthan (Jaipur and Dausa) are unsuitable for agricultural activity.

The study area under Punjab has issues of elevated nitrates (pre: 63%; post: 55%), fluoride (pre: 47%; post: 26%), sulphates (pre: 57%; post: 29%) and salinity (pre: 28%; post: 16%). In the deep zone, contamination due to high nitrate (pre: 30%; post: 13%) and fluoride (pre: 30%; post: 13%) is observed. The contaminated samples are decreased in postmonsoon season which is attributed to dilution by percolating water. The source of high nitrate and sulphate is excessive use of fertilizer while fluoride is presence of apatite minerals and salinity is due to rock-water interactions. The study area of Rajasthan has issues of high fluoride (pre: 25%; post: 71%), nitrate (pre: 40%; post: 43%) and salinity (pre: 42%; post: 86%) in the alluvial formation. For the hard rock formation contaminants like fluoride (pre: 67%; post: 75%), nitrate (pre: 20%; post: 33%) and salinity (pre: 60%; post: 92%) are found. The increased concentration of ions in postmonsoon is attributed to dissolution of salts from the vadose zone with percolating water. The high fluoride concentration in hard rock formation is attributed to increased rock-water interactions and presence of sources like fluorapatite and fluorite deposits present in the formation. The high salinity is attributed to rock-water interactions and nitrate concentrations are attributed to excessive use of fertilizer for agricultural purposes.

The ion scatter plots ascertain that the main source of Na^+ ions is ion-exchange with Ca^{2+} and Mg^{2+} ions from water, Mg^{2+} ions is a result of magnesium silicate weathering and Ca^{2+} ions is due to calcite and dolomite dissolution in shallow and deep zone of alluvial formation from study area under Punjab. For alluvial and hard rock formation of study area

under Rajasthan, same geochemical processes were found responsible for ionic concentrations.

The stable isotope signature from the alluvial formation of Muktsar and Faridkot district of Punjab indicates that shallow zone water has three main recharge sources i.e. i) canal water, ii) precipitation and regional flow contribution and iii) evaporated precipitation or irrigation return flow. The deep zone samples have a contribution from regional flow (precipitation). The stable isotope from the alluvial formation of Jaipur and Dausa districts of Rajasthan indicates two sources of recharge i.e. i) precipitation and ii) irrigation return flow. The similar signatures were observed in the hard rock formation of the study area. The signatures of delayed recharge are ascertained for alluvial and hard rock formation of Rajasthan from stable isotope and chemical data.

The uranium concentration in the alluvial formation from Muktsar and Faridkot district of Punjab has range from 1-610 $\mu\text{g/L}$ with an average value of 116 $\mu\text{g/L}$ for premonsoon season while for the postmonsoon season the concentration range from 10-565 $\mu\text{g/L}$ with an average value of 80 $\mu\text{g/L}$. 78% of the samples fall above the permissible limit by WHO which decrease to 69% in the postmonsoon season. For the alluvial formation of Jaipur and Dausa district of Rajasthan, uranium contamination in the alluvial formation ranges from 0.4-177 $\mu\text{g/L}$ with an average concentration of 30 $\mu\text{g/L}$ and 33% samples above the permissible limit of WHO for premonsoon season. For postmonsoon season, uranium concentration is in range of 5.3-142 $\mu\text{g/L}$ with an average concentration of 47 $\mu\text{g/L}$ and 61% of the samples above the permissible limits. For the hard rock formation of Jaipur and Dausa districts of Rajasthan, uranium concentrations are in range of 0.5-115 $\mu\text{g/L}$ with an average concentration of 34 $\mu\text{g/L}$ and 53% samples above the permissible limit of WHO for premonsoon season while for postmonsoon season the concentration range is 5.2-145 $\mu\text{g/L}$

with an average concentration is 51 $\mu\text{g/L}$ and 58% of the samples above the permissible limits.

Uranium contamination in the alluvial formation from Punjab shows a decrease in postmonsoon season both in average value and contaminated samples. Alluvial formation of Rajasthan indicates an increase in contaminated samples and concentration in the postmonsoon season. The hard rock formation of Rajasthan shows similar inferences as alluvial formation of Rajasthan i.e. an increase in contaminated samples and concentration of uranium is observed in postmonsoon season. The hydrochemical drivers like NO_3^- and HCO_3^- ions play a major role in uranium mobilization. It's the combined effect of aquifer conditions and concentrations of hydrochemical drivers and their correlations that led to spread in dissolved uranium concentration seasonally, spatial and temporally in the study area under Punjab and Rajasthan. The release of uranium in case of Punjab is oxidative dissolution while for Rajasthan is leaching due to limited availability of NO_3^- ions in case of Rajasthan due to delayed recharge.

The high uranium concentration in the shallow zone is associated with $\text{Na-HCO}_3\text{-Cl}$, Na-Cl-HCO_3^- , Na-HCO_3 and Na-Cl type water in a premonsoon while for the postmonsoon $\text{Na-HCO}_3\text{-Cl}$, Na-Cl-HCO_3 and Na-HCO_3 water type. For deep zone, all the contaminated samples had Na-HCO_3 as water type in both seasons. The highest values of uranium have $\text{Na-HCO}_3\text{-Cl}$ type water in both zones and both seasons for the alluvial formation of Punjab.

The high uranium concentrations in alluvial formation from Rajasthan is associated with $\text{Na-HCO}_3\text{-Cl}$ and Na-Cl-HCO_3 type in premonsoon while for the postmonsoon shift towards Na-Cl-HCO_3 type water is observed. For hard rock formation, all the contaminated samples had $\text{Na-HCO}_3\text{-Cl}$ type water in premonsoon which shifted to Na-Cl-HCO_3 water type. The highest values of uranium have Na-Cl-HCO_3 type water in both formations and

both seasons. Thus, corroborating that EC and HCO_3^- ions have a major role towards mobilization of uranium.

In the alluvial formation of Punjab, the activity ratio is in range of 0.85- 1.05 which suggests equilibrium condition while high uranium concentration suggest that aquifer is in oxidative condition. In the scatter plot of inverse uranium concentration and activity ratio, shallow zone samples follow the trend line of leaching while the deep zone samples fall on the mixing line. The mixing between deep and shallow zone is also corroborated from stable isotope signatures and chemical results.

The alluvial aquifer of Rajasthan has the $^{234}\text{U}/^{238}\text{U}$ activity ratio in range of 1.38 to 2.97 which is indicative of disequilibrium resulting from alpha recoil. The uranium is also high in the groundwater indicating that aquifer is in oxidative condition. For the hard rock formation of Rajasthan, similar activity ratio was found i.e. 1.69 to 2.38. In the scatter plot of inverse concentration versus AR, samples from both the formations follow leaching trend line. Thus, it can be concluded that similar geochemical processes are responsible for higher uranium in both the formations of Rajasthan. The stable isotope signature and chemical results indicate towards the interconnection of both the formations and delayed recharge.

By combining the chemical, stable isotopic data, uranium distribution, uranium isotope analysis, statistical and factor analysis, it can be concluded that high uranium in the shallow alluvial formation is attributed to the aquifer condition i.e. oxidative nature of the aquifer and to the extensive agricultural activity of the area, increasing nitrate concentration due to extensive use of fertilizer and bicarbonate ions due to increased pCO_2 which is result of root respiration and decaying organic matter (again due to agricultural activity) are controlling the U mobilization in groundwater of this region. The high uranium pockets in the deep zone of alluvial formation from Punjab are attributed to mixing between shallow and deep zones.

In Rajasthan, the aquifer behaves like a single unit and has signature of delayed recharge. This makes the availability of NO_3^- ions limited. The cropping intensity of Punjab is also more compared to Rajasthan that indicates the low NO_3^- ion concentration in the region that is corroborated from chemical data. Thus, overall oxidation of the mineral like in the case of Punjab is not observed. The uranium is mobilized due to limited NO_3^- ions present. Thus, a lower concentration in case of Rajasthan is observed compared to Punjab. The high activity ratio is attributed to long residence time which increases rock-water interaction. Thus, providing time for selective leaching of ^{234}U leading to increased activity ratio.

The high uranium in the study area of Punjab and Rajasthan is attributed to multiple factors including geochemical process, aquifer characteristics, aquifer condition and extensive agricultural practices. In Punjab, the main processes that causing release is oxidative dissolution from uranium minerals present in the aquifer matrix while for Rajasthan, its rock-water interactions and oxidative condition leading to leaching of uranium from the source. The selective leaching of ^{234}U is also observed in Rajasthan.

Remedial measures

Remediation is an act of correcting an error or in case of contamination the measures taken to reduce the concentration of already present contaminant. This helps in reducing the risks to human health, environment and property to acceptable levels by removing or reducing the source of contamination or by blocking exposure pathways. The treatment can be carried out in two modes, viz., in-situ (i.e. at the site) or ex-situ (i.e. after extraction) [262].

The ex situ treatment includes the following categories

1. Adsorption or ion exchange: This process comes under physical method of removal. The adsorbents like activated carbon, activated silica, resins etc are for this purpose, which are efficient methods for removal of uranium but suffer from high costs.
2. Precipitation: This is a simple and less expensive method, but leads to generation of effluent that needs proper disposal. The method involves increase the pH of the system which allows co-precipitation of uranium with ferric hydroxide.
3. Reverse osmosis: Water is passed through a semipermeable membrane under high pressure. This process of uranium removal is not cost effective and the concentrated waste generated in the process also needs to be taken care for.

In- situ remediation:

1. Making use of Redox conditions: The process work by changing the oxidation-reduction conditions leading to reduction of U(IV) to U(VI). The main disadvantage of this process is remobilization of sorbed uranium over a period of time. To invoke redox changes, sodium dithionite, microbial induced reduction, and calcium polysulfide etc are used.
2. Permeable reactive barriers (PRBs) like bone char phosphate, zero valent iron or ferric iron across the flow path of the contaminant plume has shown to lower the uranium concentration.

3. Natural zeolites: Adsorption on clinoptilolite manganese oxide coated zeolite (MOCZ) can be used for uranium removal from the groundwater system.
4. Bioremediation: Microbial reduction of U(VI) to U(IV) using *Geobacter* species. *Pseudomonas* MGF-48 is also known to help in remediation of uranium as studied by Li and Zhang (2012) ^[263]. Denitrification bacteria, ferric-iron reducing bacteria and sulphate reducing bacteria are also studied. It was found that by dosing small quantity of ethanol the reduction process of uranium is enhanced ^[261].
5. Phytoremediation: Plants like sunflower, Indian mustard, small duckweed and willow moss are known to absorb uranium from soil and water. A study by Pentyala and Eapen (2020) ^[264] concluded that *vetiveria zizanioides* grass plant can be efficiently used for removing uranium from hydroponic solutions as well as soil. At lower concentration the uranium is limited to roots while at higher concentration it spreads in the whole plant ^[264].

Remediation method that can be applied to the area under study are:

i) Punjab:

- The study area has extensive network of canal feeder hence the people can switch to surface water for their domestic necessities.
- The state government have installed large scale RO-systems throughout the affected area. The public is instructed to use RO-water for the purpose of drinking and cooking.
- Other than these measures, bioremediation and phytoremediation would be good idea for uranium removal.

ii) Rajasthan

For the people of Rajasthan, there is no other source of freshwater except the groundwater supplies. Hence, it is very important to take immediate step

towards remediation of uranium. The redox based microbial induced reduction would be a good approach. *Geobacter* species, denitrification bacteria, ferric-iron reducing bacteria and sulphate reducing bacteria can be used for the purpose.

Future Scope

Uranium is known for its radiotoxicity and also its heavy metal nature affecting the human health. In the initial study, it was known to accumulate in the kidney and affect its normal functioning. With the advancement of studies, uranium is known to impact bones, DNA, neurotransmitters, cancerous etc.

India has a diverse nature of aquifer formations. Since the distribution of uranium is not associated with any particular region or formation, it is important to conceptualize the uranium mobilization considering the local geology. Since groundwater is the major source of drinking water in India and in many other countries, it is important to conceptualize the U mobilization process in different terrains. This can be achieved through a thorough understanding of aquifer geochemistry, involving geochemical processes, source and mechanism of groundwater recharge and its dynamics, source of contamination. Considering the Uranium isotope and total uranium of groundwater four scenarios can be envisaged (Fig. 6.1).

Activity Ratio ($^{234}\text{U}/^{238}\text{U}$)	High AR, Low U	High AR, High U Rajasthan
	Low AR, Low U	Low AR, High U Punjab

Uranium Concentration

Fig. 6 1 Plausible scenarios based on AR and uranium concentration

Under this thesis work, two categories i.e. i) area with high uranium and low AR and ii) area with high uranium and high AR are studied. It is found that the study area of Rajasthan has high uranium and high AR while the study area of Punjab has High uranium low AR. The reason for high AR in Rajasthan is aquifer characteristics and dynamic that favours rock-water interaction and helps in selective leaching of ^{234}U . We have proposed a mechanism of uranium release in the two areas depicting the role of various hydrochemical drivers, geochemical processes, and human interferences. A similar study can be planned for the other two categories, viz., low uranium low AR and low uranium high AR. It would be interesting to see which of these categories are more prone to changes and how human interventions can alter the U mobilization in short term and long-term scenarios.

SYNOPSIS

The stress on earth's natural resources is increasing exponentially with the rapid population growth and rising expectation for a better life. It is of prime importance that basic resources for human survival, viz., air, water and land are managed wisely and sustainably. Groundwater constitutes 80% of the total freshwater resources on earth. Due to uncertainty in monsoons and degradation in surface water quality, the dependence on groundwater is ever increasing to meet the freshwater demand. Intensive use of groundwater resources and its contamination by anthropogenic activities pose a great threat to groundwater in terms of both quantity and quality. In Punjab, an agrarian state, the quality and quantity of groundwater are being affected by overexploitation of groundwater, excess use of fertilizers and pesticide. Rajasthan being a semi-arid to arid region, groundwater recharge is limited and abstraction of groundwater is leading to depletion in the water levels, inland salinity and other contamination. Both Punjab and Rajasthan form a sizable fraction of northwestern India and many research studies on groundwater have been carried out to evaluate the controls on groundwater recharge as well as quality. The presence of radioactive contaminants like uranium in these states poses an additional threat to human health. This research work pertains to evaluation of groundwater contamination by uranium concentration in parts of Punjab and Rajasthan states.

The selected areas i.e. Punjab (Muktsar and Faridkot districts) and Rajasthan (Jaipur and Dausa districts) are both semiarid and have cropping intensity more than 100%, which poses severe stress on the existing groundwater resources. The main aquifer system in Punjab is alluvial in nature while Rajasthan has both alluvial and hard rock formations comprising of Gneiss, Phyllites etc. Both the study areas are facing the problem of nitrate, iron and fluoride contamination in groundwater as well as salinization. In addition, Muktsar district of Punjab is

also facing waterlogging problem in addition to poor water quality. The abstraction of groundwater is very low because of its degraded quality and the water from canals and irrigational activities are further increasing the waterlogging issue. A proper evaluation of groundwater quality and factors affecting the characteristics in different aquifers is needed to ensure sustainable groundwater development and also to suggest appropriate remedial measures to combat growing contamination issues.

Geochemistry and environmental isotopes in conjunction with modelling tools have proven to be potential tools in assessing processes and factors governing groundwater chemistry, the dynamics of the aquifer system etc. The work described in this thesis deals with the assessment of groundwater quality and its suitability for potable and irrigational purposes as a first step towards understanding the groundwater characteristics. Subsequently, the chemical results along with environmental isotope, geochemical and statistical modeling tools were used to identify the factors and processes governing the mobilization of ions, the recharge sources, condition and dynamics of the aquifer system. To achieve this, the water samples were collected from both the study areas mainly from existing hand pump, tube-wells and bore wells covering spatial and vertical heterogeneities. In order to determine temporal variations, water sampling was carried out during premonsoon as well as postmonsoon seasons. The collected water samples were analyzed for major chemical ions, environmental isotopes and total uranium and its isotopes. The results helped in demarcating the low and high uranium zones and the effect of hydrochemistry on uranium mobilization. The probable hydrochemical drivers for mobilization of uranium were also evaluated and a conceptual model for groundwater uranium mobilization for both Punjab and Rajasthan states are proposed in the thesis. The work in the thesis is divided into five chapters namely;

Introduction

Methodology

Source and mobilization of uranium in groundwater of SW Punjab

Source and mobilization of uranium in groundwater of Rajasthan

Comparative analysis

CHAPTER 1: INTRODUCTION

Chapter 1 describes the importance of groundwater in the context of India and world in terms of quality and quantity. The water quality is modified during the course of its traverse through the hydrological cycle due to interaction reactions like evaporation, transpiration, selective uptake by vegetation, ion-exchange, oxidation/reduction, dissolution/precipitation of minerals, mixing of waters, leaching of fertilizers, pesticides and manure etc. Deteriorating water quality is also strongly related to increasing population and industrialization. The improper disposal of industrial waste, extensive use of fertilizers, and pesticide are impacting the quality of water in many agrarian regions. The surface water is often insufficient in fulfilling the demands for domestic, agricultural and industrial uses. Hence, the stress on groundwater resources is increasing exponentially. The additional stress on groundwater quantity arises due to uneven rainfall or failure of monsoon. Many reports have documented a rapid increase in groundwater contaminants like fluoride, chloride (inland or coastal), iron, arsenic, nitrates and uranium in India as well as abroad. These contaminants often lead to increasing human health ailments. Uranium contamination in drinking water mainly impacts the kidney functioning apart from DNA damage, bone degradation. Uranium being a toxic heavy metal also results in carcinogenic effect on the human body. High concentration of uranium was reported in Malwa region of Punjab by many researchers. The studies have not correlated the high uranium concentration to

aquifer dynamics, hydrogeology, hydrochemistry etc. To get the holistic picture on uranium mobilization, it is important to understand the role played by these factors. So, we selected two study area namely Muktsar and Faridkot district of Punjab and Jaipur and Dausa districts of Rajasthan. These chosen areas have similarities like semi-arid climate with an average annual rainfall in range of 500-600 mm received from south west monsoon. Extensive agricultural is done in the districts under study with cropping intensity of more than 150%. The districts from Punjab and Rajasthan are still different in many ways like Muktsar and Faridkot districts have principle aquifers in alluvial formation while Jaipur and Dausa districts aquifers are in both alluvial and hard rock formation. The research studies carried out on the uranium contamination and groundwater quality from these study areas are mentioned in the introductory chapter. The available research mentions about the increasing concentration of uranium and other contaminants in groundwater, but provide limited information on the source and origin of groundwater, residence time and factors leading to uranium contamination. The broad objectives of the study are i) assessment of groundwater quality and its suitability to potable and irrigation purposes, ii) identification and understanding the geochemical processes leading to the chemical characteristic of groundwater, iii) To find the source and origin of groundwater iv) to delineate the uranium-rich and poor zones v) to study uranium mobilization process.

CHAPTER 2: METHODOLOGY

Chapter 2 outlines the importance of chemistry, environmental isotopes, geochemical and statistical modeling tools in understanding the groundwater characteristics and promoting sustainable management of water resources. Water samples were mainly collected from major water-bearing formations of the study area namely, Alluvium in Muktsar and Faridkot districts of south-west Punjab; Alluvial and Hard rock formation of Jaipur and Dausa districts of

Rajasthan. The water sampling from the hand pump, tube wells, and canals in the study area of Punjab was done during October 2016 (postmonsoon) and May 2017 (premonsoon). The sampling from the study area of Rajasthan was carried out during March 2017 (premonsoon) and November 2017 (postmonsoon). The sampling locations details like latitude, longitude, elevation, well depth was noted down in the field while in situ physicochemical parameters such as electrical conductivity (EC), pH, total dissolved solids (TDS), and temperature were measured on site using Hanna multiparameter probe. The working principle of the instruments is described in this chapter. The samples for major ion chemistry (60ml), stable isotopes (30ml), tritium (500ml), total dissolved uranium (20ml) and uranium isotopes (1l) were brought to the laboratory for the measurements. The pretreatment and sampling procedure along with precautions to be taken during sampling are detailed in the chapter.

Most of the chemical analysis was carried out using ion chromatography system (DIONEX- DX 500), the working principle and operating conditions of these techniques are described under this chapter. Environmental stable isotopes (^2H & ^{18}O) were measured using isotope ratio mass spectrometer (IRMS) after adopting appropriate sample preparation method. Environmental radioisotope tritium (^3H) was measured using a liquid scintillation counter (LSC) after electrolytic enrichment. A brief description of IRMS and LSC is given in this chapter. Total dissolved uranium was measured using LED-based fluorimeter (Quantalase UA-I), the working principle and error estimation is described in the chapter under analytical techniques. For the measurement of uranium isotopes (^{234}U and ^{238}U), separation of uranium followed by electroplating was carried out. The counts were obtained using an alpha spectrometer with 1K MCA (Ortec instruments) with Maestro analysis software. The calibration, background correction and working principle of the instrument are briefly described in this chapter. Various

models commonly used for hydrochemical studies are mentioned in this chapter with detailed description.

CHAPTER 3: Source and mobilization of uranium in groundwater of South West Punjab

Chapter 3 provides the geological and hydrogeological description of the study area in Punjab, viz., Faridkot and Muktsar districts. It also includes the groundwater scenario of the region in terms of quality and quantity. The study area has a semiarid climate with 79% of its rainfall received from south-west monsoon with an average annual rainfall of 369 mm in Muktsar and 459 mm in Faridkot districts with a minimum temperature of 5°C during winter and maximum of 41°C during summers. The land of the study area is mainly used for agricultural activities with a cropping intensity of 200% in Muktsar and 193% in Faridkot district of the study area with approximate 11000 and 65000 nutrient ton of NPK of fertilizer consumption. The hydrochemical, isotope and uranium results are listed in this chapter with detailed interpretation using various graphical representations. The major cations in Muktsar are in order of $\text{Na}^+ > \text{Ca}^{2+} > \text{Mg}^{2+} > \text{K}^+$ while order for anions is $\text{HCO}_3^- > \text{SO}_4^{2-} > \text{Cl}^- > \text{NO}_3^- > \text{F}^-$ for both seasons. The order of major anions for Faridkot remains the same while the order of major cations is $\text{Na}^+ > \text{K}^+ > \text{Ca}^{2+} > \text{Mg}^{2+}$. The contaminants like TDS, TH, SO_4^{2-} , Cl^- , NO_3^- , F^- and uranium are found in both the districts during both the seasons as per the guidelines of WHO and BIS. Except for TH, all contaminants decrease in the postmonsoon season which may be attributed to dilution due to recharging precipitation water. As per the three major criteria for determining the suitability of water for drinking i.e. TDS, TH and EC; 20%, 5% and 23% of samples in Muktsar are found to be fit for drinking respectively while 39%, nil and 42% of samples are fit in the case of Faridkot district respectively. The parameters for accessing suitability of water for irrigational use are SAR, %Na, RSC, PI. According to the classification based on SAR, 89% of

samples are found to be fit for irrigation in Muktsar, which decreased to 85% in postmonsoon. In Faridkot, the acceptable samples were 73% which decreased to 58% in the postmonsoon season. As per %Na, all the samples fall in the acceptable range during both the seasons in both the districts. As per RSC, 62% of samples are suitable which decreases to 40% in postmonsoon for Muktsar. For Faridkot, 3% of samples are suitable as per RSC while none of the samples are suitable for the postmonsoon season. As per the PI values, most of the samples are in Class 1 for both seasons, whereas in Faridkot samples mostly fall in Class 2 and Class 3 in both the seasons. The composite factor for irrigation suggests none of the samples are fit for their use in Faridkot and Muktsar districts during both seasons. The premonsoon samples mostly fall under Na-Cl type water which changes to Ca-Na-HCO₃ type during postmonsoon seasons. The geochemical process involved were assessed and found that reverse ion exchange is the dominant process followed by evaporative enrichment leading to increased concentration of Na⁺ and K⁺ ions in the aquifer system while magnesium silicate weathering is the main reason for Mg²⁺ ion and calcite dissolution is the source for Ca²⁺ ions. The average uranium concentration for premonsoon is 95 µg/L and 133 µg/L for Muktsar and Faridkot districts respectively, while for the postmonsoon season, it is found to be 80 µg/L and 83 µg/L respectively. The decrease in ion concentrations in postmonsoon season is attributed to dilution due to recharging groundwater. The depth profiles for EC, nitrate, bicarbonate and uranium show contamination in the shallower zones while the deeper zones are mostly unaffected, except in a few pockets. The residence time of water in the shallower zones is low indicating modern recharge while the deeper zones show low tritium values with very narrow spread indicating higher residence time compared to shallower zones. The deeper zones seem to be fed by regional groundwater flows. The stable isotopes of water i.e. δ²H and δ¹⁸O indicates three recharge groups of samples i)

depleted $\delta^{18}\text{O}$ values due to canal water interaction, ii) values between -8‰ and -5‰ indicating precipitation recharge and iii) evaporative signature (-4‰ to -2‰) indicating contribution of irrigation return flow. The slope of best-fit lines for pre and postmonsoon season are 5.4 and 5.3 respectively indicating recharge from the evaporative body. The deeper zone samples lie near to GMWL indicating precipitation recharge and their tritium values indicate long residence time, pointing to regional flow contribution. The uranium concentration ranges from 1-610 $\mu\text{g/L}$ for the premonsoon season while for postmonsoon the concentration is in range of 5-565 $\mu\text{g/L}$. The spatial distribution shows higher concentration of uranium in south-west and northern region with patches in eastern and central locations. During the postmonsoon season, dilution is observed at northern location while an increase in uranium contaminated samples is observed in southern and eastern locations. The high and low uranium concentration samples did not show any characteristic difference in the corresponding stable isotopic values. Uranium shows a positive correlation with EC, HCO_3^- and NO_3^- ions. Uranium isotopes data was correlated with uranium concentration and it was interpreted that leaching causes high uranium in the shallower zones while mixing process contributes uranium in the deeper zone. The mobilization of uranium from mineral is a combined effect of nitrate as oxidizer and bicarbonate as a mobilizing agent. During postmonsoon, the reduction in their concentration may be affecting dissolution of uranium, which leads to a decreased uranium concentration.

CHAPTER 4: Source and mobilization of uranium in groundwater of Central Rajasthan

Chapter 4 provides the geological and hydrogeological description of the study area in Rajasthan, viz., Dausa and Jaipur districts. It also includes the current groundwater scenario in these districts. The study area has a semiarid climate with 90% of rainfall received from south-west monsoon. The average annual rainfall in Jaipur and Dausa districts is of 519 mm and 659

mm respectively. The temperature ranges from 5°C to 48°C. Agriculture is the main activity in the study area with a cropping intensity of 140% in Jaipur and 155% in Dausa district, and most of the region is irrigated using groundwater. The hydrochemical and isotope results of the pre and postmonsoon water samples are provided in this chapter. These results are interpreted in conjunction with available hydrogeology and lithology, and the findings are elaborated in this chapter. The major cations in order of $\text{Na}^+ > \text{Mg}^{2+} > \text{Ca}^{2+} > \text{K}^+$ while order for anions is $\text{HCO}_3^- > \text{Cl}^- > \text{SO}_4^{2-} > \text{NO}_3^- > \text{F}^-$ for both the seasons. The contaminants like TDS, Cl^- , NO_3^- , F^- and uranium are found in both the districts during both the seasons as per the guidelines of WHO (2012) and BIS (1991). All the contaminants show an increase in the postmonsoon season, which may be attributed to dissolution of salts with recharging water. As per the three major criteria for determining the suitability of water for drinking i.e. TDS, TH and EC, 53%, 6% and 75% of premonsoon samples in both the districts are fit for drinking while 12%, 3% and 37% of samples are fit for their use in postmonsoon season. As per the composite parameter for drinking, 69% of premonsoon samples are fit, which decreases to 33% in postmonsoon season. According to the classification based on SAR, in Jaipur, 81% of samples are fit for irrigation, which decreased to 58% in postmonsoon. As per %Na, 15% of the samples are in acceptable range during premonsoon while none of the samples are acceptable during postmonsoon season. As per RSC, 8% of samples are suitable, which decreases to 3% in postmonsoon for the study area. As per the PI values, 4% of the samples are in Class 1 for premonsoon, which decreases to 2% in postmonsoon. Overall hydrochemical facies observed are Na- HCO_3 (35%), Na- HCO_3 -Cl (57%) and Na-Cl- HCO_3 (8%) types for the premonsoon sampling. The facies observed for postmonsoon sampling are Na- HCO_3 (18%), Na- HCO_3 -Cl (46%), Na-Cl- HCO_3 (33%) and Na-Cl (3%) types. The geochemical process involved were assessed and it was found that reverse

ion exchange is the dominant process followed by evaporative enrichment leading to increased concentration of Na^+ and K^+ ions in the system while magnesium silicate weathering is the main reason for Mg^{2+} ions and calcite dissolution is the source for Ca^{2+} ions. The average uranium concentration for premonsoon is 28 $\mu\text{g/L}$, which increases to 48 $\mu\text{g/L}$ for the postmonsoon season. 33% samples are above the permissible limit given by WHO which increases to 68% in the postmonsoon season. The increase in concentration in postmonsoon season is attributed to dissolution with recharging groundwater. The depth profile for EC, F^- , NO_3^- , HCO_3^- and uranium indicates an overall groundwater contamination in all the zones. The tritium content of samples in alluvial and hard rock formation indicates modern recharge with tritium value in range of 1-4 TU. The shallow zones of the formations are more dynamic compared to deep zones. The stable isotopes of water ($\delta^2\text{H}$ and $\delta^{18}\text{O}$) indicates two main recharge sources i.e. precipitation and irrigation return flow. The isotopic values indicate an increase in the irrigational return flow during postmonsoon season. The high and low uranium samples do not show any significant difference in the corresponding stable isotopic values in premonsoon season. The isotope signatures indicate that samples with high uranium concentration are mainly recharged by evaporated precipitation. During the postmonsoon season, the isotope signatures of high uranium water samples point to two sources of recharge i.e. precipitation and irrigation return flow. Uranium shows a positive correlation with EC, HCO_3^- and NO_3^- , which is more in postmonsoon compared to the premonsoon season. Uranium isotopes data was correlated with uranium concentration and it was interpreted that uranium is contributed to groundwater mainly through leaching process. High uranium activity ratio ($^{234}\text{U}/^{238}\text{U}$) is observed in the samples from the study area, which reflect the prevalence of alpha recoil phenomenon towards uranium release into groundwater. During alpha recoil the daughter nuclei get displaced by 20nm in any

direction, therefore the fracture surfaces that are in contact with groundwater act as potential sources for accumulation of recoiled nuclei, which eventually leads to uranium mobilization. Once the uranium releases into groundwater, it gets oxidized and then form stable complexes and migrates to far off distances. Typically, NO_3^- and dissolved oxygen act as oxidizers and HCO_3^- as complexing agent in both the formations. During postmonsoon, the increase in uranium concentrations is attributed to the increased NO_3^- and HCO_3^- ions.

CHAPTER 5: Comparative analysis

This chapter consists of a detailed evaluation of similarities and dissimilarities in aquifer systems of both the study areas (Rajasthan and Punjab). The role of hydrochemical drivers like NO_3^- , pCO_2 , HCO_3^- towards uranium leaching, complexation and migration is studied considering the varied geological and hydrogeological differences in the study regions. The seasonal and temporal variations in contaminant concentrations are also studied for both the study area in light of varying groundwater dynamics. The uranium contaminated and safe zones are also delineated in both the study areas. Based on the hydrochemical, isotope and modeling inferences, conceptual models are prepared for the uranium mobilization processes in both the aquifer systems and presented in this chapter. Finally, summary and conclusions along with future scope are provided at the end of these chapter.

CHAPTER 1 Introduction

The water is present in our solar system from the beginning and was formed by the thermonuclear fusion process. The total amount of water contained in the Earth is estimated to be about 0.4% by volume, sufficient to form a sphere of ice with a diameter of almost 2500 km and a volume of $8.2 \times 10^9 \text{ km}^3$ [1]. However, most of the water (83%) is bound within rocks and minerals present in crust and mantle. Out of the freely available water, 96% is stored in oceans which is saline. Only 2.5% of available water is freshwater and is useful for humankind. 79% of this freshwater reserve is trapped in the ice caps and glaciers, and the rest occurs as groundwater (20%) and surface water (1%). The pictorial depiction of water distribution is given (Fig. 1.1).

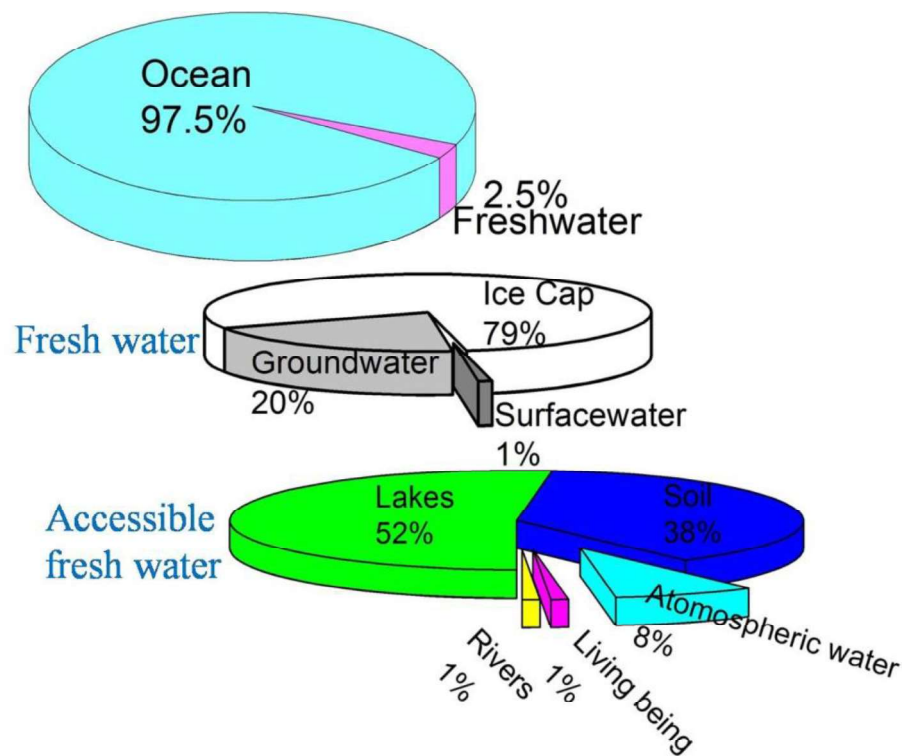


Fig. 1.1 Distribution of water on Earth

1.1 Groundwater Scenario in the world and India

An exponential increase in population and rapid industrialization has posed a severe stress on the natural resources including, water. The strong interconnections among surface water, groundwater, human being and the ecosystem necessitate a good understanding of each of these domains so that a balanced approach can be adapted for their sustainable management. Gleeson et al. (2012) ^[2] reported that 1.7 billion people already live in the regions where abstraction of groundwater resources is more than its natural recharge. United nation (2019) ^[3] estimated the total human population to be 9.7 billion by 2050. To combat the demand of the growing population, agricultural and industrial outputs need to increase further stressing the natural resources. The irrigation of agricultural fields can add upto 300 kg/ha/year ^[4]. The excessive use of fertilizers and pesticide for agricultural activity adds contaminants to the water sources.

Global warming resulted in increased evaporation, evapotranspiration and water holding capacity of atmosphere thus impacting the rainfall patterns. The extreme rain event leads to floods, increased runoff etc. In the past, most of the freshwater needs were mainly met from surface water bodies as compared to groundwater resources. However, with the growing concerns on the quantity and quality of surface water, as well as advancement in groundwater abstraction technology, there has been a shift towards the use of groundwater for freshwater needs. Groundwater was thought to be safer and less susceptible to surface contamination, resilient to seasonal changes or monsoon failure, uniformly spread and available compared to surface water.

The improvement in technology has increased abstraction of groundwater globally to about 138% over the last four decades ^[5]. Out of the countries abstracted water, Algeria uses

67%, Iran uses 58% and USA uses 45% for irrigational purposes. The main issues faced with groundwater resources are i) overdraft leading to depletion, ii) salinization and waterlogging and iii) anthropogenic contamination. Beltran and Manzur (2005) ^[6] reported that 831 million hectares of the land extended over Africa, Asia and America are affected by sodic and saline soils. A study by Konikow (2011) ^[7], estimated that 13% rise of seawater level is attributed to declining groundwater levels. The hotspots for declining groundwater levels are observed in China, India, USA, Yemen, Spain and Iran with total global depletion of $283 \pm 40 \text{ km}^3/\text{year}$ ^[5]. In northern China, a declining rate of about 0.75 m/year to 3.68 m/year was observed. Similar declining rates were also observed in Mexico, about 1.79 m/year to 3.3 m/year ^[8]. In India, the declining rate of $17.7 \pm 4.5 \text{ km}^3/\text{year}$ were observed for states of Rajasthan, Punjab and Haryana.

Though India receives an annual average rainfall of about $4000 \times 10^9 \text{ m}^3$ spread over the vast geography and varying topography, the utilizable rain is only about $1123 \times 10^9 \text{ m}^3$ ^[9]. India also has vast river channels with seven major rivers flowing through most of northern and eastern India. The Gangetic plains are most important amongst the other river plains with a spread of about 86.1 million hectares and most productive alluvial aquifer of northern India. Still, the stress on groundwater has increased due to increase for the water demand, pollution of surface water and failing monsoons. India is one of the largest users of groundwater, it abstracts $1/4^{\text{th}}$ of the world's water i.e. about $230 \text{ km}^3/\text{year}$ ^[10].

In India, the groundwater has a dominant share in irrigation water (62%), rural water supply (85%) and urban water consumptions (45%) ^[11]. The per capita water availability in India was 1816 m^3 (2001) which reduced to 1545 m^3 (2011) and it is likely to further reduce to 1367 m^3 by 2031 ^[12]. India had two major aquifer systems i.e. i) alluvial spread in Gangetic and Indus plains covering 31% of India's area and ii) hard rock aquifers spread over 65% of India

mainly covering central peninsular India ^[13]. Out of the 13,240 observation wells under CGWB, the decline in groundwater levels was observed in 55% of the sampled wells, while the rise was observed in 44% and 1% showed no change during Jan 2019. Water level decline of more than 2 m was observed in 15% wells while 9% of wells showed a rise ^[14]. For sustainable use and better management of groundwater, we need to have a holistic knowledge about the aquifer system i.e. its spread, quality and replenish ability rate etc. Groundwater in terms of quantity is expressed as groundwater draft which provides insight into its extraction. It helps in calculating the stage of development of groundwater source (Equ. 1.1)

$$\text{Stage of development} = \frac{\text{Annual groundwater draft}}{\text{Annual available resources}} \times 100 \quad (1.1)$$

When the stage of development is 100%, it means extraction is more than the availability hence the area is overexploited. Stage of development in various states of India is shown in Fig. 1.2. It is clearly observed from the figure that the states of Rajasthan, Haryana, Punjab, Delhi, Tamil Nadu and Karnataka are most stressed. The classification based on the stage of development is given in Table 1.1.

Table 1.1 Categorization based on the stage of development ^[15]

Stage of development	Category	Assessment unit (6881)
>100%	Over-exploited	1186
90-100	Critical	313
70-90	Semi-critical	972
<70	Safe	4310
Not good for use	Saline	100

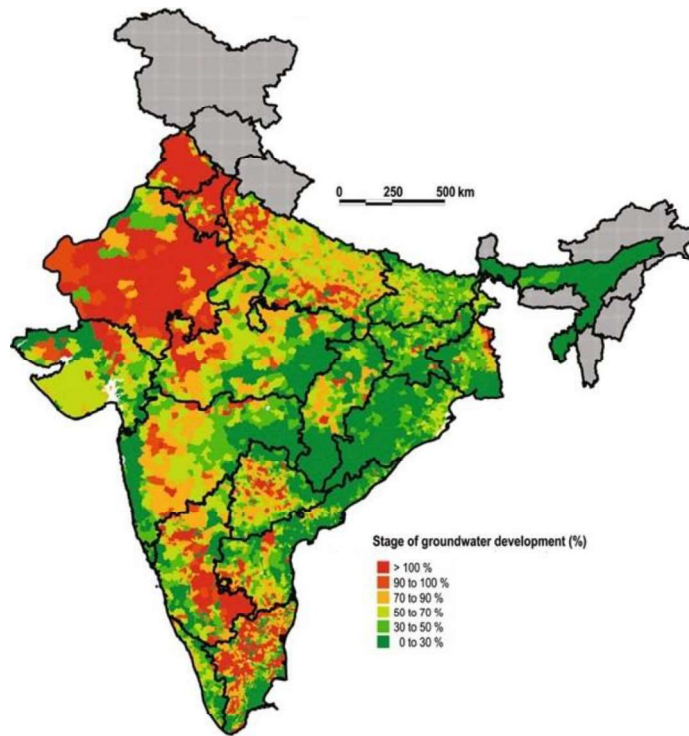


Fig. 1.2 Map of India indicating the stage of development (greyed area has no observation wells) (Cropped from Saha and Ray 2018) ^[9]

With regard to the study by Jurgens et al (2010) ^[16] in central valley, California, USA, it was observed that groundwater draft also plays an important role in mobilisation of uranium. The researchers have also observed an increase in HCO_3^- ion concentration over the past 100 years. The depth of groundwater reported in early time was shallower compared to present scenario. They reported significant correlation between the depth and uranium contamination, which decreased with increasing depths.

1.2 Groundwater contamination

Apart from over-exploitation of the groundwater resource, another major issue faced globally is groundwater contamination. The contamination can be chemical or microbial. Chemical contamination of aquifer occurs when concentrations of one or more substances are above the recommended limits, making water unsuitable for its use by human, plant and animals

^[17]. It has been reported that ~40 million people per year in the world are affected by waterborne diseases ^[18]. Duttagupta et al. (2019) ^[19], estimated death of about one lakh persons per year due to water-borne disease. Groundwater contamination and pollution mostly occurs due to human interferences like agricultural, industrial and urbanization ^[20]. The contaminants can move rapidly with recharging water through fractures in rocks, macro-pores generated by root-systems, burrows of animals etc.

The contaminant can enter the ecosystem either from point source or disperse (non-point) source. When one can identify the origin of a contaminant it is known as point source for e.g. contaminants added from industrial or sewage discharges. Disperse or non-point source type of contamination occurs when the source cannot be pin-pointed i.e. contaminants are carried by water from the path of its traverse. This contamination can occur naturally with rivers, rainfall and run off or anthropogenic from irrigation return flow etc. The recharging water carries along pesticides and fertilizers applied for agricultural purposes, industrial wastes, leakage from septic tanks etc which leads to increase in nitrogen, phosphorous, potassium (due to fertilizer), heavy metals (industrial waste) and other minerals in the groundwater ^[21]. Few potential contaminants, with their permissible limits and health impacts, are compiled in Table 1.2.

Arsenic is one of the contaminants reported in water which is a result of the natural geochemical condition of the aquifer i.e. high oxygen causes leaching of arsenic from arsenopyrite [FeAsS]. The Bengal delta i.e. flood plains of Ganga and Brahmaputra is the most impacted zone with high arsenic concentrations affecting around 36 million people ^[22, 23]. Arsenic is highly poisonous in its reduced state. It's known to have carcinogenic effects on human and long-term exposure can lead to high incidences of skin lesions, bladder, lung, skin

and kidney cancer, respiratory disease, liver and kidney disease. Höhn et al. (2006) ^[24] reported that the presence of iron, nitrate and oxygen act as a geochemical driver for arsenic mobilization. The higher arsenic concentrations are also reported around the globe, with contaminated samples reported in Myanmar, Afghanistan, Iran, Pakistan, Vietnam, Cambodia, USA, Europe and Australia etc ^[25].

Table 1.2 Chemical contaminants with their permissible limits, source and health effects on human [26]

Contaminants	Permissible limits	Source	Health effect
Dissolved solids	1000 mg/L	Natural + Manmade (landfill leachates, sewage etc)	alters the taste of water, depending on the ion concentration can affect heart or other body parts
Hardness	500 mg/L	dissolved ions especially calcium and magnesium	Diuretic effect
Arsenic	10 µg/L	Natural process, Agricultural (Pesticides) and industrial activities (processing of Copper, lead and zinc ores)	As ³⁺ is more toxic and carcinogenic, causes liver and kidney damage and anaemia
Cadmium	5 µg/L	Naturally from rocks and anthropogenic due to burning of fossil fuels and industrial waste (mining, metal plating, batteries, paints and landfill leachate)	Replaces zinc in the body, causes high blood pressure, liver and kidney damage, effects testicular tissue and anaemia
Chloride	250 mg/L	Saltwater intrusion, mineral dissolution, industrial and domestic waste.	Hyperchloremia, nausea, muscle twitching, heart and dehydration
Chromium	100 µg/L	mostly from industrial waste i.e. mining activities, fossil-fuel combustion and waste incineration	Cr ³⁺ is essential while Cr ⁶⁺ causes liver and kidney damage, internal haemorrhaging, respiratory damage, dermatitis, and ulcers on the skin
Copper	1.3 mg/L	result of metal plating, industrial and domestic waste, mining, and mineral leaching	causes stomach and intestinal distress, liver and kidney damage, anaemia
Cyanide	200 µg/L	Result of waste from electroplating, steel processing, plastics, synthetic fabrics, and fertilizer industries	damage to spleen, brain, liver and lead to death
Fluoride	1.5 mg/L	naturally or as an additive to municipal water supplies	Dental fluorosis and crippling bone disorder due to long term exposure
Iron	1 mg/L	leaching from sediment and rocks and industrial from mining, industrial waste and corroding metal	Hemochromatosis i.e. effects liver, pancreas and heart
Lead	15 µg/L	mostly result of industrial, fossil fuel and mining	effects blood, delays development in children, affects blood pressure and has carcinogenic effect
Manganese	50 µg/L	leaching from mineral and mining and industrial waste	It affects neural health like loss of memory and affects motor skills
Mercury	2 µg/L	result of industrial waste, mining, pesticides, batteries, smelting, and fossil-fuel combustion.	Effects kidney and can cause nervous system disorders, causes Minamata disease
Nickel	100 µg/L	naturally from sediments and waste from electroplating, stainless steel and alloy, mining, and refining industries	Damages heart and liver
Nitrate	45 mg/L	Main source are fertilizers, sewage and animal farm waste	reduces oxygen carrying capacity of blood and causes anaemia (methemoglobinemia) also called blue baby syndrome
Selenium	10 µg/L	naturally occurring geologic sources, sulphur, and coal-burning	Causes acute and chronic toxic effects in cattle called blind staggers
Silver	1.1 mg/L	Enters environment from ore mining and processing, product fabrication, photography industry, electroplating, alloy, and solder	Cause argyria, a blue-grey colouration of the skin, mucous membranes, eyes, and organs in humans and animals with chronic exposure.
Sodium	200 mg/L	geologically from leaching of minerals and human activities like washing products	effects on heart patient
Sulphate	250 mg/L	Saltwater intrusion, mineral dissolution, and domestic or industrial waste.	laxative effect
Thallium	2 µg/L	from electronics, pharmaceuticals manufacturing, glass, and alloy industry	Damages kidneys, liver, brain, and intestines
Zinc	5 mg/L	Found naturally and metal plating and is a major component of sludge.	Nausea, Vomiting followed by bleeding and abdominal cramps

Fluoride is another contaminant that has geogenic origin. Singh and Mahipal (2018) ^[27] reported that groundwater in 19 states of India has fluoride above the permissible limit given by WHO ^[26]. A limited quantity of fluoride ions in the human body helps improve the strength of bones and adds an acid-resistant protective layer of fluorapatite ($\text{Ca}_5(\text{PO}_4)_3\text{F}$). But prolonged consumption of fluoride contaminated water leads to formation of calcium deca-fluoride (Ca_5F_{10}) which makes bone brittle ^[28, 29] and results in dental fluorosis followed by skeletal fluorosis ^[30]. Ayoob and Gupta (2006) reported 25 nations in the world have issues of high fluoride affecting 200 million people ^[31].

The main source of nitrate to groundwater is excessive use of fertilizers ^[32] and decaying organic waste (agriculture and domestic) ^[33]. The nitrates from fertilisers solubilizes with recharging water and enter the water cycle. The nitrate ion ($>45 \text{ mg/L}$) is known to cause methemoglobinemia i.e. nitrogen from nitrate irreversibly binds to the oxygen binding site of haemoglobin decreasing the oxygen-carrying capacity of blood hence leading to anaemia. This condition is also known as blue baby syndrome in the case of infants. Nitrate also leads to enlargement of thyroid, cancer, birth defects, and hypertension ^[34]. Ward et al. (2005) ^[35], reported increased cases of stomach cancer due to consumption of high nitrate water.

High nitrate is reported in shallow aquifers in 15 states of India namely Punjab, Haryana, Andhra Pradesh, Delhi, Bihar, Karnataka, Rajasthan, West Bengal, Uttar Pradesh, Tamil Nadu, Kerala, Maharashtra, Madhya Pradesh, Himachal Pradesh and Orissa. Shomar et al. (2008) ^[36] reported high nitrate concentration in Gaza strip with 90% of the samples having nitrate above the permissible limits. Janjevic (2017) ^[37] reported 196 out of 700 sampled wells had nitrate above the permissible limit in Germany. Beutel et al. (2017) ^[38] reported that the eastern alluvial sub-region in central valley California has higher nitrate concentrations.

Iron is yet another contaminant, which when consumed in excess causes hemochromatosis i.e. it gets stored in spleen, liver etc and impacts their functioning. High iron concentrations are reported in groundwater of Assam, Orissa, West Bengal, Chhattisgarh and Karnataka with pockets in northern, north-eastern India ^[39].

Salinity is caused due to high salt content in groundwater. High salinity both inland and coastal is also reported by CGWB in India. Inland salinity is mostly affecting the arid and semi-arid regions of India. Inland salinity is mainly caused due to ill-managed irrigational practices. Chowdary et al. (2008) ^[40] reported that about 2.5-million-hectare area under water irrigation projects in the world are waterlogged and face issues related to salinization. The other reason for salinity is due to seawater intrusion. Most of the coastal aquifers of India are affected due to coastal salinity with Tamil Nadu and Saurashtra coast amongst the most affected regions. Werner et al. (2013) ^[41] reported that the hydraulic gradient at the coastal site can be reversed due to excessive pumping of groundwater leading to seawater intrusion. The coastal aquifers of the world namely Queensland Australia, Florida USA, the coastline of Spain and Lebanon are most affected.

1.3 Uranium Contamination

Uranium is ubiquitous in biosphere, lithosphere, hydrosphere and atmosphere. Uranium is last naturally occurring radionuclide with atomic number 92 and mass number of 238.03 amu. The various isotopes of uranium with their half-life and abundances are given in Table 1.3. Siegel & Bryan (2004) ^[42] estimated average concentration of uranium in the Earth's crust to be about 2.7 mg/L.

Table 1.3 Isotopes of uranium with their half-life and abundances

Isotope	Half-Life	Abundance	Specific Activity
^{238}U	4.5×10^9 years	99.28%	12.3 Bq/mg
^{235}U	7.04×10^8 years	0.72%	0.57 Bq/mg
^{234}U	2.5×10^5 years	0.005%	12.3 Bq/mg
^{233}U	1.6×10^5 years	Trace	-
^{236}U	2.3×10^7 years	Trace	-

Uranium is present as oxide (Uraninite, Pitchblende), Carbonates (Rutherfordine), silicate (Coffinite) and phosphate (Autunite, Torbernite) ores. The concentrations of uranium in various rocks are given in Table 1.4. Recife, Brazil has the highest reported uranium concentration of 30-500 mg/kg. The concentration of uranium varies in water i.e. seawater (3.3 $\mu\text{g/L}$), surface water (0.02 to 6 $\mu\text{g/L}$) and groundwater (world average of 2 $\mu\text{g/L}$)^[43].

Table 1.4 Uranium concentrations in various rocks^[44]

Rock Type	U ($\mu\text{g/g}$)
Igneous Rock	
Acid igneous	2.2-6.1
Basic igneous	1.1
Ultrabasic igneous	0.03
Granite	1-13
Basalts	0.6
Sedimentary Rock	
Unconsolidated sedimentary	1.7
Limestone	1.3
Dolomite	0.03-2
Sandstone	0.68-3.1
Black shale	1.7-6.6
Shale with oil	10-56
Phosphate rocks	77-143
Metamorphic Rock	
Gneiss	0.8-9.4

The contamination due to uranium can be from natural sources i.e. release from the high uranium source into groundwater due to rock-water interaction, geochemical changes etc. Apart from natural sources, human interferences also impact the release of uranium into the environment. Uranium is released into the environment at various stages of nuclear fuel cycle like milling, mining, fuel fabrication etc ^[45]. It is also added to environment during fuel reprocessing and waste disposal. The abandoned mining sites also pose risk to the environment. The depleted uranium is used in making bullets and shielding material. The mishandled disposal of these uranium products contaminates the environment. One of such example is the use of depleted uranium in Gulf war of 1991 which has left long terms effect on the health of the soldiers ^[46].

1.3.1 Health effects

Uranium is known to be both chemical as well as radiological toxic to human being and the chemical toxicity being more compared to later ^[47]. The chemical toxicity of uranium is due to its heavy metal nature. The heavy metal binds to proteins, enzymes of the body and replaces the useful mineral which impacts their normal functioning. WHO (2011) established the drinking water limit for uranium to be 30 µg/L taking into account both chemical and radiological toxicity, considering an average human being has an intake of 2 litres of water daily and exposure limit of 0.1mSv/yr ^[26]. The guidance value given by Atomic Energy Regulatory Board (AERB) is 60 µg/L which is calculated based on the radiological toxicity of uranium. The annual effective does of uranium is calculated using Equ. 1.2 ^[48]

$$D = C \times DWI \times 365 \times DCF \quad (1.2)$$

Where D is the annual effective dose

C= uranium concentration

DWI is daily water intake

DCF is dose conversion factor

The dose conversion factor as given by IAEA is 4.8×10^{-8} Sv/Bq ^[49]. Sharma et al 2020 ^[50], reported annual effective dose due to uranium in range of 20-208 μ Sv/year in Bathinda district of Punjab which is higher than the WHO limit (2003) ^[51] of 100 μ Sv/year.

Most of the occupational hazard is due to inhalation of uranium dust while for general public ingestion is the main mode for exposure. Bioaccumulation of contaminant along the food chain is well known, concentration factor for uranium depends on species, stage of life, exposure pathway, environment and physiology ^[52]. In plants, the accumulation is dominant in roots compared to other parts ^[53]. Muller et al. (1997) ^[54] established that cauliflowers, cucumber, mushrooms, and carrots have higher concentrations of uranium compared to other vegetables. Bergmann and Graça (2019) ^[55], states that bioaccumulation in aquatic animals is low.

As per the report by ASTDR (2013) ^[56], the daily intake of uranium through food is about 0.9 to 1.5 μ g/day out of which 70% of the annual average uptake is from potatoes, meat, fishes and bakery products ^[57,58]. ASTDR 1999 ^[45] established the annual uptake of U from water to be 1.5 μ g. Apart from food and water, uranium can also enter the human body through wind. Wind erosion can mobilise uranium particulates from soil/rock sources and makes them airborne with concentration varying from place to place and the global average value of about 1 μ Bq/m³ for ²³⁸U ^[59]. WHO (2012) ^[60] estimated annual intake of uranium through inhalation to be 4.5mBq of ²³⁸U.

Fisenne et al. (1988) ^[58] established through his study that skeleton holds up to 57% of uranium followed by muscles (20%), fats (16%), blood (3.5%) and remaining 3.5% is spread in liver, lungs and kidney. Thorne and Wilson (2015) ^[61] updated the maximum intake limit for uranium to be 2 µg/Kg/day from the earlier value of 0.5 µg/Kg/day ^[62].

The uranium is known to affect the kidney, bone degeneration, lungs etc. The retention and absorption of uranium in human body depend on the chemical compound it is present in and the organ. The kidney is the most affected part due to uranium exposure. Wrenn et al (1985) ^[63] established that out of the ingested uranium 66% is secreted out through the kidneys. Uranium causes necrosis of the proximal tubular glomeruli and its epithelium ^[64]. Uranium is retained in the kidney for longer in acidic condition of urine. As in acidic condition, the complexes dissociate and the free uranium formed binds to the epithelial tissue of the kidney. This affects the sodium reabsorption, increased excretion of protein, glucose and other essential ions from the body ^[65]. Inside the cell, uranium binds with phosphate present in lysosomes making them ineffective for functioning and also effects the functioning of mitochondria.

Bone is the other part known to be affected due to exposure to uranium. A study by Ubios et al. (1991) ^[66] has shown that bone growth and formation is affected due to the acute dose of uranium. Milgram et al. (2008) ^[67] showed that uranium dose on bone also effects osteoblast, increases reactive species, decreases alkaline phosphatase and causes genomic instability. In the exposed human population, biomarker of bone formation like osteocalcin, procollagen (amino-terminal pro-peptide-Type I), Carboxy-terminal telopeptide etc are formed and results showed a positive correlation between uranium exposure and these markers ^[68].

Uranium distribution and its removal from the lungs depend on the solubility of the compound. Uranium exposure causes congestion, haemorrhage, bronchopneumonia, fibrosis,

genotoxic lesions and tumour ^[69]. Gueguen et al. (2014) ^[70] studied the impact of uranium exposure on liver and they found that uranium causes hepatotoxicity, interferes with cholesterol metabolism and modifies xenobiotic detoxification enzymes like cytochrome P450 (CYP3A). When the brain is exposed to uranium, its effects locomotors activities, perturbs sleep and wake timing, decreases memory and increases anxiety. Uranium perturbs neurotransmitter level in hippocampus, cerebellum and frontal cortex thus affecting the brain activity. The exposure also increases the oxidative stress by producing free radical and other reactive species ^[71]. Uranium exposure is chemically genotoxic and mutagenic as it inhibits DNA binding protein and causes breaks and lesions due to the generated oxidative stress ^[72].

1.3.2 Uranium Mobilization

Release/mobilization of uranium in groundwater is the combined effect of multiple physico-chemical processes and numerous controlling factors like geology, aquifer characteristics and lithology. The physicochemical parameters include oxidation state of uranium, pH condition of the aquifer, type of ligands (NO_3^- , CO_3^{2-} , HCO_3^- , humic acid, fulvic acid etc), aquifer condition (oxidative or reductive) etc. Uranium has oxidation states in the range of +3 to +6 but mostly exists either in +4 or +6 state ^[45]. Uranium in its +4 state is sparingly soluble/insoluble, mostly found in rocks, sediments etc while in the higher oxidation state of +6, it is soluble and found in groundwater, surface water etc as uranyl complexes. Much of the aqueous geochemistry of uranium work has been done by Fox et al. (2007) ^[73], Burns and Finch (2018) ^[74] etc.

In acidic conditions ($\text{pH} < 4$), the solubility of uranyl ion is more while at high pH, the uranyl ions have high absorption on the iron-oxide present in the aquifer matrix but due to presence of carbonate ions, uranyl ions form stable and soluble carbonate complexes. Edwards

et al. (1995) ^[75] observed that the mobility of uranium is restricted due to the presence of clay and organic matter.

The bicarbonate and nitrate ions act as hydrochemical drivers for release of uranium from aquifer matrix to water. The nitrate ion is known to act as an oxidizing agent that helps convert U(IV) to U(VI) ^[76]. The reactive product like nitrite, nitrogen oxide and nitrous oxide formed can additionally oxidize U(IV) to U(VI) and enhance mobilization of uranium ^[77]. Under anaerobic conditions micro-organisms like *Geobacter metallireducens* and *Thiobacillus denitrificans* coupled with nitrate has known to oxidize U(IV) ^[78]. Nitrate driven Fe(II) oxidation reaction produces reactive Fe(III) that oxidizes U(IV) to U(VI) ^[79]. Research work by Lopez et al (2020) ^[80] suggests that nitrate play a major role in uranium mobilisation. When oxygen from the system is consumed, the nitrate comes into play and act as the next electron acceptor, which is followed by manganese, iron and sulphate present depending on their availability in a given system. The study carried out by Riedel and Kübeck (2018) ^[81] in south west-Germany also concluded that there are many factors that influence the uranium mobilization in the groundwater considering its complex geochemistry. They observed weathering and desorption of uranium from mineral surface are the main processes controlling U mobilization, which is supported by presence of calcium, nitrate, iron and sulphate reducing moieties.

The oxidized uranium is stabilized in groundwater pH condition with the help of bicarbonate ions with the formation of stable complexes like $\text{UO}_2(\text{CO}_3)$, $\text{UO}_2(\text{CO}_3)_2^{2-}$, $\text{UO}_2(\text{CO}_3)_3^{4-}$ and $\text{UO}_2(\text{CO}_3)_4^{6-}$. The other ion that helps mobilize uranium is calcium ion. The similarity in the size of UO_2^{2+} (~100pm) and Ca^{2+} (~100pm) ions favors their ion-exchange i.e. removal of the Ca^{2+} ions from water in exchange of UO_2^{2+} from aquifer matrix. The mobilized ions are then stabilized by complexing with ligands like bicarbonate, phosphates etc. Aquifer

characteristics like aquifer matrix (i.e. the concentration of uranium mineral, type of mineral etc), pore size, residence time of water are also important factors that help understand the concentration of uranium in the aquifer.

1.3.3 Uranium contamination in groundwater

1.3.3.1 World scenario

There are many studies carried out by different researchers in the world on uranium concentrations in groundwater around the world. The dissolved uranium concentrations are summarized in Table 1.5.

Table 1.5 Concentration of uranium in groundwater around the World

S. No.	Country	Uranium in water ($\mu\text{g/L}$)	Reference
1	Finland	0.01-3410	Turtiainen et al 2011 ^[82] ; Prat et al. 2009 ^[83]
2	Sweden	0.2-470	Salih et al. 2002 ^[84]
3	Norway	0.02- 170	Banks et al. (1995) ^[85]
4	Los Ratones Mine, Spain	<1 - 104	Go'mez et al, 2006) ^[86]
5	France	0.18-37.2	UNSCEAR 2000 ^[53]
6	Switzerland	0.05-92	Stalder et al. 2012 ^[87]
7	Canada	0.02-2020	Larivière et al. 2013 ^[88] ; Betcher et al. 1988 ^[89]
8	Connecticut, USA	0.2-7780	Magdo et al 2007 ^[90]
9	High Plain Aquifer, USA	0.5-2674	Nolan and Weber 2015 ^[76]
10	Central Valley Aquifer, USA	0.5-5400	Nolan and Weber 2015 ^[76]
11	Jordan	0.04–1400	Smith et al. (2000) ^[22]
12	United States	0.01-652	Cothorn and Lappenbusch (1983) ^[91]
13	Egypt, Central Eastern Desert	67-547	Dawood et al. (2004) ^[92]
14	Faisalabad, Pakistan	1.34- 24	Akram et al. (2003) ^[93]
15	Bangladesh	3.7 - 47.5	Khatun et al. (2012) ^[94]

1.3.3.1 Indian scenario

There is much work done in India regarding the groundwater concentration of uranium. The concentrations of uranium in groundwater in India are summarized in Table 1.6. The concentrations with the help of bubble plot in various aquifer formations of India are shown in Fig. 1.3

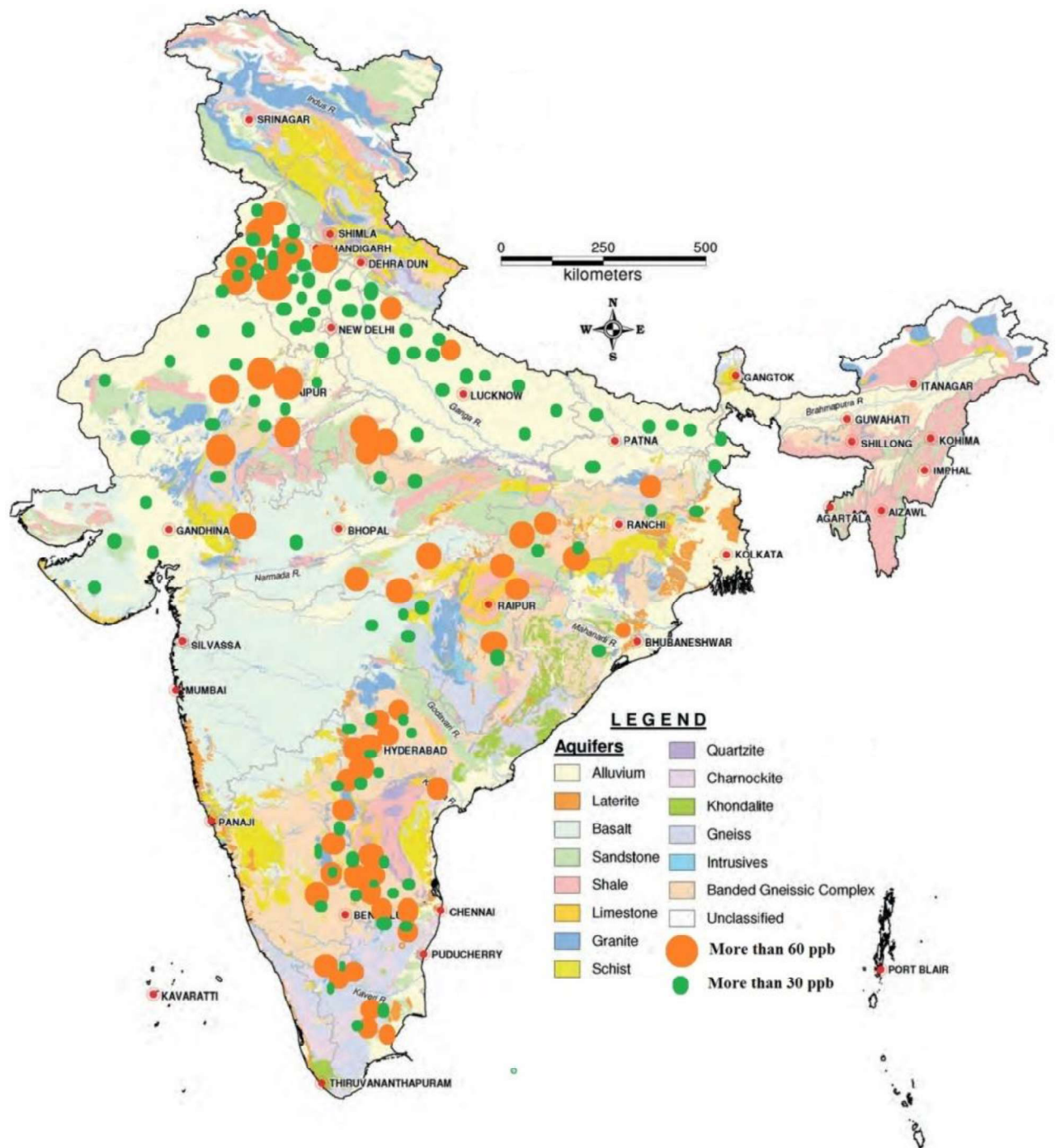


Fig. 1.3 Different aquifer of India showing uranium concentration above the WHO limit (30 $\mu\text{g/L}$)^[60] and AERB limits (60 $\mu\text{g/L}$)^[95] (modified from CGWB 2020^[96])

Table 1.6 Concentration of uranium in groundwater in India

S.No.	Place	District	Range	$^{234}\text{U}/^{238}\text{U}$	Reference
1	Punjab	Amritsar	18 -20		Singh et al. 1994 ^[97]
2		Bathinda	12-114		
3		Amritsar	3.2-46		Singh et al. 2003 ^[98]
4		Southwest (Bathinda, Mansa)	0.6-472		Kumar et al. 2011 ^[99]
5		Bathinda	<2-212		Bhalla et al. 2011 ^[100]
6		Hoshiarpur	5-11		
7		Nawanshahr	3-14		
8		BudhaNulla	2-22		
9		Bathinda	<2-212		Alrakabi et al. 2012 ^[101]
10		Malwa Region	14-173	0.94-1.85	Tripathi et al. 2012 ^[102]
11		Bathinda	0.5-572		Singh et al. 2013 ^[103]
12		Hoshiarpur	1-20		Krishan et al. 2014 ^[104]
13		Jalandhar	4-67		
14		Kapurthala	2-22		
15		Shaheed Bhagat Singh	3-37		
16		Bathinda	8-324		Saini et al. 2016 ^[48]
17		Mansa	6-645		
18		Faridkot	8-376		
19		Mansa	0.13-1340		Sharma and Singh 2016 ^[105]
20		Mohali	0.6-24		Virk et al. 2016 ^[106]
21		Fatehgarh	2.8-58		
22		Bathinda	9.7-186		Virk 2016 ^[107]
23		Bathinda	8 -374		Saini and Bajwa 2016 ^[108]
24		Mansa	6-645		
25		Faridkot	8-376		
26		Tarn Taran	3-316		
27		Hoshiarpur	0.5-25		
28		Amritsar	1-43		Bajwa et al. 2017 ^[109]
29		Bathinda	0.5-572		
30		Mansa	1.3-579		
31		Faridkot	2.4-476		
32		Ferozpur	2.8-468		Rishi et al. 2017 ^[110]
33		Bathinda	22-352		
34		Mansa	29-261		
35		Muktsar	30-284		
36		Faridkot	12-172		

37		Bathinda	2.4-529		Sharma et al. 2017 ^[111]
38		Southwest (Bathinda, Mansa)	0.13-676		Saini et al. 2017 ^[112]
39		Northeast (Hoshiarpur)	0.11-28		
40		Southwest (Bathinda, Mansa)	2.3-357		Sharma et al. 2017 ^[113]
41		Fazilika	122-366		Virk 2017 ^[114]
42		Bathinda	31-261		Singh et al. 2018 ^[115]
43		Muktsar	1.8-237		
44		Jalandhar	1.5-50		Kumar et al. 2019 ^[116]
45	Jammu and Kashmir	Jammu	0.2-21		Kumar et al. 2016 ^[117]
46		Kathua	0.3-22		Singh et al. 2016 ^[118]
47		Hamirpur	1.7-28		
48		Kangra	0.6-19		
49		Kathua	0.3-22		Sharma et al. 2017 ^[119]
50	Rajasthan	Bikaner	2.5-77		Mittal et al. 2017 ^[120]
51		Jhunjhunu	0.9-140		
52		Jodhpur	2.4-90		
53		Nagaur	15-167		
54		Hanumangarh	4-87		Duggal et al. 2017 ^[121]
55		Sikar	3-136		
56		Sri Ganganagar	2.5-171		
57		Churu	13-95		
58			BDL-320	1.53-3.97	Coyte et al. 2018 ^[122]
59	Gujarat		BDL-86	0.98-3.82	
60	Haryana	Bhiwani	19-43		Kansal et al. 2011 ^[123]
61		Fatehabad	10-18		
62		Hisar	9-17		
63		Sirsa	6-25		
64		Fatehabad	0.3-110		Singh et al. 2014 ^[124]
65		Hisar	9-17		
66		Fatehabad	1-113		Duggal et al. 2017 ^[125]
67	Andhra Pradesh	Guntur	0.5-410		Singh et al. 2002 ^[126]
68		Guntur	5.5-2075		Gupta et al. 2015 ^[127]
69	Telangana	Nalgonda	0.2-118		Brindha et al. 2013 ^[128]
70		Nalgonda	3-370		Keesari et al. 2014 ^[129]
71		Nalgonda	0.6-521		Raghavendra et al. 2014 ^[130]
72	Karnataka	Kolar	0.3-1443		Babu et al. 2008 ^[131]
73		Bangalore	0.1-2027		Mathews et al. 2015 ^[132]
74	Tamil Nadu	Madurai	0.4-68		Adithya et al. 2016 ^[133]
75		Madurai	BDL-113		Thivya et al. 2016 ^[134]

Singh et al. (1994)^[97] estimated the dissolved uranium concentration and reported higher concentrations in Bathinda compared to Amritsar. A study by Tripathi et al. (2012)^[102] in Malwa region of Punjab concluded that uranium concentrations were in the range of 14-173 µg/L and the elevated concentration are attributed to increased pCO₂ due to agricultural activity that leads to increased bicarbonate ions which mobilize uranium. The estimated activity ratio of ²³⁴U/²³⁸U in the study area was 0.94 to 1.85 with an average of 1.1. The slight disequilibrium was attributed to selective leaching of ²³⁴U. Patnaik et al. (2015) studied the fossil, palaeosol, rock and soil samples collected from Jammu Kashmir to Himachal Pradesh. They reported the uranium activity associated with Palaeosol samples in the range of 46-214 Bq/kg, while for fossil samples to be 208-4837 Bq/kg^[135]. They proposed that high uranium concentration in Malwa region are due to i) uranium-rich water percolating from Himalayan foothills that are feeding groundwater or ii) uranium-rich paleochannels of an ancient river buried below the water table keeps feeding uranium to groundwater.

Rishi et al. (2017)^[110] studied the distribution of uranium in groundwater of south-west Punjab. The spatial trend showed that uranium is more in east, west and north while the central part of the study area had a lower concentration of dissolved uranium. They attributed the high uranium to increased bicarbonate ions. Bajwa et al. (2017)^[109] worked in Bathinda, Mansa, Faridkot and Ferozpur district of Punjab. They analyzed 498 groundwater samples and found the dissolved uranium was above the permissible limit of WHO in 68% of samples. They attributed the increased concentration to leaching from the granitic base rocks and the anthropogenic activities in the area. Krishan and Chopra (2015)^[136], assessed water logging issue in Muktsar district of Punjab. They estimated the maximum rise of 18.1 m in Middu Khera

followed by 15.3 m in Brind Khera and 12.7 m in Lambi block of the district. Saini and Bajwa (2016) ^[108] estimated uranium concentration in groundwater from Mansa, Bathinda and Faridkot districts of Punjab and concluded that industries like cement, fertilizer and thermal power plant might be the possible sources for increased uranium concentration. They also attributed the increased concentration to leaching of uranium from the granitic basement ^[48]. Saini et al. (2016) ^[112] worked in the Malwa region of Punjab related to fluoride and nitrate contamination. They observed higher contamination in shallower depth and attributed contamination of fluoride and nitrate to geology and excessive fertilizer usage, poor sanitization and ill-managed irrigation.

Saini et al. (2016) ^[48] worked in Punjab covering Bathinda, Mansa, Faridkot, Tarn Taran, Hoshiarpur and Amritsar, and assessed uranium concentration and the associated risk of cancer and found that 41% of sampled location are at higher risk of cancer from south-west region of Punjab while only 10% of sampled locations were at risk from west Punjab and no risk was found for the locations from northeast Punjab. Sharma et al. (2017) ^[137] worked on the suitability of groundwater for irrigation purposes from Faridkot and Muktsar district of Punjab. They concluded that water quality is not fit for its use for irrigation. Sharma et al. (2017) ^[111] studied the distribution of uranium in groundwater of Bathinda and Mansa district of Punjab and reported a decrease in uranium concentration along the depth. They attributed the uranium concentration to leaching due to oxidative condition and bicarbonate ions.

Duggal et al. (2017) ^[121] studied the uranium concentration in groundwater of Shri Ganganagar, Hanumangarh, Churu and Sikar district of Rajasthan and found the uranium concentration in the range of 2.5–171 µg/L. They concluded that the source of high uranium was geogenic with anthropogenic activities, urbanization and excess use of phosphate fertilizer as the source. Coyte et al. (2018) ^[122] reported uranium in groundwater of Rajasthan and Gujarat. They concluded

that bicarbonate ions help in oxidation and complexing uranium. The declining water trends make the aquifer condition oxic which help in further enrichment. The uranium activity ratio ($^{234}\text{U}/^{238}\text{U}$) showed disequilibrium, which was attributed to selective leaching of ^{234}U . Coyte et al. (2019) ^[138] studied Barmer and Jodhpur district of Rajasthan for various contaminants like fluoride, nitrate and uranium. They concluded that uranium and fluoride are released due to weathering from rock and their concentration increases due to evapotranspiration, irrigation return flow and ion-exchange. Both these factors combined have led to increased concentration of uranium in groundwater of Rajasthan.

Rahman et al (2020) ^[139] studied the quality of groundwater in Sanganer block of Jaipur. They concluded the groundwater quality is not fit for both drinking and irrigational purposes. Ion-exchange and silicate weathering are the major ions contributors. Mondal et al. (2016) ^[140] studied the water quality of Dausa district of Rajasthan and attributed pollution of groundwater to the mixing of anthropogenic contaminant and the occurrence of rock weathering in the region. The quality of water was also found to be unfit for its use for the purpose of irrigation and drinking. Aggarwal (2016) ^[141] worked on nitrate contamination in Rajasthan and estimated the concentration in the range of 10-415 mg/L and attributed the higher concentration to excessive use of NPK fertilizer.

The groundwater of Jaipur and Dausa districts has issues of salinity and high concentrations of NO_3^- ions, Cl^- ions, F^- ions and iron. As per the CGWB reports ^[142,143], issues of high salinity in groundwater ($\text{EC} > 2000 \mu\text{S}/\text{cm}$) is observed in Bassi, Chaksu, Dudu, Phagi and Sambhar block of Jaipur and Dausa and Mahwa blocks of Dausa district. All the blocks of Jaipur and Dausa districts have the issue of NO_3^- ions ($> 45 \text{ mg}/\text{L}$) and F^- ions ($> 1.5 \text{ mg}/\text{L}$) above the permissible limit for drinking laid by BIS (2012) ^[144]. The blocks showing NO_3^-

>100mg/L are Dudu, Phagi, Govindgarh and Jamwa Ramgarh under Jaipur district and Dausa and Mahwa blocks of Dausa district. $F^{-} > 3\text{mg/L}$ were observed Dudu, Phagi and Sambhar blocks of the Jaipur district. High F^{-} ion contamination was reported in Dausa, Mahwa and Sikrai blocks of Dausa district. The high concentration of $Fe^{3+} > 1\text{ mg/L}$ is observed in Dudu, Phagi, Sanganer, Chaksu, Bassi, Amer and Jamwa Ramgarh blocks of Jaipur district and Bandikui and Lalsot blocks of Dausa district.

1.4 Limitations and motivation for the study

India consists of different type of formations like alluvial, sandstone, Laterite, Basalt, Shale, Limestone, Charnockite, Khondalite, Gneiss, Quartzite, Schist, BGC, Granite and Intrusives. The study by CGWB (2020) ^[96] shows the concentration of uranium in the shallower aquifer of different formations (Fig. 1.3). The dissolved uranium concentrations in the shallow aquifers of different states with dominant formations are given in Table 1.7. Since the distribution of uranium is not associated with any particular region or formation, it is important to conceptualize uranium mobilization into groundwater considering the local geological and hydrological conditions. The studies done in India estimates the dissolved uranium concentrations and mostly deal with the quality of water in terms of its suitability but there is no holistic approach for understanding the reasons for uranium mobilization. The sources and processes responsible for higher concentration of uranium in groundwater are also not well established. The relative impact of source and release mechanism i.e. the high concentration is due to the source (aquifer matrix or anthropogenic sources) or due to the geochemical conditions is not well perceived. Hydrochemical drivers such as nitrate, bicarbonate and oxygen favor uranium mobilization while other geochemical processes like ion exchange, leaching, sorption, desorption etc alter the uranium distribution in groundwater. There is no clarity on how these

factors behave in different formations. There is no mechanistic understanding of uranium release/mobilization in Indian groundwaters. A thorough understanding of aquifer geochemistry, geochemical processes, source and mechanism of groundwater recharge and its dynamics, source of uranium and uranium isotopic ratios are needed to achieve a better understanding of uranium mobilization in groundwater. Establishing a holistic picture of the uranium release mechanism throughout India is need of the hour considering the number of locations uranium contamination is found in groundwater. Thus, the study was taken up employing basic aspects of geology, hydrogeology and hydrochemistry of the aquifers of two different states with varied geological features as well as advanced tools such as environmental isotopes, residence time tracer and uranium isotopes to study the uranium mobilization process in selected Indian waters.

Table 1.7 Principle aquifer system with dissolved uranium concentrations and percent samples exceeding the WHO permissible limits

(compiled from CGWB report 2020 ^[96])

State	Principle Aquifer	No. of samples	% exceeding WHO limits (30 µg/L)	Range
Andhra Pradesh	BGC, Shale, Sandstone, Alluvium, Granite and Schist	588	5	0.3-2875
Assam	Alluvium and BGC with sandstone and Shale at few locations	454	0	0-10.7
Bihar	Alluvium with BGC and Sandstone	634	2	0-57
Chhattisgarh	BGC, Sandstone, Gneiss, Shale and limestone dominant	917	1.3	0-138
Delhi	Alluvium with few locations in Quartzite	60	12	0-89
Gujarat	Basalt, Alluvium in dominance	543	0.92	0-57
Haryana	Alluvium with few places under Sandstone and Quartzite	451	20	0-131
Himachal Pradesh	Schist, Sandstone, Limestone and Quartzite	122	0.82	0-71
Jammu and Kashmir	Sandstone, Granite, Shale and Alluvium	314	0	0-24
Jharkhand	BGC, Schist and Alluvium	399	1.5	0-70
Karnataka	BGC, Basalt, Schist and Charnockite	737	1.9	0-201
Kerala	Charnockite, Gneiss, Khondalite and Alluvium	423	0	0-1.5
Madhya Pradesh	Basalt, Sandstone, BGC, Alluvium and Shale	1191	1.3	0-234
Maharashtra	Basalt, Gneiss and alluvium	1085	0.3	0-48
Odisha	BGC, Alluvium, Khondolite and Charnockite	1114	0.4	0-59
Punjab	Alluvium and Sandstone	302	24	0-160
Rajasthan	alluvium, Sandstone, BGC, Gneiss and Shale	671	7.2	0-181
Tamil Nadu	Gneiss, Charnockite, Alluvium, Sandstone and BGC	1208	1.6	0-302
Telangana	BGC, Shale, Sandstone, Alluvium, Granite, Schist	345	10	0-158
Uttarakhand	Schist, Alluvium, Quartzite, Gneiss and BGC	186	0	0-24
Uttar Pradesh	Alluvium and BGC	826	2.7	0-189
West Bengal	Alluvium, Laterite and BGC	935	0.11	0-34

Two different geographic locations i.e. Punjab (Muktsar and Faridkot districts) and Rajasthan (Jaipur and Dausa districts) were chosen for the thesis work (Table 1.8). All the districts under study are agriculture dominant with extensive irrigation by groundwater, high evapotranspiration, irrigation return flow and use of fertilizer.

Table 1.8 Characteristics of the study area (compiled from CGWB reports ^[145-148])

Parameters	Faridkot	Muktsar	Jaipur	Dausa
Population (Census 2011)	618008	902702	6626178	1634409
Climate	Semi-Arid	Semi-Arid	Semi-Arid	Semi-Arid
Rainfall	449mm	431mm	591mm	659mm
Temperature	5°C-41°C	5°C -41°C	5°C -48°C	5°C -48°C
Cropping Intensity	200%	200%	140%	155%
Water scenario	Was waterlogged now showing declining water trends	waterlogged	declining	declining
Contamination	Nitrate, Iron, Fluoride, Salinity	Nitrate, Fluoride, Salinity	Nitrate, Iron, Fluoride, Salinity	Nitrate, Iron, Fluoride, Salinity
Formation	Alluvial	Alluvial	Alluvial + Hard Rock	Alluvial +Hard rock

1.5 Objectives

The broad objectives of the study are

- i) To understand uranium contamination in the different geological formation
- ii) Assessment of groundwater quality and its suitability to potable and irrigation purposes
- iii) Identification and understanding the geochemical processes leading to the chemical characteristic of groundwater
- iv) To find the source and origin of groundwater
- v) To delineate the uranium-rich and poor zones
- vi) To study uranium mobilization process and its plausible reason or favoring factor
- vii) Propose a mechanism for uranium release.

1.6 Thesis outline

To achieve the above objectives Muktsar and Faridkot districts of Punjab and Dausa and Jaipur districts of Rajasthan were chosen. The work done is described in the following chapters

Chapter 2 outlines the importance of chemistry, environmental isotopes, geochemical and statistical modelling in understanding groundwater characteristics for sustainable management of these resources. Water samples were mainly collected from major water-bearing formations of the study area namely, alluvium in Muktsar and Faridkot region of south-west Punjab; alluvial and hard rock formation in Jaipur and Dausa districts of Rajasthan. The water sampling from the hand pump, tube wells, and canals in the study area of Punjab was done during October 2016 (70 samples, postmonsoon) and May 2017 (37 samples, premonsoon). The samplings from Rajasthan study area was carried out during March 2017 (72 samples, premonsoon) and November 2017 (33 samples, postmonsoon). The physicochemical parameters were measured in-situ in the field and the samples for major ion chemistry (60ml), stable isotopes (30ml), tritium (500ml), total dissolved uranium (20ml) and uranium isotopes (1L) were brought to the laboratory for the measurements. The measurement procedure and instrumental details are included in this chapter.

Chapter 3 includes a brief description of the geological and hydrogeological of the study area in Punjab, viz., Faridkot and Muktsar districts followed by general water chemistry. It also includes the groundwater scenario of the region in terms of quality and quantity. The results are provided in this chapter with detailed interpretation using various graphical representations. The geochemical processes involved in the study area were established using ionic ratio plots. The uranium in the study area ranges from 1-610 $\mu\text{g/L}$ in shallow zone and 21-260 $\mu\text{g/L}$ in the deep zones with 79% and 90% samples above the permissible limits respectively in premonsoon season. For postmonsoon season, uranium

concentration ranges from 10-565 µg/L in shallow and 16-135 µg/L deep zones with 71% and 62% samples above the permissible limits respectively. The uranium contour helped in demarcating contaminations zones with higher concentrations in south- west and northern region of the study area. The stable isotope indicates three signatures in the shallower zones namely i) depleted $\delta^{18}\text{O}$ values due to canal water interaction, ii) values between -8‰ to -5‰ indicating precipitation recharge and iii) evaporative signature (-4‰ to -2‰) indicating irrigation return flow. The deeper zone samples fall near to GMWL indicating precipitation recharge and their tritium values indicate long residence times and possible contribution from regional groundwater flows. Uranium shows a positive correlation with EC, bicarbonate and nitrate. The uranium activity ratio ($^{234}\text{U}/^{238}\text{U}$) is in range of 0.85-1.05 for shallow zone and 0.89-0.96 for deep zones. Uranium isotopes data was correlated with uranium concentration and it was interpreted that uranium concentration is due to leaching in the shallower zones while in the deeper zone it is mainly due to the mixing process. The mobilization of uranium from mineral is a combined effect of nitrate as oxidizer and bicarbonate as a mobilizing agent.

Chapter 4 includes the brief description of geological and hydrogeological of the study area in Rajasthan, viz., Dausa and Jaipur districts followed by general water chemistry. The geochemical processes involved were assessed using ionic ratio plots. The stable isotopes indicate towards two main recharge sources i.e. precipitation and irrigation return flow. The uranium concentration ranges from 0.4-177 µg/L in alluvial formation and 0.5-142 µg/L in hard rock formation with 33% and 53% samples above the permissible limit in premonsoon season respectively. For postmonsoon season, uranium concentration ranges from 5.3-142 µg/L for alluvial formation and 5.2-145 µg/L for hard rock formation with 61% and 58% samples above the permissible limits respectively.

Uranium shows a positive correlation with EC, bicarbonate and nitrate, which is more in postmonsoon season. Uranium isotope data was correlated with uranium concentration and it was interpreted that uranium concentration is mainly due to leaching. High uranium activity ratio ($^{234}\text{U}/^{238}\text{U}$) i.e. 1.44-2.85 for alluvial formation and 1.38-2.97 for hard rock formation is observed in the samples from the study area, which reflect the prevalence of alpha recoil phenomenon towards uranium release into groundwater. Once the uranium releases into groundwater, it gets oxidized and then complexes to form stable compound and migrates too far off distances.

Chapter 5 consists of a detailed evaluation of similarities and dissimilarities in aquifer systems of both the study areas (Rajasthan and Punjab). The role of hydrochemical drivers like nitrates, pCO_2 , bicarbonates towards uranium leaching, complexation and migration is studied considering the varied geological and hydrogeological differences in these study regions. The seasonal and temporal variations in contaminant concentrations are also studied for both the study area in light of varying groundwater dynamics. Based on the hydrochemical, isotope and modelling inferences, conceptual models are prepared for the uranium mobilization processes in both the aquifer systems and presented in this chapter. Finally, summary and conclusions along with future scopes are provided at the end of these chapters.

CHAPTER 2 Methodology

To fulfill the objectives a work plan was emulated which included i) sampling ii) measurement and iii) data interpretation. The physicochemical parameters were measured in the field and samples were collected for chemical analysis, isotopic analysis ($\delta^{18}\text{O}$, $\delta^2\text{H}$ and ^3H), uranium and its isotopes (^{234}U and ^{238}U) from both the study areas. The sampling procedure and analytical technique used are explained in this chapter.

2.1 In situ analysis

The location parameters like latitude, longitude, elevation etc were measured using in-build global positioning system and physicochemical parameters like electrical conductivity (EC), pH, total dissolved solids (TDS), temperature, dissolved oxygen (DO) etc were measured in situ in the field using HI 9829-11042 multiparameter meter with GPS, PH / ORP / EC / DO / Turbidity and 4m probe (Fig. 2.1). The pH sensor of the system is made of durable polyetherimide (PEI) body. It has two compartments, one containing Ag/AgCl reference electrode and glass pH sensing tip in gel electrolyte and the external compartment containing reference wire. This double jacket system ensures that no silver is leaked from the electrode to the sample or precipitated at the junction. The range of measurement is 0 to 14 with the resolution of $\pm 0.01/\pm 0.1\text{mV}$ and accuracy of $\pm 0.02/\pm 0.5\text{mV}$.

The conductivity probe is made up of ABS (Acrylonitrile Butadiene Styrene) sensor body containing 4 ring electrodes made up of AISI 316 stainless steel that prevents polarization or surface coating effects. It works on the polarographic measurement principal. The range of measurement is 0 to 200 mS/cm with a resolution of 1 $\mu\text{S}/\text{cm}$ for lower values and 0.1 mS/cm for higher conductivity values and accuracy is $\pm 1\%$ of reading. The dissolved oxygen sensor consists of a silver cathode and zinc anode with an HDPE membrane

containing the zero DO solution. The range of measurement is 0 to 50 ppm (500%) with a resolution of 0.1% and an accuracy of $\pm 1.5\%$.



Fig. 2. 1 Field sampling along with in-situ field parameter measurement

Titration method was followed to measure alkalinity in the field. 10 ml of the groundwater sample was titrated using 0.02N H_2SO_4 with methyl orange as an indicator. Change of orange colour to pink colour determines the endpoint of the titration. As the pH of the groundwater samples is neutral to alkaline, the alkalinity values are used to calculate bicarbonate concentration by multiplying the measured titer value with the factor of 122.

2.2 Major ion chemistry

The main ions analyzed in the water samples are sodium (Na^+), potassium (K^+), calcium (Ca^{2+}), magnesium (Mg^{2+}), chloride (Cl^-), nitrate (NO_3^-), sulphate (SO_4^{2-}), bicarbonate (HCO_3^-) and fluoride (F^-). From the field, approximately 60 ml water sample was filtered through 0.45 μm filter paper and collected in tarson make bottles for both cations and anions. To avoid precipitation of major cations, the samples are preserved by adding ultrapure concentrated nitric acid ^[149]. Major ions can be measured with the help of UV-Spectrophotometer, atomic absorption spectrophotometer, flame photometry and inductively coupled plasma optical emission spectroscopy (ICP-OES). For the study, Dionex DX-500 ion chromatography (IC) system was used to measure ionic species (Fig. 2.2).



Fig. 2.2 Dionex ion chromatography system

Chromatography is an analytical technique used to separate a mixture of chemical components. The different component of the mixture can swap from one phase to another and the rate of migration depends on the affinity of each component towards the stationary phase, its charge and size. Ion chromatography works on the principle of reversible ion exchange between the stationary phase and mobile phase. Thus, the time required to pass through the stationary phase is characteristic to each component and is known as retention time that depends on species type and size.

2.2.1 Working principle

The eluent is pumped into the analytical column with the help of a pump under a typical pressure of 1100 psi for cations and 650 psi for anions. The measurement is carried out in gradient mode for anions using 3–15 mN NaOH while in the isocratic mode for cations using 21 mN H₂SO₄ as eluent. The sample is injected into the sample loading loop and with the eluent flow, 25 μ L of sample is taken into the system. The sample then passes through the guard column which protects the main column from getting contaminated and removes impurities.

For cations, the resin contains sulphonic or carboxylic acid groups and for anions quaternary ammonium salts. The analytical column for anion is AS-11+AG-11 and the cation is CS12A+CG12A. The mobile phase contains ions i.e. H^+ and OH^- that create high background conductivity, making it difficult to measure analyte ions. This is overcome by selectively removing the ions generated by the mobile phase after the analytical column and before the detector. This is accompanied by converting the mobile phase ions to a neutral form or removing them with the eluent suppressor, which consists of ion-exchange column or membranes. For cations, the eluent used is H_2SO_4 (conductivity due to H^+) which is suppressed by the suppressor eluent that supplies OH^- . The SO_4^{2-} is removed by the suppressor column or membrane. The same principle holds for anion analysis. The mobile phase is usually NaOH (conductivity due to OH^-) and the suppressor eluent supplies H^+ to neutralize OH^- ions.

The ion detection is done in conductivity mode after eluent suppression with an electrochemical detector (ED 40). The concentration of analyte ions is calculated from the area under the peak (Fig. 2.3). The instrument performance is checked by running blanks and calibrations standards after every 10 samples. Accuracy of the chemical analysis is checked using charge balance error (CBE) as shown by Equ. 2.1. The CBE was within the allowed limit of $\pm 5\%$ [150].

$$CBE (\%) = \frac{\text{meq(cations)} - \text{meq(anions)}}{\text{meq(cations)} + \text{meq(anions)}} \times 100 \quad (2.1)$$

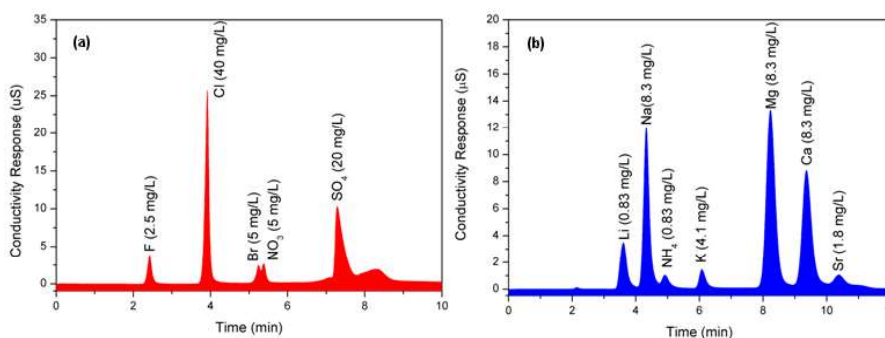


Fig. 2.3 A typical ion chromatograph for a) anions and b) cations

2.2.2 Applications

Hydrochemistry plays role in defining the quality of water and the impact of geogenic and anthropogenic activity. The characterization of water spatially and temporally provides insights into the changes occurring and factors influencing changes ^[145,146]. Numerous studies have been carried out in India on the role of hydrochemistry on water quality, its suitability for drinking and irrigation etc ^[151-157]. The major ion data is used to analyze i) suitability of water for drinking as well as irrigational purposes, ii) geochemical evolution and processes involved.

2.2.2.1 Suitability of water

The concentration of ions in water determines its suitability for drinking and irrigation.

A) Drinking:

Suitability of groundwater for the purposes of domestic activity mainly drinking is determined based on permissible limits given by the BIS (2012) ^[144] and the WHO (2011) ^[26]. The respective permissible values are given in the result part of chapter 3 and 4.

B) Irrigation

The suitability of water for irrigation is determined based on EC, TDS, sodium absorption ratio (SAR), percent sodium (%Na), permeability index (PI), residual sodium carbonate (RSC), magnesium hazard (MH), Kelley's ratio (KR) and corrosion ratio (CR). The desired values for these parameters are given in the result part of chapter 3 and chapter 4. The formula to calculate the parameters is given in Table 2.1

Table 2.1 Irrigation quality parameters calculation formulas

Parameter	Formula and values taken in	Reference
SAR	$SAR = \frac{Na^+}{\sqrt{\frac{Ca^{2+}+Mg^{2+}}{2}}}$, meq/L	Richard 1954 ^[158]
Percent sodium	$\%Na = \frac{(Na^++K^+)}{(Na^++K^++Ca^{2+}+Mg^{2+})} \times 100$, meq/L	Wilcox 1948 ^[159]
Residual sodium carbonate	$RSC = (HCO_3^- + CO_3^{2-}) - (Ca^{2+} + Mg^{2+})$, meq/L	Ragunath et al. 1987 ^[160]
Permeability Index	$PI = \frac{Na^+ + \sqrt{HCO_3^-}}{Ca^{2+}+Mg^{2+}+Na^+} \times 100$, meq/L	Doneen et al. 1964 ^[161]
Magnesium Hazard	$MH = \frac{Mg^{2+}}{Ca^{2+} + Mg^{2+}} \times 100$, meq/L	Szabolcs and Darab 1964 ^[162]
Kelly's ratio	$KR = \frac{Na^+}{Ca^{2+} + Mg^{2+}}$, meq/L	Kelley 1946 ^[163]
Corrosivity ratio	$CR = \frac{(Cl/35.5)+2(SO_4/96)}{2\{(CO_3 + HCO_3)/100\}}$, meq/L	Balasubramanian 1986 ^[164]

C) Composite water quality index

Composite parameters give a realistic view of water quality compared to impact by individual parameter. Weighted means of the parameters as per the suitability standards are used to calculate the drinking water quality index (DWQI) and irrigation water quality index (IWQI) ^[165]. The parameter considered for DWQI (WHO standards) ^[26] and IWQI ^[166] along with their weighting factors is calculated using Equ. 2.2 to 2.5 and are given in Table 2.3 and Table 2.4.

$$DWQI (IWQI) = \frac{\sum q_n W_n}{\sum W_n} \quad (2.2)$$

Where W_n is the unit weight of n^{th} parameters, calculated using Equ. 2.3

$$W_n = \frac{K}{S_n} \quad (2.3)$$

K = constant of proportionality and calculated using Equ. 2.4

$$K = \frac{1}{\sum \frac{1}{S_n}} \quad (2.4)$$

And q_n is the quality rating calculated as (Equ. 2.5)

$$q_n = 100 \times \frac{V_n - V_{i0}}{S_n - V_{i0}} \quad (2.5)$$

Where,

n = represents parameters

q_n = quality rating of the n^{th} parameter

V_n = value of the sample

S_n = standard value of the n^{th} parameter

V_{i0} = ideal value of the n^{th} parameter in pure water

Table 2.2 Parameters and standards for DWQI

Parameters	Standards (WHO 2011) ^[26]	W_n
pH	8.5	0.1416
EC	1500	0.0008
TDS	1000	0.0012
Ca²⁺	300	0.004
Mg²⁺	100	0.012
Cl⁻	250	0.0048
SO₄²⁻	250	0.0048
NO₃⁻	50	0.0241
F⁻	1.5	0.8023
total alkalinity	600	0.002

Table 2.3 Parameters with their weighting factor and standards for IWQI

Parameters	Standards ^[166]	W_n
MH	50	0.0396
RSC	2.5	0.793
Na%	60	0.033
SAR	18	0.1101
EC	2250	0.0009
PI	85	0.0233

2.2.2.2 Geochemical processes

The water while traversing interacts with the aquifer matrix through different process like ion-exchange, sorption/desorption, dissolution and precipitation. There are different

indices and plots to identify the geochemical processes. One such plot is Gibbs plot, TDS vs. $\text{Na}^+ / (\text{Na}^+ + \text{Ca}^{2+})$ and $\text{Cl}^- / (\text{Cl}^- + \text{HCO}_3^-)$ that helps to ascertain the mechanism, processes and type of reactions responsible for the chemical constituent of water via main governing processes like evaporation, precipitation and water-rock interaction ^[152].

Rock-weathering has three major processes that govern the groundwater chemistry of the study area namely carbonate weathering, silicate weathering and evaporate dissolution ^[167]. To understand the rock- weathering mechanism, bivariate mixing between Na^+ -normalized Ca^{2+} versus Na^+ normalized HCO_3^- and Na^+ normalized Mg^{2+} are done. Mineral dissolution and weathering occur due to interaction with carbonic acid water formed due to dissolution of pore CO_2 . The ionic ratios also give insight into the process like ion-exchange, weathering etc. The ratio of $\text{Ca}^{2+}/\text{Mg}^{2+}$ and Na^+/Cl^- is used to get insight into geochemical processes like weathering ion-exchange, evaporative enrichment, dissolution etc. Similarly, trilinear piper's plot is a widely used graphical representation for evaluating the hydrochemical processes ^[168].

2.3 Uranium and its isotopes

Uranium is the last naturally occurring radioactive element with atomic number 92. Its isotopes along with half-life's, abundance and specific activity are mentioned in Table 1.3.

2.3.1 Total Uranium determination

For uranium measurement, approximately 20 ml of groundwater sample were collected after filtration through $0.45\mu\text{m}$ filter paper in pre-leached (soaked in 10% HNO_3 solution overnight) tarson bottles. Uranium in groundwater samples is analyzed using LED fluorimeter i.e. UA1, Quantalase (Fig. 2.4). The fluorimeter works in the range of 0.5-1000 $\mu\text{g/L}$ with a minimum detection limit of 0.2 $\mu\text{g/L}$.



Fig. 2.4 LED fluorimeter i.e. UA1, Quantalase

2.3.1.1 Measurement

For uranium measurement, 5ml of samples is taken in the cuvette and 500 μ L of 5% w/v sodium pyrophosphate ($\text{Na}_4\text{P}_2\text{O}_7 \cdot 10\text{H}_2\text{O}$) solution is added. The pH of the mixture maintained at 7 by adding ortho-phosphoric acid. The uranyl phosphate complex thus formed has enhanced stability and fluorescence. The standard addition method with three successive increments of 10 $\mu\text{g/L}$ each (Sigma Aldrich supplied 100 mg/L natural uranium) is added to nullify the matrix effect. The same procedure is followed for distill water to estimate the background count, which are subtracted from the sample for background correction. The plot for the concentration of successive addition vs. fluorescence output is made for each sample to obtain the uranium concentration in the sample. The measurement is carried out at neutral pH as uranyl phosphate complex is stable at neutral pH. The higher or lower pH leads to quenching of fluorescence. The sodium pyrophosphate solution acts as a buffer and maintains the pH of the solution.

2.3.1.2 Working principle

The LEDs with a wavelength of 410 nm are arranged in floret of 7 LEDs on both the sides with a pulse power of 1.4 watts of peak powered pulse. The group of LEDs can give 100 mW in pulses shorter than 100 μs and with the duty cycle of less than 0.1. This excites the uranyl complex and fluorescence is measured using PMT placed at 90° to the incidence

pulse. The fluorescence lifetime of organics is about 100 ns and fluorescence peak at 400 nm. The fluorescence lifetime for uranyl complex is 200 μ S and its fluorescence peak ranges from 464-565 nm with a maximum at 510 nm ^[169]. This causes interference in fluorescence estimation. Hence, two modifications have been introduced into the instrument i.e. time-gated technologies that allow transmission only for 100 μ s period starting from 30 μ s after the LED pulse, so that pulse due to organics is cut off. The second modification is the optical filter at 450 nm that again cuts off the contribution of organic matters ^[170].

2.3.2 Uranium isotope determination

For isotopic measurement of uranium, 1 litre sample after filtration with 0.45 μ m filter paper is brought from the field. To preserve the sample approximately 2ml of ultrapure concentrated nitric acid is added. As the uranium concentration is low hence pre-concentration is carried out followed by separation, electroplating and counting using an alpha spectrometer.

2.3.2.1 Measurement

The pre-concentration is carried out by evaporating 1L sample and uranium is separated from all the other ions through column separation. To know the recovery and efficiency of separation ²³²U standard is added to each sample at the beginning of the procedure. For column preparation, approximately 2g of Dowex 1x8 anionic resin with 100-200 mesh size is soaked for overnight. The Dowex is packed into the cylindrical glass column of dimension 20cm x 0.8 cm and is pre-conditioned with 8M HCl (5mL x 5times) with a flow rate of about 1.5 to 2 mL/min (Fig. 2.5).

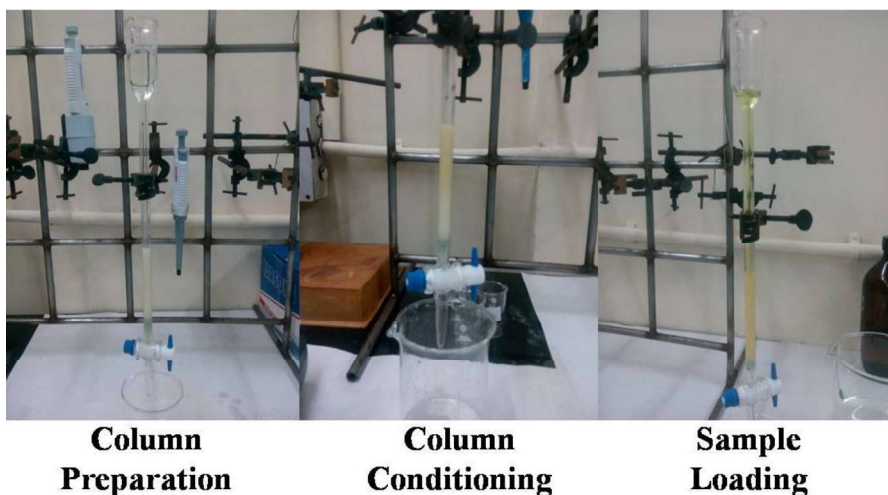


Fig. 2.5 Stages of column preparation and uranium stripping

The precipitate formed by evaporating the water sample is then re-dissolved in aqua-regia (1:3 HNO_3 : HCl). The stock/loading solution is prepared in 8M HCl ^[102]. The stock solution is loaded into the conditioned column. As uranium forms an anionic complex with HCl i.e. $\text{UO}_2\text{Cl}_4^{2-}$, it exchanges with Cl^- ion present in the conditioned resin. The uranium is stripped from the column with help of 1M HNO_3 (5mL x 5times), as uranium forms a neutral complex with nitrate ion i.e. $\text{UO}_2(\text{NO}_3)_2$ hence it is released from the column. The stripped uranium is then converted to the electroplating solution using the steps shown in the flow diagram (Fig. 2.6).

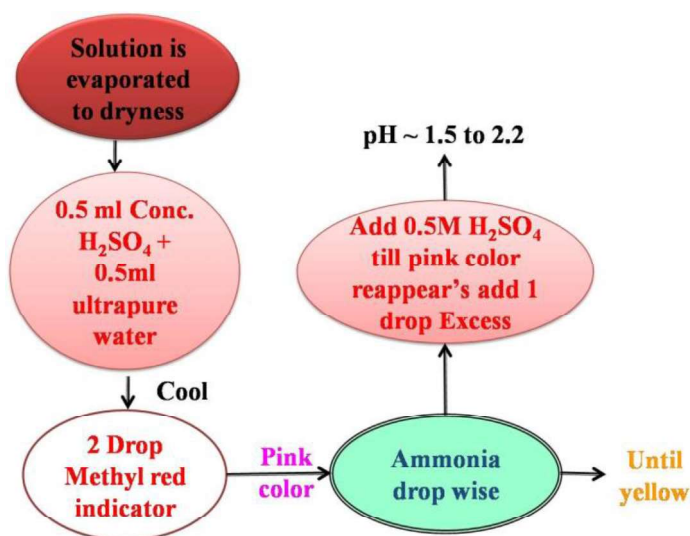
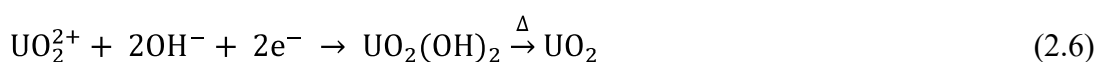


Fig. 2.6 Flow diagram showing step involved in preparation of electroplating solution

The solution was then transferred to deposition assembly (Fig. 2.7) which consists of cathode i.e. stainless steel plachets with 2.5 cm diameter and 0.5 mm thickness and anode i.e. platinum wire of 10 cm length and 2 mm diameter. For electroplating, the voltage of 6V and 0.3A of current is applied for 2.5 hours ^[171]. The reaction at cathode and anode are mentioned in Equ. 2.6 and 2.7 respectively.

At cathode: stainless steel (-ve):



At anode: Platinum wire (+ve):



After completion electroplating, 2 mL of ammonium was added into the solution. So, the plated uranium is not released back to the solution after switching off the current due to the acidic condition of the plating solution. The plachet is then washed with ethyl alcohol and burned to fix the activity on the disc. This is followed by counting in an alpha spectrometer for 24 hours under vacuum condition (Fig. 2.7).

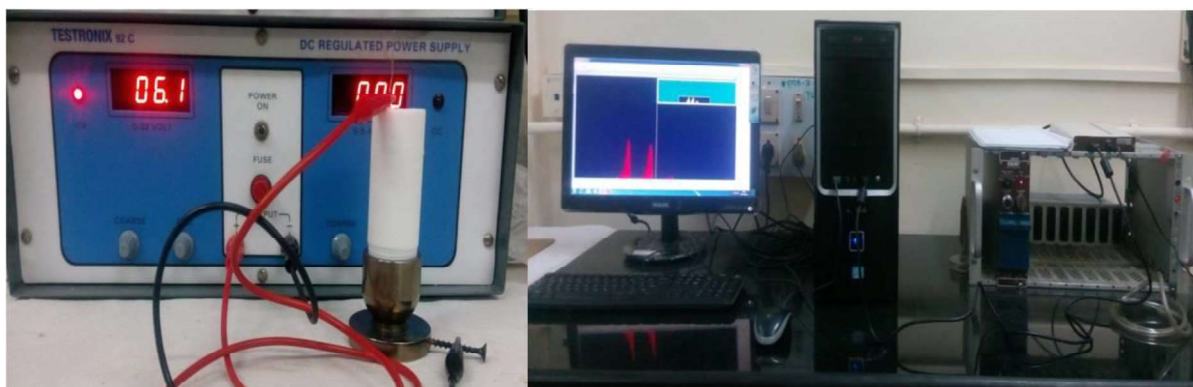


Fig. 2.7 Electroplating setup and alpha spectrometer

2.3.2.2 Working principle

Alpha spectroscopy system consists of passivated ion-implanted planar semiconductor detector (PIPS) with an area of 450mm². PIPS detector is made by introducing doping impurities at the surface of the semiconductor by exposing that surface

to a beam of ions produced by an accelerator. This method is known as ion implantation and can be used to form n^+ or p^+ layers by hitting the surface with accelerating particles, for example, either phosphorus or boron ions respectively [172]. The advantages of ion-implanted detectors are thinner depletion zone with rugged front contact, better energy resolution and lower electronic noise. The counting is done in a vacuum to reduce attenuation hence increasing the resolution of the system. The signal is then amplified and the resultant signal is displayed on the computer. The area under the peak is used to calculate the cpm which is converted to activity by applying the efficiency parameter of the system.

Calibration is done using a standard alpha source containing two or more distinct alpha energies. We use a mixed standard of ^{239}Pu and ^{241}Am (5.15 MeV and 5.486 MeV respectively) in the same geometry as that of the sample. The pulse height spectrum of the standard alpha source is recorded. Using the energies and respective position (channel no.) of the peaks calibration of the analyzer is carried out. Assuming, the energy and position have a linear relationship, the calibration factor is calculated by the following Equ. 2.8.

$$m = \frac{E_2 - E_1}{n_2 - n_1 + 1} \quad (2.8)$$

Where E_1 and E_2 are the energies and peak channels are n_1 and n_2 respectively.

For quantitative estimation of activity of the sample, it is essential to know the efficiency of the spectrometer as a function of energy. The efficiency of the system in percentage can be calculated as follows (Equ. 2.9)

$$\text{Efficiency (\%)} = \frac{\text{CPS}}{\text{dps}} \times 100 \quad (2.9)$$

Where cps is the count rate in the region of interest (area under the peak) and dps is the activity (disintegration/sec) of the standard source.

2.3.3 Applications

The study of uranium isotopes serves as a tool to study radioactive pollution and is widely used for tracing groundwater over the long period. Studies by many researchers

indicated that disequilibrium between ^{234}U and ^{238}U occurs in groundwater ^[173], its related sediments ^[174,175] and seawater ^[176]. The application of activity ratio of $^{234}\text{U}/^{238}\text{U}$ was demonstrated by Osmond et al in 1968 ^[177] and became a well-established technique thereafter ^[178,179]. Activity ratio ($^{234}\text{U}/^{238}\text{U}$) of uranium act as a fingerprint to trace water masses under different environmental conditions. The main reason for disequilibrium is alpha recoil i.e. daughter nuclide is displaced by 20nm through mineral and the alpha tracks formed makes mineral more vulnerable to leaching. This alpha recoil phenomenon makes insoluble species (^{230}Th , ^{234}Th) also mobile for a short time enhancing disequilibrium ^[180]. The recoiled thorium nuclide then decays to $^{234\text{m}}\text{Pa}$ by beta decay which further decays to ^{234}U . The uranium due to the presence of oxidizing species like nitrate and oxygen in water oxidizes to U^{6+} state and is mobilized in water.

The AR ($^{234}\text{U}/^{238}\text{U}$) of uranium varies from 0.7 to 20 based on the aquifer conditions ^[181]. Under oxidizing conditions, the concentration of dissolved uranium is high as uranium converts to U^{6+} state i.e. highly mobile and the AR is mostly upto 1 i.e. equilibrium condition as uniform leaching occurs due to oxidizing condition and selective leaching is minimal i.e. water is in augmenting regime (Fig. 2.8). This scenario is mostly at the beginning of recharge zones or in unsaturated zones. The water then travels further and comes in contact with the redox front i.e. change from oxidizing to reducing conditions. The dissolved uranium (U^{6+}) converts to reduced (U^{4+}) state which is insoluble hence precipitates and reduction in uranium concentrations are observed. Over a long period, the redox front shows a secondary deposit of uranium mineral ^[182]. The AR shows values ranging from 2 to 20 in the redox front region. The increase in AR in reducing condition is attributed to alpha recoil and selective leaching of ^{234}U . Long residence time in reductive condition leads to decay of uranium. The decay of ^{234}U is more compared to ^{238}U due to their half-life difference hence

decrease in AR is observed i.e. water is in decaying regime (Fig. 2.8). Hence by measuring uranium concentration and AR one can predict the aquifer condition ^[183].

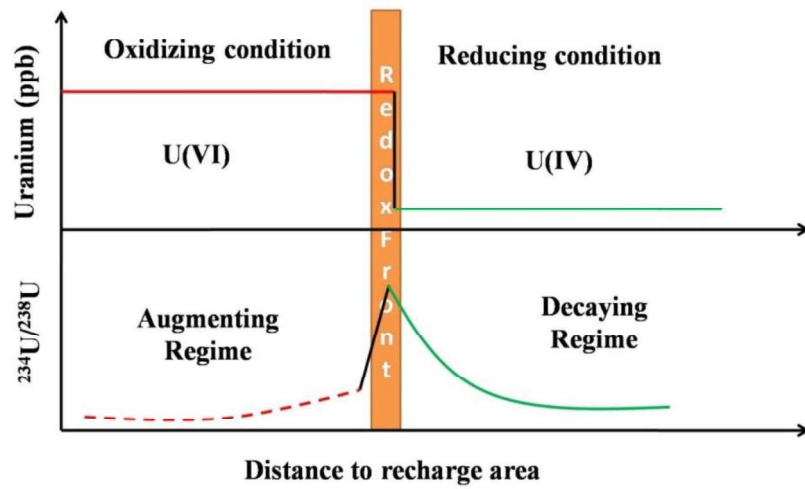


Fig. 2.8 Variation in uranium concentration and AR ($^{234}\text{U}/^{238}\text{U}$) with distance from recharge

From the plot of inverse uranium concentration versus AR, one can predict the processes leading to the release of uranium from the aquifer system. The plot has various trend lines and the sample following a particular trend line defines the process of uranium release. For example, if uranium is mobilized due to leaching it will follow the brown colour trend line shown in Fig. 2.9.

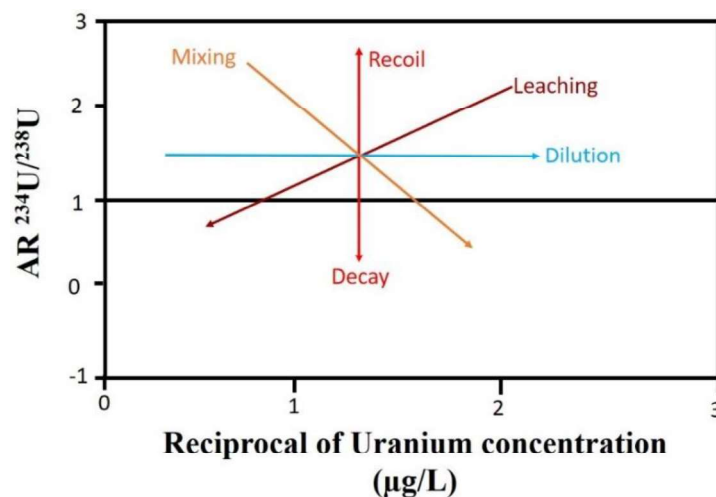


Fig. 2.9 Uranium mobilization processes (modified from Osmond and Cowart ^[177])

From the plot of inverse uranium concentration versus AR, one can predict the process leading to release of uranium from aquifer system. The plot has various trend lines and the sample data following a particular trend line defines the process of uranium release. The blue colour trend line shown in Fig. 2.9 indicates dilution process, in which only the concentration of dissolved uranium will decrease while the activity ratio ($^{234}\text{U}/^{238}\text{U}$) is not be affected. Hence sample data fall along the blue trend line. In the case of mixing between two samples having different concentrations and different activity ratios ($^{234}\text{U}/^{238}\text{U}$), the sample data fall between the two end members, as shown by the yellow trend line. In case of radioactive decay, the activity ratio ($^{234}\text{U}/^{238}\text{U}$) shows a decrease due to difference in half lives of two uranium isotopes. During the recoil process, ^{234}U will be selectively available for mobilization hence the activity ratio ($^{234}\text{U}/^{238}\text{U}$) increases and sample data fall on the orange trend line. Brown trend line shows the process of leaching, in which the activity ratio is high due to selective leaching of readily available ^{234}U and the concentration of dissolved uranium also increases.

2.4 Environmental isotopes of water ($\delta^2\text{H}$ and $\delta^{18}\text{O}$)

Isotopes are elements having the same atomic number but different mass number i.e. have different physical property and slightly different chemical property. This leads to a difference in the abundance of isotopes which is represented as (Equ. 2.10)

$$R = \frac{\text{abundance of rare isotope}}{\text{abundance of abundant isotope}} = \frac{{}^{18}_8\text{O}}{{}^{16}_8\text{O}} \text{ or } \frac{{}^{13}_6\text{C}}{{}^{12}_6\text{C}} \text{ or } \frac{{}^2_1\text{H}}{{}^1_1\text{H}} \quad (2.10)$$

The relative abundance of isotopes varies from one physical phase to other or one chemical state to others. This phenomenon is known as isotopic fractionation. Fractionation occurs during physical processes like evaporation, diffusion etc due to difference in mobility of lighter and heavy isotope and chemical processes due to difference in binding energies. For example, evaporation of water from ocean, ^{18}O being heavy has lower mobility and prefers to stay in water phase compared to vapour phase and chemical dissolution of calcium carbonate with acid, $\text{Ca}^{12}\text{CO}_3$ dissolves faster than $\text{Ca}^{13}\text{CO}_3$ in acidic medium. This difference in abundances due to different processes acts as a potential tool for hydrological applications. But these processes lead to smaller differences making it difficult to determine

the absolute values, for example, average abundance of oxygen-18 is close to 2000 ppm while it ranges from 1900 to 2100 ppm from compound to compound due to fractionation [1]. For isotope hydrology studies, the relative abundance is more important than absolute values. The relative difference is called δ value and is defined as (Equ. 2.11)

$$\delta = \left(\frac{R - R_{\text{std}}}{R_{\text{std}}} \right) \times 1000 \quad (2.11)$$

Where, R represents the isotope ratio of a sample ($^2\text{H}/^1\text{H}$, $^{13}\text{C}/^{12}\text{C}$, $^{18}\text{O}/^{16}\text{O}$, etc) and R_{std} represents ratio in a standard. As these values are small, they are generally expressed in parts per thousand (per mil., ‰). The universal standard used for $\delta^{18}\text{O}$ and $\delta^2\text{H}$ is Vienna Standard Mean Oceanic Water (VSMOW) with $\delta^{18}\text{O}$ and $\delta^2\text{H}$ values as 0‰ [184].

Craig in 1961 collected the precipitation samples over the whole globe and analyzed them for $\delta^{18}\text{O}$ and $\delta^2\text{H}$ [185]. The samples fitted in a straight line with a slope of 8 and intercept of 10, it is known as Global Meteoric Water Line (GMWL). The line serves as a reference line to understand physicochemical processes i.e. evaporation, condensation, rock-water exchange etc (Fig. 2.10). The various shifts from the GMWL are depicted in Fig. 2.10 depending on the environmental conditions. For example, the meteoric water line shows a shift towards left in case of humid environment and right in case of arid environment. The samples having depleted values are due to cooler temperature, higher latitude or altitude while the enriched values are due to warmer climate, lower latitude and altitude. The samples from lagoons fall in the enriched region due to evaporation. The enrichment is observed in $\delta^{18}\text{O}$ due to exchange under high temperature conditions like in geothermal water. The exchange in $\delta^2\text{H}$ is observed when the exchange is with clay or hydrocarbons in the aquifer this occurs in case of paleowater.

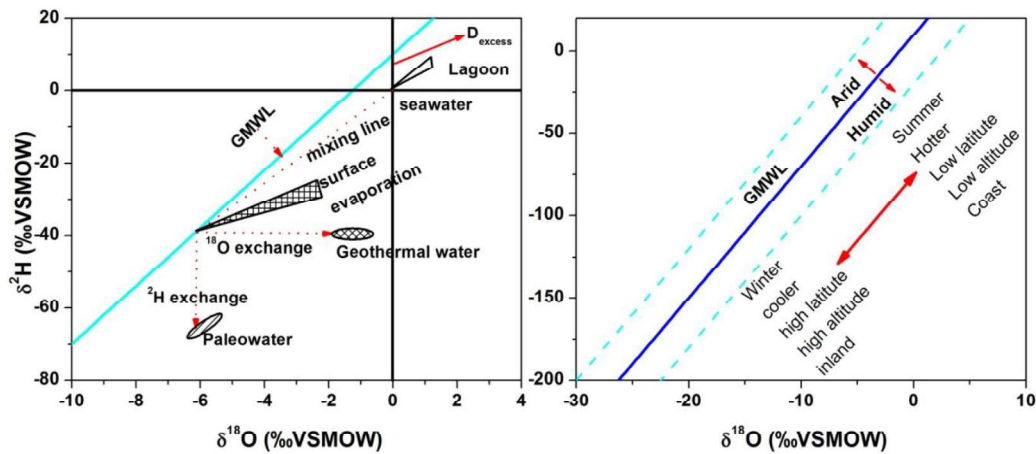


Fig. 2.10 The scatter plot of $\delta^{18}\text{O}$ and $\delta^2\text{H}$ indicating phenomenon leading to change in isotopic values.

The degree of depletion in heavy isotope is also related to parameters such as latitude, altitude and distance from the coast and fraction precipitated from the vapour mass. Latitude effect is decrease or depletion of the heavy isotopic concentration when going from lower to higher latitude. Rainwater from the northern and southern hemispheres is depleted in $\delta^{18}\text{O}$ and $\delta^2\text{H}$ compared to those located near the equator. This occurs due to successive rainouts from the clouds during moisture transport [186]. A depletion of about -0.5‰ per degree of latitude for $\delta^{18}\text{O}$ was observed over the North American continent by Yurtsever, 1975 [187]. As the moisture moves inland depletion in $\delta^{18}\text{O}$ and $\delta^2\text{H}$ is observed, it's called the continental effect. A decrease in $\delta^{18}\text{O}$ and $\delta^2\text{H}$ content with increasing altitude is observed. The magnitude of the altitude effect depends on local climate and topography. An altitude effect of about 3.8‰ per 100 m for $\delta^2\text{H}$ and 0.5‰ per 100 m for $\delta^{18}\text{O}$ were observed in eastern Himalayas [188]. Seasonal variation of $\delta^{18}\text{O}$ and $\delta^2\text{H}$ is related to seasonal variation in temperature. These are predominant in places far away from coastal stations. A strong negative correlation between $\delta^{18}\text{O}$ or $\delta^2\text{H}$ and the amount of rainfall is observed. This is due to the evaporation of the falling raindrops and exchange with atmospheric water vapour

during periods of light rain. This combined effect of these phenomena provides an isotopic signature to the water molecule which is exploited for isotope hydrological applications.

2.4.1 Stable Isotopes ($\delta^{18}\text{O}$ and $\delta^2\text{H}$)

2.4.1.1 Measurement

The samples are collected in 60 ml tarson bottles for stable isotope analysis using Isotope Ratio Mass Spectrometer (IRMS- Isoprime100). While collecting the sample a precaution is taken that bottle doesn't have any bubble and is leak-proof to avoid fractionation of the sample due to evaporation. The first IRMS was developed by Alfred Nier in 1936, with 180° magnetic sector. The basic design of the system has not been changed, just improvement in the optics. In 1988, advancement in IRMS came with the introduction of continuous flow unit to the mass spectrometer. With the advancement in the field of laser's, off-axis integrated cavity output spectroscopy (OA-ICOS) lasers were used for isotopic analysis. The instrument works on the principle of spatial separation by reflections through highly reflective mirrors that extend average optical path length to 3000 m. For measurement i) either the gas is prepared offline by reducing water in presence of zinc as a catalyst at 450°C and then injected into mass spectrometer or ii) equilibration method is followed.

For our analysis, we used mass spectrometer attached to Multi-flow unit which is an automated sample injection system for the measurement of $\delta^2\text{H}$ and $\delta^{18}\text{O}$ in aqueous samples (Fig. 2.11). In the lab, automated sample equilibration and analysis of 60 sample vials in each batch is carried out. The batch consists of samples bracketed with standard vials i.e. after every 10 samples there is a standard vial. For $\delta^{18}\text{O}$ analysis 200 μl of aqueous sample is equilibrated with a gas having the composition of 5% CO_2 in Helium at two bar pressure with a flushing time is 5 min. per sample. Equilibration temperature is maintained at 300°C for 6 hours ^[189]. The temperature is maintained uniformly using an automated system as

fractionation is temperature depended phenomenon. After the equilibration, the headspace gas is sampled with the needle and passed to the Isoprime for isotopic analysis. The equilibration reaction can be written as (Equ. 2.12)



Fig. 2.11 Multiflow-IRMS-Isoprime100 system



For $\delta^2\text{H}$, around 1 ml of the water sample is equilibrated with mix gas (10% H_2 in He) at two bar pressure in presence of reusable Hokko bead platinum catalyst. Equilibration temperature is maintained at 50°C for 90 minutes ^[189]. The equilibrated gas present in the headspace is then introduced into the mass spectrometer. The analysis is done using pure reference H_2 gas. The equilibrium reaction can be written as (Equ. 2.13):



The measured values are then normalized on VSMOW scale. Precision is measured by comparing the spread in the ratio for standards. For accuracy, the deviation in isotopic ratio of standard from the calibrated value i.e. true value is done for each batch. Quality assurance is done by participating in IAEA inter-comparison exercises. The precision of measurement for $\delta^2\text{H}$ is $\pm 0.5 \text{ ‰}$ (2σ). The precision of measurement for $\delta^{18}\text{O}$ is $\pm 0.1 \text{ ‰}$ (2σ).

2.4.1.2 Working principle

The mass spectrometer has four parts namely ionisation source, separation system, detector and data system. The ionisation source, separation system and detectors are under high vacuum. The vacuum reduces ion scattering due to the collision of the ion with residual gas molecules that modifies their trajectories, resulting in peak broadening. And it also limits contamination by residual gases in the ionising chamber. The equilibrated gas then enters the IRMS through flight tube. The ionization is through an electron beam source which bombards the gas and ionizes it. The ionized gas formed is collimated and accelerated with the help of the electric field. The beam enters a magnetic field applied perpendicular to the beam direction, which deflects the ions into circular paths based on its mass/charge ratio. In the collector, ions of the selected mass are transmitted and detected by a Faraday cup. The ion current from the cup is proportional to the number of incident ions and therefore to the partial pressure of the equivalent isotopic molecular species in the sample gas. Multiple faraday cups are often used to obtain simultaneous detection of different isotopes. Amplifiers connected to the collectors then convert the ion currents into voltages by using very high resistance. The voltages are next converted to frequencies that are counted by a counter for a fixed time to get respective numbers. The ratios of the numbers are taken as isotope ratios.

2.4.2 Radioisotope (Tritium (^3H))

Water exists in 18 different isotopic combinations out of which HTO is one of the forms. Tritium being an integral part of the water system plays an important role in isotope hydrology. Tritium is produced in the stratosphere by spallation of cosmic-ray neutron on nitrogen atom present in the environment with a steady-state inventory of 3.6 kg ^[190]. From stratosphere tritium enter troposphere through spring leak. It takes approximately 11-15 days for tritium to enter the water cycle. It is also produced in lithosphere by the spallation of neutron on lithium-6 atom. Tritium was also added to the environment via anthropogenic

activities of nuclear bomb testing carried out in the stratosphere. It is also a byproduct of the paint industry and watch industries as it's a component of luminescent paints and dials.

The concentration of tritium atom being low i.e. $^3\text{H}/^1\text{H}=10^{-18}$ hence, pre-concentration of tritium needs to be done before determining its content at environmental levels. After enrichment, it is counted either by liquid scintillation counter or using gas proportional counters. For gas counting, water is reduced using magnesium forming hydrogen gas which is converted to ethane by reacting it with dead ethylene in presence of nickel. The procedure for sample preparation is tedious involves high temperature of around 600°C . Thus, counting using LSC is preferred.

2.4.2.1 Measurement

For measurement, approximately 500 ml of the sample is brought to the lab from the field in airtight polyethylene terephthalate bottles. The procedure for electrolytic enrichment (preconcentration) of tritium is as follows [191-192].

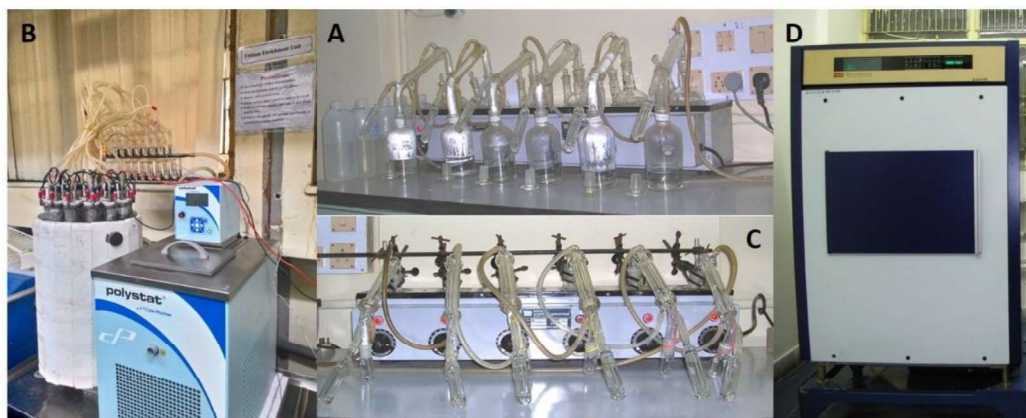


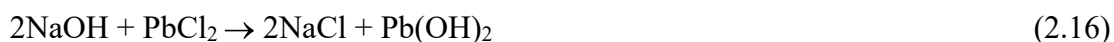
Fig. 2.12 Tritium electrolytic enrichment setup

The first step is distillations of sample (Fig. 2.12A) to bring its EC to avoid corrosion followed by addition of sodium peroxide to make water conducting. 250g by weight of this solution is added to electrolytic cells. Enrichment is done in the batch of twenty cells out of these three are the standard spiked solution of known concentration, three are background samples and fourteen are the sample cells (Fig. 2.12B). A total of 705 AH are passed to attain

enrichment factor of 19. The reactions of electrolytic enrichment process are given in Equ. 2.14 and 2.15



Enrichment is followed by neutralization of solution by adding lead chloride (~2g) (Equ. 2.16). This solution is heated at ~150°C and the condensate is collected through closed system setup (Fig. 2.12C).



14 ml of Scintillator is added to the 8g of the enriched sample in high-density polythene scintillation vials are counted in Quantallus 1220 liquid scintillation counter (Fig. 2.12D). The sample is counted for 500 min. each (50 min each sample for 10 cycles). After counting, the cpm values are obtained by selecting the channel that has the best figure of merits (square of efficiency /background). For quality assurance of the lab generated data in every batch spiked samples and distilled water samples are added to keep the check on the consistency of measurement. Secondly, we regularly participate in IAEA inter-comparison studies. The tritium values are reported in terms of tritium Units (TU) where 1 TU is equal to 0.118 Bq/Kg or 3.19 pCi/Kg.

2.4.2.2 Working principle

The basic principle of LSC is the measurement of scintillation caused by the interaction of radionuclide with the scintillator material. The radiation emitted by analyte excites the solute molecule in the scintillator mixture. The solute molecule transfers the energy to secondary solute that acts as a wavelength shifter and brings the fluorescence in the detection range of the PMT. These scintillations are measured with the help of the photomultiplier tube (PMT). The main advantage with Quantallus 1220 liquid scintillation counter is their reduced backgrounds due to asymmetric lead shield that reduces the entry of

natural radiation into the counting area. Secondly, its coincidence and anticoincidence system which help in background cancellation. After background cancellation, the counts are sent to ADC and registered into MCA. The minimum detection limit for tritium after electrolytic enrichment is 0.5 TU (1σ).

2.4.3 Applications

Environmental isotopes act as tracers for movement of water over time and space both short term and long term. These isotopes are also useful in understanding

1. Source and origin of groundwater ^[193,194]
2. Groundwater interconnections with surface water ^[195,196]
3. Recharge of groundwater ^[197,198]
4. Recharge to spring water ^[199]
5. To understand atmospheric circulation patterns ^[200,201]
6. Source and origin of contamination ^[202]
7. Residence time of water ^[203,204]
8. To quantify infiltration rates ^[205]
9. To identify primary recharge seasons ^[206]
10. To identify the pathways of groundwater ^[207,208]

2.5 Spatial, geochemical and statistical Methods

2.5.1 Geographic Information System (GIS)

The software is used to make geographic location maps for the sampling site and also used for spatial display of data in form of contours. We used Quantum GIS (Q-GIS) for our work. It was developed by Gary Sherman in python, Qt and C++ language. Its desktop-based software that supports shape files, coverage, personal geodata bases, dxf files, map-info, post-GIS, and other formats. Location maps and various spatial contour plots were made using this software.

2.5.2 Aquachem

The software AQUACHEM 3.70 was used for Piper, Stiff, Durov, Schoeller Wilcox diagrams as well as and statistical plots such as box and whisker and histogram. This software allows preparation of multiple plots simultaneously from the same data set. The software also helps in calculating charge balances, unit transformations and statistical analysis.

2.5.3 Origin

Origin (version 8.0) is data analysis and graphical software with a wide range of plotting options. It was used to make scatter plots, box plots and for statistical analysis.

2.5.4 WATEQ4F

It is a chemical speciation code used for natural water to estimate distribution of aqueous species, ionic activities and mineral saturation indices. It uses the field and analytical parameters like temperature, EC, PH, TDS, alkalinity and dissolved ions present in the groundwater. The code works on the assumption of homogenous phase and equilibrium condition for non-redox species.

The thermodynamic stability of mineral in groundwater provides insight into the saturation index value. There are a considerable number of algorithms and programs for calculating chemical equilibrium by using the computer, which introduces either of the two ways of simulating water-rock interactions: (a) computation by using the equilibrium constants of chemical reactions, and (b) calculation by the method of free energy minimization.

The value of ionic activity product (IAP) for a mineral equilibrium reaction in natural water may be compared with the value of K_{sp} , the solubility product of the mineral. If a mineral dissolve according to the reaction (Equ. 2.17)



IAP is given by Fetter (1988) ^[209] as (Equ. 2.18):

$$\text{IAP} = (\alpha_x)^x \times (\alpha_y)^y \quad (2.18)$$

Where, $\alpha = \gamma m$; m is the mole concentrate for the specific ion, γ is calculated using (Equ. 2.19)

$$\log \gamma_i = \frac{-AZ_i^2\sqrt{I}}{1+a_iB\sqrt{I}} \quad (2.19)$$

Where γ_i is the activity coefficient of ionic species i, Z_i is the charge of ionic species i, I is the ionic strength of the solution. A is a constant equal to 0.5085 at 25°C, B is a constant equal to 0.3281 at 25°C, and a_i is the effective diameter of the ion.

The WATEQ4F code uses continued fraction method to solve nonlinear mass balance equations given by Wigely (1977) ^[210] and uses Davies (1962) equation to estimate activity coefficients for solute species required for Debye Huckel equation ^[211].

The standard Gibbs free energy (ΔG_r°) of a reaction is the difference between the sum of the free energy of the products and the sum of the free energy of the reactants. It is also given as (Equ. 2.20)

$$\Delta G_r^\circ = RT \ln K_{sp} \quad (2.20)$$

Where R is the gas constant and equal to 0.00199 kcal/(mole·°K), T is the temperature in degrees Kelvin. The values of ΔG_r° have been measured for many reactions, the value of K_{sp} can be computed if ΔG_r° is known ^[209].

Saturation indices are given as $\log (\text{IAP}/K_{sp})$ if; i) $\text{SI} = \log \text{IAP}/K_{sp} = 0$; ii) equilibrium state $\text{SI} = \log \text{IAP}/K_{sp} < 0$; under saturation state (mineral dissolution condition) and iii) $\text{SI} = \log \text{IAP}/K_{sp} > 0$; oversaturation state (mineral precipitation condition). The software is used for theoretical calculation of probable species based on the chemical data. For our study, we calculated the probable species of uranium present in the system. These theoretical species help us in predicting the role of ions on the release and mobilization.

2.5.5 Multivariate analysis

IBM SPSS statistics (version 20) was used for estimation of Pearson's correlation and factor analysis, which includes principal component analysis (PCA). The software allows advanced statistical, provides machine learning algorithms for analysis. It helps in data validation, anomaly detection. The software uses python and R language.

2.5.5.1 Pearson's correlation

The correlation coefficient is to measure the strength of association between the two variables. It is mostly calculation through linear regression. The value ranges from -1 to 1. Where -1 mean strong negative correlation and 1 means a strong positive correlation between the variable. The main drawback of Pearson's correlation is that it doesn't distinguish between dependent and independent variable. We need to have prior knowledge about the dependence of two variables. It is calculated using the Equ. 2.21 ^[212]

$$r = \frac{n(\sum XY) - (\sum X) \times (\sum Y)}{\sqrt{[n \times \sum X^2 - (\sum X)^2] \times [n \times \sum Y^2 - (\sum Y)^2]}} \quad (2.21)$$

Where n is the sample size, X is the first variable, Y is the second variable.

2.5.5.2 Principle Component Analysis (PCA)

When data consist of a large number of interrelated variables, PCA helps to reduce the dimensionality of a data set keeping the information of data intact. The first step to PCA is standardization of the variables. This is an important step as it brings the data to the same level hence each variable contributes equally towards component generation i.e. each variable is normalized to unit variance ^[213]. This is calculated using formula (Equ. 2.22) for every variable.

$$z = \frac{\text{value} - \text{mean}}{\text{Std dev}} \quad (2.22)$$

The second step is generation of the matrix. This helps us to understand how the variables of the input data set are varying from the mean with respect to each other i.e.

correlation among variables. The third step is to compute eigenvalue and eigenvector ^[214]. After applying PCA to the data set we generate the principal components (PCs), which are non-correlated (orthogonal) to each other and carry the information of the original data set. Thus, larger the covariance carried by a line more the information about the data set carried by the particular component. The principal component score is obtained by projecting the eigenvector onto the principal axes. The variables that contribute towards the component's generation are called principal component loadings. Varifactors (VFs), a new group of variables that are obtained by rotating the axis. This is done with the help of singular value decomposition (SVD). In varimax rotation, dispersion of PC loading values is maximized by minimizing the coefficients ^[215]. This grouping of the variables into PC's or rotated components helps provide insight into the data and is very useful for data interpretation.

CHAPTER 3 Source and mobilization of uranium in groundwater of Southwest Punjab

3.1 Study area description

Under this study, two districts of Punjab viz. Faridkot and Muktsar were chosen. Both the districts have a semi-arid climate, with winter from November to February (5°C-18°C) and summer from April to June (35°C to 41°C). The monsoon season stretches between the end of June and September with 79% of the rainfall received from the southwest monsoon while remaining 21% is received via western disturbances. The annual average rainfall during year 2010 to 2019 was 459 mm for Faridkot district and 369 mm for Muktsar district ^[216].

Faridkot district is located in the south-west part of Punjab. It is bounded by Moga & Bathinda districts (east), Ferozpur district (North & West) and Muktsar district (South). It stretches between 29.9° and 34.9° N latitudes and 74.25° and 75.42° E longitudes covering a total area of 1419 km². The district is divided into 2 administrative blocks with a total population of 6,18,008 ^[217]. The district is devoid of the natural stream but is covered by the canal on the east, west and north side of the district namely Rajasthan feeder, Sirhind feeder and Bikaner canal.

Out of the total area of the district, the area under cultivation is 1282 km² with the cropping intensity of 198%. Out of the remaining area, the forest cover is 20.04 km², fallow land is 22.4 km², barren land is 45 km², pastures cover is 52 km², land not good for cultivation is 356 km², remaining land of 170 km² is used for non-agricultural activities like school, houses etc. The main source of irrigation in the district is canal water mainly the Sirhind feeder, which covers the length of about 228.4 km ^[142].

Muktsar district is located in the south-west part of Punjab. It is bounded by Bathinda district (east), Ferozpur district (North-west and eastern side), Faridkot district (North and North-east) and Hanumangarh district (Rajasthan) & Sirsa district (Haryana) on the south. It stretches between 29.91° and 30.67°N latitudes and 74.25° and 75.32°E longitudes covering a total area of 2630 km². The district is divided into 4 administrative blocks with a total population of 9,02,702 ^[211]. The district is devoid of the natural stream but is covered by canal feeders namely Sirhind feeder and Bathinda branch canal.

Out of the total area of the district, the area under cultivation is 2240 km² with the cropping intensity of 193%. Out of the remaining area, the forest cover is 20.04 km², fallow land is 170 km², barren land is 55 km², pastures cover is 45 km², land not good for cultivation is 400 km², remaining land of 150 km² is used for non-agricultural activities like school, houses etc. The district uses groundwater and canal water as irrigational sources. The Sirhind feeder is the main canal, which covers the length of about 523 km ^[143]. The area irrigated by canal water is 2000 km² and by groundwater is 250 km².

Geologically, the study area consists of thick Quaternary deposits of younger, older alluvium and aeolian deposits. The older alluvium belongs to the middle to late Pleistocene period while younger alluvium belongs to Holocene period. The older alluvium is composed of reddish clay, sand, silt and coarse kankar which are calcareous and the young alluvium mainly consists of mica sand with clay.

Hydro-geologically, Faridkot district falls under Sutlej basin and is composed of sand, silt, silty clay with an occasional patch of mica flakes with an elevation of about 226m amsl and a slope towards the south-west. The bands of silty clay with kankar deposits and lenticular clay are found at various depths. A lithological cross-section of deposits with depth is shown in Fig. 3.1. The exploratory studies by CGWB (2013) in Faridkot district revealed a multiple aquifer system upto the depth of 408m bgl with the first aquifer upto the depth of

57 m separated by a thick clay layer of about 10m followed by the second aquifer which goes down upto 120m ^[142]. After the depth of 120 m, the study area has semiconfined to confined multiple aquifers with thin sand layers alternating with a thick clay layer.

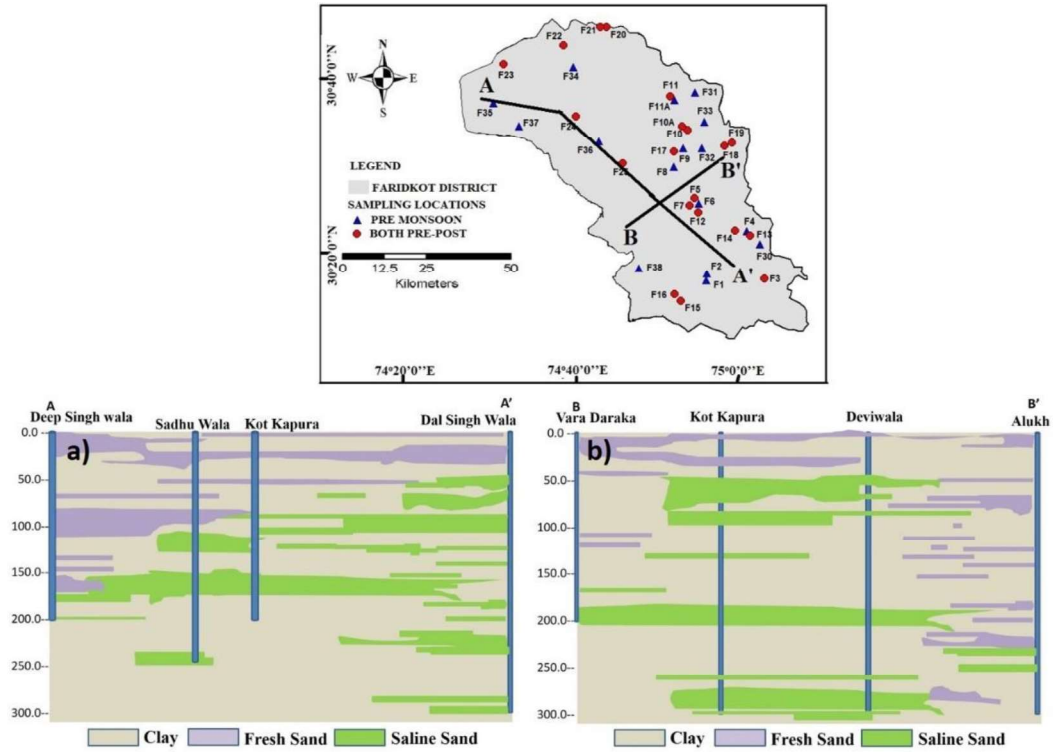


Fig. 3 1 Lithological cross-section of Faridkot district a) transect A-A' and b) transect B-B'

Muktsar district falls on the Indus basin with both confined and unconfined aquifers with alluvial thickness upto 416m bgl at Nagaur and an elevation of 200 m amsl with a gentle slope towards south to the south-west. The study area has a multiple aquifer system with a maximum depth of 300m. The area consists of sand, silt and clay with mostly saline water except for a few freshwater pockets. The aquifer system has granular structures alternating with thick and thin clay lenses or layers. A lithological cross-section of deposits with depth is shown in Fig. 3.2. The exploratory work by CGWB (2013) in Muktsar district indicates that unconfined aquifer exists up to 30m bgl ^[143]. The second and third aquifers are separated by 10m thick clay layer.

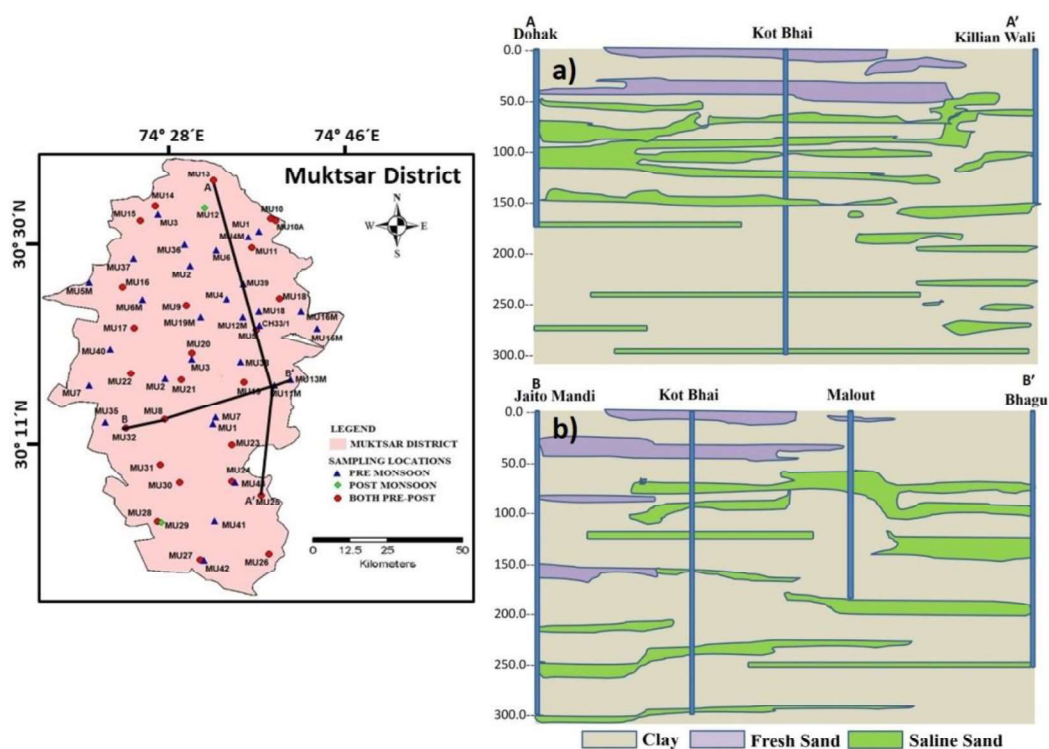


Fig. 3.2 Lithological cross-section of Muktsar district a) transect A-A' and b) transect B-B'

3.2 Sampling

The sample location selection was done by dividing the total area into 1km X 1km grid. At least one sample from each grid was collected depending on the availability of water source, electricity and consents of the well's owners. Samples were collected for both premonsoon during May 2017 (70 nos.) and postmonsoon seasons during October 2016 (39 nos.). Samples were collected from shallow zone tapping depths from 3 m to 50 m and deep zone tapping the depth of 60 m to 250 m. The percentage of samples collected from shallow and deep zones are given in Table 4.5

Table 3.1 Percentage of samples from the different depths

Depths	% samples	
	Premonsoon	Postmonsoon
Shallow (3m- 50 m)	86	79
Deep (60m-250m)	14	21

The sample location details like latitude, longitude, elevation etc along with date and time of sampling were noted for every sample. Physico-chemical parameters like EC, pH, temp., DO etc. were measured in the field using a hand-held multiparameter probe (HANNA-HI9829-11042). Samples for major ion, environmental stable isotopes (^{18}O and ^2H), environmental radioisotope (^3H), total dissolved uranium and its isotopes were collected and brought to the lab for their respective measurements. The details of the measurement protocol and instruments used are given in chapter 2.

3.3 Results and discussion

3.3.1 General water quality

The summary of field parameters and chemical parameters of groundwater samples from shallow and deep zones for both pre and postmonsoon season of Muktsar and Faridkot districts of Punjab are shown in Table 3.2.

3.3.1.1 Physicochemical parameters

The pH values for the shallow zone ranges from 6.8 to 9.3 with an average of 7.7 for premonsoon season and 6.1 to 8.9 with an average of 7.3 for the postmonsoon season. The value in the deep zone is 7.4 to 9.8 with an average of 8.3 for premonsoon season and 6.7 to 8 with an average of 7.6 for the postmonsoon season (Fig.3.4). The WHO (2011) ^[26] and BIS(2012) ^[144] permissible limit for pH are 6.5 – 8.5, 7% of the samples from shallow zone and 30% samples from the deep zone in premonsoon season are above the suggested limits, while for the postmonsoon season all the samples are in permissible limits for both the zones. The variation in pH values is more in the shallow zone compared to the deep zone, which indicates the vulnerability of shallow zone to changes due to recharging water.

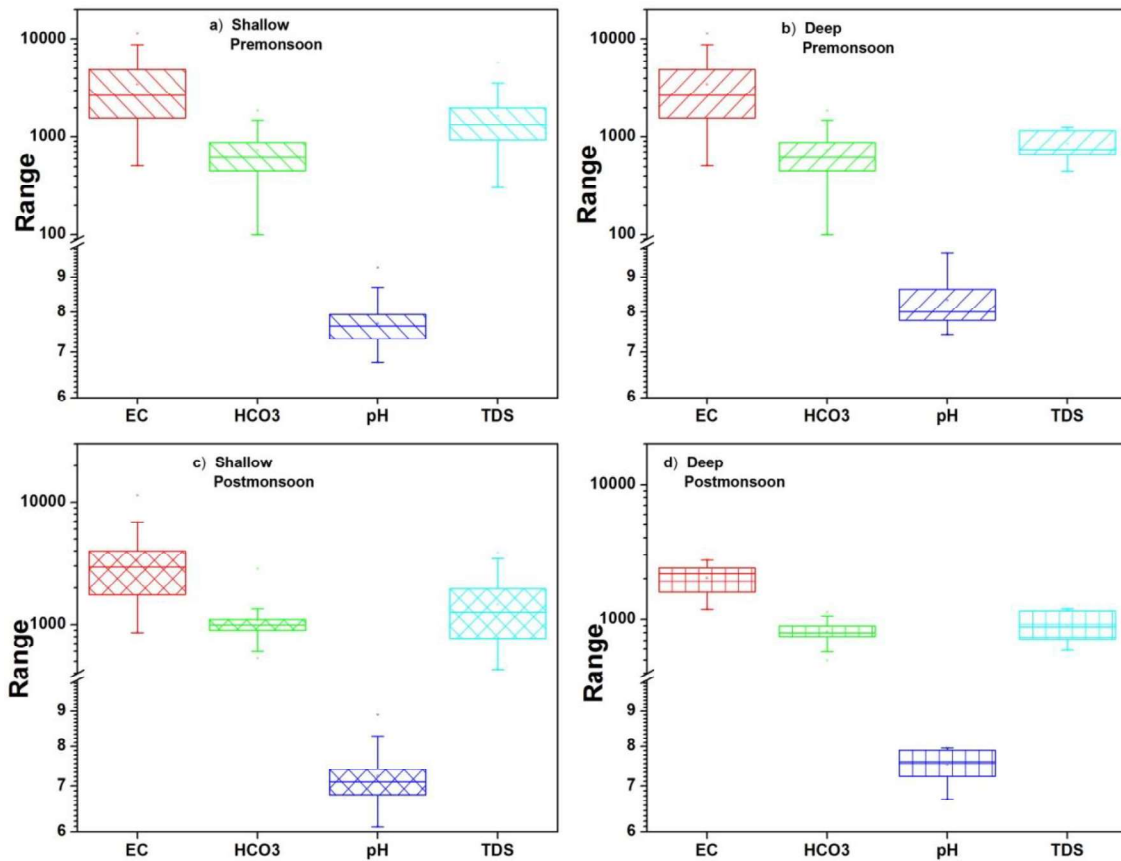


Fig. 3.4 Box plot for physiochemical parameters a) premonsoon of the shallow zone, b) premonsoon of deep zone c) postmonsoon of the shallow zone and d) postmonsoon of the deep zone

The averaged EC value for premonsoon and postmonsoon season from the shallow zone is 3588 $\mu\text{S}/\text{cm}$ (Fig. 3.4a) and 3106 $\mu\text{S}/\text{cm}$ (Fig 3.4c) while for the deep zone is 1830 $\mu\text{S}/\text{cm}$ (Fig. 3.4b) and 1973 $\mu\text{S}/\text{cm}$ (Fig. 3.4d) respectively. The exceptionally high EC value at the location from Muktsar block (Khuade Halal) having the value of 11500 $\mu\text{S}/\text{cm}$ (premonsoon) and 11390 $\mu\text{S}/\text{cm}$ (postmonsoon) was observed, which may be attributed to local contamination like leakage in household pipes etc. The decrease in average EC values of shallow groundwater during the postmonsoon season is observed, which can be attributed to dilution with the recharging water. A slight increase in average EC is observed for deep groundwater during the postmonsoon season, which can be attributed to slow recharge to deeper zones.

Table 3.2 Summary of physicochemical and chemical parameters for both the seasons of shallow and deep zones

Parameters	Shallow zone						Deep zone					
	Premonsoon			Postmonsoon			Premonsoon			Postmonsoon		
	Min.	Max.	Mean	Min.	Max.	Mean	Min.	Max.	Mean	Min.	Max.	Mean
pH	6.8	9.3	7.7	6.1	8.9	7.3	7.4	9.8	8.3	6.7	8	7.6
EC ($\mu\text{S}/\text{cm}$)	513	11500	3588	857	11390	3106	891	2826	1830	1189	2765	1973
TDS (mg/L)	303	5785	1675	429	7290	1538	446	1251	861	590	1173	844
TH (mg/L)	9.08	7858	1716	26	1311	446	14	288	117	47	402	163
Alkalinity (mg/L)	82	1230	559	66	1407	784	102	900	522	410	938	648
F ⁻ (mg/L)	0.23	12	2.1	0.13	9	1.8	0.6	2.88	1.36	0.13	2.88	1.01
Cl ⁻ (mg/L)	14	2020	405	27	1040	217	17	232	114	37	185	95
NO ₃ ⁻ (mg/L)	6.5	710	124	8	365	89	0.62	77	27	0.72	51	15
SO ₄ ²⁻ (mg/L)	28	2500	642	41	1477	374	59	606	271	78	526	224
HCO ₃ ⁻ (mg/L)	100	1500	682	528	1716	979	125	1098	637	500	1144	791
Na ⁺ (mg/L)	32	1900	555	100	1200	393	181	553	346	236	450	330
K ⁺ (mg/L)	1	492	44	2.22	386	43	0.8	8.1	4.04	2.7	18	6.3
Mg ²⁺ (mg/L)	1.6	348	75	4	170	52	1.7	44	19	6.4	48	23
Ca ²⁺ (mg/L)	1	408	93	3.8	292	93	3	43	16	8.3	85	28
Uranium ($\mu\text{g}/\text{L}$)	1.02	610	120	10	565	90	21	260	95	16	135	43
DWQI	22	645	132	12	490	108	51	177	91	15	166	62

The spread in EC values indicates the variability of leaching and dilutions due to recharging water, which is further linked to variation in soil type and other agriculture-related activities in the study area. From the depth profile of EC (Fig 3.5), the decreasing trend is observed. The shallow zones have more spread and the higher concentration of EC, which can be attributed to dissolution of salts from the vadose zone with the recharging water and contribution from irrigation return flow. The deep zones are less affected by the salinity and are fresh. This also indicates that the two zones are not interconnected. The study carried out by Sharma et al (2017) ^[137] found that the average pH values for Faridkot district were 7.5 (pre) and 7.6 (post) while for Muktsar district were 7.5 (pre) and 7.8 (post). This change in pH was attributed to recharging water. The average EC values for Faridkot district was 1760 $\mu\text{S}/\text{cm}$, which increased to 1963 $\mu\text{S}/\text{cm}$ while for Muktsar district was 2566 $\mu\text{S}/\text{cm}$, which increased to 2976 $\mu\text{S}/\text{cm}$. The slight increase in concentration during the postmonsoon season is attributed to the salts dissolved by the recharging water as per the authors ^[137].

The average alkalinity for pre and postmonsoon seasons in the shallow zone is 559 mg/L (Fig. 3.4a) and 784 mg/L (Fig. 3.4c) respectively. The average value of alkalinity for the deep zones for pre and postmonsoon seasons is 522 mg/L (Fig. 3.4b) and 648 mg/L (Fig. 3.4d) respectively. 88% of samples from shallow zone and 64% of samples from deep zone show increase in alkalinity. This increase in average alkalinity value for postmonsoon samples can be attributed to carbonate weathering or dissolution of pCO_2 generated due to root respiration and organic matter decay. A larger spread is observed in the shallow zone compared to the deep zone, which can be attributed to more inputs from unsaturated zones to the shallow region with recharging water compared to the deeper zone. The groundwater alkalinity shows a decrease with increasing well depths. This again corroborates that

contamination is limited to shallow zone and the deep zone are comparatively less affected by anthropogenic activities.

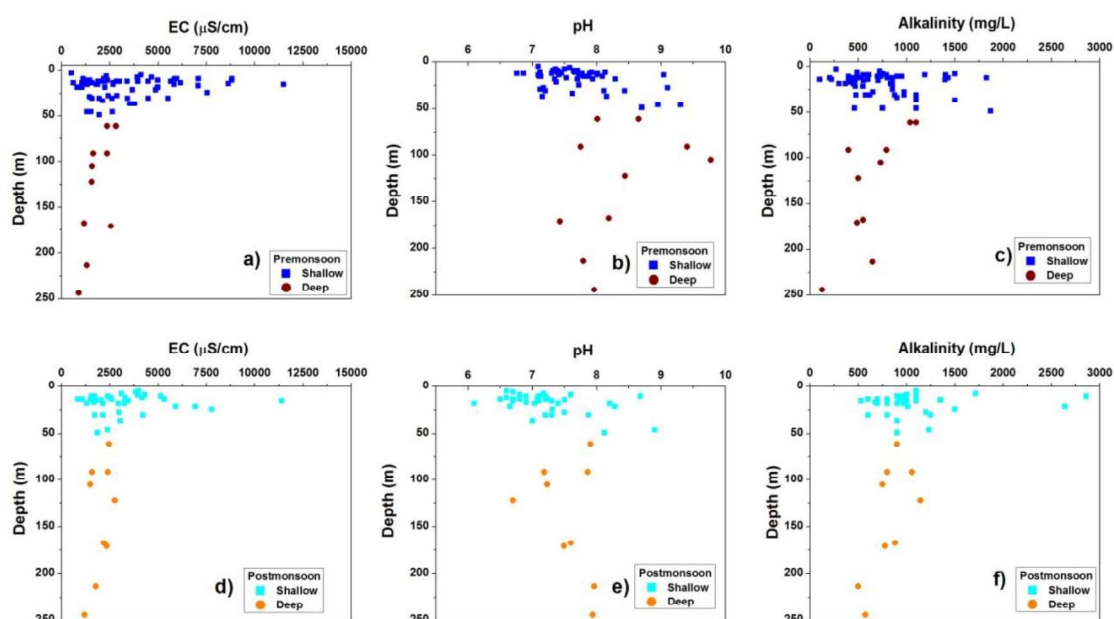


Fig. 3.5 Depth profile for physicochemical parameters a) EC, b) alkalinity and c) pH for premonsoon season and d) EC, e) alkalinity and f) pH for postmonsoon season of both the zones

3.3.1.2 Chemical parameters

The major cations are in the order of $\text{Na}^+ > \text{Ca}^{2+} > \text{Mg}^{2+} > \text{K}^+$ for both the seasons of the shallow zone. The order of major cations for the deep zone is $\text{Na}^+ > \text{Mg}^{2+} \approx \text{Ca}^{2+} > \text{K}^+$ and $\text{Na}^+ > \text{Ca}^{2+} > \text{Mg}^{2+} > \text{K}^+$ for pre and postmonsoon seasons respectively. The major anions for the shallow zone are in the order of $\text{HCO}_3^- \approx \text{SO}_4^{2-} > \text{Cl}^- > \text{NO}_3^-$ and $\text{HCO}_3^- > \text{SO}_4^{2-} > \text{Cl}^- > \text{NO}_3^-$ for pre and postmonsoon seasons respectively. The order for anions in deep zone is $\text{HCO}_3^- > \text{SO}_4^{2-} > \text{Cl}^- > \text{NO}_3^-$ for both pre and postmonsoon seasons. The box plots for various major ions present in the groundwater of shallow and deep zones of the study area for both the seasons are shown in Fig. 3.6. The health effects of the ions and the permissible concentrations are mentioned in Chapter 1 Table 1.2.

The Na^+ ion concentration in shallow zone range from 32-1900 mg/L with an average value of 555 mg/L for the premonsoon season while 100-1200 mg/L with an average value of 393 mg/L for the postmonsoon season (Table 3.2). The Na^+ ions in the deep zone range from 181-553 mg/L with an average value of 346 mg/L for the premonsoon season while 236-450 mg/L with an average value of 330 mg/L for postmonsoon season (Table 3.2.2). The average concentration of Na^+ ion decreases in the shallow zone in postmonsoon season which can be attributed to dilution with percolating water. The deep zone doesn't show much variation seasonally which indicates that deep zone is less prone to local environmental changes. The average Na^+ ion concentration is reported as 177 mg/L in premonsoon, which is increased to 190 mg/L during the postmonsoon season for Faridkot district while for Muktsar district the average concentration for premonsoon is 183 mg/L which increased to 210 mg/L. The increase in concentration is attributed to dissolution of salts from the unsaturated zone by recharging water, as per the authors ^[137]. The K^+ ions in the shallow zone ranges from 1-492 mg/L with an average value of 44 mg/L for premonsoon while for postmonsoon the range is 2.2-386 mg/L with an average of 43 mg/L. The concentration of K^+ ion in deep zone ranges from 0.8-8 mg/L with an average value of 4 mg/L for premonsoon season while for postmonsoon season the concentration ranges from 2.7-18 mg/L with an average value of 6.3 mg/L. The high concentration of K^+ ion in the shallow zone can be attributed to excessive use of fertiliser in the study area for agricultural activities. High concentration of K^+ ion in the shallow zone were also reported by Sharma et al. (2016) ^[134] in Muktsar (upto 869 mg/L) and Faridkot (upto 108 mg/L) districts.

The Ca^{2+} ions in the premonsoon season ranges from 1-408 mg/L with an average value of 93 mg/L while 3.8-292 mg/L with an average of 93 mg/L for the postmonsoon season in the shallow zone of the study area (Table 3.2). For deep zone, the concentration range for Ca^{2+} ion is 3-43 mg/L with an average of 16 mg/L for premonsoon while 8.3-85

mg/L with an average of 28 mg/L for postmonsoon season (Table 3.2). The Mg^{2+} ion concentration in shallow zone ranges from 1.6-348 mg/L with an average value of 75 mg/L for the premonsoon while 4-170 mg/L with an average of 52 mg/L for the postmonsoon season (Table 3.2). The Mg^{2+} ion concentration for the deep zone is in range of 1.7-44 mg/L with an average of 19 mg/L for the premonsoon season while 6.4-48 mg/L with an average of 23 mg/L in postmonsoon season (Table 3.2). The shallow zone shows a decrease in the average concentration of Mg^{2+} ion in the postmonsoon season which can be attributed to dilution due to recharging water. The deep zone shows an increase in the average concentration of Ca^{2+} and Mg^{2+} in postmonsoon season, which is attributed to long residence time leading to more rock water interactions thus increasing the concentrations.

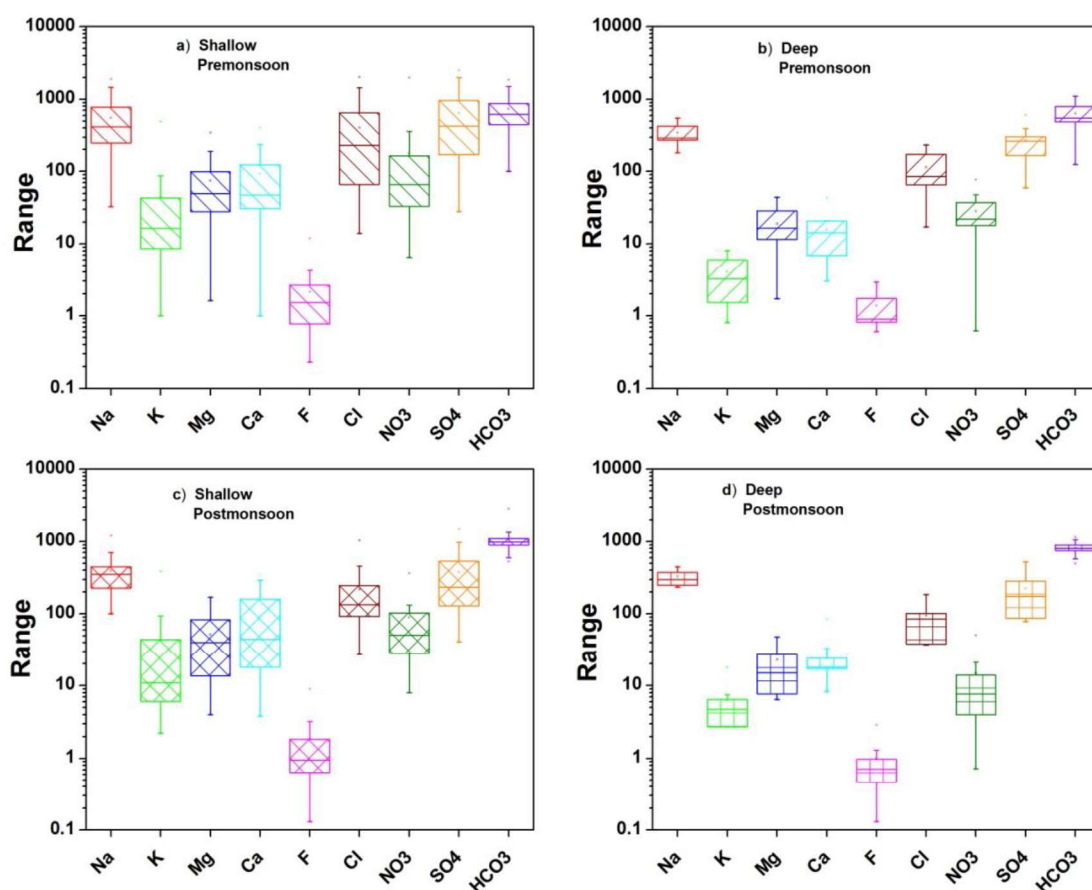


Fig. 3.6 Box plot for major ions present in groundwater from shallow and deep zone in both the seasons

The HCO_3^- ion concentration in the shallow zone is in the range of 100-1500 mg/L with an average value of 682 mg/L for the premonsoon season while 528-1716 mg/L with an average value of 979 mg/L for the postmonsoon season (Table 3.2). The HCO_3^- ion concentration for the deep zone in premonsoon season are 125-1098 mg/L with an average value of 637 mg/L while 500-1144 mg/L with an average value of 791 mg/L for the postmonsoon season (Table 3.2).

The Cl^- ion concentration in shallow zone ranges from 14-2020 mg/L with an average value of 405 mg/L for the premonsoon season while 27-1040 mg/L with an average value of 217 mg/L for the postmonsoon season (Table 3.2). The deep zone has Cl^- ion concentration in the range of 17-232 mg/L with an average value of 114 mg/L for the premonsoon season while 37-185 mg/L with an average value of 95 mg/L for postmonsoon season (Table 3.2).

The SO_4^{2-} ion concentration for the premonsoon season in the shallow zone are 28-2500 mg/L with an average value of 642 mg/L while 41-1477 mg/L with an average value of 374 mg/L for postmonsoon season (Table 3.2). The SO_4^{2-} ion concentration for the deep zone are 59-606 mg/L with an average value of 271 mg/L for the premonsoon season while 78-526 mg/L with an average of 224 mg/L for the postmonsoon season (Table 3.2).

The shallow zone has concentration of NO_3^- ion in the range of 6.5-710 mg/L with an average of 124 mg/L for the premonsoon season while 8-365 mg/L with an average of 89 mg/L for the postmonsoon season (Table 3.2). The deep zone has NO_3^- ion concentration in the range of 0.6-77 mg/L with an average of 27 mg/L for the premonsoon season while 0.7-51 mg/L with an average of 15 mg/L for the postmonsoon season (Table 3.2). The higher NO_3^- ion concentration in the shallow zone is attributed to the excess use of NPK fertilizer by Tripathi et al. (2000)^[12] and decaying organic which is waste product of agriculture and domestic waste by David and Gentry (2000)^[13]. Sharma et al. (2016)^[137] reported NO_3^- ion concentration upto 600 mg/L in Muktsar district and 128 mg/L in Faridkot district.

The F^- ion concentration in the shallow zone are in the range of 0.23-12 mg/L with an average of 2.1 mg/L for the premonsoon season while 0.13-9 mg/L with an average value of 1.8 mg/L for the postmonsoon season (Table 3.2). The F^- ion concentration in the deep zone are 0.6-2.9 mg/L with an average of 1.4 mg/L for the premonsoon season while 0.13–2.9 mg/L with an average of 1 mg/L for the postmonsoon season (Table 3.2).

The concentration of cations and anions decreases in postmonsoon season except for HCO_3^- ions. The decrease can be attributed to dilution with recharging water while the content of HCO_3^- ions is increased which is due to the dissolution of pCO_2 generated due to root respiration and organic matter decay in the soil along with percolating water.

The depth profile for NO_3^- and F^- ions indicates that contamination is localized to shallow zone (Fig.3.7). Few samples from the deep zone have concentration above the permissible range which can be attributed to some mixing with shallow zone or vertical leakage in the wells.

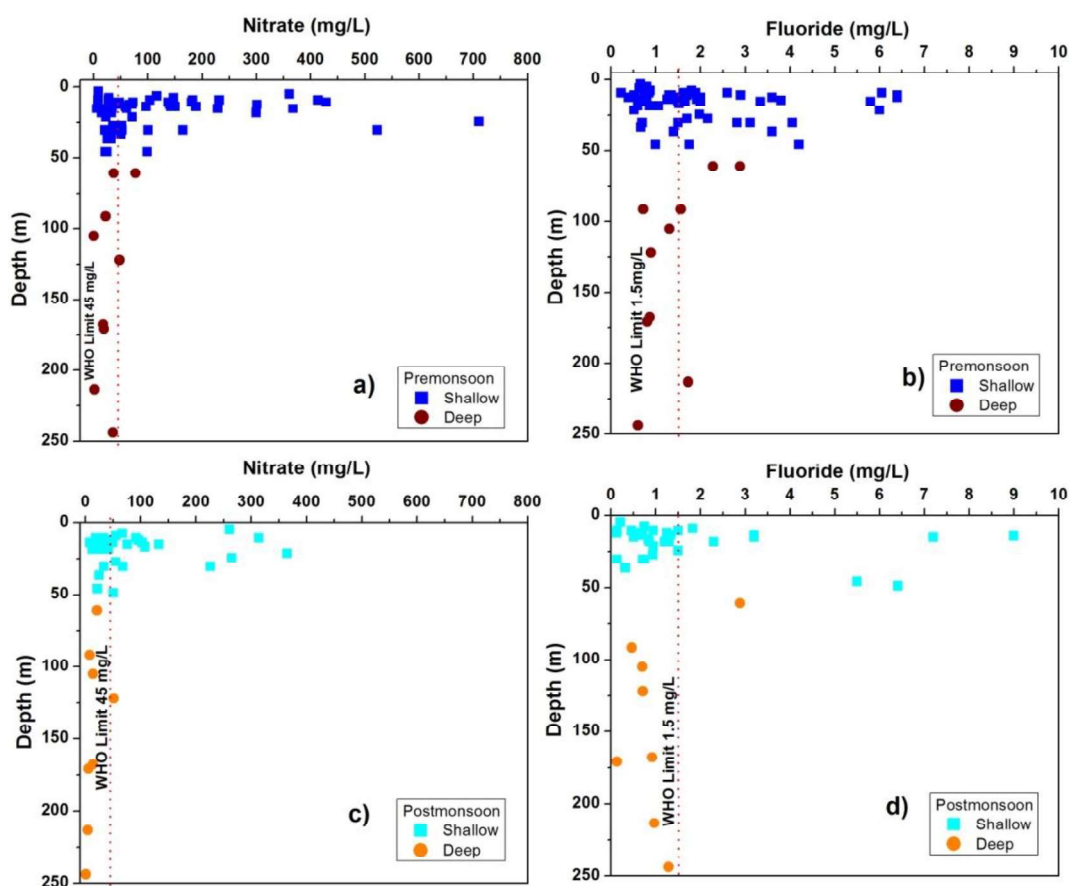


Fig. 3.7 Depth profile for a) NO_3^- ion concentration in premonsoon b) F^- ion concentration in premonsoon c) NO_3^- ion concentration in postmonsoon and d) F^- ion concentration in postmonsoon season

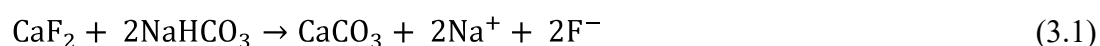
3.3.2 Suitability of water

3.3.2.1 Suitability for drinking

Suitability of groundwater for drinking was assessed by comparing the concentration of ions with permissible limits given by the BIS (2012) ^[144] and WHO (2011) ^[26]. The compiled data for water quality for both seasons of the shallow and deep zones is shown in Table 3.3.3. According to the permissible limits laid by BIS (2012) (Table 3.3), it was observed that contamination in the study area is mainly caused by NO_3^- ions (63%) followed by SO_4^{2-} ions (57%), TH (57%) and F^- ions (47%) in shallow zone. In the deep zone, the contamination due to NO_3^- ions (30%) and F^- ions (30%) is observed during the premonsoon season. High NO_3^- ions (55%), SO_4^{2-} ions (29%), TH (29%) and F^- ions (26%) are found in the shallow zone while the deep zone shows contamination by F^- ions (13%) and NO_3^- ions (13%) for the postmonsoon season. According to the permissible limit of ions in drinking water given by WHO (2011) ^[26] (Table 3.33), in the premonsoon season, the contamination is due to Na^+ ions (82%), TDS (73%) followed by SO_4^{2-} ions (65%), NO_3^- ions (60%), TH (60%) and F^- ions (47%) while for the postmonsoon season, the major contamination is due to Na^+ ions (77%), TDS (61%), NO_3^- ions (55%), SO_4^{2-} ions (48%) in shallow zone. For the deep zone, the contamination in premonsoon season is due to Na^+ ions (90%), SO_4^{2-} ions (60%) and TDS (40%) while in postmonsoon season contamination by Na^+ ions (100%), TDS (25%) and SO_4^{2-} ions (38%).

The decrease in the number of contaminated samples is observed in both the zones during the postmonsoon season which is attributed to dilution with recharging water. The main source of NO_3^- ions is the excess use of nitrogen fertilizers, use of manure and irrigation

with wastewater ^[218]. NO₃⁻ ions are highly soluble and easily leache with percolating water ^[219]. Saxena et al. (2014) ^[220] correlated the amount of rainfall with NO₃⁻contamination and concluded that low rainfall areas mostly have higher NO₃⁻ contamination as the dilution effect is low. Mondal et al. (2009) ^[221] attributed high NO₃⁻ion concentration to prolonged leaching from the minerals via rock-weathering present in the aquifer matrix. Vikas (2009) ^[222] attributed a higher concentration of contaminants in groundwater to increased alkalinity, semi-arid conditions and mineral in the aquifer matrix. The exchange reaction for F⁻ ions is (Equ. 3.1)



Kumar et al. (2007) ^[153] reported the NO₃⁻ ion concentration of 7.5-120 mg/L for premonsoon and 15-120 mg/L for postmonsoon with 60% samples above the permissible limit of 45 mg/L in Muktsar district and they attributed the high concentration of NO₃⁻ ion to extensive use of fertilisers. Their study concluded that the contamination is increasing in postmonsoon season. Sharma et al. (2016) ^[155], also found high F⁻ and NO₃⁻ ions contamination in the alluvial formation from the adjacent district of Bathinda. They reported 72% of the samples having F⁻ ion concentration above the permissible limit of WHO which decreased to 50% in the postmonsoon season while 22% of the samples show contamination due to NO₃⁻ ions during both seasons.

Another parameter for determining the suitability of water for drinking is total hardness (TH) which is determined using the equation given by Todd in 1980 (Equ. 3.2) ^[223] and its values are expressed in mg/L of CaCO₃.

$$\text{TH} = 2.497 \times \text{Ca}^{2+} + 4.115 \times \text{Mg}^{2+} \quad (3.2)$$

Table 3.3 Compiled water quality data for shallow and deep zones of the study area for both the seasons

Parameter	Permissible Limits		Shallow				Deep			
			% of samples exceeding BIS		% of samples exceeding WHO		% of samples exceeding BIS		% of samples exceeding WHO	
	BIS	WHO	Pre	Post	Pre	Post	Pre	Post	Pre	Post
			60	31	60	31	10	8	10	8
pH	6.5-8.5	6.5-8.5	7	0	7	0	30	0	30	0
TH	600	500	57	29	60	32	0	0	0	0
TDS	2000	1000	28	16	73	61	0	0	40	25
Na ⁺		200	0	0	82	77	0	0	90	100
K ⁺		20	0	0	42	29	0	0	0	0
Ca ²⁺	200	300	15	23	7	0	0	0	0	0
Mg ²⁺	100	100	25	10	25	10	0	0	0	0
F ⁻	1.5	1.5	47	26	47	26	30	13	30	13
Cl ⁻	1000	250	10	3	48	23	0	0	0	0
NO ₃ ⁻	45	50	63	55	60	55	30	13	20	13
SO ₄ ²⁻	400	250	57	29	65	48	10	13	60	38

Table 3.4 Suitability of water for drinking and irrigation on basis of TDS, TH and EC

Water class		Shallow		Deep	
		% of samples in premonsoon	% of samples in Postmonsoon	% of samples in premonsoon	% of samples in Postmonsoon
		60	31	10	8
TDS (mg/L)					
< 500	Desirable for drinking	3	6	10	0
500-1000	Permissible for drinking	23	32	60	75
1000-3000	Useful for Irrigation, Unfit for drinking	62	55	30	25
> 3000	Unfit for drinking as well as irrigation	12	6	0	0
TH (mg CaCO ₃ /L)					
< 60	Soft	2	13	20	13
60-120	Moderately hard	5	10	50	38
121-180	Hard	5	6	10	25
> 180	Very Hard	88	71	20	25
EC (μS/cm)					
< 250	Excellent	0	0	0	0
250-750	Good	3	0	0	0
750-2000	Permissible	30	35	60	50
2000-3000	Doubtful	20	29	40	50
> 3000	Unsuitable	47	35	0	0

According to TH ^[224], only 2% samples are soft which increases to 13% during the postmonsoon season for shallow zone. For the deep zone, 20% samples are soft for the premonsoon season while 13% of the samples remains soft during the postmonsoon season (Table 3.4)

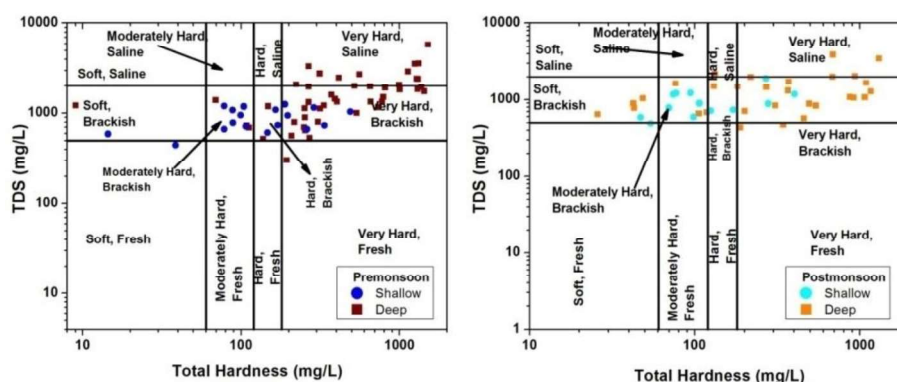


Fig. 3.8 TDS vs TH plot to understand water type.

From the plot of TDS vs TH (Fig. 3.8), it can be interpreted that the groundwater is mostly moderately hard to very hard with brackish to saline nature thus making it unsuitable for its use for drinking purposes. EC is yet another parameter that defines the quality of water for drinking. According to EC, 33% of the samples fall in the permissible range which increases to only 35% samples for the shallow zone (Table 3.4). For deep zone, 60% of samples are in the permissible range which reduces to 50% during the postmonsoon season.

3.3.2.2 Suitability for irrigation

EC, TDS, SAR, Na%, PI and RSC are the parameters used to determine the suitability of water for its use in irrigation. The compiled data for these parameters are given in Table 3.4 and Table 3.5. The water classification given by Richards (1954) ^[158] for EC is shown in Table 3.4.5 and it is observed that 47% of the samples are unsuitable for irrigation purpose for premonsoon which decreases to 35% for the postmonsoon season for the shallow zone. For deep zone, the water is suitable for its use for irrigation as per EC. Based on TDS, 12% of samples are unsuitable for their use for irrigation for the premonsoon season which decreases to 6% for the postmonsoon season for the shallow zone. The deep zone samples

are good for their use for irrigation as per TDS for both the seasons. The water classification based on other parameters such as SAR, RSC and Na% for both seasons is shown in Table 3.6.

A) Sodium absorption ratio (SAR)

The calculation of parameter is done using equation given in Chapter 2 (Table 2.1). The SAR values range from 0.99-51 with an average value of 12.6 for premonsoon and 1.5-38.5 with an average value of 12.5 for postmonsoon of shallow zone. The values for deep zone are 9.1-31 with an average value of 16 for premonsoon season while for the postmonsoon season are 7.9-23.8 with an average value of 13 (Table 3.5). According to the classification based on SAR, it was observed that 8% of samples are unsuitable for their use in the premonsoon season which increases to 16% for the postmonsoon season in shallow zone. For the deep zone, 10% of samples from premonsoon season and no sample from postmonsoon season fall under the unsuitable category (Table 3.5). This corroborates the fact that recharging water is decreasing the alkalinity related hazard making the water fit for irrigation purpose. The United States Salinity Laboratory plot (USSL) ^[225] between sodium hazard and conductivity of samples collected for both seasons for the shallow and deep zones is shown in Fig. 3.9.

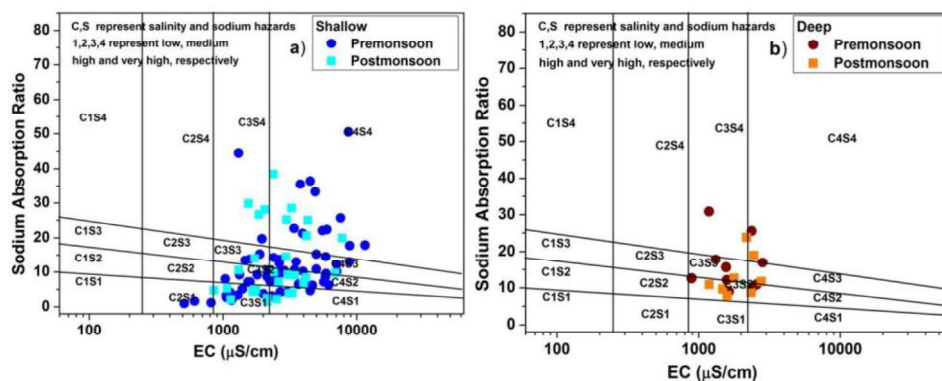


Fig. 3.9 USSL plot of groundwater from a) shallow and b) deep zones for premonsoon and postmonsoon seasons

Table 3.5 Compiled irrigation water quality data for shallow and deep zones of the study area for both the seasons

Parameters	Shallow						Deep					
	Pre			Post			Pre			Post		
	Min.	Max.	Mean	Min.	Max.	Mean	Min.	Max.	Mean	Min.	Max.	Mean
SAR	0.999	50.6	12.6	1.5	38.4	12.5	9.1	31	16	7.85	23.8	13.0
Na%	24.4	99	67	19.7	97	64	77	98	87	68	94	82
PI	44.5	125	81	34	120	84	88	123	106	82	117	104
RSC	-42.3	23.2	0.4	-9.6	21.2	7.14	1.28	16	8.1	4.7	13.5	9.7
MH	34.3	81	59	20.7	92	53.1	48	82	63.9	42.6	70.4	57
KR	0.35	74	4.8	0.25	38	6.2	3.23	41	10.6	2.17	17.4	6.63
CR	0.07	12.5	2.2	0.08	2.9	0.7	0.35	1.96	0.77	0.17	1.04	0.49
IWQI	-21.7	34.2	11.3	-1.4	30	15.7	11	27	18	12.8	23.3	18.2

Table 3.6 Suitability of water for irrigation on basis of SAR, Na% and RSC

Water class		Shallow		Deep	
		% samples in premonsoon	% samples in Postmonsoon	% samples in premonsoon	% samples in Postmonsoon
		57	21	15	12
Alkalinity Hazard (SAR)					
< 10	Excellent	50	61	20	37.5
10-18	Good	32	10	60	37.5
18-26	Doubtful	10	13	10	25
> 26	Unsuitable	8	16	10	0
Percent Sodium					
< 20	Excellent	0	3	0	0
20-40	Good	10	16	0	0
40-60	Permissible	27	26	0	0
60-80	Doubtful	35	19	20	50
> 80	Unsuitable	28	36	80	50
Residual Sodium Carbonate					
< 1.25	Good	23	0	0	23
1.25-2.5	Doubtful	0	20	0	0
>2.5	Unsuitable	77	80	100	77

The premonsoon samples of the study area shows scatter from medium to very high salinity hazard and low to very high sodium hazard for shallow zone while for the postmonsoon season, sample fall in high to very high salinity and sodium related hazards zones. During the postmonsoon season salinity related hazard tends to increase. For deep zone, less scatter is observed with samples falling in the high range of salinity and low to high zones for sodium related hazard. During the postmonsoon season decrease in scatter is observed related to alkalinity and salinity for the deep zone.

B) Sodium percentage (Na%)

Sodium percent is calculated using equation given in Chapter 2 (Table 2.1). The Na% values for premonsoon are in the range of 24%-99% with an average of 67% for premonsoon while for the postmonsoon season the values ranges from 19.7%-97% with an average of 64% for the shallow zone (Table 3.5). For deep zone, the Na% value ranges from 76.5%-98% with an average value of 87% for premonsoon while for the postmonsoon season the values range from 68%-94% with an average value of 82%. A decrease in Na% is observed in the postmonsoon season of both the zones. The value for Na% is more in deep zone which can be attributed to increased rock water interaction due to longer residence time. 37% of samples from shallow zone for premonsoon falls in the permissible range which increases to 45% samples during the postmonsoon season (Table 3.6). None of the samples fall in permissible range for the deep zone in both the seasons. The high values of Na% and high EC both can play a key role as they decrease the osmotic activity of plants limiting the absorption of water and nutrients from the soil.

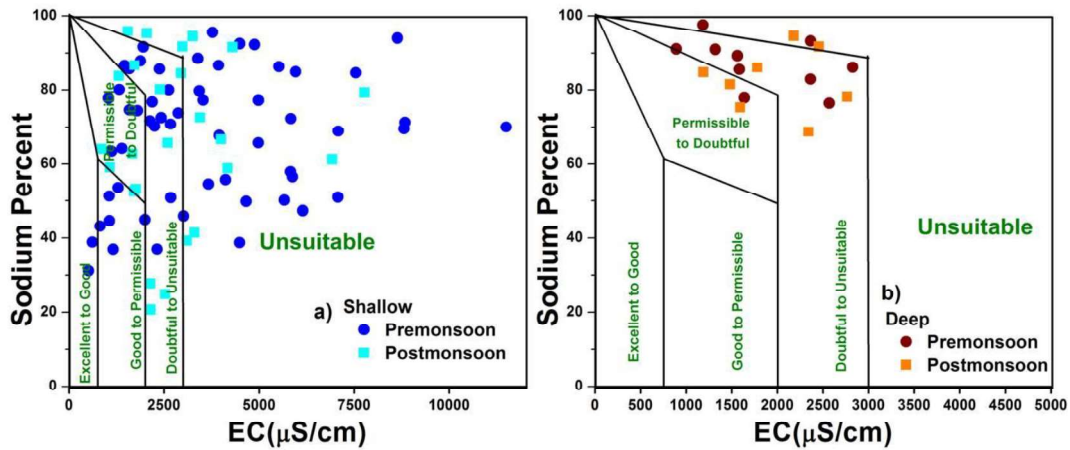


Fig. 3.10 Wilcox plot of groundwater from a) shallow and b) deep zone for premonsoon and postmonsoon seasons

The Na% is plotted against EC i.e. Wilcox plot (Fig. 3.10), it is observed that all the postmonsoon samples fall in doubtful to the unsuitable range while premonsoon samples show much larger scatter ranging from excellent to permissible to the doubtful and unsuitable range for shallow zone. Only 23% of the samples fall in permissible category for the premonsoon period which decreases to 13% in postmonsoon season. For deep zone, most of the pre and postmonsoon samples fall in permissible to doubtful to unsuitable category. Only 20% of samples fall in the permissible range which increases to 37.5% during the postmonsoon season.

C) Residual sodium carbonate (RSC)

It is calculated using equation given in Chapter 2 (Table 2.1). The RSC values for premonsoon season ranges from -42 to 23 meq/L with an average value of 0.42 meq/L while for postmonsoon the values range from -9.6 to 21 meq/L with an average value of 7 meq/L for the shallow zone. For deep zone, the value ranges from 1.3 to 16 meq/L with an average value of 8 meq/L for the premonsoon season while for the postmonsoon season, the value ranges from 4.7 to 14 meq/L with an average value of 10 meq/L (Table 3.5). The samples are categorised in three groups: i) value < 1.25: good for irrigation, ii) values in the range of 1.25 to 2.5: doubtful and iii) values > 2.5: unsuitable. For the premonsoon season, only 40%

of samples are suitable for irrigation which decreases to 23% during postmonsoon season for the shallow zone. This indicates, degradation of water quality with recharging water. For deep zone, none of the samples is suitable for its use during both the seasons.

D) Permeability index (PI)

It is calculated using equation given in Chapter 2 (Table 2.1). For shallow zone, the PI values range from 44.5–125 with an average value of 81 while for the postmonsoon season the value ranges from 34-120 with an average value of 84. For deep zone, the values range from 88-123 with an average value of 106 for the premonsoon season while for the postmonsoon season, the values range from 82-117 with an average value of 104 (Table 3.5). PI is classified into three categories i) class I: suitable for irrigation, ii) class II: marginally suitable for irrigation and iii) class III: unsuitable for irrigation (Fig.3.11). For the shallow zone, 33% of samples fall under class I which decreases to 32% for the postmonsoon season while 54% of samples fall under class II which falls to 23% in postmonsoon season and 13% of samples fall in class III which increases to 45% during the postmonsoon season. This indicates the increase in unsuitability of water for irrigation during postmonsoon season in shallow zones. For deep zone, none of the samples falls under class I for both the seasons while 10% of samples fall in class II which increases to 25% during the postmonsoon season and 90% of the samples fall in class III which decreases to 75% of samples. This indicates that during the postmonsoon season the water is becoming less unfit for deep zone.

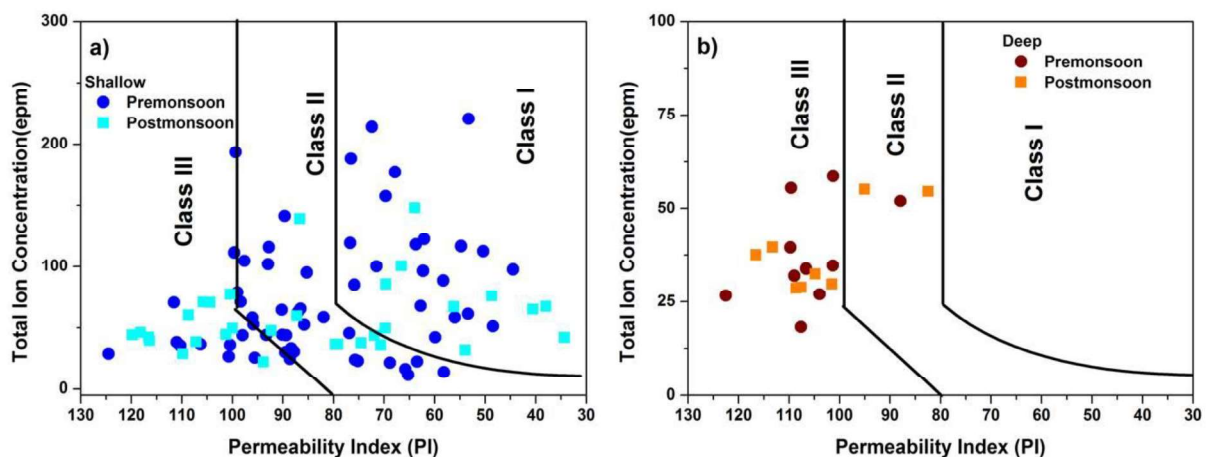


Fig. 3.11 Permeability index of groundwater from a) shallow and b) deep zones for premonsoon and postmonsoon seasons

E) Magnesium Hazard (MH)

It is calculated using equation given in Chapter 2 (Table 2.1). The MH for the shallow zone ranges from 34%-81% with an average value of 59% for the premonsoon season and 21%-92% with an average value of 53% for postmonsoon season. 77% of samples exceed the permissible MH value in premonsoon season that decreases to 71% of samples in the postmonsoon season for the shallow zone. For deep zone, the values range from 48%-82% with an average of 64% and 90% of the samples unsuitable for their use in the premonsoon season. For the postmonsoon season, the values range from 43%-70% with an average value of 57% and 75% of the samples unsuitable for their use in the deep zone. The suitability of water as per MH increases in the postmonsoon season for both the zones.

F) Kelley's ratio (KR)

It is calculated using equation given in Chapter 2 (Table 2.1). $KR < 1$ indicates the suitability of water to irrigation while $KR > 1$ is harmful. The KR values range from 0.35- 74 with an average value of 4.8 for the premonsoon season while for postmonsoon the values are in the range of 0.25-38 with an average of 6.2 for the shallow zone. 78% of the premonsoon samples and 81% of the postmonsoon samples are harmful as per KR ratio for the shallow zone. For deep zone, the KR values range from 3.23–41 with an average of 10.6 for the premonsoon season while for the postmonsoon season the values range from 2.2-17 with an average value of 6.6. 100% of the samples from both the seasons for deep zone are unsuitable for their use.

G) Corrosive Ratio (CR)

It is calculated using equation given in Chapter 2 (Table 2.1). For shallow zone, the values range from 0.07–12.5 with an average of 2.2 for the premonsoon season while for the

postmonsoon season the values range from 0.08–2.9 with an average of 0.7. 45% of the samples are fit for their use in the premonsoon season which increases to 81% for the postmonsoon season. For deep zone, the values range from 0.35- 1.96 with an average of 0.8 for the premonsoon season while for the postmonsoon season the values range from 0.17–1.04 with an average of 0.49. 90% of the samples from premonsoon season are suitable for their use which falls to 88% for the postmonsoon season.

3.3.2.3 Composite water quality index

Composite water quality index is calculated for drinking (DWQI) and irrigation (IWQI) using Equ. 2.2 to Equ. 2.5 (Chapter 2). Parameters used to calculate DWQI were; pH, EC, TDS, TH, total alkalinity, Mg^{2+} , Cl^- , F^- , SO_4^{2-} and NO_3^- based on WHO standards. IWQI is calculated based on MH, RSC, EC, Na%, PI and SAR. The weighting factor along with standard values for DWQI and IWQI are given in Table 2.2 and Table 2.3 respectively. The DWQI values range from 22-645 with an average of 132 for the premonsoon season and 12-490 with an average of 108 for postmonsoon season for the shallow zone (Table 3.2). For deep zone, the values range from 51-177 with an average of 91 and 15-166 with an average value of 62 for postmonsoon season (Table 3.2). The IWQI values range from -21.7 to 34.2 with an average of 11.3 for the premonsoon season and -1.4 to 30.4 with an average of 15.7 for postmonsoon season for the shallow zone (Table 3.5). For deep zone, the values range from 11 to 27 with an average value of 18 for the premonsoon season and 12.8 to 23.3 with an average value of 18 for postmonsoon season (Table 3.5). According to the composite parameters for drinking, for shallow zone 57% of samples are suitable in premonsoon season which increases to 71% in postmonsoon season. For deep zone, suitable samples for the premonsoon season are 70% that increases to 88% for postmonsoon season. The suitability of water increases in postmonsoon season which may be attributed to dilution with recharging water. The composite parameter for irrigation indicates that 100% of samples are

unsuitable for their use in premonsoon and postmonsoon seasons respectively for both the zones. The study by Sharma et al. (2017) ^[137] in Muktsar and Faridkot district of Punjab concluded that the water quality is unsuitable for the uses in majority of the locations. The study carried out in nearby districts of Bathinda by Sharma et al (2016) ^[156] concluded that parameters like F^- , TH, NO_3^- and SO_4^{2-} are above the permissible limit at most of the sampled locations. The irrigation parameters also indicate increased unsuitability during the postmonsoon season.

3.3.3 Geochemical evolution

From the piper trilinear plot ^[168] (Fig. 3.12), overall facies observed for shallow zone were Na-HCO₃ (10%), Ca-HCO₃ (12%), Na-Cl (38%), Mixed Ca-Mg-Cl (15%) and Mix Ca-Na-HCO₃ (25%) water type for the premonsoon samples. The facies observed for postmonsoon samples were Na-HCO₃ (23%), Ca-HCO₃ (23%), Na-Cl (6%), Mixed Ca-Mg-Cl (6%) and Mix Ca-Na-HCO₃ (43%) water type. The dominance of HCO₃⁻ type water is observed in postmonsoon season. This is a clear indication of increase in the pCO₂ as a result of root respiration and decaying organic etc with percolating water. The same is corroborated with increased HCO₃⁻ ions (average values: Pre: 682 mg/L and Post: 979 mg/L) and decrease in Cl⁻ ions (average value: Pre: 405 mg/L and Post: 217 mg/L) during the postmonsoon (Table 3.2).

The deep zone shows Na-HCO₃ (80%) and Na-HCO₃-Cl (20%) as dominant water type for premonsoon and Na-HCO₃ (88%) and Na-HCO₃-Cl (12%) water type for postmonsoon. A clear observation of ion change/addition can be made from the changing water types. The same is corroborated with increased HCO₃⁻ ions (average values: Pre: 637 mg/L and Post: 791 mg/L) and decrease in Cl⁻ ions (average values: Pre: 114 mg/L and Post: 95 mg/L) during the postmonsoon season (Table 3.2). A clear dominance of HCO₃⁻ ions is observed in pre and postmonsoon seasons for both the zones which can be attributed to

extensive agricultural activity of the area. This also indicates the contribution of irrigation return flow to the groundwater. The major water type reported by Sharma et al. (2016) ^[156] for the Bathinda district were Na–Mg–Cl, Na–Mg–HCO₃ and Mg–Na(Ca)–HCO₃ in the pre-monsoon and Na–Mg–Cl, Ca–Mg–HCO₃ and Mg–Ca–HCO₃ in the post-monsoon. A similar variation in water facies were found in this study.

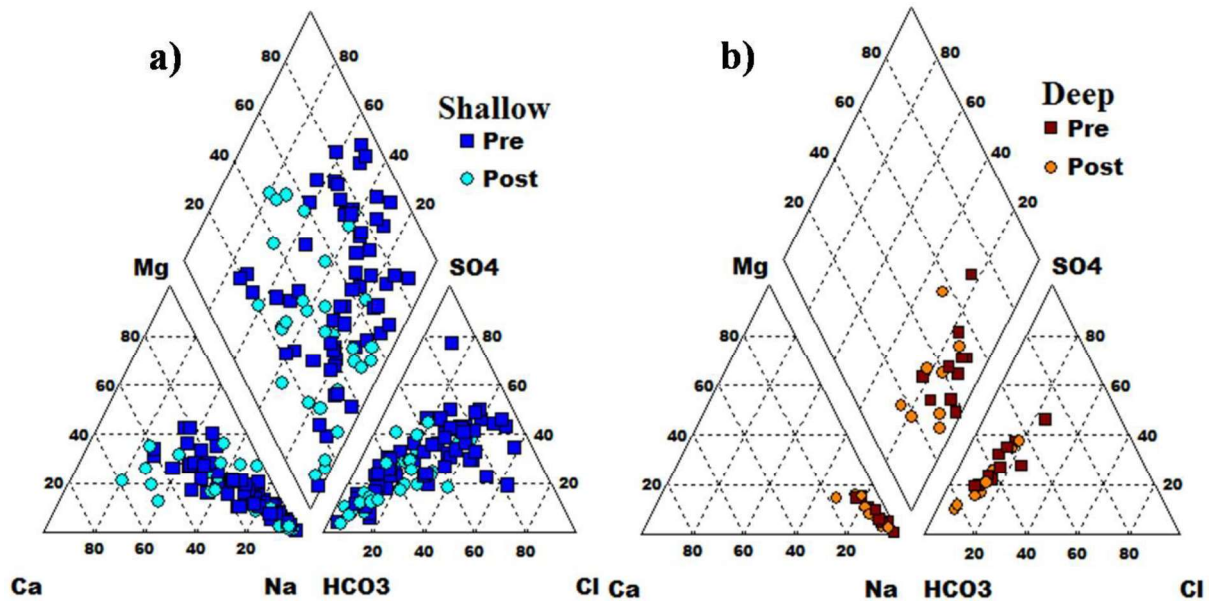


Fig. 3.12 Piper trilinear plot showing water facies for a) shallow and b) deep zones during both the seasons

It is clear from the Gibbs plot ^[152] that rock-weathering and evaporation are the dominant processes in the premonsoon and postmonsoon seasons for the shallow zone (Fig. 3.13 a, b). Deep zone groundwater shows rock weathering as the dominant process in both the seasons (Fig. 3.14 a, b).

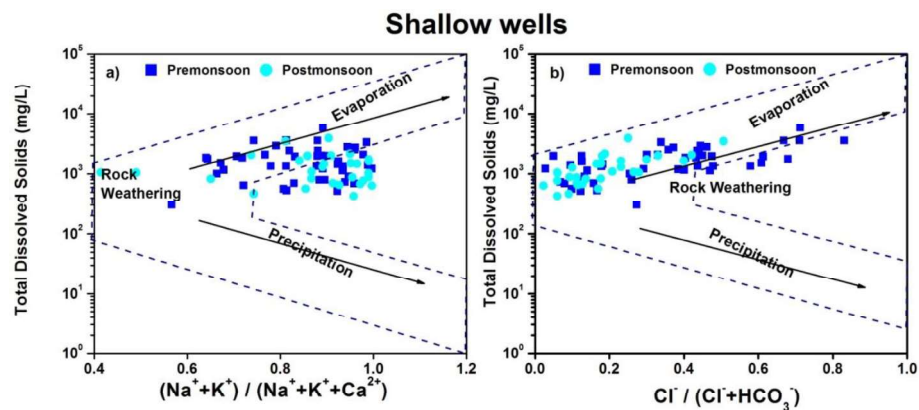


Fig. 3.13 Gibbs plot a) cationic and b) anionic for both the seasons in the shallow zone

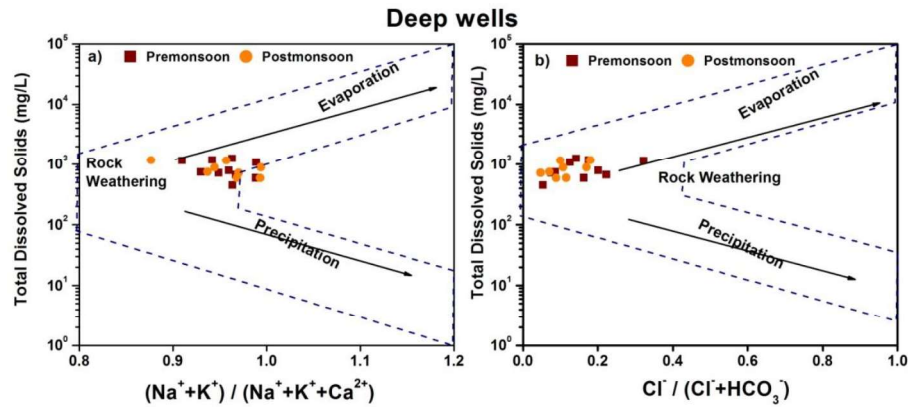
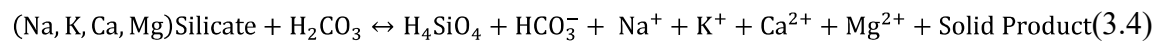


Fig. 3.14 Gibbs plot a) cationic and b) anionic for both the seasons in the deep zone

Rock-water interaction has three major processes that govern the groundwater chemistry of the study area namely carbonate weathering, silicate weathering and evaporate dissolution [167,226]. To understand the rock-water weathering mechanism, bivariate mixing plots between Na^+ -normalized Ca^{2+} versus Na^+ normalized HCO_3^- and Na^+ normalized Mg^{2+} were used. From the plot, Na^+ -normalized Ca^{2+} versus Na^+ normalized HCO_3^- (Fig. 3.15 a, b) and Na^+ -normalized Ca^{2+} versus Na^+ normalized Mg^{2+} (Fig. 3.15c, d), it can be interpreted that silicate weathering is the dominant process for both premonsoon and postmonsoon seasons of shallow and deep zones. The formation of carbonic acid and subsequent weathering of silicate minerals is shown as follows (Equ.3.3& 3.4) [227]:



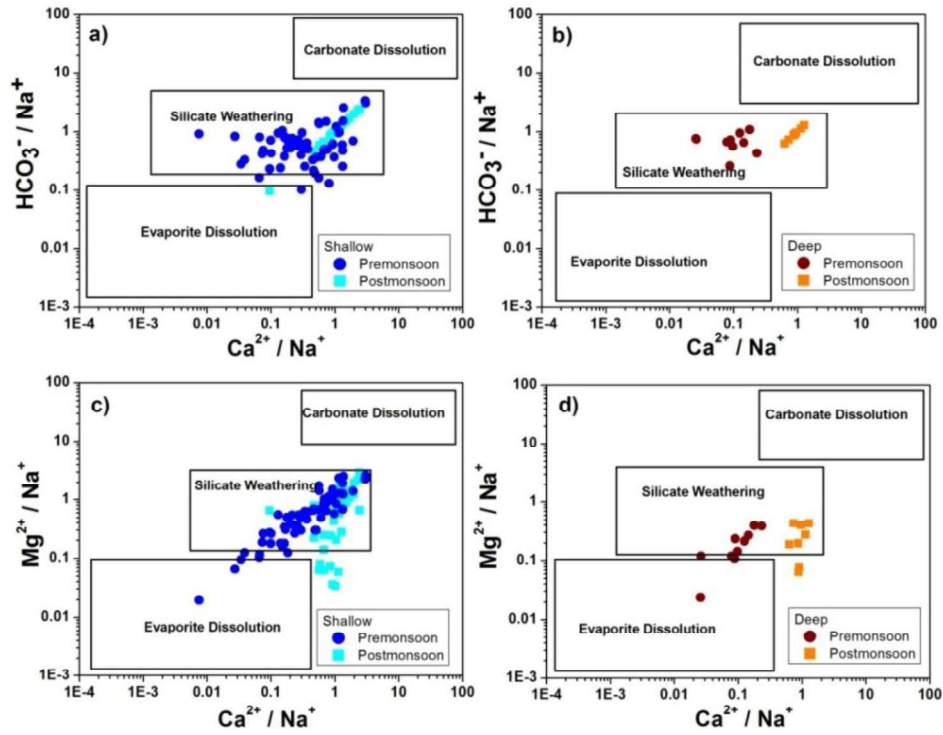


Fig. 3.15 Bivariate plots a) Shallow: Na^+ -normalized Ca^{2+} versus Na^+ normalized HCO_3^- , b) Deep: Na^+ -normalized Ca^{2+} versus Na^+ normalized HCO_3^- , c) Shallow: Na^+ -normalized Ca^{2+} versus Na^+ normalized Mg^{2+} and d) Deep: Na^+ -normalized Ca^{2+} versus Na^+ normalized Mg^{2+}

The value of Na^+/Cl^- ratio i) near to 1 is indicative of evaporation, ii) ratio between 1 and 3 is indicative of evapotranspiration and irrigation return flows (enrichment from recirculated water) and iii) higher ratio (>3) is indicative of ion exchange or silicate weathering^[150]. From the plot (Fig.3.16), it is clearly seen that most of the samples fall in the field having ratio > 3 which indicates ion exchange or silicate weathering as a dominant process in the study area. For shallow zone in the premonsoon season, 10% of the samples show evaporation effect while 43% of the samples indicate the occurrence of evaporative enrichment and 48% of the samples indicate the occurrence of ion exchange or silicate weathering process. In the postmonsoon season, the effect of evaporation decreases i.e. 7% of samples indicates evaporation process while 29% of the samples shows sign of

evaporative enrichment and 64% of the samples shows ion exchange or silicate weathering as the dominant process. In case of deep zone, for premonsoon season none of the samples has Na^+/Cl^- the ratio of one while 10% samples indicate evaporative enrichment or irrigation return flow and 90% indicates ion exchange or silicate weathering as the dominant process. During the postmonsoon season 100% of samples indicate ion exchange or silicate weathering. In the postmonsoon season of both the zone, the contribution due to ion exchange or silicate weathering shows an increase, this could be due to increased rock-water interactions. Due to longer residence time of water in the deep zone, the processes like ion exchange and silicate weathering are dominant compared to the shallow zone.

The $\text{Ca}^{2+}/\text{Mg}^{2+}$ ratio of equals 1 is indicative of the dissolution of dolomite while a higher ratio is because of the dominance of calcite dissolution [228]. The molar ratio of $\text{Ca}^{2+}/\text{Mg}^{2+} > 2$ indicates the dissolution of calcite minerals or calcium silicate weathering, while the ratio < 1 is indicative of magnesium silicate weathering [229]. These reactions contribute Ca^{2+} and Mg^{2+} to the groundwater. From the trends observed in the $\text{Ca}^{2+}/\text{Mg}^{2+}$ ratio plot (Fig. 3.16), it can be inferred that dolomite dissolution process occurs in 22% and 10% of the samples from the shallow and deep zones in premonsoon season which increases to 32% and 25% respectively during the postmonsoon season. This is corroborated with increased alkalinity in the postmonsoon season of both shallow and deep groundwater. Calcite weathering occurs in 10% of shallow zone samples from the postmonsoon season. In the study area, magnesium silicate weathering is the dominating process in 78% and 90% of the samples from shallow and deep zones from premonsoon which decreases to 58% and 75% respectively in the postmonsoon season. This is again corroborated with enhanced pCO_2 leading to formation of carbonic acid with percolating water leading to enhanced weathering.

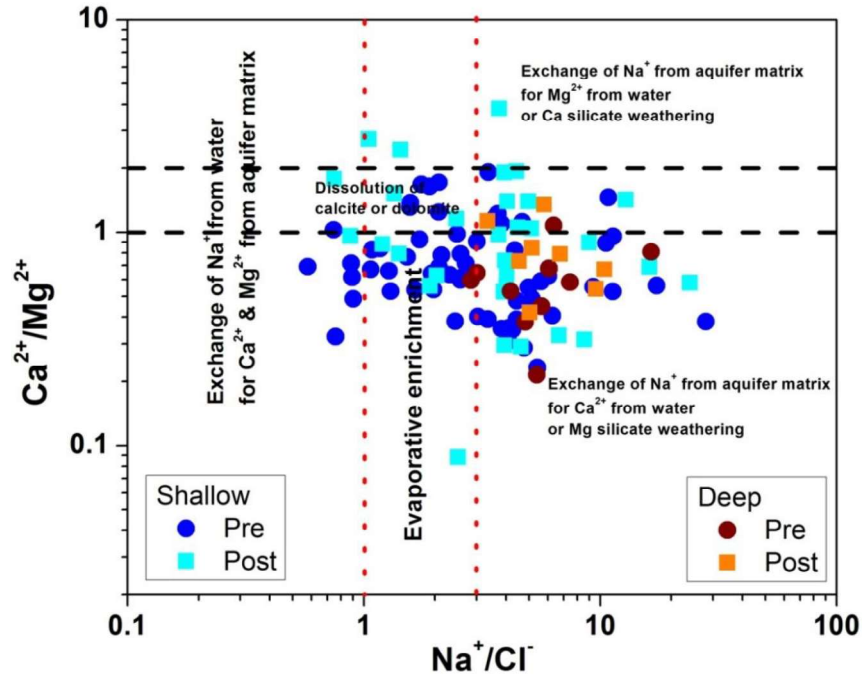


Fig. 3.16 Plot of $\text{Ca}^{2+}+\text{Mg}^{2+}$ vs $\text{Na}^{+}+\text{K}^{+}$ of groundwater samples from the study area

3.3.3.1 Ion Exchange

Ion exchange encompasses reactions between the aquifer minerals especially clay minerals and groundwater, which play a significant role in influencing the water quality ^[150]. Ion exchange processes are interpreted using chloro-alkaline indices (CAI 1 and 2) calculated using Equ. 3.5 and Equ. 3.6 ^[230].

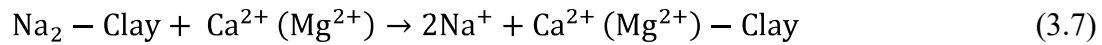
$$\text{CAI 1} = \frac{\text{Cl}^{-}-(\text{Na}^{+}+\text{K}^{+})}{\text{Cl}^{-}} \quad (3.5)$$

$$\text{CAI 2} = \frac{\text{Cl}^{-}-(\text{Na}^{+}+\text{K}^{+})}{\text{SO}_4^{2-}+\text{HCO}_3^{-}+\text{CO}_3^{2-}+\text{NO}_3^{-}} \quad (3.6)$$

If both the indices are positive, it indicates exchange between Na^{+} or K^{+} in water with Ca^{2+} or Mg^{2+} in clay and reverse exchange takes place when both the indices will be negative ^[231].

For shallow zone, the CAI-1 values range from -27 to 0.4 for the premonsoon season, while the values range from -23.03 to 0.22 for the postmonsoon season. The CAI-2 for premonsoon and postmonsoon samples ranges from -1.08 to 0.62 and -0.93 to 0.09 respectively in the shallow zone. For deep zone, the CAI-1 values are in the range of -15.5

to -1.87 for premonsoon season and -9.54 to -2.37 for postmonsoon season while the range for CAI-2 is -0.83 to -0.58 for premonsoon season and -0.79 to -0.52 for the postmonsoon season. The values indicate that the exchange of Na^+ or K^+ from rock to water in place of Ca^{2+} and Mg^{2+} from water is the dominant process in 92% of samples from premonsoon which increases to 97% in shallow zones. In the deep zone, the exchange of Na^+ or K^+ from rock to water in place of Ca^{2+} and Mg^{2+} from water is the dominant process in 100% of samples during both pre and postmonsoon seasons. The ion exchange can be written as Equ. 3.7



The plot of $(\text{Ca}^{2+} + \text{Mg}^{2+}) - (\text{HCO}_3^- + \text{SO}_4^{2-})$ versus $(\text{Na}^+ - \text{Cl}^-)$ is used to ascertain the ion exchange process occurring in the aquifer system. The linearity of this plot with a negative one slope is an indicator of the dominance of the ion exchange process [232].

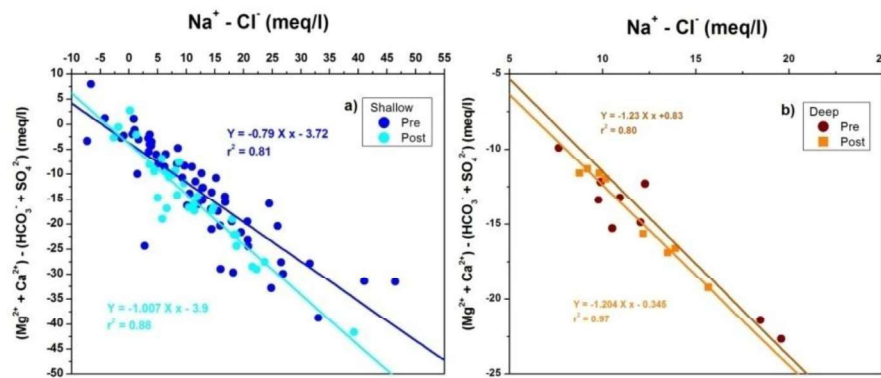


Fig. 3.17 Plot of $(\text{Na}^+ - \text{Cl}^-)$ vs. $(\text{Mg}^{2+} + \text{Ca}^{2+}) - (\text{HCO}_3^- - \text{SO}_4^{2-})$ illustrating reverse ion exchange

The groundwater samples from the shallow zone of the study area fall on the slope of -0.79 and -1.007 for premonsoon and postmonsoon seasons respectively. The samples from deep zone fall on the slope of -1.23 and -1.2 in pre and postmonsoon seasons respectively (Fig. 3.17). The tendency of deep samples is more towards the slope of -1 indicating the

dominance of exchange reaction in the deep zone. The same is also corroborated from Na^+/Cl^- ratio (Fig. 3.16) and CAI values.

3.3.3.2 Carbonate Weathering

The recharging water from irrigation or rainfall has led to high concentrations of HCO_3^- ion and moderately higher amounts of Ca^{2+} and Mg^{2+} ions in groundwater. The samples lie close to equiline (i.e. 1:1) in the plot of $(\text{Ca}^{2+} + \text{Mg}^{2+})$ vs. $(\text{SO}_4^{2-} + \text{HCO}_3^-)$ when the dissolution of calcite, dolomite and gypsum are the dominant processes occurring in the aquifer. The shift in the samples either to left and right is observed due to processes like ion exchange, reverse ion exchange and silicate weathering [232, 233].

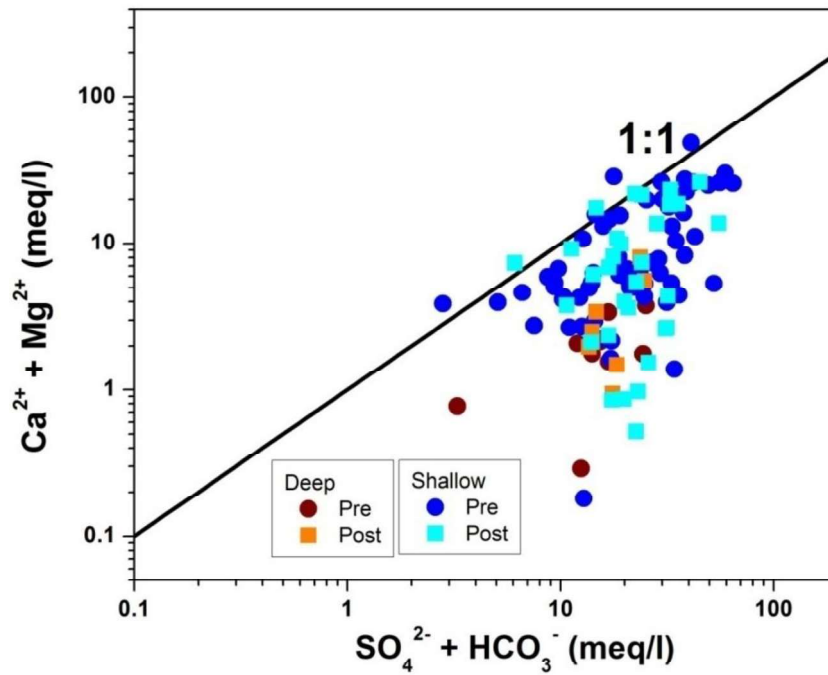


Fig. 3.18 Plot of $(\text{Ca}^{2+} + \text{Mg}^{2+})$ vs. $(\text{SO}_4^{2-} + \text{HCO}_3^-)$ of groundwater samples from the study area

From the plot (Fig. 3.18) of $(\text{Ca}^{2+} + \text{Mg}^{2+})$ vs. $(\text{SO}_4^{2-} + \text{HCO}_3^-)$, it was observed that most of the samples fall below the equimolar line indicating more concentration of $\text{SO}_4^{2-} + \text{HCO}_3^-$ over $\text{Ca}^{2+} + \text{Mg}^{2+}$. This higher HCO_3^- ions is attributed to the reaction of feldspar minerals with carbonic acid [234] or organic matter oxidation and root respiration leading to higher pCO_2 in soil pores. The higher SO_4^{2-} ions can be due to pyrite oxidation or gypsum

dissolution from the use of fertilizers. The SO_4^{2-} ions solubilize with irrigation return flow and groundwater shows $\text{SO}_4^{2-}/\text{Cl}^-$ ratio >0.05 [235] which is observed in samples from both shallow and deep zones. The other reason for the shift to $\text{SO}_4^{2-} + \text{HCO}_3^-$ is the exchange of Ca^{2+} and Mg^{2+} ions in water for Na^+ and K^+ ions in the aquifer matrix. The inference from Fig. 3.17 confirms that ion exchange process is controlling the alkaline earth metal concentration in the groundwater. Few samples lie close to equiline which indicates dolomite dissolution and samples lying above equiline indicates the exchange of Ca^{2+} and Mg^{2+} from rock to water in place of Na^+ in water.

3.3.3.3 Silicate Weathering

The silicate weathering process is an important process that controls the groundwater chemistry and can be evaluated by the relationships among the major ions present in the groundwater. In the study area, alkali metals ($\text{Na}^+ + \text{K}^+$) ions dominate over alkaline earth metal ions ($\text{Ca}^{2+} + \text{Mg}^{2+}$) which are clear from Fig. 3.19.

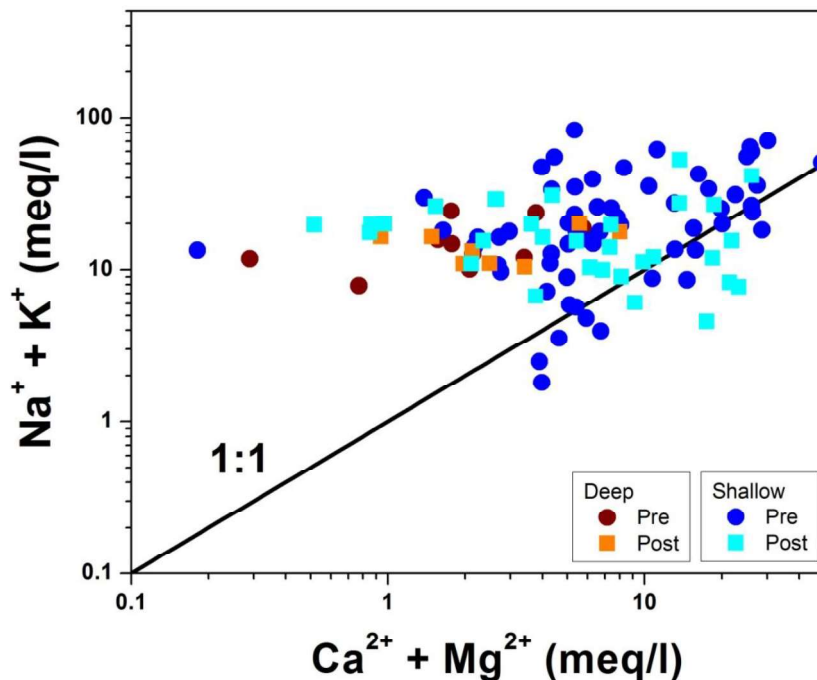


Fig. 3.19 Plot of ($\text{Na}^+ + \text{K}^+$) vs ($\text{Ca}^{2+} + \text{Mg}^{2+}$) for groundwater samples from the study area

The lower concentration of alkaline earth metals is also corroborated from Fig. 3.16. Thus, excess of HCO_3^- and SO_4^{2-} (Fig. 3.18) is balanced by ions due to silicate weathering or evaporate dissolution. To ascertain the silicate weathering occurring in these groundwaters, the relationship between the total ion concentration and the sum of Na^+ and K^+ (Fig. 3.20) is evaluated, the samples fall on or above 1:1 line. This indicates that Na and K- silicate weathering is not the dominant process contributing alkali metal ions to groundwater.

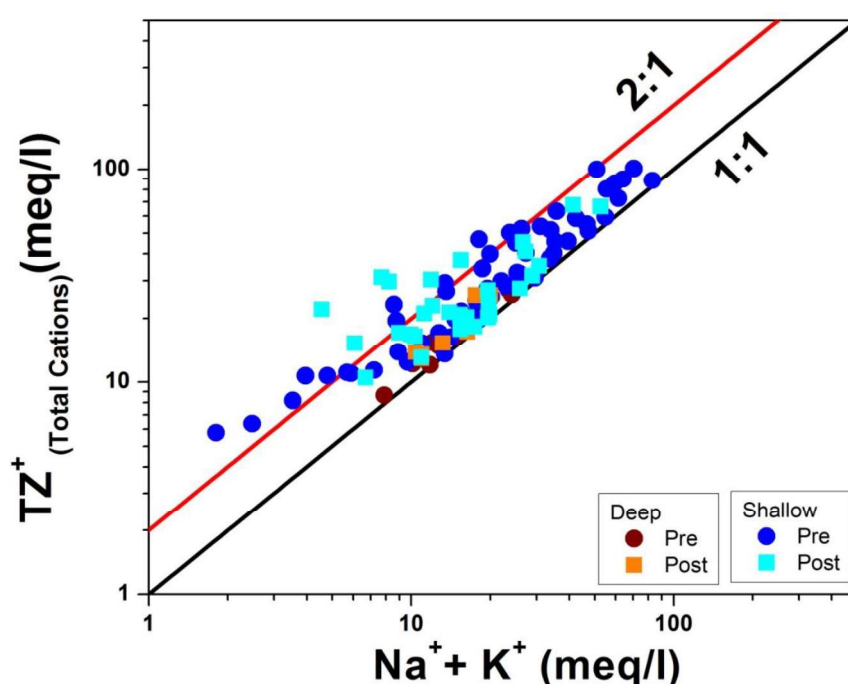


Fig. 3.20 Plot of TZ^+ vs $\text{Na}^+ + \text{K}^+$ of groundwater samples from the study area

Hence it can be concluded that Na^+ ions from the aquifer matrix is replaced with Ca^{2+} and Mg^{2+} ions from water. Thus ion-exchange is the source for Na^+ ions. The source of Mg^{2+} ions is magnesium silicate weathering and Ca^{2+} ions is the result of calcite or dolomite dissolution. Similar geochemical processes were observed by Kumar et al. (2007) in Muktsar district of Punjab [152].

3.3.4 Source and recharge mechanism of groundwater

The environmental deuterium ($\delta^2\text{H}$) in the groundwater ranges from -68.24‰ to -18.41‰ and -71.07‰ to -29.29‰ for premonsoon and postmonsoon seasons respectively in samples from shallow zone. The $\delta^2\text{H}$ ranges for the premonsoon and postmonsoon season are -53.43‰ to -31.13‰ and -62.31‰ to -46.37‰ respectively in samples from the deep zone. The environmental oxygen-18 ($\delta^{18}\text{O}$) in the groundwater from shallow zone is in range of -10.16‰ to -1.94‰ for the premonsoon season while its value for the postmonsoon season ranges from -10.04‰ to -3.28‰. The $\delta^{18}\text{O}$ values in samples from deep zone for premonsoon and postmonsoon samples are in the range of -8.88‰ to -5.64‰ and -11.3‰ to -7.24‰ respectively. From the box plot of isotopic values, it can be clearly seen that more spread is seen in shallow zone compared to the deep zone in both the seasons (Fig. 3.21) indicating multiple sources contributing to the recharge of the shallow zone groundwater.

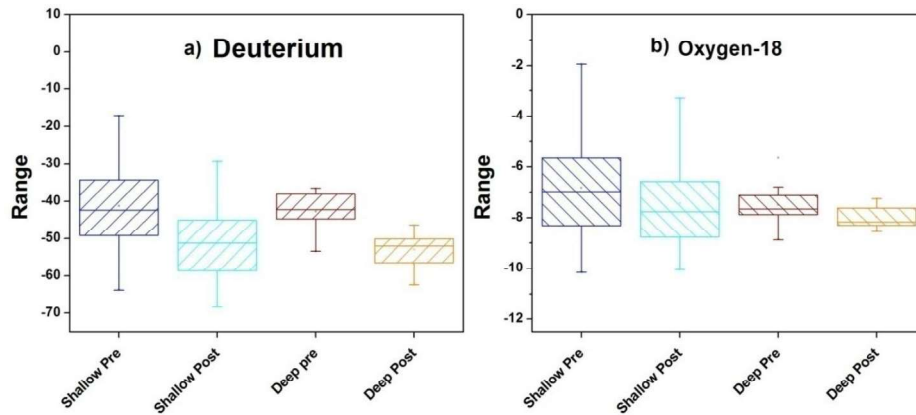


Fig. 3.21 Box plot for a) Deuterium and b) Oxygen-18 for both the seasons and both the zones

Deuterium excess ($D_{\text{excess}} = \delta^2\text{H} - 8 \times \delta^{18}\text{O}$) assesses the control of the relative humidity and evaporation of precipitation in a given area ^[190]. D_{excess} values $<10\text{‰}$ represent evaporative enrichment and values $>10\text{‰}$ represent the contribution of recycled moisture. The D_{excess} value for samples in the shallow zone of the study area ranges from -1.44‰ to

27.79‰ for premonsoon and -9.97‰ to 19.12‰ for the postmonsoon season. In the deep zone, the D_{excess} ranges from 8.38‰ to 22.06‰ and 4.86‰ to 18.96‰ for premonsoon and postmonsoon seasons respectively. The samples can be categorized based on the D_{excess} values and they were grouped into categories i.e. $<5\text{‰}$, 5‰ to 15‰ and $>15\text{‰}$ (Fig. 3.22). The variations in the D_{excess} values of groundwater depend on characteristic local hydro-meteorological processes. 11% and 27% of the premonsoon and postmonsoon samples respectively have $D_{\text{excess}} < 5\text{‰}$ from the shallow zone (Fig. 3.22a). For deep zone, none of the premonsoon samples has $D_{\text{excess}} < 5\text{‰}$ while 11% of the postmonsoon samples have $D_{\text{excess}} < 5\text{‰}$ (Fig. 3.22b). The samples having D_{excess} between 5‰ to 15‰ for the shallow zone are 52% and 68% for premonsoon and postmonsoon seasons respectively (Fig. 3.22 a). For deep zone, 20% of premonsoon and 78% of the postmonsoon samples fall under the category of D_{excess} in range of 5‰ to 15‰ (Fig. 3.22 b). The samples having $D_{\text{excess}} > 15\text{‰}$ are 37% and 5% for the pre and postmonsoon seasons respectively for shallow zone while for the deep zone are 80% and 11% respectively (Fig. 3.22 a, b).

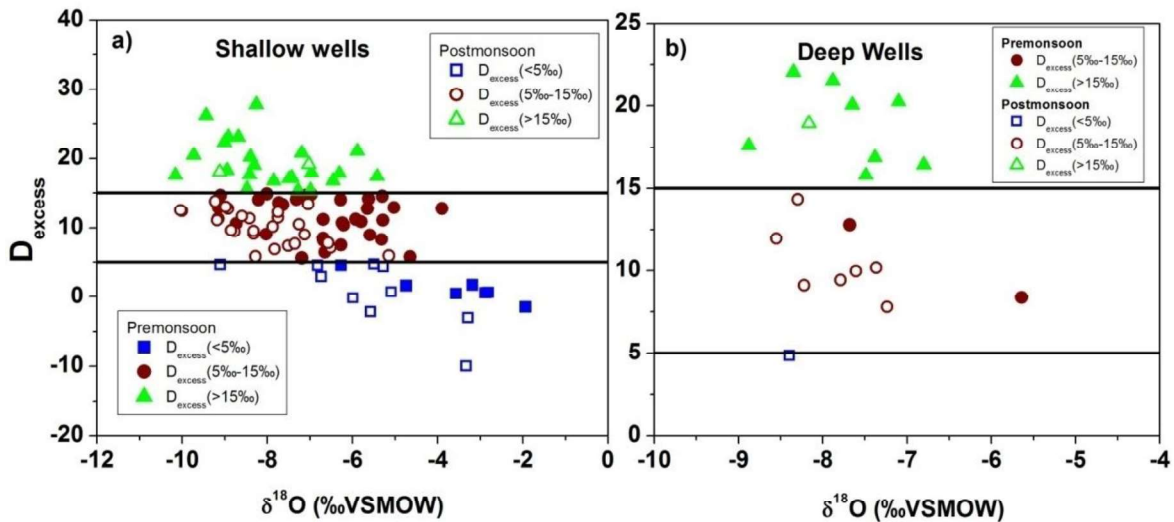


Fig. 3.22 D_{excess} vs $\delta^{18}\text{O}$ plot for both the seasons from the shallow and deep zones

The samples having D_{excess} values less than 15‰ fall close to the global meteoric water line (GMWL) established by Rozanski et al. (1992) ^[236] and local meteoric water line

(LMWL) for Chandigarh ^[237]. The equation for GMWL and LMWL are given as Equ. 3.8 and Equ. 3.9 respectively (Fig. 3.23).

$$\text{GMWL: } \delta^2\text{H} = 8.17(\pm 0.06) \times \delta^{18}\text{O} + 10.35(\pm 0.65) \quad n=206; r^2=0.99 \quad (3.8)$$

$$\text{Chandigarh (LMWL): } \delta^2\text{H} = 7.6 (\pm 0.10) \times \delta^{18}\text{O} + 4.4 (\pm 0.50) \quad r^2=0.95 \quad (3.9)$$

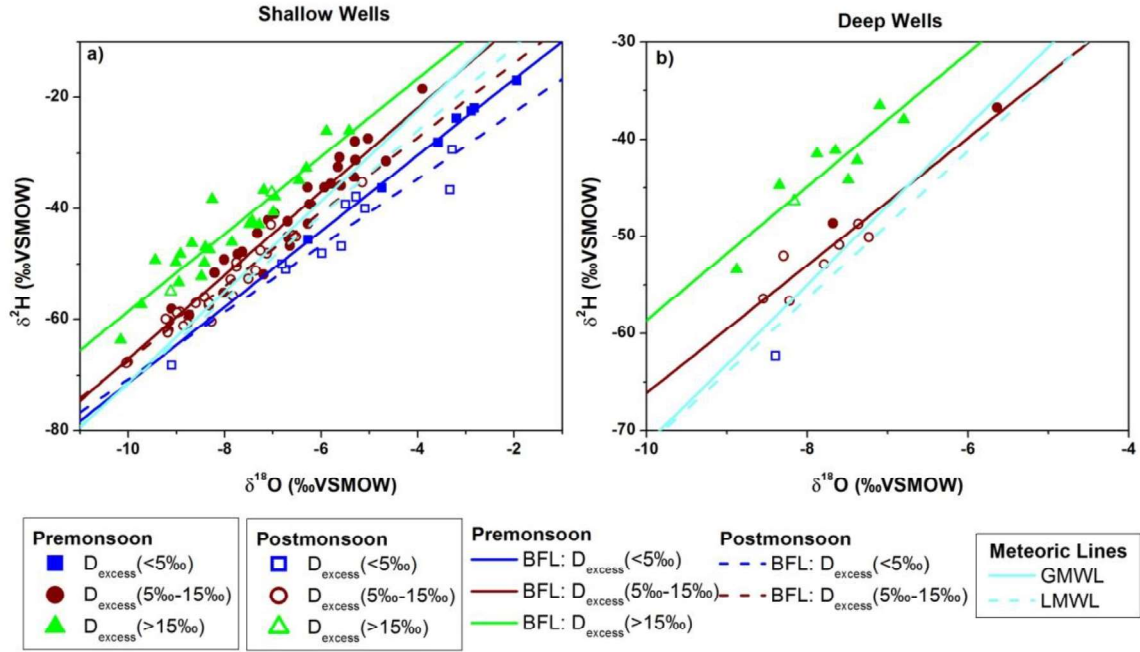


Fig. 3.23 Stable isotope plot for a) shallow and b) deep zone for both the seasons

The BFL for premonsoon having $D_{\text{excess}} < 5\text{‰}$, 5‰ to 15‰ and $> 15\text{‰}$ are given in Equ. 3.10 to Equ. 3.12 for the shallow zone (Fig. 3.23 a).

$$D_{\text{excess}} < 5\text{‰}: \delta^2\text{H} = 6.84(\pm 0.06) \times \delta^{18}\text{O} - 3.03(\pm 0.51) \quad n=7; r^2=0.99 \quad (3.10)$$

$$D_{\text{excess}} 5\text{‰}-15\text{‰}: \delta^2\text{H} = 7.5(\pm 0.06) \times \delta^{18}\text{O} + 8.26 (\pm 0.51) \quad n=32; r^2=0.93 \quad (3.11)$$

$$D_{\text{excess}} > 15\text{‰}: \delta^2\text{H} = 6.99 (\pm 0.06) \times \delta^{18}\text{O} + 11.36 (\pm 0.51) \quad n=23; r^2=0.88 \quad (3.12)$$

The BFL for postmonsoon having $D_{\text{excess}} < 5\text{‰}$, 5‰ to 15‰ and $> 15\text{‰}$ are given in Equ. 3.13 to Equ. 3.14 for the shallow zone (Fig. 3.23 a).

$$D_{\text{excess}} < 5\text{‰}: \delta^2\text{H} = 6.01(\pm 0.06) \times \delta^{18}\text{O} - 10.63(\pm 0.51) \quad n=10; r^2=0.91 \quad (3.13)$$

$$D_{\text{excess}} 5\text{‰}-15\text{‰}: \delta^2\text{H} = 6.7 (\pm 0.06) \times \delta^{18}\text{O} - 0.41 (\pm 0.51) \quad n=25; r^2=0.94 \quad (3.14)$$

$D_{\text{excess}} > 15\text{‰}$: similar to premonsoon

The BFL for premonsoon having D_{excess} 5‰ to 15‰ and postmonsoon samples having $D_{\text{excess}} > 15‰$ are given in Equ. 3.15 to Equ.3.16 respectively for the deep zone (Fig. 3.23 b).

$$D_{\text{excess}} \text{ 5‰-15‰: } \delta^2\text{H} = 6.84 (\pm 0.06) \times \delta^{18}\text{O} + 9.9 (\pm 0.51) \quad n=8; r^2=0.8 \quad (3.15)$$

$$D_{\text{excess}} > 15‰: \delta^2\text{H} = 5.18 (\pm 0.06) \times \delta^{18}\text{O} - 11.78 (\pm 0.51) \quad n=7; r^2=0.72 \quad (3.16)$$

From these plots, it can be concluded that post precipitation evaporation and mixing while passing through the soil are the reasons for the observed isotopic signatures in groundwater of this region. Similar trend lines were observed by Gupta et al. (2004) in central India [238]. The precipitation water gets modified isotopically before it recharges the aquifer via processes like mixing and evapotranspiration. Mixing is a process in which different rainfall events gets mixed before recharging. Precipitation while passing through the soil zone involves diffusion and dispersion, expansion and drainage of soil moisture storage and vapour phase movement. As a result of these processes, the isotopic composition of groundwater at any location tends to reach a characteristic value.

The samples showing $D_{\text{excess}} < 5‰$, show slight enrichment with the slope of 6.84 and intercept of -3.03 for the shallow zone which may be due to evaporation of soil moisture before adding to the groundwater (Fig. 3.23a). Gupta et al. (2004) observed the slope of 6.5 and intercept of -2.8 which is close to observation made in the study [238]. They also concluded the evaporation of moisture before recharging the aquifer system. In the postmonsoon, the slope and intercept are 6.01 and -10.63 respectively, more evaporation effect is observed for the postmonsoon season in the shallow zone. The premonsoon samples with D_{excess} values between 5‰ to 15‰ have the slope of 7.53 and intercept of 8.26 which is very close to the LMWL with the slope of 7.6 and intercept of 4.4 indicating precipitation as a source of recharge to the shallow zone (Fig. 3.23a). Postmonsoon samples have a slope of 6.7 and intercept of -0.41, which indicates slight evaporation of water before contributing to the groundwater. The BFL of premonsoon samples with $D_{\text{excess}} > 15‰$ from the shallow

zone have the slope of 6.99 and intercept of 11.36, the samples show slight enrichment but fall close to GMWL indicating contribution of regional groundwater flow. Postmonsoon samples also follow a similar trend. This indicates that few samples are receiving recharge from regional flow in both the seasons in the shallow zone.

For the premonsoon season of the deep zone, the slope and intercept of BFL of samples having D_{excess} values in the range of $>15\text{‰}$ are 6.84 and 9.9 respectively, which is close to GMWL. These samples also show slight enrichment and have the signatures of regional groundwater. In the postmonsoon, samples from deep zone having D_{excess} in range of 5‰ to 12‰ have a slope of 5.18 and intercept of -11.78. These samples show the evaporation effect and contribution from slight mixing with the shallow zones.

Hence, it can be concluded that the source of recharge to groundwater in shallow zone is evaporated local rain i.e. irrigation return flow, direct local precipitation and minor contribution from regional groundwater flow. The recharge source to deep zone is regional groundwater flow and minor contributions from irrigation return flow through vertical leakage.

The chemical inferences like Na^+ ions and TDS etc corroborate the same. The average value for Na^+ ion in the premonsoon and postmonsoon seasons for deep zone is 346 mg/L and 330 mg/L respectively while for TDS are 861 mg/L and 844 mg/L. The high concentration of Na^+ and TDS indicates long residence time hence increased rock-water interaction leading to increased concentrations (Table 3.2).

Keesari et al. (2017), worked in the south-west region of Punjab and observed the recharge source to shallow groundwater as canal influence and recharge by precipitation and irrigation return flow ^[239]. The deep zone receives the recharge from the regional flow.

The BFL of the samples indicated evaporation of water before recharging the groundwater as it had a slope of 5.3 and intercept of -15. Sharma et al. (2017) ^[240] worked in

Bathinda and Mansa district of Punjab and observed multiple sources contributing to the shallow zone of the study area namely irrigation return flow, canal contribution, precipitation etc. The BFL of their samples had a slope of 5.7 and intercept of -12.1 which is indicative of evaporation effect. The results from their finding corroborate results of this study.

The precipitation signature of south-west Punjab was taken from Keesari et al (2017) [239]. The canal water isotopic signature values were taken from Sharma et al. (2017) [240]. From the depth profile of $\delta^{18}\text{O}$ (Fig. 3.24), it can be concluded that sample from shallow zone lie in three regions i.e. i) close to canal water which is indicative of mixing with canal water (-10 ‰ to -9‰), ii) in the region of precipitation i.e. in $\delta^{18}\text{O}$ between -8‰ to -6‰ which indicates precipitation as the recharge source and iii) samples showing evaporative signature (-4‰ to -2‰) which is indicative of evaporated local rain i.e. irrigation return flow. The deep zones show the signature of slight mixing with shallow zone due to vertical well leakage and precipitational recharge. As observed from Fig. 3.24b during the postmonsoon season the contribution from irrigation return flow is reduced which can be attributed to increased regional flows during the postmonsoon season flushing out the signature of irrigation return flow. This is also corroborated by the BFL for D_{excess} values >15‰ for the postmonsoon season of both shallow and deep zones.

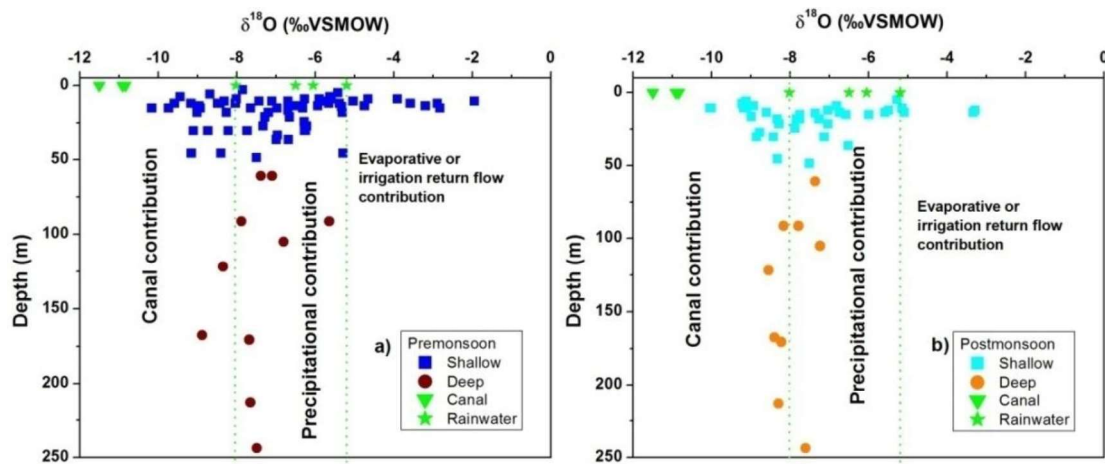


Fig. 3.24 Stable isotope plots for a) shallow and b) deep zones for both the seasons

The tritium values range from 1.5 TU to 8.2 TU in shallow zone while for deep zone, the tritium content is in range of 1 TU to 2.5 TU. One deep zone sample shows high tritium content of 4 TU which may be attributed to vertical leakage (Fig. 3.25). Presence of modern tritium in both the zones indicate modern recharge but the shallow zone is more dynamic compared to deep zones. This is also corroborated from the increased Na^+ and TDS values for the deep zones, which is the result of enhanced rock-water interactions due to long residence time.

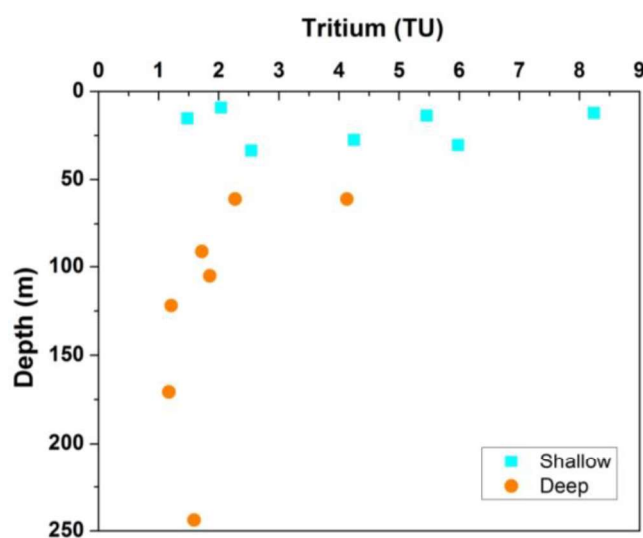


Fig. 3.25 Depth profile for tritium for shallow and deep zones

From the stable isotope and tritium values, it can be concluded that shallow zone is getting recharged from evaporated local rain i.e. irrigation return flow, local precipitation, canal contribution while deep zone gets recharged by regional flow and some location shows the signature of mixing with shallow zone. The same can be corroborated from increased NO_3^- ion concentration in the few samples from deep zones. The schematic diagram for the groundwater system and flow is given in Fig. 3.26

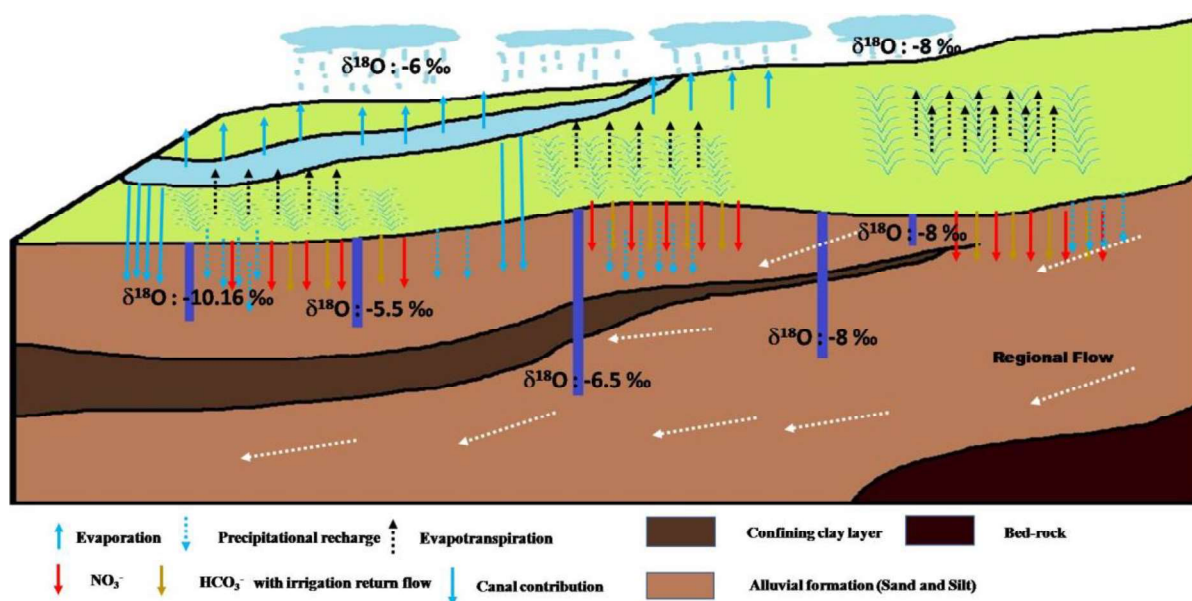


Fig. 3.26 Schematic diagram for groundwater recharge and flow

3.3.5 Factors impacting uranium distribution in groundwater

3.3.5.1 Uranium distribution: Spatial and Temporal

A) Uranium distribution and seasonal variation

The total dissolved uranium ranges from 1-610 $\mu\text{g/L}$ with an average value of 210 $\mu\text{g/L}$ for the premonsoon season and 10-565 $\mu\text{g/L}$ with an average value of 90 $\mu\text{g/L}$ for the postmonsoon season for the shallow zone. For deep zone, the dissolved uranium concentration ranges from 21-260 $\mu\text{g/L}$ with an average of 95 $\mu\text{g/L}$ for the premonsoon season while for postmonsoon the value ranges from 16-135 $\mu\text{g/L}$ with an average value of 3 $\mu\text{g/L}$ (Table. 3.2). The deep zone has a low average concentration of dissolved uranium compared to shallow zone in both the seasons (Fig. 3.27). This indicates that deep zones are comparatively less vulnerable to local anthropogenic activities/contamination. The decrease in uranium concentration in the postmonsoon season of both the zones can be attributed to dilution with recharging water.

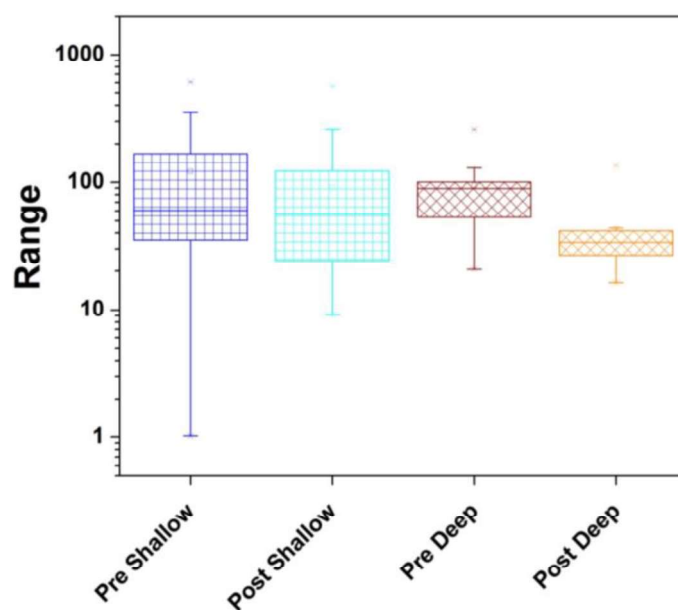


Fig. 3.27 Box plot of uranium in both the zones and both the seasons

The drinking water permissible guidelines as per WHO ^[60] and AERB ^[95] are 30 µg/L and 60µg/L respectively. 79% and 49% of the samples are above the guidance values of WHO ^[60] and AERB ^[95] for the premonsoon season while for postmonsoon season 71% and 45% of the samples are above the guideline values respectively for the shallow zones (Fig. 3.28). In deep zones, 90% and 60% of the samples are above the permissible limits by WHO ^[60] and AERB ^[95] respectively for premonsoon season which decreases to 62% and 12% respectively in postmonsoon season. A decrease in uranium contamination can be attributed to dilution with recharging water or decrease in the physico-chemical parameters promoting release of uranium from aquifer matrix to groundwater. Similar uranium concentration was reported by researchers in different districts of Punjab ^[97-116].

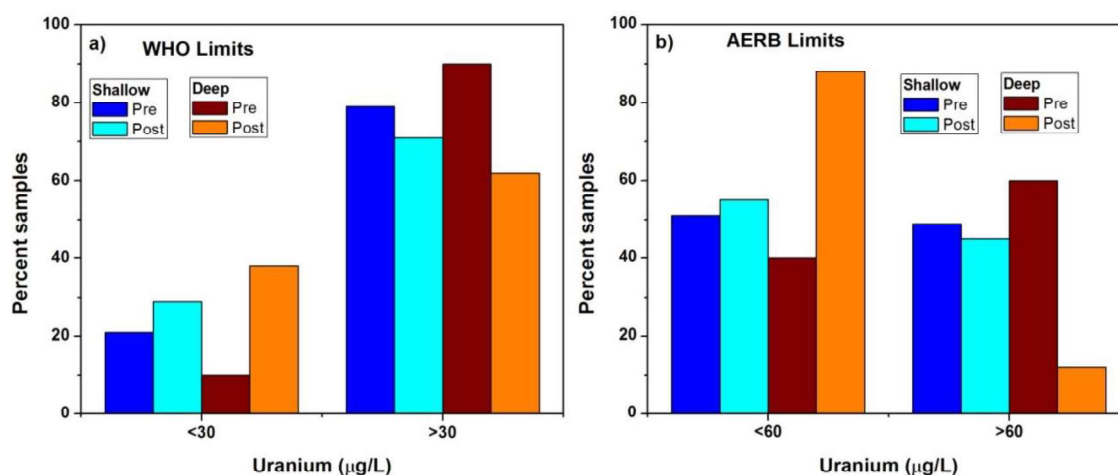


Fig. 3.28 Percent samples above a) WHO and b) AERB limits

B) Spatial distribution

Spatial distribution of dissolved uranium concentration is shown in Fig. 3.29. During the premonsoon season, the high uranium concentration is observed in the northern, eastern and southern part of the study area with patches in the central region (Fig. 3.29a). The highest concentrations are observed in the south-west locations of the study area. During the postmonsoon season, the trend remains more or less the same with an increased concentration in the south-western location and dilution in the central and eastern locations of the study area (Fig. 3.29b). Similar spatial trends for uranium were observed by Rishi et al. 2017^[110] for south-west Punjab.

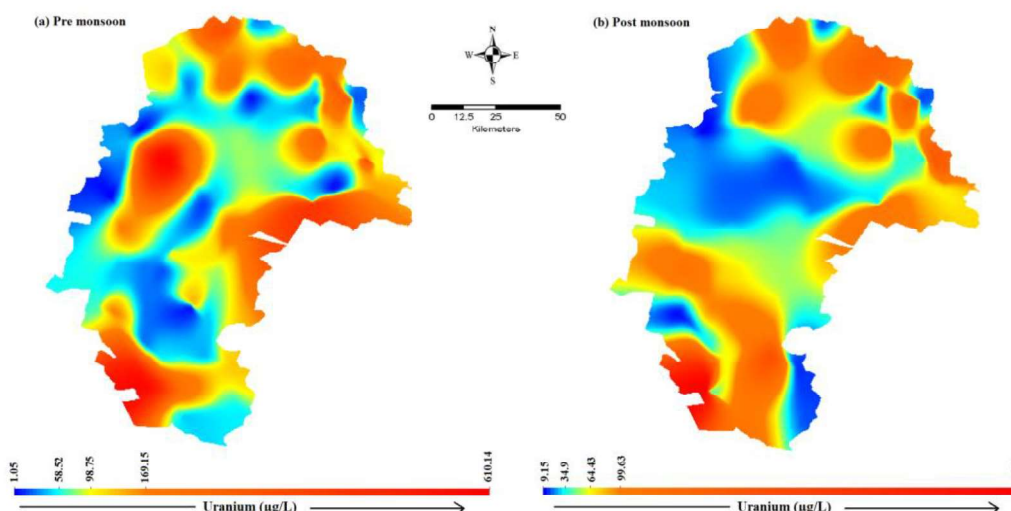


Fig. 3.29 Spatial distribution of dissolved uranium a) premonsoon and b) postmonsoon

From the spatial distribution of HCO_3^- ions, higher concentration is observed in the northern, eastern and southern location with patches in central locations which are similar to the uranium spatial trends during the premonsoon season. For the postmonsoon season, high concentration of HCO_3^- ions is observed in the northern, eastern and central locations. During the postmonsoon season, increased HCO_3^- ion concentration is observed in south-east location and central locations. From the spatial distribution, an increase in HCO_3^- concentration during the postmonsoon season is observed that is attributed to the increased dissolution from the root zone CO_2 percolating along with recharging water (Fig. 3.30). A correlation between HCO_3^- ions and uranium can be observed in the premonsoon season which corroborated the high concentration of uranium during the premonsoon season while during the postmonsoon season a weak correlation can be seen from the spatial distribution plot. Thus, decreasing the uranium concentration during the postmonsoon season (Fig. 3.29 b).

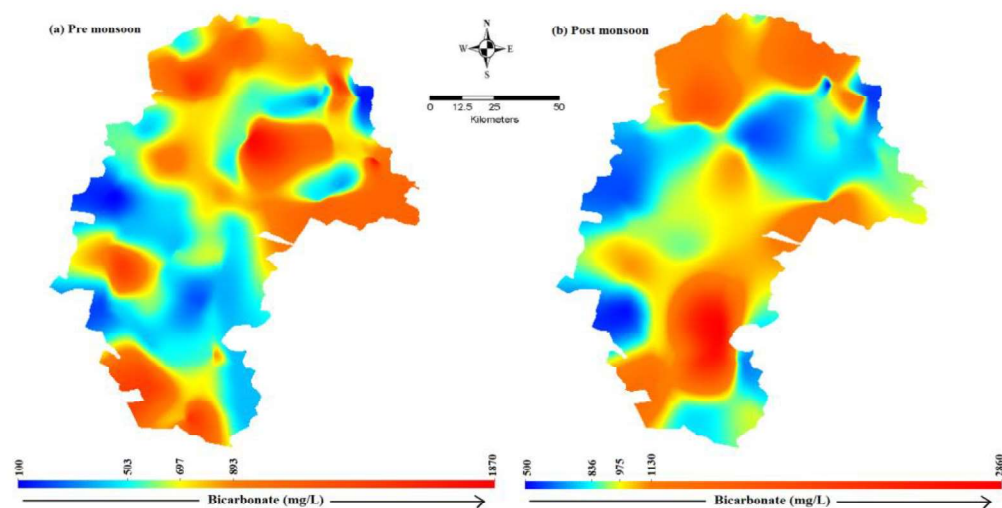


Fig. 3.30 Spatial distribution of HCO_3^- in a) premonsoon and b) postmonsoon seasons

The NO_3^- ion concentration is found to be high in the south-west, south-east, northern and patches in west and east locations of the study area during the premonsoon season. The NO_3^- ion concentration from premonsoon season again corroborate high uranium

concentration at similar locations. In the postmonsoon season, high NO_3^- ion values are observed in the northern, central and eastern part of the district. During the postmonsoon season, the correlation between uranium and NO_3^- ions is very weak. This corroborates the decrease in uranium concentration observed in the postmonsoon season. It is clear from the spatial trends in pre and postmonsoon seasons that location having high uranium either has high HCO_3^- ions or high NO_3^- ions or both.

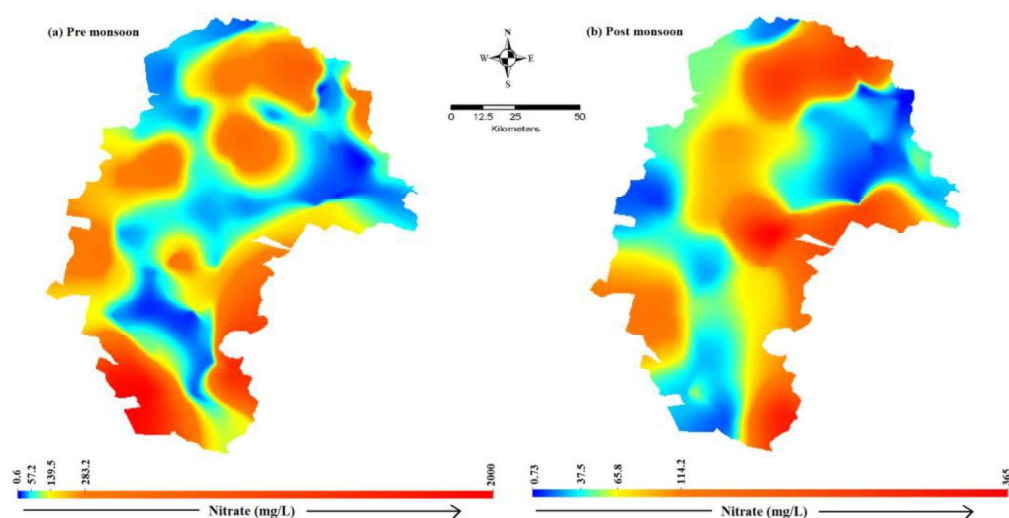


Fig. 3.31 Spatial distribution of NO_3^- in a) premonsoon and b) postmonsoon seasons

A similar interpretation was made by Sharma et al. 2017^[111] in Bathinda and Mansa district of Punjab. They concluded that HCO_3^- ions help in complexing uranium and migrating to far regions. Tripathi et al. (2012)^[102] attributed the elevated concentration to increased pCO_2 due to agricultural activity that led to increased HCO_3^- ions which mobilize uranium.

C) Depth profile

The depth profile (Fig. 3.34) of uranium indicates that the contamination due to uranium is limited to shallow zone with few patches in the deep zone. The high value in uranium in the deep zone can be attributed to mixing from the shallow zone at few locations. During the postmonsoon season, a decrease is observed in for both shallow and deep zones.

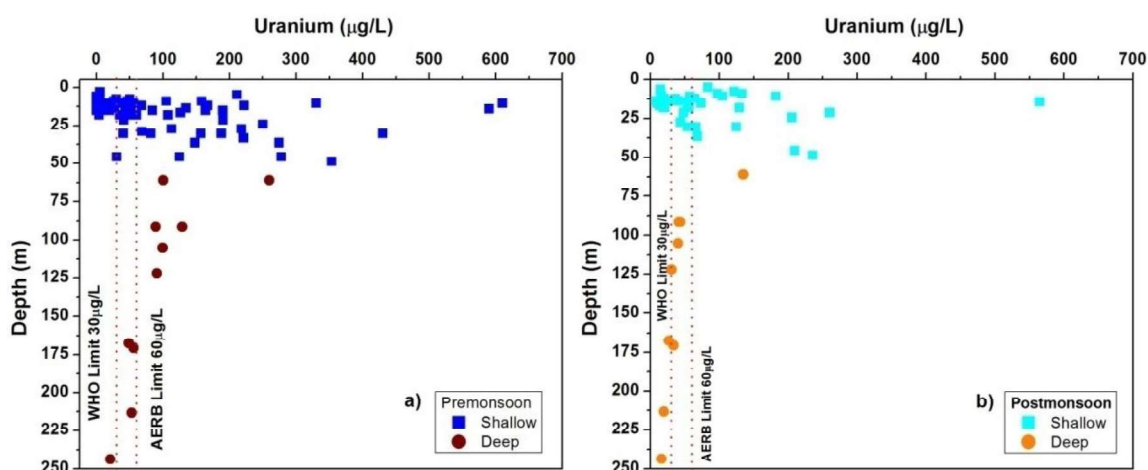


Fig. 3.32 Depth profile of uranium for a) shallow and b) deep zone for both the seasons

From the correlation plot between uranium and HCO_3^- ions, a positive correlation is inferred for the premonsoon season, which decreases during the postmonsoon season for both shallow and deep zones (Fig. 3.33).

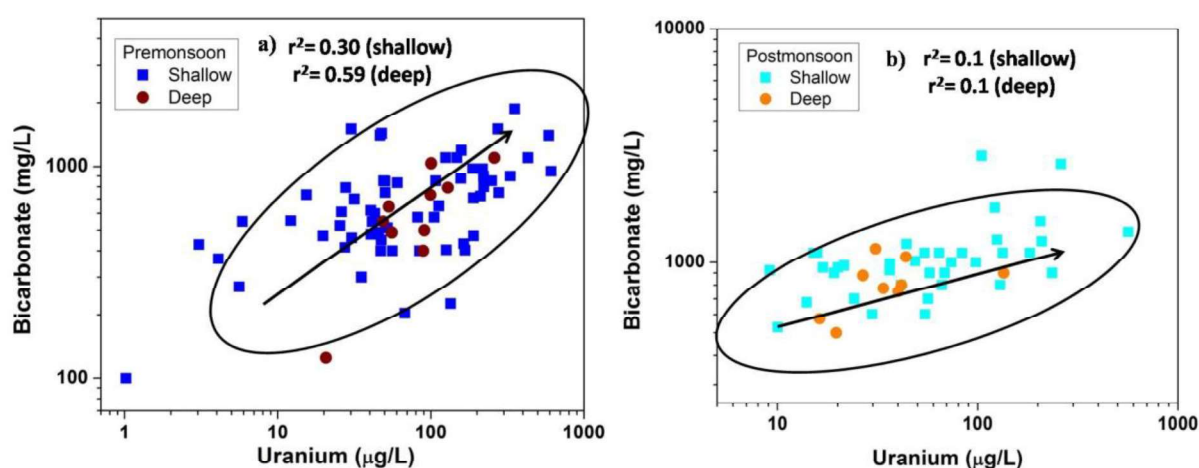


Fig. 3.33 Correlation of uranium with HCO_3^- ions in a) premonsoon and b) postmonsoon seasons for both the zones

From the plot of NO_3^- ions vs. uranium (Fig. 3.34), a strong positive correlation is observed in the premonsoon season which is also corroborated from the spatial distribution (Fig. 3.31). For postmonsoon season correlation is not much evident.

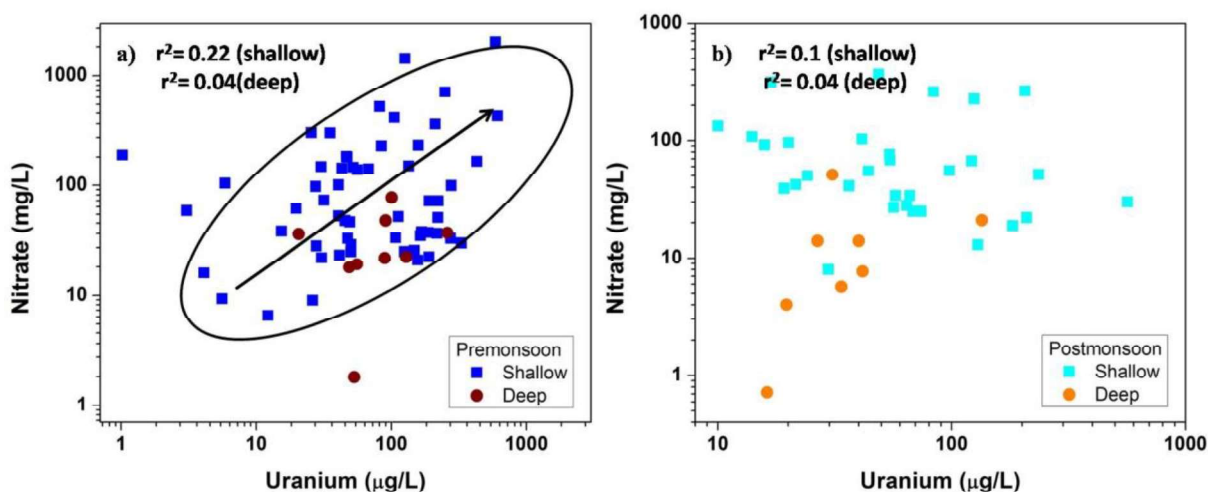


Fig. 3.34 Correlation of uranium with NO_3^- ions in a) premonsoon and b) postmonsoon seasons for both the zones

Uranium also shows a positive correlation with EC (Fig. 3.35) during both the seasons in both the zones. The correlation decreases in postmonsoon season.

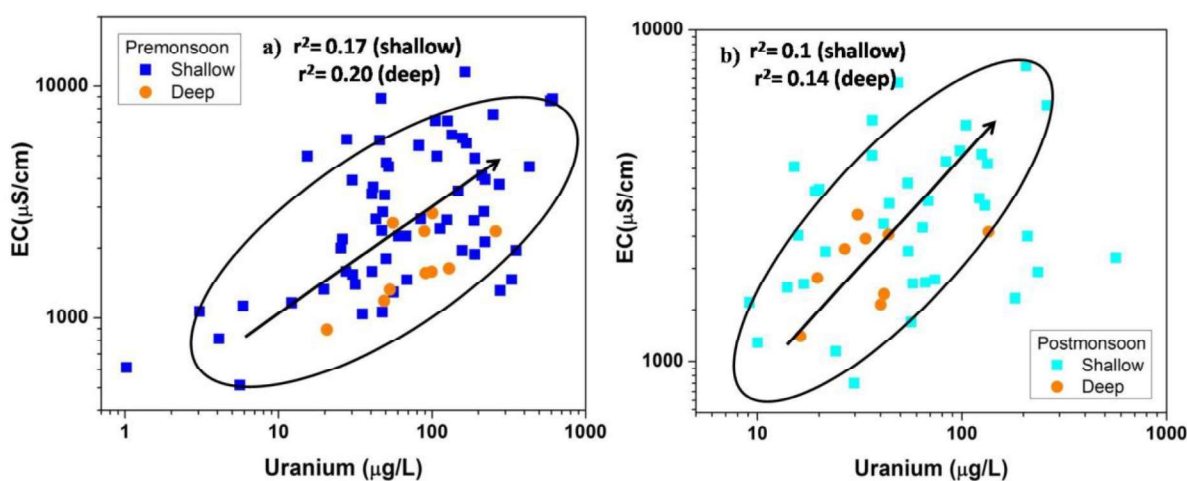


Fig. 3.35 Correlation of uranium with EC in a) premonsoon and b) postmonsoon season.

The HCO_3^- ions, NO_3^- ions and EC all show decreased correlation for the postmonsoon season of both shallow and deep zones. Thus, corroborating the decreased uranium concentration for the postmonsoon season. The details on the release mechanism is given under chapter 5

From the depth profile of $\delta^{18}\text{O}$ (Fig. 3.24), it is observed that shallow zone samples show signatures of irrigation return flow and precipitational recharge. The irrigational return flow

and precipitation water mostly has high NO_3^- ions and HCO_3^- ions, which leaches the uranium from the minerals. Hence attributing to contamination in the shallower zone of the study area. The high concentration of uranium at few deep locations is attributed to mixing or vertical well leakage taking along-with HCO_3^- ions and NO_3^- ions leading to increased leaching. This is also corroborated by stable isotope signature.

3.3.5.2 Correlations of uranium

Pearson's correlation of uranium with different physicochemical parameter and major ions are shown with the help of bar graph (Fig. 3.36). For the shallow zone samples (Fig. 3.36 a), it was observed that uranium shows a positive correlation with almost all parameters except Ca^{2+} ions (-0.13) in premonsoon season. The correlation is dominant with F-ions (0.62) followed by Na^+ ions (0.52), HCO_3^- ions (0.48) and NO_3^- ions (0.42) in premonsoon. The average concentration of HCO_3^- ions in premonsoon season of the shallow zone is 682 mg/L. Thus, the high concentration of uranium in the premonsoon season of shallow zones can be linked to the combined role of NO_3^- ions, Ca^{2+} ions and HCO_3^- ions. Thus, it can be concluded that uranium is released from the aquifer matrix under the influence of NO_3^- , HCO_3^- and Ca^{2+} ions explained in details under chapter 5

For the postmonsoon season of the shallow zone, a negative correlation with Ca^{2+} ions (-0.24) and NO_3^- ions (-0.09) is observed and a positive correlation with HCO_3^- ions (0.48). Thus, it can be inferred that the release of uranium from the aquifer matrix is controlled mainly by only Ca^{2+} ions via the process of ion-exchange. The released uranium ion is stabilized by HCO_3^- ions. The decrease in concentration in postmonsoon can be justified by the decrease in NO_3^- ion concentration during the postmonsoon season i.e. 89 mg/L compared to premonsoon concentration of 124 mg/L. Thus, decrease in available U(VI) in the aquifer matrix for ion exchange leading to decrease in contaminated locations.

In the deep zone, during the premonsoon season uranium shows a positive with HCO_3^- ions (0.78) followed by Na^+ ions (0.61) and negative correlation with NO_3^- ions (-0.33) and weak correlation with Ca^{2+} ions (-0.15). Thus, a low concentration of uranium in the deep zone is justified as explained for the postmonsoon season of the shallow zone. The high concentration pocket in the deep zone can be attributed to mixing with shallow zones at few locations which are corroborated with stable isotope signature bringing along-with NO_3^- ions and HCO_3^- ions that help in mobilizing uranium.

For the postmonsoon season, weak correlation with HCO_3^- ions is observed compared to premonsoon season and positive correlation with Ca^{2+} ions both these factors combined acts negatively for uranium dissolution. Thus, low uranium concentrations in the postmonsoon season for deep zones.

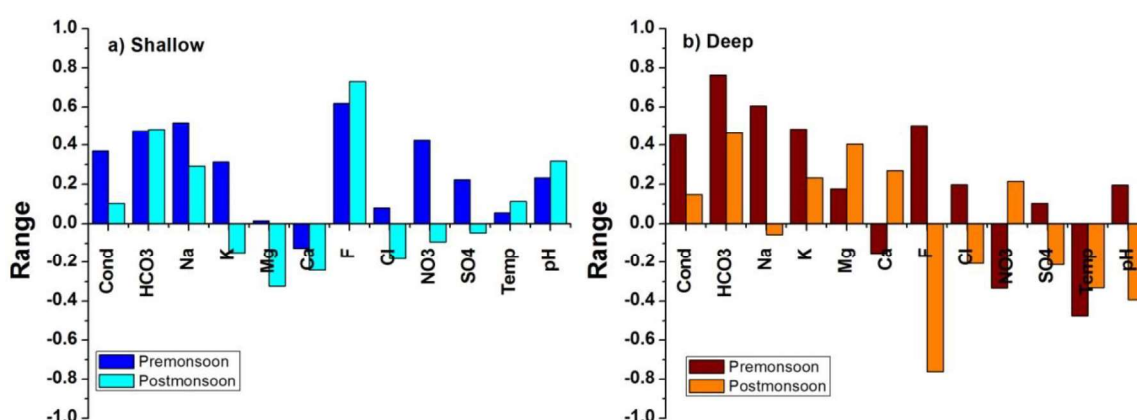


Fig. 3.36 Correlation of physicochemical parameters and major ions with uranium for a) shallow and b) deep zones for both the seasons

Rishi et al. (2017) ^[110] also attributed the high uranium to increased HCO_3^- ions in the south-west region of Punjab. Sharma et al. 2017 ^[111] worked in Bathinda and Mansa districts of Punjab and attributed the uranium concentration to leaching due to oxidative condition and HCO_3^- ions.

The high uranium concentrations in the shallow zone are associated with Na- HCO_3 -Cl (19%), Na-Cl- HCO_3 (14%), Na- HCO_3 (41%) and Na-Cl (26%) type in a premonsoon

while for the postmonsoon Na-HCO₃-Cl (50%), Na-Cl-HCO₃ (7%) and Na-HCO₃ (43%) type. For deep zone, all the contaminated samples had Na-HCO₃ type water in both seasons. The highest values of uranium have Na-HCO₃-Cl type water in both the zones and both the seasons. Thus, corroborating that Cl⁻ and HCO₃⁻ ions influence mobilization of uranium.

3.3.5.3 Factor analysis or Principal Component Analysis

On applying PCA to the data set, thirteen variables namely EC, temperature, pH, Na⁺, K⁺, Ca²⁺, Mg²⁺, F⁻, Cl⁻, NO₃⁻, SO₄²⁻, HCO₃⁻ and Uranium were considered as they had commonalities more than 0.7. Hence, all these variables were suitable for loading on the principle components. Kaiser normalization was followed to select the PC covering the maximum variance of the data [241].

A) Shallow zone

For samples from the shallow zone, five components were found that covers 80.7% of the variance for premonsoon season. PC1 corresponds for 37.5% of the variance and it shows high correlation with EC, Ca²⁺, Mg²⁺, Cl⁻ and SO₄²⁻. The PC1 represents the anthropogenic contamination caused due to excess use of fertilizer for agricultural activity. The high correlation of PC1 with Ca²⁺ and SO₄²⁻ indicates anthropogenic contamination from gypsum-based fertilizers. The PC2 corresponds to 18.9% of the variance and shows a positive correlation with uranium, Na⁺, F⁻ and NO₃⁻ ions while a negative correlation with Ca²⁺ ions. The positive correlation of PC2 with NO₃⁻ ions indicates oxidation of uranium in aquifer matrix from U(IV) to U(VI) with NO₃⁻ ions as an oxidizer. The role of NO₃⁻ ions for uranium mobilization is studied by many researchers and they concluded positive correlation [78]. The negative correlation with Ca²⁺ indicates ion exchange (discussed under chapter 5). This is also corroborated with the dominance of ion exchange reaction in the study area (Fig. 3.17) and CAI 1 and CAI 2 (Chapter 3 section 3.3.3.1). The positive correlation with Na⁺ and Cl⁻ ions indicates the role of EC in leaching of uranium. PC3 corresponds to 9.3% of the

variance and is positively correlated to K^+ and F^- ions indicate towards rock weathering, fertilizers and brick industry as a source for these ions. PC4 and PC5 correspond for 7.8% and 7.3% of the variance and show a weak correlation with the variables.

For the postmonsoon season, four components with a total variance of 74.9% were estimated. PC1 corresponds to 34.9% of the variance and shows a strong positive correlation with EC, Na^+ , SO_4^{2-} , Cl^- , NO_3^- and HCO_3^- ions which indicates ion-exchange between Ca^{2+} and Mg^{2+} ions from the water with Na^+ ions from aquifer matrix. The increased SO_4^{2-} (fertilizer), NO_3^- (fertilizer) and HCO_3^- (soil pore CO_2) ions correlation with PC1 indicate irrigation return flow. The PC2 component with 22% variance shows a positive correlation with Ca^{2+} and Mg^{2+} ions which indicate dolomite dissolution as the source for the ions. The PC3 component with 10% variance shows a positive correlation of uranium with HCO_3^- ions and negative with Ca^{2+} ions which indicates ion exchange with Ca^{2+} ions followed by stabilization of uranyl ion as uranyl-carbonate complexes. The same is corroborated with the uranium and HCO_3^- correlation plot (Fig. 3.33). The PC4 corresponds for 7.8% of the variance and has a positive correlation with NO_3^- and K^+ ions which indicate irrigation return flow bringing along dissolved NO_3^- and K^+ ions from fertilizers. The same is corroborated with stable isotopic value for the postmonsoon season.

B) Deep zone

For the deep zone during premonsoon season four-component were identified with a total variance of 90.95%. The PC1 corresponds for 50.8% of the variance. It has a positive correlation with Ca^{2+} , Mg^{2+} , Cl^- , SO_4^{2-} , K^+ ions and EC which can be due to anthropogenic contamination from gypsum-based fertilizer [235]. Similarly, high correlation with K^+ again indicates anthropogenic contamination from excess use of NPK fertilizers [242]. The PC2 correspond for 20.8% of the variance. It has a positive correlation with uranium F^- , Na^+ and HCO_3^- ions while the weak negative correlation with Ca^{2+} ions which indicates mobilization

of uranyl ion via the process of ion exchange and stabilization as uranyl carbonates, which is corroborated by correlation plot (Fig. 3.33). PC3 and PC4 correspond for 10.7% and 8.7% of the variance and have weak correlations.

For the postmonsoon season, PCA yielded a total variance of 95.4% with four components. The PC1 corresponds to 50.8% of the variance and has a positive correlation with Na^+ , K^+ , NO_3^- and HCO_3^- ions which indicates irrigation return flow adding dissolved fertilizer components like K^+ , NO_3^- and SO_4^{2-} ions and dissolved CO_2 as HCO_3^- ions. The PC2 corresponds to 22.5% of the variance and has a positive correlation with Mg^{2+} , Ca^{2+} , Na^+ , Cl^- , SO_4^{2-} which points to dolomite, gypsum and halite dissolution. The PC3 corresponds to 14.7% variance and correlates with uranium while the weak correlation with other variables. This explains the low uranium in the deep zones during the postmonsoon season. PC4 corresponds for 7.5% of the variance and show very weak correlations with variables.

Table 3.7 PCA output Varimax rotated for the shallow and deep zones for both the seasons

Parameters /Components	Shallow									Deep							
	Premonsoon					Postmonsoon				Premonsoon				Postmonsoon			
	PC1	PC2	PC3	PC4	PC5	PC1	PC2	PC3	PC4	PC1	PC2	PC3	PC4	PC1	PC2	PC3	PC4
Cond.	.813	.476	.163	.043	.156	.946	.220	.101	.089	.690	.524	.188	.193	.739	.555	.130	.321
HCO₃	-.126	.685	.093	-.401	.262	.500	.090	.628	-.071	.209	.867	.323	-.206	.899	.073	.275	-.047
U	-.060	.753	.497	.095	-.035	.094	-.205	.863	-.042	.038	.819	.107	-.186	.229	-.183	.934	-.172
Na	.599	.739	.068	-.090	.136	.920	-.166	.242	.041	.448	.791	.143	.284	.663	.655	-.072	.243
K	.317	-.096	.809	.039	.089	.271	.322	-.207	.628	.848	.493	.061	-.161	.867	.326	.106	-.138
Mg	.860	-.052	.122	.345	-.040	.231	.811	-.161	.270	.970	.141	.117	-.040	.507	.646	.424	-.239
Ca	.900	-.150	.009	-.090	-.076	.152	.859	-.088	.012	.944	-.250	.172	.045	-.060	.873	.448	-.178
F	.032	.455	.723	-.059	-.073	-.198	-.281	.810	.098	.062	.852	.179	.216	-.102	-.455	-.884	-.030
Cl	.911	.145	.050	.220	.052	.662	.536	-.139	.308	.619	.316	.330	.574	.220	.964	-.064	.131
NO₃	.323	.645	-.091	.159	-.155	.597	.115	-.196	.554	-.188	-.186	-.920	.018	.992	.051	-.024	-.098
SO₄	.860	.292	.142	-.036	.027	.863	.339	-.024	.027	.791	.145	.292	.501	-.010	.994	-.018	.062
Temp	-.055	.086	.079	-.061	.893	.573	-.480	-.154	-.101	-.075	-.527	-.804	.137	-.135	.069	-.124	.972
pH	-.353	.164	.337	-.339	-.512	.065	-.663	.358	.041	-.052	.125	.196	-.944	-.861	-.183	-.148	.326
Eigen Values	5.24	2.64	1.30	1.09	1.02	4.89	3.09	1.41	1.10	7.11	2.91	1.49	1.22	7.10	3.15	2.05	1.05
% Variance	37.46	18.89	9.31	7.79	7.26	34.94	22.07	10.04	7.84	50.81	20.79	10.66	8.69	50.73	22.51	14.65	7.51
Cumulative %	37.46	56.35	65.66	73.46	80.71	34.94	57.00	67.04	74.88	50.81	71.60	82.26	90.95	50.73	73.25	87.90	95.41

Table 3.8 The correlation of components with the various variables in both shallow and deep zones for both the seasons

Components	Shallow		Deep	
	Premonsoon	Postmonsoon	Premonsoon	Postmonsoon
PC1	Positively correlated with EC, Ca^{2+} , Mg^{2+} , SO_4^{2-} , Cl^-	Positively correlated with EC, Na^+ , SO_4^{2-} , Cl^- , NO_3^- , HCO_3^-	Positively correlated with EC, Ca^{2+} , Mg^{2+} , Na^+ , SO_4^{2-} , Cl^- , K^+	Positively correlated with EC, HCO_3^- , Mg^{2+} , Na^+ , NO_3^- , Cl^- , K^+ weak with U
PC2	Positively correlated with U, Na^+ , NO_3^- and HCO_3^-	Positively correlated with Mg^{2+} , Ca^{2+}	Positively with HCO_3^- , F^- , Na^+ and U	Positive with Na^+ , Ca^{2+} , Cl^- , SO_4^{2-} , Mg^{2+}
		Negatively correlated with pH	Negatively correlated with Ca^{2+} and temp.	
PC3	Positively correlated with K^+ and F^-	Positively with HCO_3^- , F^- , U	Negatively correlated with HCO_3^- and temp.	Positive with U, HCO_3^-
		Negatively correlated with Ca^{2+}		Negative with F^- , Ca^{2+} , Mg^{2+}
PC4	Positively correlated with Mg^{2+}	Positively correlated with NO_3^- and K^+	Positively with Cl^- and SO_4^{2-}	Positive with temp.
	Negatively correlated with pH and HCO_3^-		Negatively correlated with pH	Negative with pH
PC5	Positively correlated with temperature			
	Negatively correlated with pH			

Thus, it can be observed that uranium shows a correlation with PC2 during the premonsoon season for both shallow and deep zone while it shows a correlation with PC3 during the postmonsoon season for both shallow and deep zones which corroborated by the decrease in uranium concentration during the postmonsoon season in both the zones. The correlation for the premonsoon season is high for shallow zone compared to deep zones thus corroborating the high concentration of uranium in the shallow zones compared to deep zones. PCA also indicates the role played by EC , NO_3^- and HCO_3^- ions in uranium mobilisation. This is explained in details under chapter 5

3.3.5.4 Uranium Speciation

The uranyl ion when mobilized to groundwater complexes with various ligands such as HCO_3^- ions, hydroxyl ions, phosphate ions, fulvic acid etc. The complexes formed either solubilizes or precipitates depending on the solubility of the complex formed. The complexation depends on factor like uranium concentration, pH, concentration of ligands, stability constants of the product being formed etc. The mobilization of uranyl ion depends on its complexation and is more mobile in the complexed state than in free uranyl ionic state. It has been studied that uranium-carbonate complexes like $\text{UO}_2(\text{CO}_3)_2$, $\text{UO}_2(\text{CO}_3)_2^{2-}$, $\text{UO}_2(\text{CO}_3)_3^{4-}$ and $(\text{UO}_2)_3(\text{CO}_3)_6^{6-}$ have greater solubility ^[243] with stability constant of 9.94, 16.61, 21.84 and 54 respectively. They are most commonly occurring species in groundwater with pH in the range of 6.5 to 8.5 ^[244]. Uranyl ion also forms complexes with NO_3^- ions, SO_4^{2-} ions etc. The commonly found species are $\text{UO}_2(\text{NO}_3)^+$, $\text{UO}_2(\text{NO}_3)_2$, $\text{UO}_2(\text{NO}_3)_3^-$, $\text{UO}_2(\text{SO}_4)$ and $\text{UO}_2(\text{SO}_4)_2^{2-}$ with $\log \beta$ values of 0.3, 0.76, 0.796, 3.15 and 4.14 respectively ^[245].

The species of uranium were estimated using WATEQ4F software. Only those uranium species having a concentration in $\mu\text{g/L}$ (ppb) range were selected and the results are compiled in Table 3.9.

Table 3.9 Various species formed by uranyl ion in groundwater from both the zones

Zone	Season/ Species	UO ₂ (CO ₃) ₂ ²⁻ (µg/L)			UO ₂ (CO ₃) ₃ ⁴⁻ (µg/L)		
		Min.	Max	Average	Min.	Max	Average
Shallow	Pre	0.5	140	49	2	980	410
	Post	2	129	22	6.4	931	174
Deep	Pre	5.5	139	28	18	487	182
	Post	3.6	25	15	26	232	63

The main uranium species found in the groundwater of the study area are UO₂(CO₃)₂²⁻ and UO₂(CO₃)₃⁴⁻. Similar complexes in groundwater of in alluvial formation were reported by researchers [99, 111]. The UO₂(CO₃)₃⁴⁻ complex is dominant species in pre and postmonsoon season of both the zone. The concentration of UO₂(CO₃)₂²⁻ and UO₂(CO₃)₃⁴⁻ complex is more in the premonsoon season compared to postmonsoon which can be attributed to the availability of uranyl ion and complexing ions. Despite the high concentration of ions like NO₃⁻ ions, SO₄²⁻ ions etc their complexes with uranyl ions were not identified as they have lower stability compared to carbonate complexes. The complexation reactions are discussed later in chapter 5

3.3.5.5 Saturation Index

Uranium is mostly found as UO₃(C), gummite, coffinite, uraninite, rutherfordine, schoepite, etc. All the common occurring uranium minerals were considered while estimating the saturation index by WATEQ4F. Uraninite is uranium oxide mineral having formula UO₂ but due to oxidative condition, it is mainly found in variable oxidation state like pitchblende i.e. U₃O₈. Rutherfordine is uranyl carbonate mineral having the formula as UO₂CO₃. It is usually formed from uraninite by the process of weathering. When uraninite mineral is exposed to the hydrothermal condition it forms schoepite. Its empirical formula (UO₂)₈O₂(OH)₁₂.12(H₂O). The silicate mineral of uranium is coffinite with the empirical formula of [U(SiO₄)_{1-x}(OH)_{4x}]. Coffinite is known to occur with uraninite, pyrite, clay

minerals. Gummite is an amorphous mixture of uranium as oxides, silicates, and hydroxides etc. The generated output for the shallow and deep zones is represented in the box plot (Fig. 4.37). The saturation index values indicate that the groundwater is tending to supersaturation with respect to uraninite in premonsoon of both the zones. The decrease in saturation index i.e. unsaturation is observed for uraninite in the postmonsoon season compared to the premonsoon season for both the zones. This can be attributed to decreased uranium concentration in postmonsoon season. The other uranium minerals like Rutherfordine, Schoepite, $\text{UO}_3(\text{c})$, $\text{UO}_2(\text{a})$, $\text{B-UO}_2(\text{OH})_2$ and Gummite are undersaturated (Fig. 3.37). As the water is undersaturated w.r.t uranium minerals, it is more prone to contamination in the study area. The favorable condition can lead to further U contamination in both the zones of the study area.

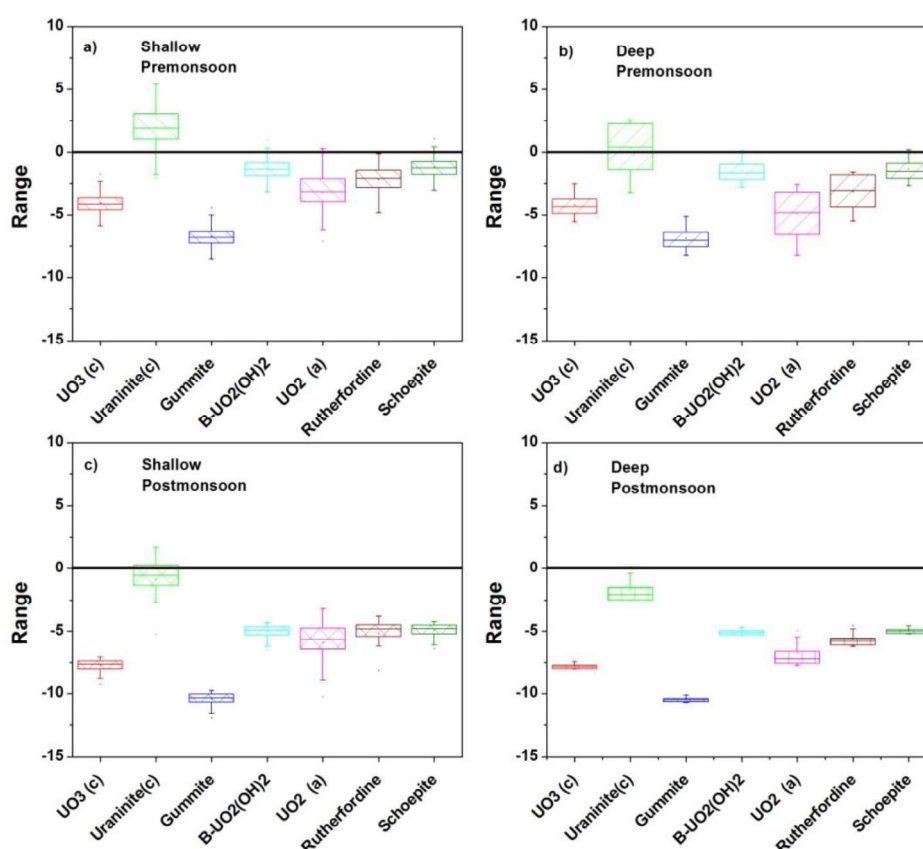


Fig. 3.37 Box plot of saturation indices for common uranium minerals for a) shallow and b) deep zones for both the seasons

3.3.5.6 Uranium isotopes

The uranium activity ratio ($^{234}\text{U}/^{238}\text{U}$) ranges from 0.85 to 1.05 with an average value of 0.96 in the shallow zone and 0.89 to 0.96 with an average value of 0.90 in the deep zone. Activity ratio in the range of 0.94 to 1.85 with average of 1.1 was estimated by Tripathi et al. (2012) ^[102] in Malwa region of Punjab. Authors attribute the slight disequilibrium to selective leaching of ^{234}U . The activity ratio of $^{234}\text{U}/^{238}\text{U}$ from this study showed equilibrium condition. Thus, dissolution of uranium can be considered as a result of oxidative leaching process that shows an activity ratio of 1 representing equilibrium condition.

From the depth profile (Fig. 4.40), it is observed that spread in AR is larger in the shallow zones which can be attributed to variability in the U isotopic composition of the local sediments. In the case of deeper zones, the spread is less i.e. 0.885 to 0.89 except for one sample showing AR of 0.96 which could be due to mixing between the two zones. This is also corroborated with pockets of high uranium concentration in the depth zone of 60m to 100 m.

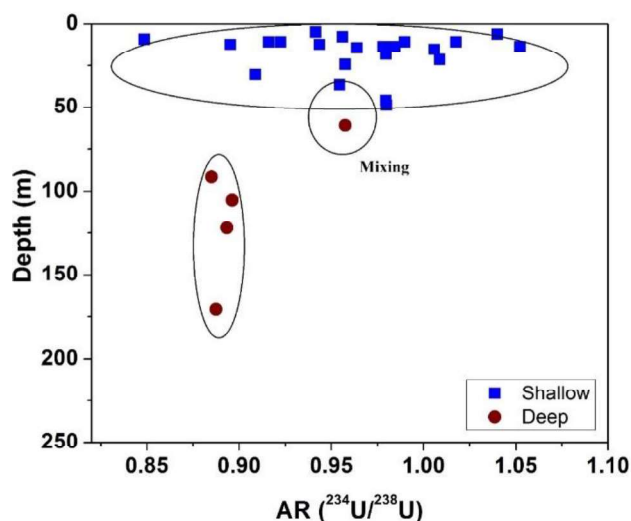


Fig. 3.38 Depth profile for AR ($^{234}\text{U}/^{238}\text{U}$)

A study by Yamaguchi (2009) ^[248] concluded that the nature of the soil, dilution by ploughing, hydrochemical characteristics lead to accumulation of uranium in the soil. The study area is agriculture intensive with extensive use of fertilizers. The phosphate fertilizer

is known to have a high concentration of uranium up to 100-150 ppm^[247]. Thus, there is a high chance of uranium accumulation in the shallow zone of the soil. A study by Sharma et al. 2017^[249] concluded that sediment from the agricultural field and non-agricultural field had the same uranium concentrations i.e. in the natural sediment range. The depth profile of the uranium in sediment also showed not much variation. So, the authors conclude that the increased uranium concentration in water is controlled by water chemistry, redox condition etc.

Comparing the plot of activity ratio versus inverse uranium concentration with the standard plot by Osmond and Cowart (Chapter 2, Fig. 2.9), it is observed that leaching of uranium from its mineral is the main process responsible for uranium concentration in the shallow zone of the study area (Fig. 4.41). The samples from deep zone fall on the mixing trend line which was also corroborated from chemical and isotopic data of the study area.

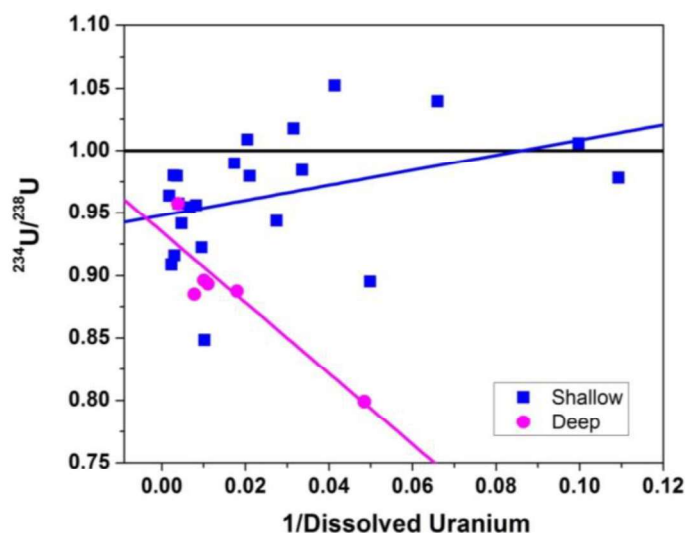


Fig. 3.39 Activity ratio vs. inverse concentration plot to identify the process for uranium mobilization for both the zones

3.4 Conclusions

The water from shallow and deep zones are both unsuitable for the purpose of drinking and irrigation. According to DWQI, 43% of the premonsoon samples are unsuitable

which decreases to 29% in postmonsoon season for the shallow zone. For the deep zone, 30% of the samples are unsuitable for premonsoon which decreases to 12% in the postmonsoon period. According to the IWQI parameter, 100% of the samples from both the seasons and zones are unsuitable for their use. The shallow zone and deep zones seem to be separate (apart for few pockets) as a decreasing trend in contamination along the depth is observed for NO_3^- ions, uranium and F^- ions. The geochemical processes occurring in the study area are i) ion-exchange which is mainly responsible for Na^+ ions in the water, ii) magnesium silicate weathering is responsible for Mg^{2+} ions and iii) calcite dissolution that increases Ca^{2+} ions. The $\delta^2\text{H}$ ranges from -68.24‰ to -18.41‰ for premonsoon season while it is in range of -71.07‰ to -29.29‰ for the postmonsoon season. The $\delta^{18}\text{O}$ values for premonsoon season are in range of -10.2‰ to -1.94‰ while for postmonsoon season the value ranges from -11.30‰ to -3.28‰. The source of recharge to groundwater for the shallow zone is i) precipitation, ii) canal recharge and iii) irrigation return flow while the recharge source to the deep zone is the regional flow along with mixing with shallow zone at few locations. The irrigation return flow signature is diluted by the percolating rain in the postmonsoon season. The uranium concentration in the study area ranges from 1-610 $\mu\text{g/L}$ for premonsoon season while for the postmonsoon season the values are 10-565 $\mu\text{g/L}$. As per the permissible limit given by WHO, 78% of the premonsoon samples are above which decrease to 68% in postmonsoon season. The decrease in concentration can be attributed to dilution caused due to the recharging water. The spatial distribution of uranium shows higher concentrations in Southwest, Northern, north-eastern and central locations of the study area during the premonsoon season while during the postmonsoon dilution is observed in central and eastern location but increase is observed in the south-west and northern regions. The spatial variations in the uranium concentration are attributed to the local hydrogeology of the region. The high uranium concentration samples of the region are associated with Na-

HCO₃-Cl water type indicating that both HCO₃⁻ and EC (Na⁺ and Cl⁻ ions) are playing major role in the mobilization of uranium from the aquifer matrix. The area under study is characterised by high agriculture activity with excess use of fertilisers. The NO₃⁻ ions from fertilisers reaches the aquifer system along with the recharging water through irrigation return flow. The increased agricultural activity also leads to increased pCO₂ concentration, which facilitates the carbonate dissolution and increases HCO₃⁻ ions in the aquifer water. Higher uranium concentrations with larger spread are observed in the shallow zone which shows the vulnerability of shallow aquifer for contamination. Shallow zones have higher uranium concentrations compared to deep zones. The statistical analysis, factor analysis and speciation studies suggest that uranium in the aquifer matrix is oxidized due to high concentration of NO₃⁻ ions from the irrigation return flow. Thus, the main reason for uranium release is found to be oxidative dissolution. The uranyl ion released in groundwater, complexes with HCO₃⁻ ions under the favourable pH condition forming the major species as UO₂(CO₃)₂²⁻ and UO₂(CO₃)₃⁴⁻ in the aquifer system. The decrease concentration of uranium in the postmonsoon season is attributed to decreased concentration and correlation with NO₃⁻ ions. The activity ratio of ²³⁴U/²³⁸U is one i.e. equilibrium condition which can be attributed to oxidative dissolution. As, complete dissolution takes place in the study area hence signature of alpha recoil is not noticed in the aquifer formation. Thus, it is concluded that release of uranium is occurring via two processes i) NO₃⁻ ion help in oxidizing uranium from the aquifer matrix and ii) ion-exchange with Ca²⁺ ions plays the role in uranium release from aquifer matrix. The first process leads to the formation of oxidized uranium species i.e. the uranyl ion which is soluble and mobile in nature. The second process further promotes the release of oxidized uranium from the aquifer matrix. Under the groundwater pH condition, uranyl ions forms carbonate complexes which stabilize the uranyl ion in the aquifer system. The proposed mechanism for uranium release in the zone is discussed in chapter 5.

CHAPTER 4 Source and mobilization of uranium in groundwater of Central Rajasthan

4.1 Study area description

Under this study, two districts of Rajasthan viz. Jaipur and Dausa were chosen. Both the districts have a semi-arid climate, with winter from November to February (5°C - 18°C) and summer from April to June (35°C to 48°C) and monsoon between the end of June and September with 90% of the rainfall received from the southwest monsoon. The annual average rainfall from the year 1971 to 2019 was 519 mm for Jaipur district and 659 mm for Dausa district ^[216]. Over the last decade (2010-2019), the annual average rainfall in Jaipur and Dausa district was 601.6 mm and 678.6 mm respectively ^[250].

Jaipur district is located in the eastern part of Rajasthan. It is bounded by Alwar district (east), Ajmer & Nagaur districts (west), Sikar district (North) and Tonk district (South). It stretches between 26.436° and 27.865° N latitudes and 74.915° and 76.293° E longitudes covering a total area of 11,152 km². The district is divided into 13 administrative blocks with a total population of 66,26,178 ^[217]. The district is drained by ephemeral rivers like Banganga, Banas, Sabi and Shekhawati. The important river to Jaipur is Sabi which originates in eastern slopes of the Saiwar protected forest hills in Aravalli range near Jitgarh and Manoharpur in Sikar district with a catchment area of 4608 km² ^[251] and Banganga which originates in Aravalli Hills, proximity with the Bairath and the Arnasar hills of Jaipur with a catchment area of 8879 km² ^[252].

Out of the total area of the district, the area under cultivation is 6412 km² with the cropping intensity of 140%. Out of the remaining area, the forest cover is 818 km², fallow land is 1340 km², barren land is 563 km², pastures cover is 769 km², land not good for cultivation is 356 km², remaining land of 786 km² is used for non-agricultural activities like

school, houses etc. The main source of irrigation in the district is groundwater, with the gross irrigated area of 3884 km² and the rainfed area is 5071 km². Out of the irrigated area of 3884 km², 51% of the irrigation is from open wells, 47% is from bore wells and the remaining 2% is through canal of the area ^[253].

Geologically, Jaipur district has formations ranging from Archean to Recent age. The north-eastern part of the district is covered mostly by younger and older alluvium (sandy and clayey) with alluvial thickness ranging from 90m to 100m with a maximum thickness at Risani village. Lesser alluvial thickness is found in southern and south-western blocks of the region (Table 4.1). Alluvial deposits are followed by formations belonging to Post Delhi age, Alwar and Ajabgarh group of Delhi supergroup and Bhilwara supergroup. The southern half of the district is mainly occupied by Gneiss and Schist of Bhilwara Super Group ^[254].

Topographically, the district is characterized by a wide spectrum of landscapes that include hillocks, pediments, undulating fluvial plains, aeolian dune fields, ravines, paleochannels etc with an elevation of 250m to 750m amsl ^[254].

Table 4.1 Geological succession of Jaipur district, Rajasthan.

Geological succession		
Super Group	Group	Formation
	Recent to sub-Recent	Sand, Clay, Kankar
	Post Delhi	Granite, Pegmatite, Amphibolite (Intrusive)
Delhi	Ajabgarh	Schists, Phyllites, Marble and Quartzite
	Alwar	Quartzite, Conglomerate and Schists
	Raialo	Dolomitic Marble and Quartzite
-Unconformity-		
Bhilwara		Gneiss, Schists and Migmatites

Hydro-geologically, the district has unconfined to confined aquifers with varying formations (Table 4.2). 67% of the area is occupied by alluvial aquifer (38.9%: young and 28.1%: older alluvial) (Fig. 4.1). Young alluvial is spread mostly in northern parts of the district while the older alluvial aquifer is found in southern parts of Bassi, Jaipur, Renwal

and Kishangarh blocks. Out of the total area covered under alluvial aquifers, 2% area is saline and is found in Bagru block. Remaining 37% area is occupied by Schist, Quartzite, Granite, and Gneiss. Aquifers with saline pockets are also found in Schists and Gneiss formations ^[142].

Table 4.2 Hydrogeology of Jaipur district, Rajasthan

Aquifer	Percentage area occupied	Description
Younger Alluvium	38.8	Unconsolidated to semi consolidated clay, sand, gravel, pebble etc. northern part: younger alluvium southern parts: older alluvium
Older Alluvium	26.2	
Younger Alluvium Saline Area	0.1	Mainly in the south of Bagru
Older alluvium Saline Area	1.9	
Schist	6.4	Weathered and fractured cleavage with medium to fine-grained rock, found in Sambhar, Northeast of Jamwa Ramgarh and north and south of Chaksu.
Schist Saline Area	0.2	Found North of Chaksu alongside Dhund Nadi
Quartzite	6.4	Fled-spathic Grit to Serictic Quartzite medium to coarse grain in west Chakshu, Amber, Northwest in Kotputli and Shapur and between Bassi and Virtnagar
Granite	0.4	Porphyritic texture of light grey to pink medium to coarse-grained rock found in north-eastern edge of Jamwa-Ramgarh
Gneiss	13.9	weathered and fractured grey to dark coloured medium to coarse-grained rock, occur in south-western part of Dudu and Phagi block
Gneiss Saline Area	2.4	mostly found in Phagi

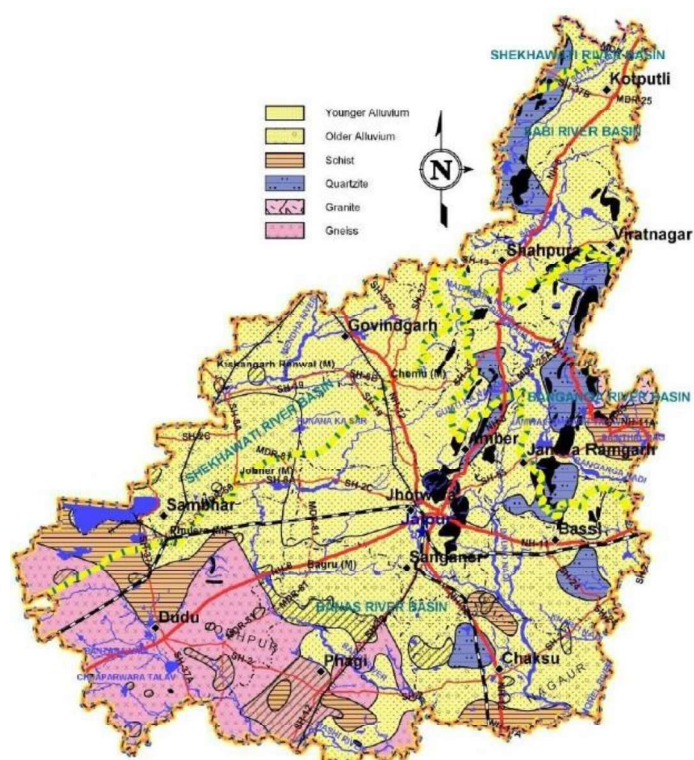


Fig. 4.1 Aquifer map of Jaipur district showing the area covered under various formations
(cropped from PHED 2013 ^[254])

Dausa district is located in the eastern part of Rajasthan. It is bounded by Bharatpur district (east), Jaipur district (west), Alwar district (North) and Sawai Madhopur and Karauli districts (South). It stretches between 26.37° and 27.243° N latitudes and 76.143° and 77.08° E longitudes covering an area of 3,418 km² divided into 5 administrative blocks with a population of 16,34,409 ^[217]. The district is drained by ephemeral rivers namely Banganga and Sawa rivers.

Out of the total area of the district, the area under cultivation is 2180 km² with the cropping intensity of 155%. Out of the remaining area, the forest-covered area is 247 km², fallow land is 269 km², barren land is 174 km², permanent pastures are 262 km², land not good for cultivation is 72 km², the land under non-agricultural activities like school, houses etc is 378 km². The main source of irrigation in the district is groundwater, with a gross

irrigated area of 1648 km² and the rainfed area is 1734 km². Out of the irrigated area of 1648 km², 48% of the irrigation is from open wells, 52% is from bore wells ^[255].

Geologically, the northeast and southwest blocks mainly in Mahwa and Lalsot have alluvial and wind-blown sand deposits underlain formation from Delhi Supergroup comprising Raialo (dolomite/marble) and Alwar Groups (quartzite & schist). This is followed by older formations from the Bhilwara Super Group rocks which consist of gneisses, schist and migmatites ^[256]. The geological succession is given in Table 4.3.

Table 4.3 Geological succession of Dausa district, Rajasthan

Geological succession		
Super Group	Group	Formation
	Recent to sub-Recent	Alluvium-Sand, Silt, Gravel, Clay and Kankar and wind-blown sand
-Unconformity-		
Delhi	Ajabgarh	Schists, Phyllites, Marble and Quartzite
	Alwar	Quartzite, Conglomerate and Schists
	Raialo	Dolomitic Marble
-Unconformity-		
Bhilwara	Mangalwar Complex	Gneiss, Schists and Migmatites

The district is characterized by relatively flat topography along with occasional hills in the southwestern part with an elevation of 200m to 600m amsl. The aquifer system of Dausa district is present in alluvial (young and older), Phyllites, Quartzite and Gneiss (Fig. 4.2) covering an area of 80%, 2.2 %, 9.1% and 3.1% respectively (Table 4.4). The dominant aquifer of the region is older alluvial with the thickness of about 90 m to 100m and water under unconfined to confined type. North-western part and the south-eastern borders of the district mainly have hard rock formations of Bhilwara supergroup and groundwater occurs under unconfined to semi-confined conditions with thickness from 2 m to 25 m ^[143].

Table 4.4 Hydrogeology of Dausa district, Rajasthan

Aquifer	Percentage area occupied	Description
Younger Alluvium	21.6	Aeolian and Fluvial sand, clay, silt, gravel and pebbles in varying proportions
Older Alluvium	58.4	
Phyllite	2.2	fine to medium-grained sand, Silt and Kankar
Quartzite	9.1	Meta sediments represented by Carbonaceous Phyllite
Gneiss	3.1	Porphyritic and non-porphyritic gneiss complex

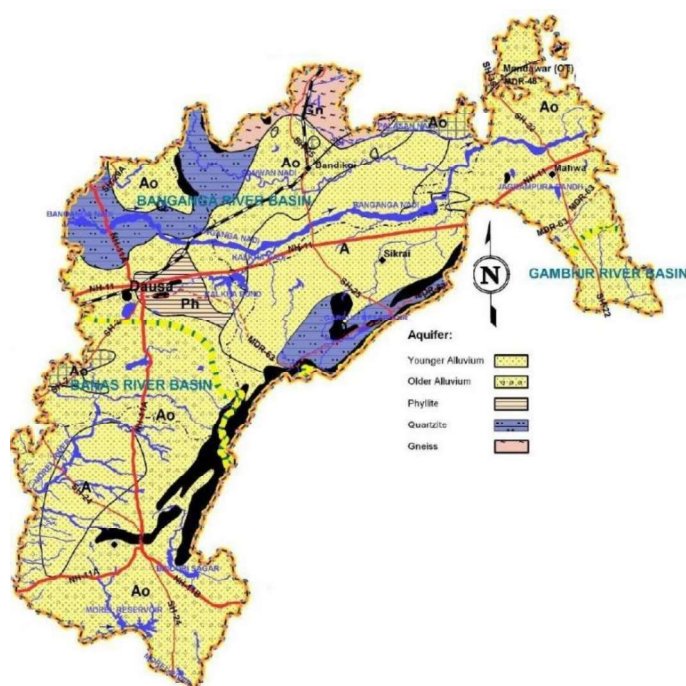


Fig. 4.2 Aquifer map of Dausa district showing the area covered under various formation
(cropped from PHED 2013 ^[256])

The stage of development (Chapter 1, Equ. 1.1) of Jaipur and Dausa district is $>100\%$ indicating that groundwater is overexploited in both the districts. Bassi, Shahpura, Govindgarh, Sanganer, Sambhar, Amber and Jhotwa blocks of Jaipur are under the notified condition of overexploitation which means no abstraction for other than drinking purpose is allowed in these regions while the Phagi block of Jaipur comes under critical condition.

4.2 Sampling

The sampling methodology same as Punjab (chapter 3 section 3.2) was followed. Samples were collected for both premonsoon during March 2017 (72 nos.) and postmonsoon seasons during November 2017 (33 nos.). Samples were collected from different formations present in the study area namely alluvial (young and old) and hard rock (Quartzite, Phyllites, Schists and Gneiss) tapping depths from 30m to 170m. The percentage of samples collected from each formation is given in Table 4.5

Table 4.5 Percentage of samples from the different formations

Type of Formation		% samples	
		Premonsoon	Postmonsoon
Alluvium	Young	33	21
	Old	44	43
Hard Rock	Phyllites	4.5	9
	Schists	4.5	3
	Quartzite	3	0
	Gneiss	11	24

32% of the collected samples were from tube wells and 68% were from handpumps for the premonsoon season while for postmonsoon, the samples from tube wells were 15% and from hand pump were 85%. The sampling locations are shown in Fig. 4.3. The details of the measurement protocol and instruments used are given in chapter 2.

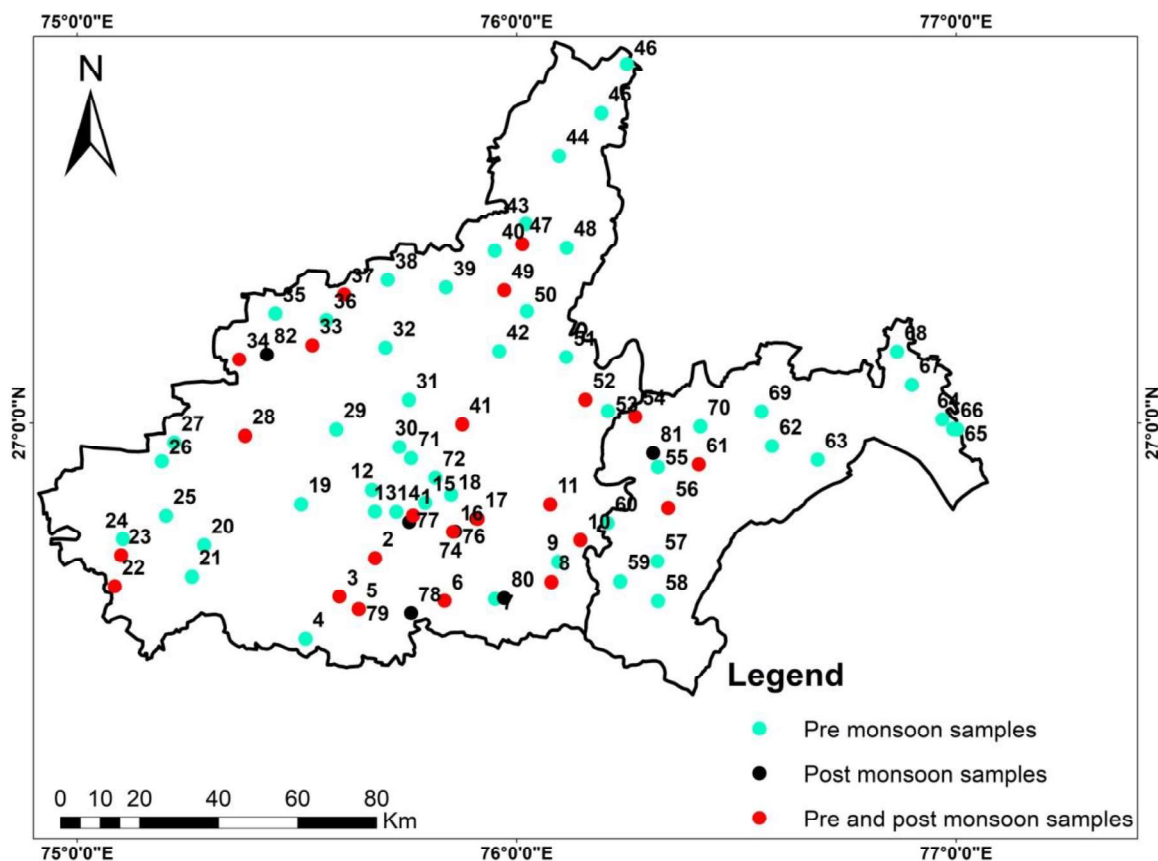


Fig. 4.3 Sample location map showing different colour for samples collected only in premonsoon (Cyan), postmonsoon (Black) and collected in both the seasons (Red)

4.3 Results and discussion

4.3.1 General water quality

The summary of field parameters and chemical parameters of groundwater samples from alluvium and hard rock formations for both pre and postmonsoon seasons of Dausa and Jaipur districts of Rajasthan are shown in Table 3.2.

4.3.1.1 Physicochemical parameters

The pH values are in the permissible range of 6.5 to 8.5 for both the formations of both the seasons (pre and post) of the study area. The average pH value for pre and postmonsoon seasons is 7.9 and 7.5 respectively (Fig. 4.4) for both the formations, which indicate that the groundwater is slightly alkaline. The averaged EC value for premonsoon

and postmonsoon seasons from alluvium formation is 2078 $\mu\text{S}/\text{cm}$ (Fig. 4.4a) and 3655 $\mu\text{S}/\text{cm}$ (Fig 4.4c) while for the hard rock formation is 2005 $\mu\text{S}/\text{cm}$ (Fig. 4.4b) and 3017 $\mu\text{S}/\text{cm}$ (Fig. 4.4d) for pre and postmonsoon seasons respectively. The exceptionally high EC values at locations from Naraina i.e. 12100 $\mu\text{S}/\text{cm}$ (premonsoon) and Sambhar i.e. 23120 $\mu\text{S}/\text{cm}$ (postmonsoon) were observed, which may be attributed to local contamination, due to salt pan activity ^[257]. The increase in EC values of groundwater during the postmonsoon season can be attributed to dissolution of salts present in the unsaturated zone that are brought along with the recharging water. Groundwater in alluvium and hard rock formations showed an increase in EC values in 75% and 70% of the samples respectively. The spatial variation in EC values indicates the variability of leaching and dilutions due to recharging water, which is further linked to variation in soil type and other agriculture-related activities in the study area. The average alkalinity for pre and postmonsoon in the alluvial formation is 527 mg/L (Fig. 4.4 a) and 600 mg/L (Fig. 4.4 c) respectively. The average value for the hard rock formation for premonsoon and postmonsoon seasons is 585 mg/L (Fig. 4.4 b) and 659 mg/L (Fig. 4.4 d) respectively. This increase in average alkalinity value for postmonsoon samples can be attributed to carbonate weathering. An overall increase in EC values is observed in postmonsoon in 63% and 71% of samples compared to premonsoon. The study carried out by Mondal et al. (2016) ^[142] in Dausa district, found that the average pH values were 8.7 (pre) and 8.6 (post). The average EC values were 2029 $\mu\text{S}/\text{cm}$ which increased to 2179 $\mu\text{S}/\text{cm}$. The slight increase in concentration during the postmonsoon season is attributed to dissolution of salts present in the unsaturated zone through recharging water, as per the authors ^[142].

Table 4.6 Summary of physicochemical and chemical parameters for both the seasons of alluvium and hard rock formations

Parameters	Alluvium Formation						Hardrock Formation					
	Premonsoon			Postmonsoon			Premonsoon			Postmonsoon		
	Min.	Max.	Mean	Min.	Max.	Mean	Min.	Max.	Mean	Min.	Max.	Mean
pH	7.2	8.3	7.9	6.8	8.4	7.5	7.20	8.20	7.99	6.79	8.09	7.51
EC ($\mu\text{S}/\text{cm}$)	470	12100	2078	761	23120	3655	660	6300	2005	740	5437	3017
TDS (mg/L)	301	7744	1330	487	14797	2339	422	4032	1283	474	3480	1931
TH (mg/L)	37	518	180	54	4163	362	59	1349	210	114	974	241
Alkalinity (mg/L)	150	1400	527	170	1020	600	180	850	585	200	1050	659
F ⁻ (mg/L)	0.07	5.0	1.4	0.04	8.1	3.4	0.79	5.31	2.40	0.30	8.2	3.88
Cl ⁻ (mg/L)	7.5	5125	372	4.5	5315	610	20	707	183	15.44	992	434
NO ₃ ⁻ (mg/L)	0.3	242	47	0.3	205	50	0.36	528	56	2.86	382	74
SO ₄ ²⁻ (mg/L)	1.9	1750	115	2.2	5278	339	7.79	324	69	13	391	138
HCO ₃ ⁻ (mg/L)	183	1708	643	207	1244	732	220	1037	713	244	1281	804
Na ⁺ (mg/L)	55	7199	567	54	4607	662	68	665	360	78	849	525
K ⁺ (mg/L)	1.6	44	6.7	1.55	14	5.3	2.27	267	23	2.66	282	28.5
Mg ²⁺ (mg/L)	5.2	93	32	8.9	752	70	9.9	197	36	17	229	52
Ca ²⁺ (mg/L)	2.6	74	19	2.2	428	30	1.77	216	24	2.69	18	10
Uranium ($\mu\text{g}/\text{L}$)	0.38	177	30	5.3	142	47	0.49	115	34	5.16	145	51
DWQI	15	477	94	11	452	218	52	297	142	38	348	175

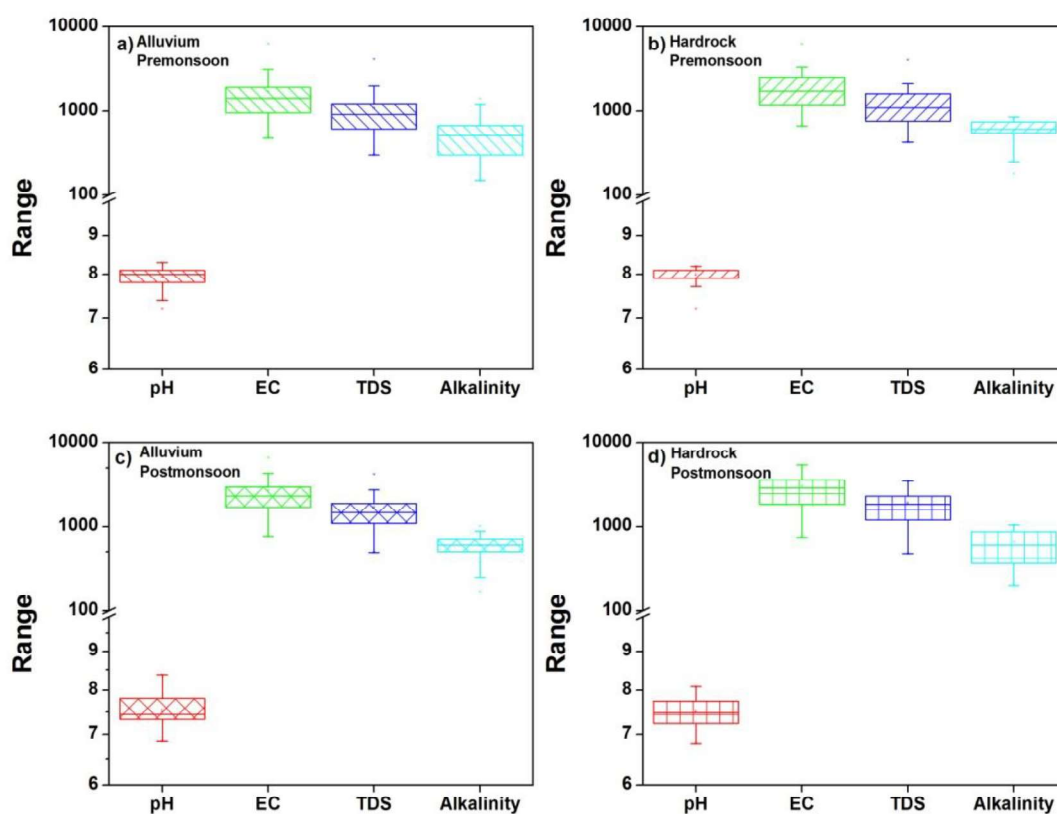


Fig. 4.4 Box plot for physiochemical parameters a) premonsoon of alluvial formation, b) premonsoon of hard rock formation c) postmonsoon of alluvial formation and d) postmonsoon of hard rock formation

From the depth profiles of EC, pH and alkalinity (Fig 4.5), an overall spread is observed in both alluvium and hard rock formations. The higher EC and alkalinity values are also observed in deeper zones.

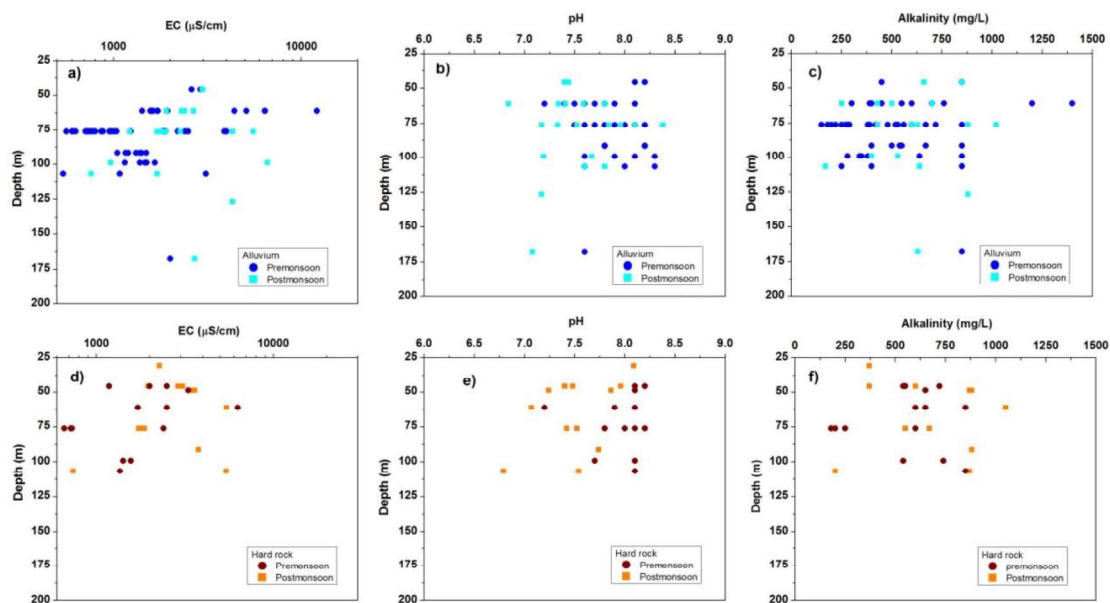


Fig. 4.5 Depth profile for physicochemical parameters a) EC, b) alkalinity and c) pH for alluvial formation and d) EC, e) alkalinity and f) pH for hard rock formation of both the seasons

4.3.1.2 Chemical parameters

The major cations are in the order of $\text{Na}^+ > \text{Mg}^{2+} > \text{Ca}^{2+} > \text{K}^+$ for both alluvial and hardrock formations for both the seasons. The major anions are in the order of $\text{HCO}_3^- > \text{Cl}^- > \text{SO}_4^{2-} \approx \text{NO}_3^- > \text{F}^-$ for both alluvial and hard rock formations for both the seasons. The box plots for various major ions present in the groundwater of alluvial and hard rock formations of the study area for the premonsoon and postmonsoon seasons are shown in Fig. 4.6. The Na^+ ions in alluvial formation range from 55-1990 mg/L with an average value of 356 mg/L for the premonsoon season while 54-991 mg/L with an average value of 660 mg/L for the postmonsoon season. An exceptionally high Na^+ ion concentration of 7200 mg/L and 4600 mg/L is observed for premonsoon and postmonsoon seasons respectively in Naraina and Sambhar blocks of Jaipur district, which may be attributed to local contamination such as salt pan activity occurring in the area (Table 3.2). The Na^+ ions in the hard rock formation range from 68-665 mg/L with an average value of 360 mg/L for the premonsoon season

while 78-850 mg/L with an average value of 525 mg/L for postmonsoon season (Table 3.2). The average Na^+ ion concentration is reported as 321 mg/L in premonsoon, which is increased to 388 mg/L during the postmonsoon season. The increase in concentration is attributed to ions brought along with recharging water, as per the authors [141].

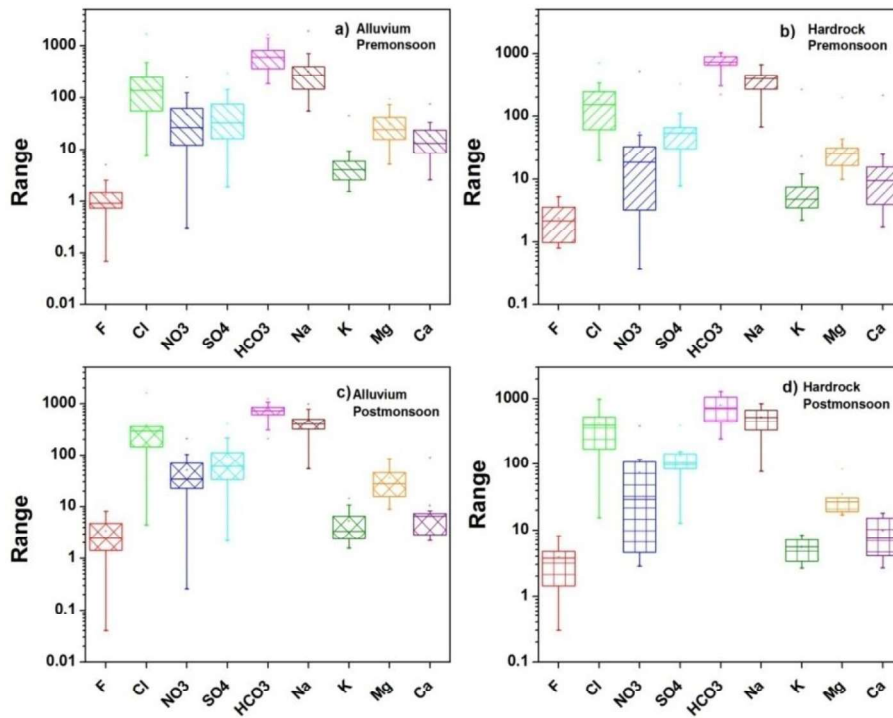


Fig. 4.6 Box plot for major ions present in groundwater from a) premonsoon alluvial, b) premonsoon hard rock, c) postmonsoon alluvial and d) postmonsoon hard rock formations

The Ca^{2+} ion concentration for the premonsoon season ranges from 2.6-74 mg/L with an average value of 19 mg/L while 2.2-90 mg/L with an average of 10 mg/L for the postmonsoon season in the alluvial formation of the study area (Table 4.6). The concentration range for the hard rock formation in the premonsoon season range from 2-35 mg/L with an average of 10 mg/L and while 3-18 mg/L with an average of 10 mg/L (Table 4.6). The variation in concentrations in pre and postmonsoon seasons of both the formations is less indicating similar spread in both the formations. The Mg^{2+} ion concentration in alluvial formation ranges from 5.2-93 mg/L with an average value of 32 mg/L for the

premonsoon while 9-85 mg/L with an average value of 36 mg/L for the postmonsoon season (Table 4.6). The Mg^{2+} ion concentration for hard rock formation is in range of 10-197 mg/L with an average of 36 mg/L for the premonsoon season while 17-84 mg/L with an average of 36 mg/L in postmonsoon season (Table 4.6). The seasonal variations in Mg^{2+} ion concentration in both formations are very less. All the cations show an increase in the postmonsoon season which is attributed to dissolution of ions from unsaturated zones with recharging water. All the ions are distributed equally in both formations indicating mixing or interconnection of groundwater. The concentration of K^+ ion is higher in hard rock formation compared to the alluvial formation which can be attributed to mineral sources of K^+ ion in hard rock formations.

The HCO_3^- ion concentration in alluvial formation is in the range of 183-1708 mg/L with an average value of 567 mg/L for the premonsoon season while 207-1244 mg/L with an average value of 732 mg/L for the postmonsoon season (Table 4.6). The HCO_3^- ion concentrations for hard rock formations in premonsoon season are 220-1037 mg/L with an average value of 713 mg/L while 244-1281 mg/L with an average value of 804 mg/L for the postmonsoon season (Table 4.6). The Cl^- ion concentration in alluvial formations ranges from 7.5-1742 mg/L with an average value of 227 mg/L for the premonsoon season while 4.5-1618 mg/L with an average value of 375 mg/L for the postmonsoon season (Table 4.6). Exceptionally high Cl^- ion concentration of 5125 mg/L (Naraina) and 5315 mg/L (Sambhar) are observed in pre and postmonsoon season respectively. The same location has high EC, Na^+ and Cl^- ions. This is attributed to local salt pan activity observed in that area [257]. The hard rock formation has Cl^- ion concentration in the range of 20-708 mg/L with an average value of 183 mg/L for the premonsoon season while 15-992 mg/L with an average value of 434 mg/L (Table 4.6). The SO_4^{2-} ion concentrations for the premonsoon season in alluvial formation are 2-300 mg/L with an average value of 60 mg/L while 2-407 mg/L with an

average value of 92 mg/L (Table 4.6). The concentration of SO_4^{2-} ion for hard rock formation are 8-324 mg/L with an average value of 69 mg/L for the premonsoon season while 13-392 mg/L with an average of 138 mg/L for the postmonsoon season (Table 4.6). The alluvial formation has NO_3^- ion concentrations in the range of 0.3-242 mg/L with an average of 47 mg/L for the premonsoon season while 0.3-205 mg/L with an average of 50 mg/L for the postmonsoon season (Table 4.6). The hard rock formation has concentrations in the range of 0.4-528 mg/L with an average of 56 mg/L for the premonsoon season while 3-382 mg/L with an average of 74 mg/L for postmonsoon season (Table 4.6). The higher concentrations of NO_3^- ion can be attributed to the excess use of NPK fertilizer and decaying organic matter [12, 13]. The F^- ion concentrations in alluvial formation are in the range of 0.07-5 mg/L with an average of 1.4 mg/L for the premonsoon season while 0.04-8 mg/L with an average value of 3.5 mg/L for the postmonsoon season (Table 4.6). The F^- ion concentrations in hard rock formation are 0.8-5.3 mg/L with an average of 2.4 mg/L for the premonsoon season while 0.3 mg/L-8 mg/L with an average of 3.9 mg/L for the postmonsoon season (Table 4.6). The anions show a similar trend in the postmonsoon season as cations. The depth profile for major cations and anions indicates contamination in shallow as well as deeper zones (Fig. 4.7). The NO_3^- and F^- ions contamination is also observed in both the formations indicating mixing/interconnections between two formations with an increase in concentration in postmonsoon season.

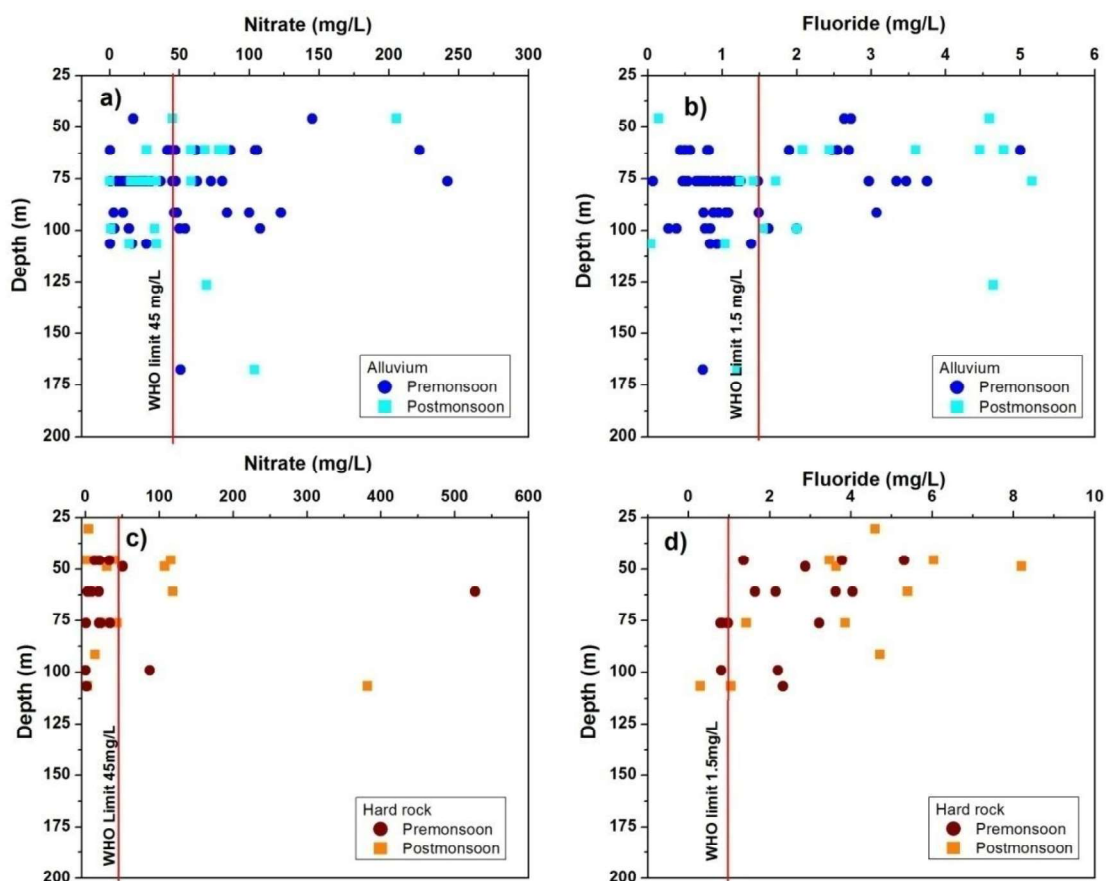


Fig. 4.7 Depth profile for a) NO_3^- ions in alluvial formation, b) F^- ions in alluvial formation c) NO_3^- ions in hard rock formation and d) F^- ions in hard rock formation in both the seasons

4.3.2 Suitability of water

4.3.2.1 Suitability for drinking

The compiled data for water quality for both seasons of the alluvial and hard rock formation is shown in Table 3.3. According to the permissible limits laid by BIS (2012) ^[144] (Table 3.3), it was observed that contamination in the study area is mainly caused by NO_3^- ions (40%) followed by F^- ions (25%) and TDS (11%) in alluvial formation. In hard rock formation, the contamination due to F^- ions is found in 67% of samples followed by NO_3^- ions (20%) and TDS (13%) during the premonsoon season. High F^- ion concentration in 71% of samples followed by NO_3^- ions in 43% and TDS (24%) in alluvial formation. The hard

rock formation shows contamination of F^- ions in 75% of the samples followed by TDS (42%) and NO_3^- ions (33%) for the postmonsoon season. According to the permissible limit of ions in drinking water given by WHO (2011) ^[26] (Table 3.3), in the premonsoon season, the contamination is due to Na^+ ions (63%), TDS (42%) followed by NO_3^- ions (40%), Cl^- ions (26%) and F^- ions (25%) while for the postmonsoon season, the major contamination is due to Na^+ ions (90%), TDS (86%) followed by F^- ions (71%), Cl^- ions (62%) and NO_3^- ions (43%) in alluvial formation. The contamination in premonsoon season is due to Na^+ ions (80%), TDS (60%) followed by F^- ions (67%), Cl^- ions (27%) and NO_3^- ions (20%) while in postmonsoon season contamination by Na^+ ions (92%), TDS (92%) followed by F^- ions (75%), Cl^- ions (67%) and NO_3^- ions (33%) in the hard rock formation.

The increase in the number of contaminated samples is observed in both the formations during the postmonsoon season. The main source of NO_3^- ions is the excess use of nitrogen fertilizers, use of manure and irrigation with wastewater ^[218]. NO_3^- ions are highly soluble and easily leaches with percolating water ^[219]. Saxena et al. (2014) ^[220] reported high NO_3^- ion concentration in Bassi Tehsil of Jaipur due to leakage from the sewage system, septic tanks etc, extensive use of fertilisers and use of wastewater for irrigation. Contamination due to NO_3^- ion is found in 40% of the samples from alluvial formation and 20% of the samples from the hard rock formation. This can be attributed to the amount of recharge received by the formations.

Table 4.7 Compiled water quality data for alluvium and hard rock formations of the study area for both the seasons

Parameter	Permissible Limits		Alluvium				Hard rock			
			% of samples exceeding BIS		% of samples exceeding WHO		% of samples exceeding BIS		% of samples exceeding WHO	
	BIS	WHO	Pre	Post	Pre	Post	Pre	Post	Pre	Post
			57	21	57	21	15	12	15	12
pH	6.5-8.5	6.5-8.5	0	0	0	0	0	0	0	0
TH	600	500	0	5	2	10	7	8	7	8
TDS	2000	1000	11	24	42	86	13	42	60	92
Na⁺		200	0	0	63	90	0	0	80	92
K⁺		20	0	0	5	0	0	0	0	0
Ca²⁺	200	300	0	5	0	5	7	0	0	0
Mg²⁺	100	100	0	5	0	5	7	8	7	8
F⁻	1.5	1.5	25	71	25	71	67	75	67	75
Cl⁻	1000	250	4	10	26	62	0	0	27	67
NO₃⁻	45	50	40	43	40	43	20	33	20	33
SO₄²⁻	400	250	2	10	5	14	0	0	7	17

The high F^- ion values are observed in 25% of samples from alluvial formation and 67% of samples from the hard rock formation. High TDS is observed in 42% of samples from the alluvial formation and 60% of samples from the hard rock formation. Many researchers have confirmed that F^- ions bearing minerals in weathered and fractured hard rock aquifers are the main source of F^- ions ^[256]. The source of high F^- ions and TDS is mostly prolonged leaching from the minerals via rock-weathering present in the aquifer matrix ^[221]. Rajasthan has high fluorapatite and fluorite deposits which are a rich source of F^- ions ^[257]. Saxena et al. (2014) ^[220] reported the F^- ions concentration in the range of 0.3-11.5 mg/L and TDS in range of 770-11200 mg/L and they attributed high F^- ions and TDS concentrations to rock-weathering. Vikas (2009) ^[222] also estimated the F^- ions concentration in the range of 0.12-17 mg/L in central Rajasthan.

In granitic terrain of Medak, Telangana the F^- ion concentration was estimated in the range of 0.2-7.4 mg/L with 57% of samples above WHO permissible limits and increased concentration were attributed to increased alkalinity which leads to leaching from mineral source ^[258].

Table 4.8 Suitability of water for drinking and irrigation on basis of TDS, TH and EC

Water class		Alluvium		Hard rock	
		% of samples in premonsoon	% of samples in Postmonsoon	% of samples in premonsoon	% of samples in Postmonsoon
		57	21	15	12
TDS (mg/L)					
< 500	Desirable for drinking	18	5	20	8
500-1000	Permissible for drinking	40	10	27	0
1000-3000	Useful for Irrigation, Unfit for drinking	37	71	47	75
> 3000	Unfit for drinking as well as irrigation	5	14	7	17
TH (mg CaCO ₃ /L)					
< 60	Soft	7	5	7	0
60-120	Moderately hard	30	38	33	17
121-180	Hard	23	14	33	50
> 180	Very Hard	40	43	27	33
EC (µS/cm)					
< 250	Excellent	0	0	0	0
250-750	Good	16	5	20	8
750-2000	Permissible	61	33	47	25
2000-3000	Doubtful	11	38	20	25
> 3000	Unsuitable	12	24	13	42

According to total hardness parameter ^[223], only 7% samples are soft which falls to 5% during the postmonsoon season for alluvial formation while for hard rock formation, 7% samples are soft for the premonsoon season while none of the samples remains soft during the postmonsoon season (Table 4.8).

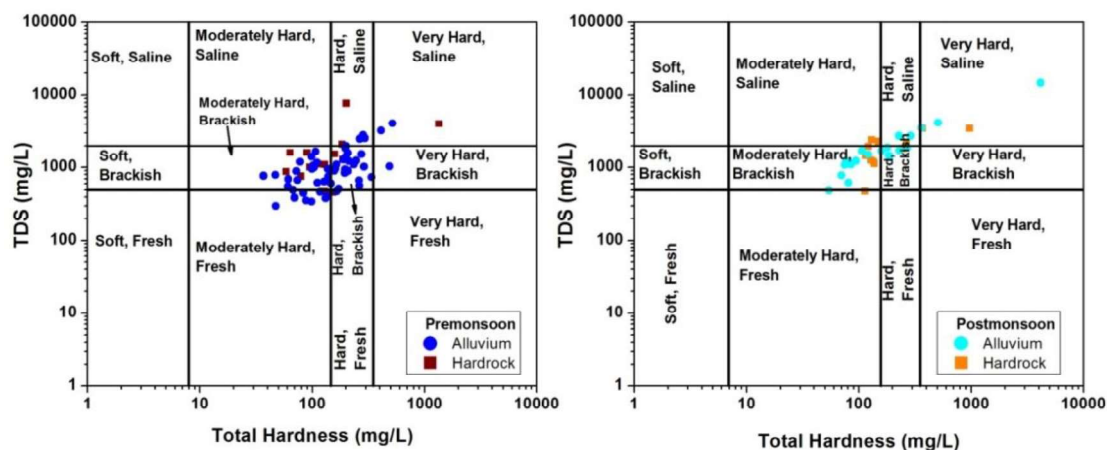


Fig. 4.8 TDS vs TH plot to understand water type for pre and postmonsoon seasons for both the formations.

From the plot of TDS vs TH (Fig. 4.8), it can be clearly interpreted that the groundwater is mostly hard with brackish to saline nature thus making it unsuitable for its use for drinking purposes. According to EC, 77% of the samples fall in the permissible range during the premonsoon season which falls to only 38% samples in the postmonsoon season (Table 4.8) for alluvial formation. For hard rock formation, 67% of samples are in the permissible range during the premonsoon season which falls to 33% during the postmonsoon season.

4.3.2.2 Suitability for irrigation

The compiled data for these parameters are given in Table 4.7 and Table 3.5. The water classification given by Richards (1954) ^[158] for EC is shown in Table 3.4 and it is observed that 12% of the samples are unsuitable for irrigation purpose for premonsoon which increases to 24% for the postmonsoon season for alluvial formation while the unsuitable samples from hard rock formations are 13% for the premonsoon season which

increases to 42% during postmonsoon. Based on TDS, 5% of samples are unsuitable for irrigational purposes during premonsoon season which increases to 14% for the postmonsoon season for alluvial formation. 7% of samples are unsuitable for their use for irrigation for the premonsoon season that increases to 17% samples for the postmonsoon season from the hard rock formation. The water classification based on other parameters such as SAR, RSC and Na% for both seasons is shown in Table 4.10.

A) Sodium absorption ratio (SAR)

The calculation of parameter is done using the equation given in chapter 2 Table 2.1. The SAR values range from 1.9–38 with an average value of 11.8 for premonsoon and 3.2–31 with an average value of 16 for postmonsoon for alluvial formation. An exceptionally high value of 220 is observed for the premonsoon season of alluvial formation (Table 4.10). The values for hard rock formation are 2.5–25 with an average value of 13 for premonsoon season while 3.2–29 with an average value of 17 for postmonsoon season (Table 4.10). According to the classification based on SAR, it is observed that 16% of samples are unsuitable for their use in the premonsoon season which increases to 38% for the postmonsoon season in alluvial formation. The unsuitable samples are 20% in premonsoon which increases to 33% samples in the postmonsoon season for hard rock formation (Table 4.8). This corroborates the fact that recharging water is increasing the alkalinity related hazard making the water unfit for irrigation purpose.

Table 4.9 Compiled irrigation water quality data for alluvium and hard rock formations of the study area for both the seasons

Parameters	Alluvium						Hardrock					
	Pre			Post			Pre			Post		
	Min.	Max.	Mean	Min.	Max.	Mean	Min.	Max.	Mean	Min.	Max.	Mean
SAR	1.89	220	19	3.2	31	16	2.49	25	13	3.18	29	17
Na%	39	99	77	69	92	84	52	94	79	61	92	83
PI	56	118	97	72	116	102	59	116	99	65	105	97
RSC	1.71	26	10	-13	20	10	2.71	17	10	3.14	20	12
MH	23	95	64	38	96	77	40	95	70	48	96	77
KR	0.63	78	7.5	2.17	12	6.38	1.05	15	6.46	1.22	12	7
CR	0.04	5.29	0.67	0.04	25	1.96	0.10	1.28	0.43	0.14	2.0	0.92
IWQI	5.23	62	17	-43	37	17	4.19	26	17	8.90	28	19

Table 4.10 Suitability of water for irrigation on basis of SAR, sodium percent and residual sodium carbonate

Water class		Alluvial		Hardrock	
		% samples in premonsoon	% samples in Postmonsoon	% samples in premonsoon	% samples in Postmonsoon
		57	21	15	12
Alkalinity Hazard (SAR)					
< 10	Excellent	47	14	33	17
10-18	Good	37	48	47	50
18-26	Doubtful	11	33	20	8
> 26	Unsuitable	5	5	0	25
Sodium Percent					
< 20	Excellent	0	0	0	0
20-40	Good	4	0	0	0
40-60	Permissible	9	0	27	0
60-80	Doubtful	35	33	7	17
> 80	Unsuitable	52	67	67	83
Residual Sodium Carbonate					
< 1.25	Good	0	5	0	0
1.25-2.5	Doubtful	11	0	0	0
>2.5	Unsuitable	89	95	100	100

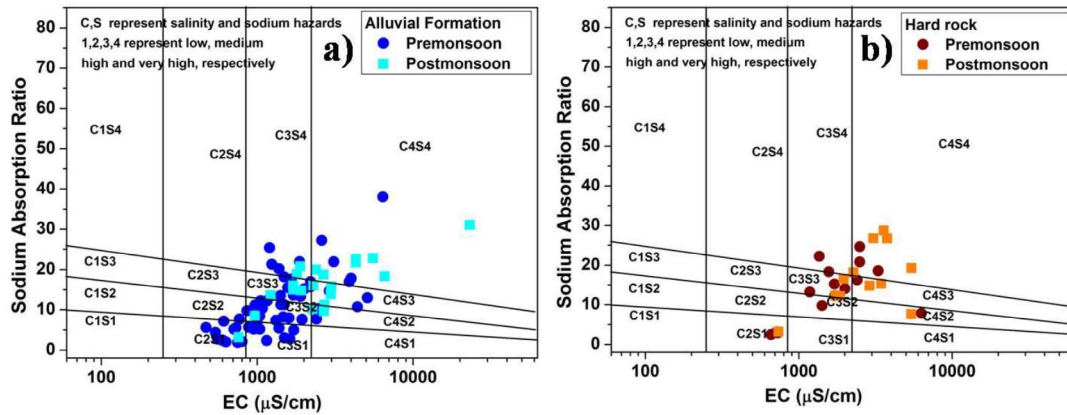


Fig. 4.9 USSL plot of groundwater from a) alluvial and b) hard rock formation for premonsoon and postmonsoon seasons

From the USSL plot (Fig. 4.9), it is observed that samples from pre and postmonsoon seasons shows scatter from low to very high salinity hazard as well as sodium hazard for both alluvial as well as hard rock formations. The salinity and sodium hazard increases in postmonsoon season.

B) Sodium percent (Na%)

Sodium percent is calculated using the equation given in chapter 2 Table 2.1. The Na% values for premonsoon are in the range of 39% - 99% with an average of 77% for premonsoon while 61% - 92% with an average of 84% for postmonsoon season for alluvial formation (Table 4.9). For hard rock formation, the Na% value ranges from 52% - 94% with an average value of 79% for premonsoon while for the postmonsoon season the values range from 61% - 92% with an average value of 83%. An increase is observed in the postmonsoon season of both the formations. The value for Na% is more in hard rock formation which is attributed to increased rock water interaction due to longer residence time. Only 13% and 26% of samples from alluvial and hard rock formations respectively for premonsoon falls in the permissible range while none of the sample is in the permissible range during the postmonsoon season for both the formations (Table 4.10).

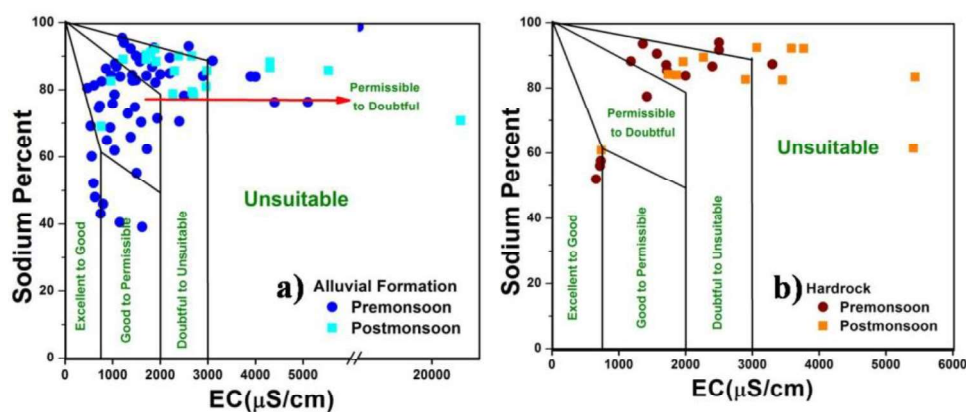


Fig. 4.10 Wilcox plot for a) alluvial formation and b) hard rock formation for premonsoon and postmonsoon seasons

From the Wilcox plot (Fig. 4.10), it is observed that all the postmonsoon samples fall in doubtful to the unsuitable range while premonsoon sample shows much scatter ranging from good to permissible to doubtful and unsuitable for alluvial formation. Only 14 % samples fall in permissible category for the premonsoon season with no sample in permissible category for the postmonsoon season. For hard rock formation, most of the pre and postmonsoon samples fall in doubtful to unsuitable category. Only 20% of samples fall in the permissible range which falls to 8% for the postmonsoon season for hard rock formation.

C) Residual sodium carbonate (RSC)

It is calculated using the equation given in chapter 2 Table 2.1. The RSC values for premonsoon season ranges from 1.7-26 meq/L with an average value of 10 meq/L while for postmonsoon the values range from 3.1-20 meq/L with an average value of 10 meq/L for alluvial formation. For hard rock formation, the value ranges from 2.7-17 meq/L with an average value of 10 meq/L for the premonsoon season while for the postmonsoon season, the value ranges from 3.1-20 meq/L with an average value of 12 meq/L. For the premonsoon season, only 11% of samples are suitable for irrigation while for postmonsoon only 5% of samples are suitable from the alluvial formation. This indicates, degradation of water quality

with recharging water. For hard rock formation, none of the samples are suitable for their use in both the seasons.

D) Permeability index (PI)

It is calculated using the equation given in chapter 2 Table 2.1. For alluvial formation, the PI values range from 56-118 with an average value of 97 while 72-116 with an average value of 102 for postmonsoon season. For hard rock formation, the values range from 59-116 with an average value of 99 for the premonsoon season while 65-105 with an average value of 97 for postmonsoon season (Table 4.9). 3.5% samples fall under class I which increases to 5% for the postmonsoon season while 9% of samples fall under class II which falls to 5% in postmonsoon season and rest fall in class III for alluvial formation. For hard rock formation, 6% of samples fall under class I which increases to 8% in the postmonsoon season while rest samples fall under class III (Fig.4.11).

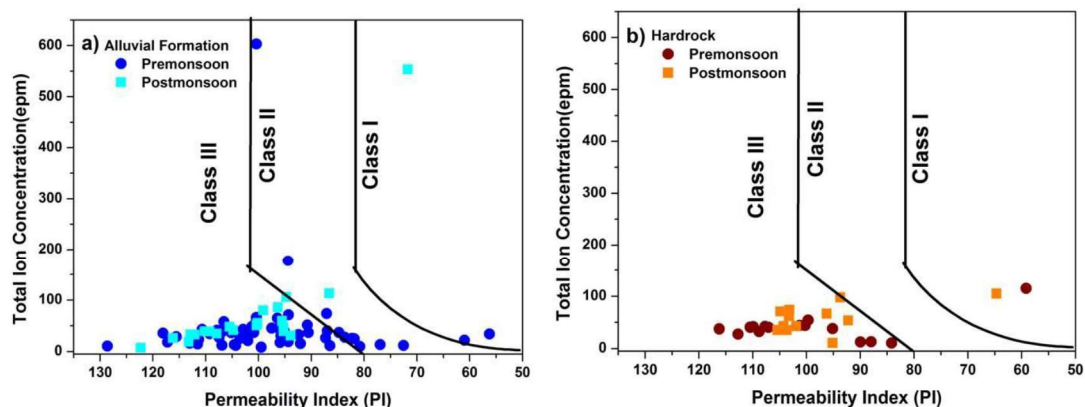


Fig. 4.11 Permeability index of groundwater from a) alluvial and b) hard rock formation for premonsoon and postmonsoon seasons

E) Magnesium Hazard (MH)

It is calculated using the equation given in chapter 2 Table 2.1. The MH values range from 23%-95% with an average value of 64% for the premonsoon season while for postmonsoon season range from 38%-96% with an average value of 77% for alluvial formation. 77% of samples exceed the permissible MH values that increase to 90% of

samples in the postmonsoon season for alluvial formation. For hard rock formation, the values range from 40%-95% with an average of 70% with 80% of the samples unsuitable for their use in the premonsoon season while for the postmonsoon season, the values range from 48%-96% with an average value of 77% with 92% of the samples unsuitable for their use.

F) Kelley's ratio (KR)

It is calculated using the equation given in chapter 2 Table 2.1. The KR values range from 0.6-78 with an average value of 7.5 for the premonsoon season while for postmonsoon season the values are in the range of 2.2-12 with an average of 6.4 for alluvial formation. 91% of the premonsoon samples and 100% of the postmonsoon samples are harmful as per KR ratio from alluvial formation. For hard rock formation, the KR values range from 1.05-15 with an average of 6.5 for the premonsoon season while for the postmonsoon season the values range from 1.2-12 with an average value of 7. 100% of the samples from both pre and the postmonsoon season for hard rock formation are unsuitable for their use.

G) Corrosive Ratio (CR)

It is calculated using the equation given in chapter 2 Table 2.1. For alluvial formation, the values range from 0.04-5.3 with an average of 0.7 for the premonsoon season while for the postmonsoon season the values range from 0.04-3.9 with an average of 0.8. 89 % of the samples are fit for their use in the premonsoon season which falls to 67% samples during the postmonsoon season for alluvial formation. For hard rock formation, the values range from 0.1-1.3 with an average of 0.4 for the premonsoon season while for the postmonsoon season the values range from 0.1-2 with an average of 0.9. 93% of the samples are suitable for their use which falls to 58% during postmonsoon season.

4.3.2.3 Composite water quality index

Composite water quality index is calculated for drinking (DWQI) and irrigation (IWQI) using Equ. 2.2 to 2.5 (Chapter 2). The DWQI values range from 15-477 with an average of 94 for the premonsoon season while the values for the postmonsoon season are 11-452 with an average of 218 for alluvial formation (Table 3.2). For hard rock formation, the values range from 52-297 with an average of 142 while for the postmonsoon season, the values range from 38-348 with an average value of 175 (Table 3.2). The IWQI values range from 5.2-62 with an average of 17 for the premonsoon season while for the postmonsoon season; the value ranges from 9.4-37 with an average of 20 for alluvial formation (Table 3.5). For hard rock formation, the values range from 4.2-26 with an average value of 17 for the premonsoon season while for the postmonsoon season the value ranges from 8.9-28 with an average value of 19 (Table 3.5). As per the categorization of DWQI and IWQI, given in chapter 3 section 3.2.3. For DWQI, 75% of samples are suitable in premonsoon season for alluvial formation, which decreases to 29% in postmonsoon season while for hard rock formation suitable samples for the premonsoon and postmonsoon season are 40%. The composite parameter for irrigation estimates 99% and 100% of samples are unsuitable for their use in pre and postmonsoon seasons respectively for alluvial formation while for hard rock formation all the samples are unsuitable for both the seasons. The study done by Mondal et al. (2016) ^[140] in Dausa district, concluded that the water quality is unsuitable for its uses for the purpose of drinking and irrigation. Rahman et al (2020) ^[139] studied the quality of groundwater in Sanganer block of Jaipur. They concluded the groundwater quality is not fit for both drinking and irrigational purposes. Ion-exchange and silicate weathering are the major ions contributors. Mondal et al. (2016) ^[140] studied the water quality of Dausa district of Rajasthan and attributed pollution of groundwater to the mixing of anthropogenic

contaminant and the occurrence of rock weathering in the region. The quality of water was also found to be unfit for its use for the purpose of irrigation and drinking.

4.3.3 Geochemical evolution

From the piper trilinear plot ^[168] (Fig. 4.12), the water facies observed are Na-HCO₃ (35%), Na-HCO₃-Cl (57%) and Na-Cl-HCO₃ (8%) type for the premonsoon samples. The water facies observed for postmonsoon samples are Na-HCO₃ (18%), Na-HCO₃-Cl (46%), Na-Cl-HCO₃ (33%) and Na-Cl (3%) type. The dominance of Cl⁻ type water is observed in postmonsoon season.

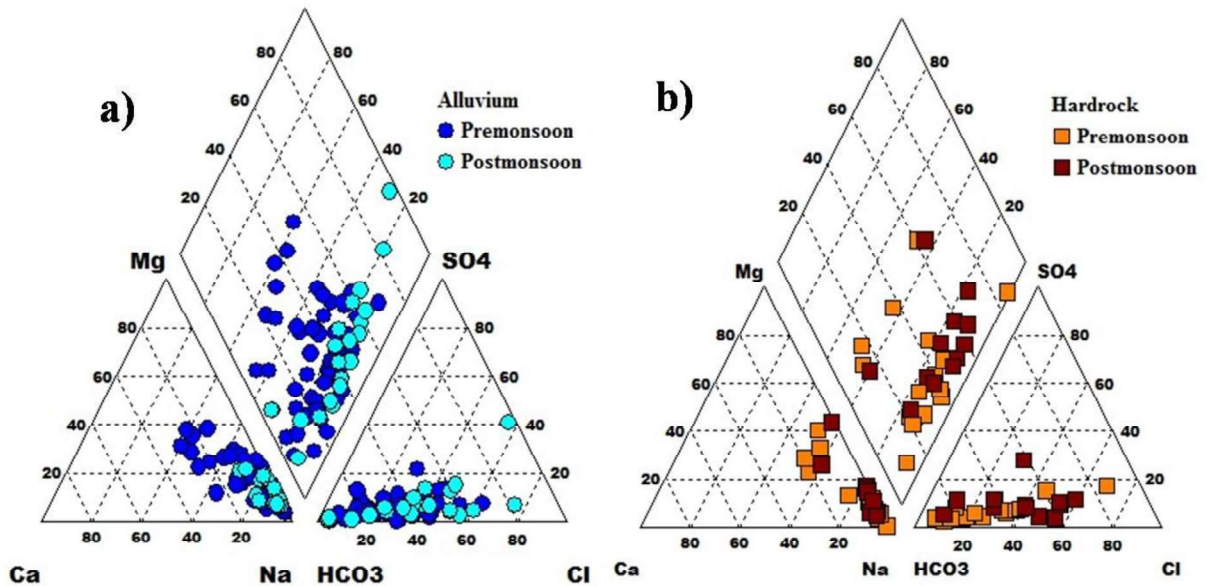


Fig. 4.12 Piper trilinear plot showing water facies for a) alluvial and b) hard rock formations

The samples from the aquifer falling in alluvial formation have Na-HCO₃ (35%), Na-HCO₃-Cl (56%) and Na-Cl-HCO₃ (9%) water type for the premonsoon while for postmonsoon, the water type are Na-HCO₃ (19%), Na-HCO₃-Cl (48%), Na-Cl-HCO₃ (24%) and Na-Cl (9%). This is a clear indication of the dissolution of salt from the vadose zone with percolating water. The same is corroborated with increased TDS values (average values: Pre: 1330 mg/L and Post: 2339 mg/L) and Cl⁻ ions (average value: Pre: 372 mg/L and Post: 610 mg/L) during the postmonsoon (Table 4.6) compared to the change in

concentration of HCO_3^- ions (average value: Pre: 643 mg/L and Post: 732 mg/L) which is not much. The hard rock formation shows Na- HCO_3 (40%), Na- HCO_3 -Cl (53%) and Na-Cl- HCO_3 (7%) as dominant water type for premonsoon season. The dominant water types for the postmonsoon season are Na- HCO_3 (16%), Na- HCO_3 -Cl (42%) and Na-Cl- HCO_3 (42%). A clear observation of ion change/addition can be made from the changing water types. The same is corroborated with increased TDS value (average values: Pre: 1283 mg/L and Post: 1931 mg/L) and Cl^- ions (average values: Pre: 183 mg/L and Post: 434 mg/L) during the postmonsoon (Table 4.6) compared to the change in concentration of HCO_3^- ions in postmonsoon season (average value: Pre: 713 mg/L and Post: 804mg/L). The major water type reported by Tatawat and Chandel (2008) ^[259] for the Jaipur district were Na-Mg-Cl, Na- HCO_3 and Mg-Na(Ca)- HCO_3 -Cl. Similar water facies were found in area under this study.

It is clear from the Gibbs plot ^[152] that rock-weathering is the dominant process in the premonsoon season while in the postmonsoon season the major role is played by the rock weathering and evaporation process for both alluvial (Fig. 4.13 a, b) and hard rock formations (Fig. 4.14 a, b).

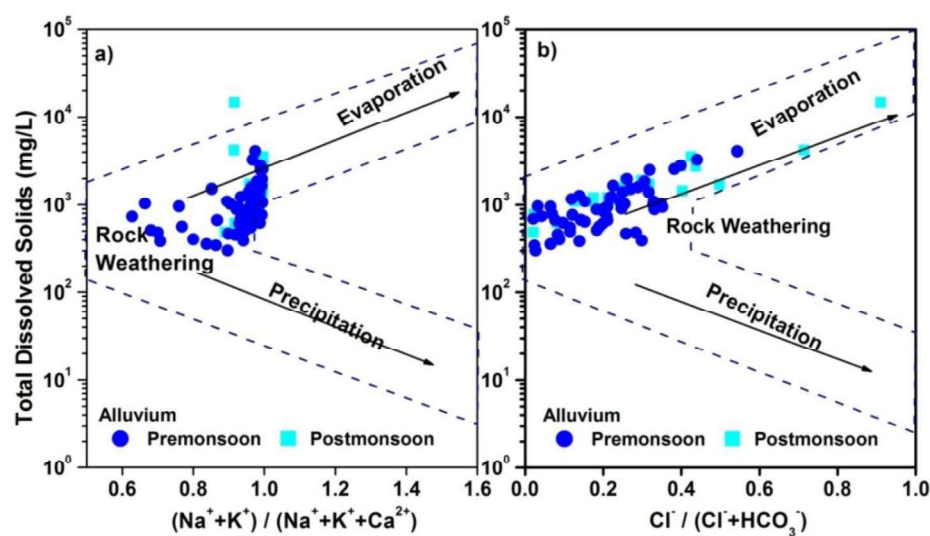


Fig. 4.13 Gibbs plot a) cationic and b) anionic in the premonsoon and postmonsoon seasons for the alluvial formation

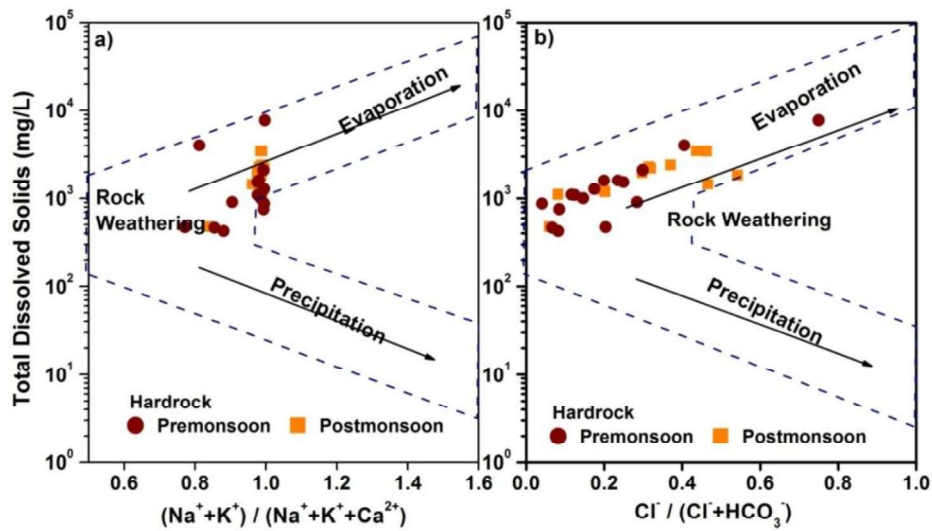


Fig. 4.14 Gibbs plot a) cationic and b) anionic in the premonsoon and postmonsoon seasons for the hard rock formation

From the plot Na^+ -normalized Ca^{2+} versus Na^+ normalized HCO_3^- (Fig. 4.15a, b), it can be interpreted that silicate weathering is the dominant process for both premonsoon and postmonsoon seasons of both alluvial and hard rock formations. From the plot of Na^+ -normalized Ca^{2+} versus Na^+ normalized Mg^{2+} (Fig. 4.15c, d), the dominant process leading to the concentration of Ca^{2+} and Mg^{2+} ions are evaporite dissolution like gypsum, anhydrite, dolomite, calcite, magnesite etc. for both the seasons in the alluvial and hard rock formations.

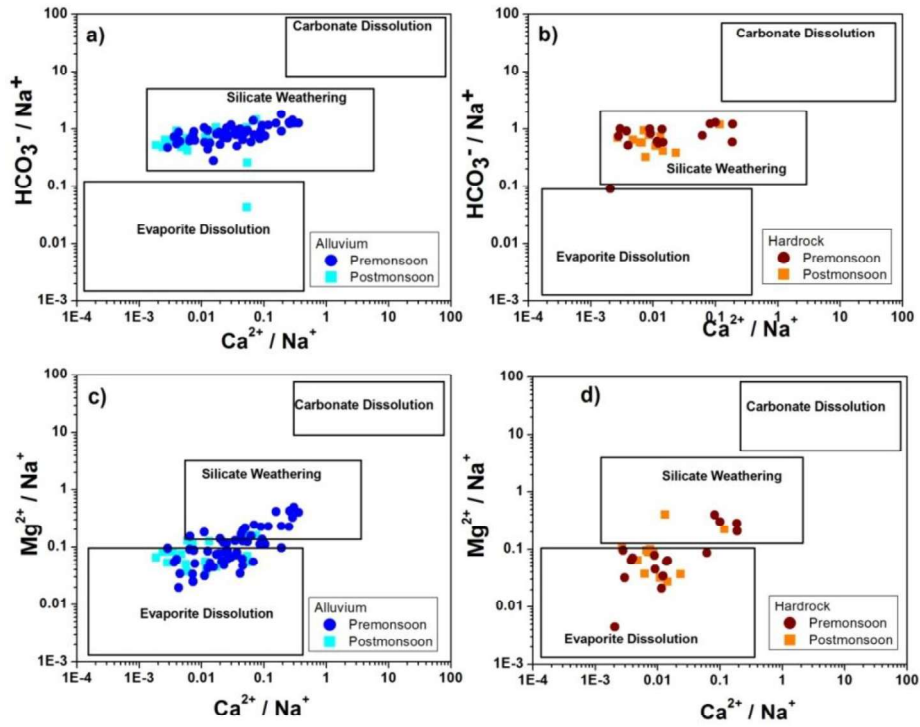


Fig. 4.15 Bivariate plots a) Alluvial: Na^+ -normalized Ca^{2+} versus Na^+ normalized HCO_3^- , b) Hard rock: Na^+ -normalized Ca^{2+} versus Na^+ normalized HCO_3^- , c) Alluvial: Na^+ -normalized Ca^{2+} versus Na^+ normalized Mg^{2+} and d) Hard rock: Na^+ -normalized Ca^{2+} versus Na^+ normalized Mg^{2+}

From the plot of $\text{Ca}^{2+}/\text{Mg}^{2+}$ vs Na^+/Cl^- (Fig. 4.16), it is clearly seen that most of the samples fall in the field having ratio > 3 which is the sign of ion exchange or silicate weathering as a dominant process in the study area. For alluvial formation in the premonsoon season, 1% of the samples shows evaporation effect while 53% of the samples indicate evaporative enrichment and 46% of the samples indicates ion exchange or silicate weathering process. In the postmonsoon season, the effect of evaporation increases i.e. 5% of samples indicates evaporation process while 62% of the samples shows sign of evaporative enrichment and 33% of the samples shows ion exchange or silicate weathering as the dominant process.

In case of hard rock formation, for premonsoon season none of the samples has Na^+/Cl^- ratio of one while 33% samples indicate evaporative enrichment or irrigation return

flow and 67% indicates ion exchange or silicate weathering as the dominant process. During postmonsoon season, 8% samples indicates evaporation process, 58% indicated irrigation return flow and 34% indicated dominance of ion exchange or silicate weathering. In the postmonsoon season of both the formation, the samples under evaporative enrichment category is increased this indicates increased irrigation return flow that is signature of delayed recharge as the premonsoon signatures are observed in postmonsoon seasons. The processes like ion exchange and silicate weathering are dominant in hard rock formations compared to the alluvial formation which is corroborated with increased K^+ and F^- ions in hard rock formation which are mainly contributed from rock weathering.

From the ratio plot, (Fig. 4.16), it is inferred that dolomite dissolution process occurs in 7% and 5% of the samples from the alluvial and hard rock formations in premonsoon season. Calcite dissolution is dominant only in 5% of samples in premonsoon season from the hard rock formation. In the study area, magnesium silicate weathering is dominating in 93% and 90% of the samples from alluvial and hard rock formations from premonsoon which increases to 100% and 95% respectively in the postmonsoon season.

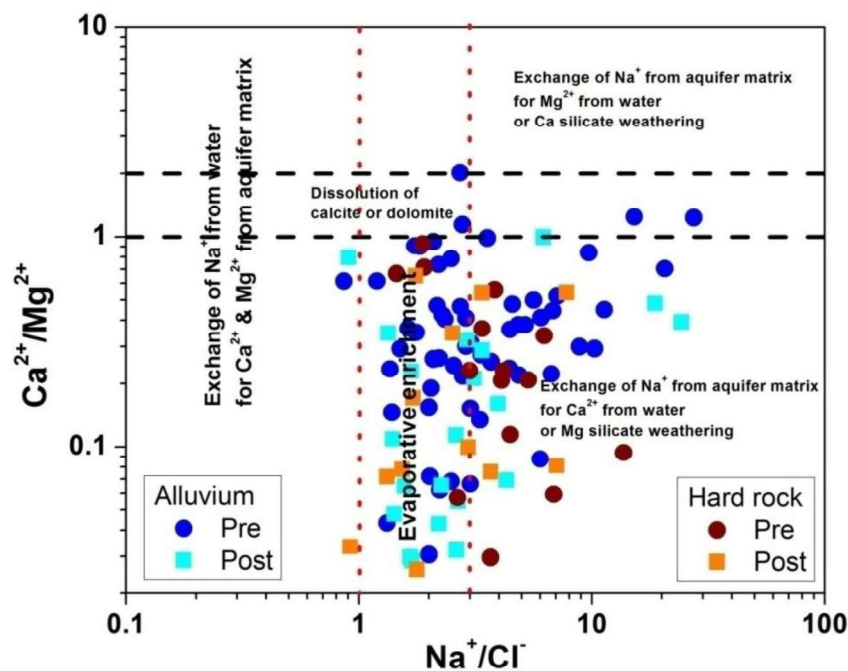


Fig. 4.16 Plot of $Ca^{2+}+Mg^{2+}$ vs $Na^+ + K^+$ of groundwater samples from the study area

4.3.3.1 Ion Exchange

Ion exchange processes are interpreted using chloro-alkaline indices (CAI 1 and 2) that are calculated using Equ. 3.5 and Equ. 3.6 (Chapter 3) ^[230]. For alluvial formation, the CAI-1 values range from -26.65 to -0.23 for the premonsoon season, while the values range from -23.39 to -0.34 for the postmonsoon season. The CAI-2 for premonsoon and postmonsoon ranges from -1.42 to -0.13 and -0.98 to -0.36 respectively. For hard rock formation, the CAI-1 values are in the range of -12.8 to -0.8 for premonsoon and -7.1 to -0.2 for postmonsoon while the range for CAI-2 is -1.11 to -0.38 for premonsoon and -1 to -0.2 for the postmonsoon season. The values indicate that the exchange of Na^+ or K^+ ions from rock to water in place of Ca^{2+} and Mg^{2+} from water is the dominant process. the ion exchange recation is given in chapter 3 Equ. 3.7

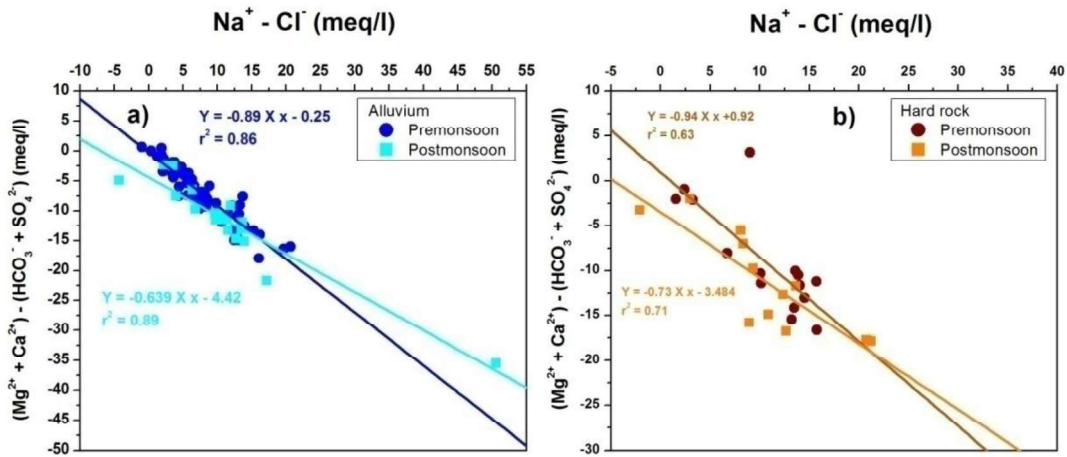


Fig. 4.17 Plot of $(\text{Na}^+ - \text{Cl}^-)$ vs. $(\text{Mg}^{2+} + \text{Ca}^{2+}) - (\text{HCO}_3^- - \text{SO}_4^{2-})$ illustrating reverse ion exchange

The groundwater samples from the alluvial formation of the study area fall on the slope of -0.89 and -0.64 for premonsoon and postmonsoon respectively. The samples from hard rock formation fall on the slope of -0.94 and -0.73 in pre and postmonsoon seasons respectively (Fig. 4.17). The tendency of hard rock samples is more towards the slope of -1

indicating the dominance of exchange reaction in the hard rock formation. The same is also corroborated from Na^+/Cl^- ratio (Fig. 4.16).

4.3.3.2 Carbonate Weathering

The plot of $(\text{Ca}^{2+} + \text{Mg}^{2+})$ vs. $(\text{SO}_4^{2-} + \text{HCO}_3^-)$ predicts the occurrence of dissolution of calcite, dolomite and gypsum (samples fall on equiline), replacement or addition of Ca^{2+} and Mg^{2+} ions during ion exchange or reverse ion exchange or silicate weathering [232,233]. From the plot (Fig. 4.18) of $(\text{Ca}^{2+} + \text{Mg}^{2+})$ vs. $(\text{SO}_4^{2-} + \text{HCO}_3^-)$, it was observed that all the samples fall below the equimolar line indicating more concentration of $\text{SO}_4^{2-} + \text{HCO}_3^-$ over $\text{Ca}^{2+} + \text{Mg}^{2+}$. This higher HCO_3^- is attributed to the weathering of feldspar minerals [234] or organic matter oxidation and root respiration leading to higher pCO_2 in soil pores which dissolves and adds to HCO_3^- ions with recharging water. The higher SO_4^{2-} ions is attributed to excessive use of fertilizers or oxidation reaction occurring in the aquifer matrix [235]. The exchange of Ca^{2+} and Mg^{2+} ions from water with Na^+ and K^+ in the aquifer matrix is also one of the possible reasons for decreased Ca^{2+} and Mg^{2+} ions. The exchange process is corroborated from Fig. 4.17.

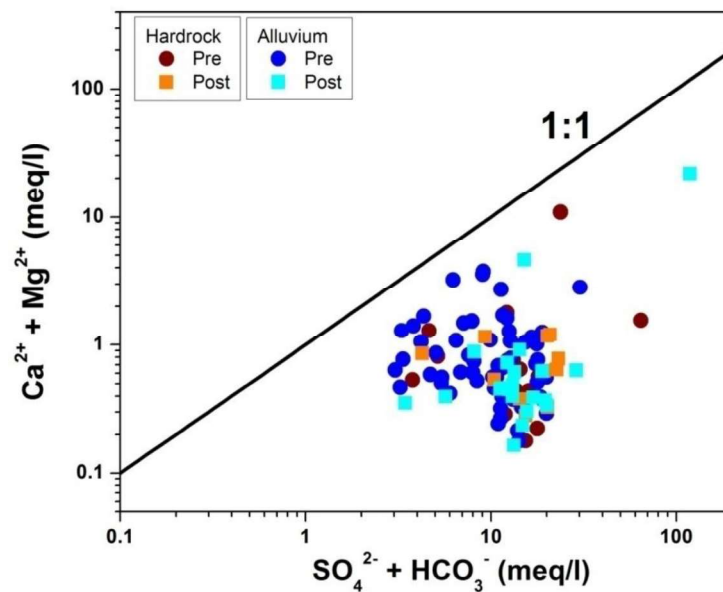


Fig. 4.18 Plot of $(\text{Ca}^{2+} + \text{Mg}^{2+})$ vs. $(\text{SO}_4^{2-} + \text{HCO}_3^-)$ of groundwater samples from the study area

4.3.3.3 Silicate Weathering

To ascertain the silicate weathering occurring in these groundwaters, the relationship between the total ion concentration and the sum of Na^+ and K^+ (Fig. 4.19) is evaluated, the samples fall on or above 1:1 line. This indicates that Na- or K-silicate weathering is not a dominant process for release of alkali metals.

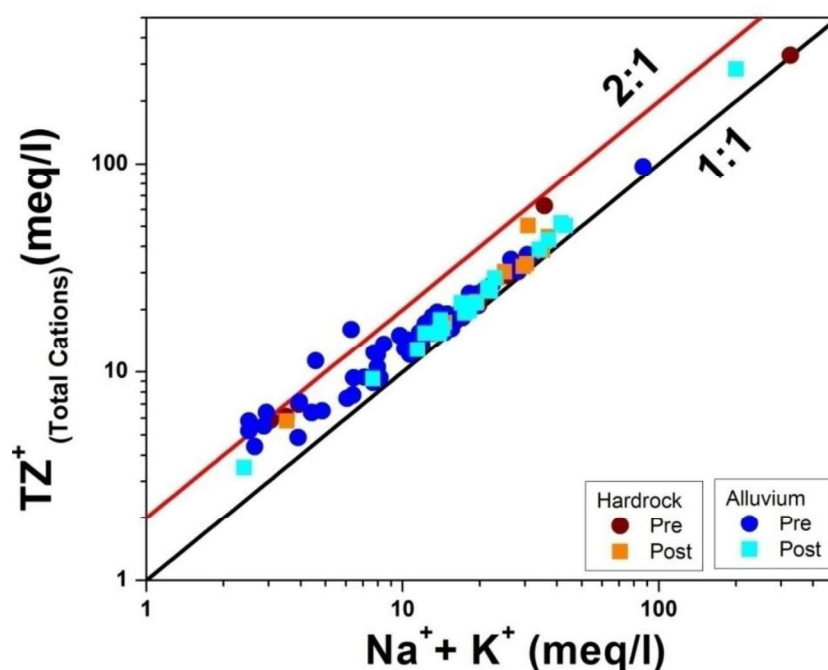


Fig. 4.19 Plot of TZ^+ vs $\text{Na}^+ + \text{K}^+$ of groundwater samples from the study area

Hence it can be concluded that Na^+ ions from the aquifer matrix is replaced with Ca^{2+} and Mg^{2+} ions from water. Thus ion-exchange is the source for Na^+ ion. The source of Mg^{2+} is magnesium silicate weathering and Ca^{2+} ions is the result of calcite or dolomite dissolution. Similar geochemical processes were observed by Coyte et al. (2019) ^[141] in Barmer, Jodhpur, Jaipur, Ajmer, Tonk, Dausa, Kota and Bundi districts of Rajasthan.

4.3.4 Source and recharge mechanism of groundwater

The environmental deuterium ($\delta^2\text{H}$) in the groundwater ranges from -43.44‰ to -15.68‰ and -41.49‰ to -24.7‰ for premonsoon and postmonsoon seasons respectively in samples from the alluvial formation. The $\delta^2\text{H}$ ranges for the premonsoon and postmonsoon

season are -36.44‰ to -8.44‰ and -39.01‰ to -15.5‰ respectively in samples from the hard rock formation. The environmental oxygen-18 ($\delta^{18}\text{O}$) content in the groundwater from alluvial formation are -7.08‰ to -2.88‰ for the premonsoon season while its value for the postmonsoon season ranges from -6.05‰ to -3.19‰. The $\delta^{18}\text{O}$ values in samples from hard rock formation for premonsoon and postmonsoon samples are in the range of -5.99‰ to -1.85‰ and -5.27‰ to -1.67‰ respectively. A widespread in both the isotopes values is observed in both the seasons. From the box plot of isotopic values, it can be clearly seen that more spread is seen in alluvial formation compared to the hard rock formation in both the season (Fig. 4.20).

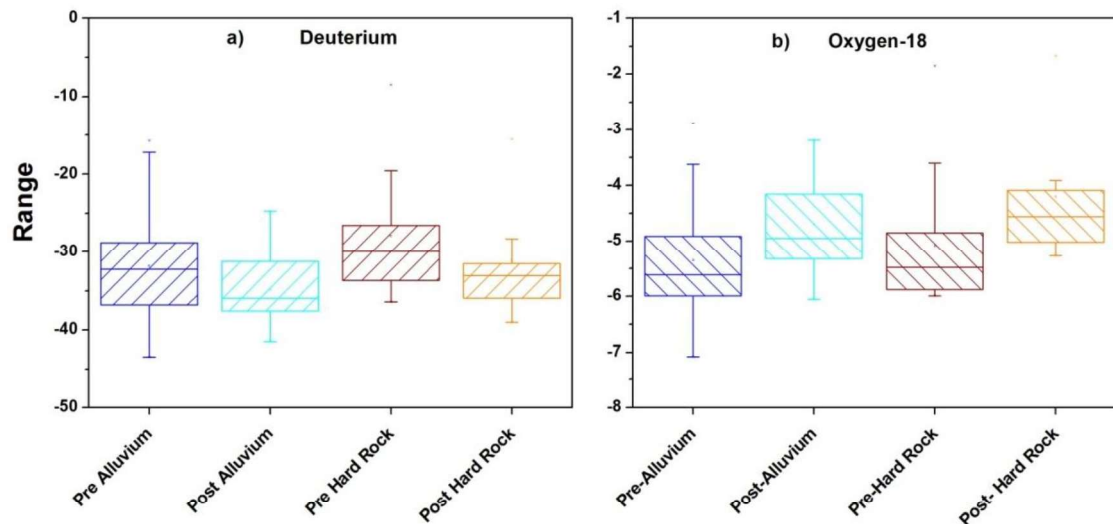


Fig. 4. 20 Box plot for a) Deuterium and b) Oxygen-18 for both season of both formation

The D_{excess} value for samples in the alluvial formation of the study area ranges from -0.39‰ to 19.3‰ for premonsoon and -1.29‰ to 8.0‰ for the postmonsoon season. Samples from the hard rock formation, the D_{excess} ranges from 6.3‰ to 18.5‰ and -2.17‰ to 7.92‰ for premonsoon and postmonsoon seasons respectively. The samples can be categorized based on the D_{excess} values and they were grouped into categories i.e. <5‰, 5‰ to 12‰ and >12‰ (Fig. 4.21). The variations in the D_{excess} values of groundwaters depend on characteristic local hydro-meteorological processes. 10% and 67% of the premonsoon

and postmonsoon samples respectively have $D_{\text{excess}} < 5\text{‰}$ from the alluvial formation (Fig. 4.21 a). For hard rock formation, none of the premonsoon samples has $D_{\text{excess}} < 5\text{‰}$ while 83% of the postmonsoon samples have $D_{\text{excess}} < 5\text{‰}$ (Fig. 4.21 b). The samples having D_{excess} between 5‰ to 12‰ for alluvial formation are 45% and 33% for premonsoon and postmonsoon season respectively (Fig. 4.21 a). For hard rock formation, 37.5% of premonsoon and 17% of the postmonsoon samples fall under the category of D_{excess} in range of 5‰ to 12‰ (Fig. 4.21 b). The samples having $D_{\text{excess}} > 12\text{‰}$ are observed only in premonsoon season for both alluvial and hard rock formation with 45% and 62.5% of samples (Fig. 4.21 a, b).

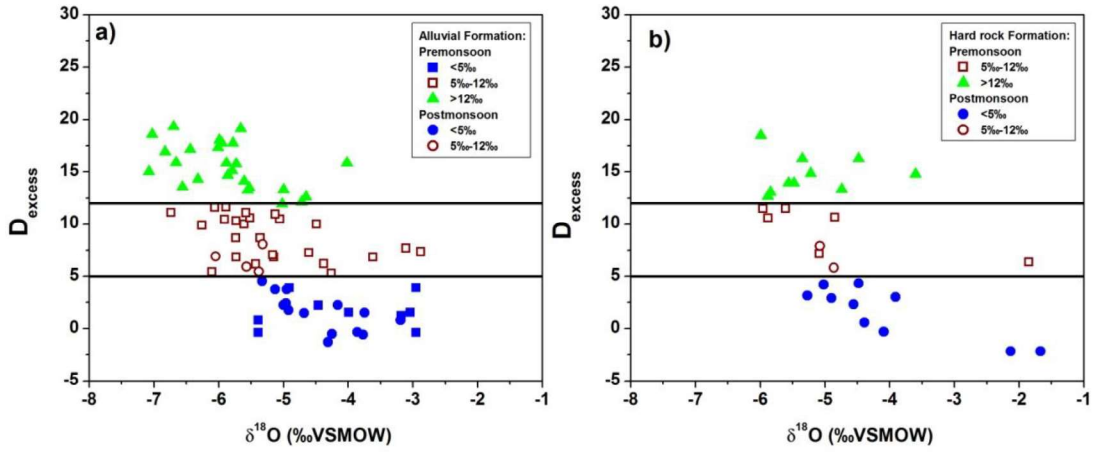


Fig. 4.21 D_{excess} vs $\delta^{18}\text{O}$ plot for both seasons from the alluvial and hard rock formations for both the seasons

The samples having D_{excess} values less than 12‰ fall close to the global meteoric water line (GMWL) by Rozanski et al. (1992) ^[236] and local meteoric water line (LMWL) for Delhi ^[237] are given in Equ. 3.8 and Equ. 4.1 respectively (Fig. 4.23).

$$\text{Delhi (LMWL): } \delta^2\text{H} = 7.2 (\pm 0.10) \times \delta^{18}\text{O} + 4.6 (\pm 0.50) \quad r^2 = 0.95 \quad (4.1)$$

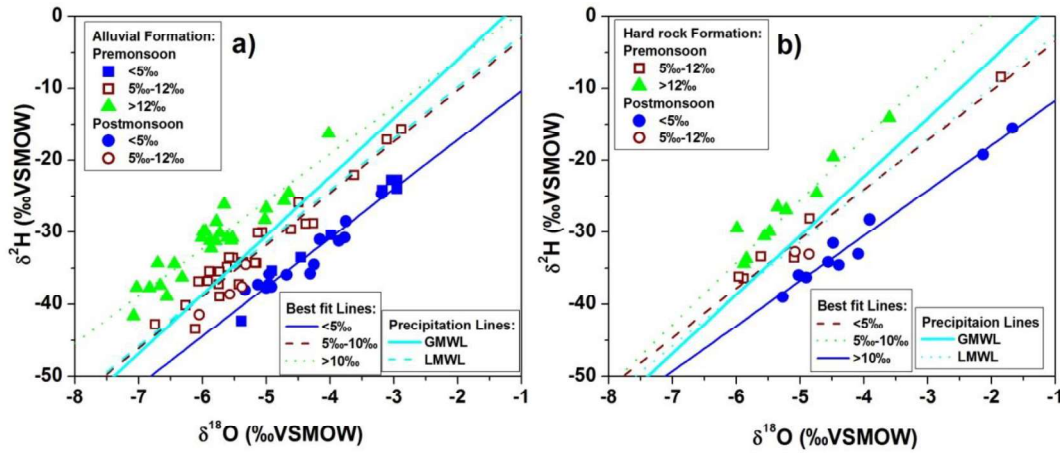


Fig. 4.22 Stable isotope plots for a) alluvium and b) hard rock formations for both the seasons

The BFL for premonsoon and postmonsoon samples having $D_{\text{excess}} < 5\text{‰}$, 5‰ to 12‰ and $> 12\text{‰}$ are given in Equ. 4.2 to Equ. 4.4 for alluvial formation (Fig. 4.22 a).

$$D_{\text{excess}} < 5\text{‰}: \delta^2\text{H} = 6.82(\pm 0.06) \times \delta^{18}\text{O} - 3.52(\pm 0.51) \quad n = 20; r^2 = 0.94 \quad (4.2)$$

$$D_{\text{excess}} 5\text{‰}-12\text{‰}: \delta^2\text{H} = 7.17(\pm 0.06) \times \delta^{18}\text{O} + 4.08(\pm 0.51) \quad n = 29; r^2 = 0.92 \quad (4.3)$$

$$D_{\text{excess}} > 12\text{‰}: \delta^2\text{H} = 6.58(\pm 0.06) \times \delta^{18}\text{O} + 7.2(\pm 0.51) \quad n = 25; r^2 = 0.87 \quad (4.4)$$

The best fit line for premonsoon and postmonsoon samples having $D_{\text{excess}} < 5\text{‰}$, 5‰ to 12‰ and $> 12\text{‰}$ are given in Equ. 4.5 to Equ. 4.7 respectively for the hard rock formation (Fig. 4.22 b).

$$D_{\text{excess}} < 5\text{‰}: \delta^2\text{H} = 6.27(\pm 0.06) \times \delta^{18}\text{O} - 5.40(\pm 0.51) \quad n = 10; r^2 = 0.97 \quad (4.5)$$

$$D_{\text{excess}} 5\text{‰}-12\text{‰}: \delta^2\text{H} = 6.87(\pm 0.06) \times \delta^{18}\text{O} + 3.39(\pm 0.51) \quad n = 8; r^2 = 0.96 \quad (4.6)$$

$$D_{\text{excess}} > 12\text{‰}: \delta^2\text{H} = 8.07(\pm 0.06) \times \delta^{18}\text{O} + 15.11(\pm 0.51) \quad n = 10; r^2 = 0.92 \quad (4.7)$$

The samples with $D_{\text{excess}} < 5\text{‰}$, show slight enrichment with the slope of 6.82 and intercept of -3.52 for alluvial formation which may be due to evaporation of soil moisture before adding to the groundwater (Fig. 4.22a). The samples with D_{excess} values between 5‰ to 12‰ have the slope of 7.17 and intercept of 4.08 which is very close to the LMWL with the slope of 7.2 and intercept of 4.6 indicating precipitation as a source of recharge to the alluvial formation (Fig. 4.22a). The BFL of samples with $D_{\text{excess}} > 12\text{‰}$ from alluvial

formation have the slope of 6.58 and intercept of 7.2, the samples show slight enrichment but lie close to LMWL indicative of slight evaporation of local precipitation before recharging.

For hard rock formation, the BFL of samples having $D_{\text{excess}} < 5\text{‰}$, has a slope of 6.27 and intercept of -5.4 indicative of slight evaporation (Fig. 4.22 b). The slope and intercept of the BFL for samples having D_{excess} values in the range of 5‰ to 12‰ is 6.87 and 3.39 respectively which is close to LMWL. These samples also show slight enrichment which may be attributed to evaporation of local precipitation before recharging. The samples having $D_{\text{excess}} > 12\text{‰}$ from hard rock formation have a slope of 8.07 and intercept of 15.11. These samples lie close to GMWL and indicate recharge from the regional flow. Hence, it can be concluded that the source of recharge to groundwater in alluvial formation is evaporated local rain i.e. irrigation return flow and local precipitation. The recharge source to hard rock formation is evaporated local rain i.e. irrigation return flow and regional flow. The high concentration of F^- , K^+ and TDS are observed in samples from a hard rock formation which indicates long residence time hence increased rock-water interaction leading to increased concentrations (Table 4.6).

Sinha and Navada (2008) ^[260], from their study in Jaisalmer, got the regression line with a slope of 7.4 and intercept of 2.4 which is similar to the samples of the study with D_{excess} between 5‰-12‰ from alluvial formation. They concluded that precipitation is getting infiltrated which modifies in the soil before recharging the aquifer system. Samples from Barmer and Jalore region of their study showed vertical infiltration of evaporated precipitation.

The depth profile of $\delta^{18}\text{O}$ (Fig. 4.23) also corroborates the fact that the source of recharge to groundwater is precipitation and evaporated local rain i.e. irrigation return flow.

The precipitation signature of Delhi was considered ^[238] as samples lie close to LMWL from Delhi (Fig. 4.23).

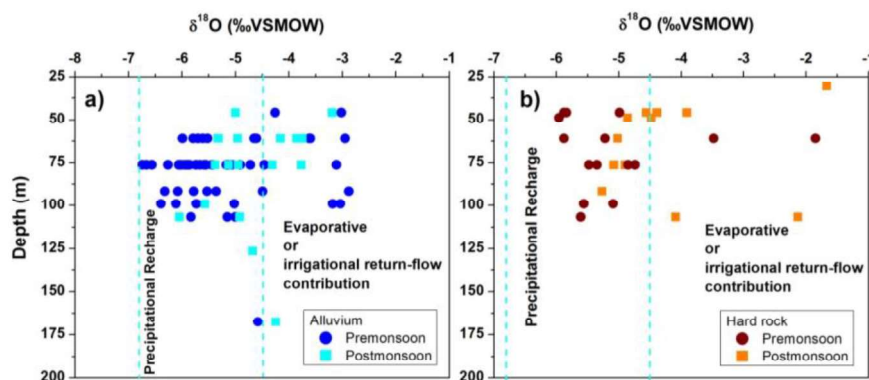


Fig. 4.23 Stable isotope plots for a) alluvium and b) hard rock formations for both the seasons

The tritium values range from 1 TU to 3.5 TU in alluvial formation while for hard rock formation, the tritium content is in range of 1.2 TU to 4.5 TU (Fig. 4.24). Both the formations are getting modern recharge. The tritium values for shallower zones is 1.5 TU to 4.5 TU and the deeper zone is 1 TU to 2.5 TU, indicates that shallower zones in the study area are more dynamic compared to deeper zones.

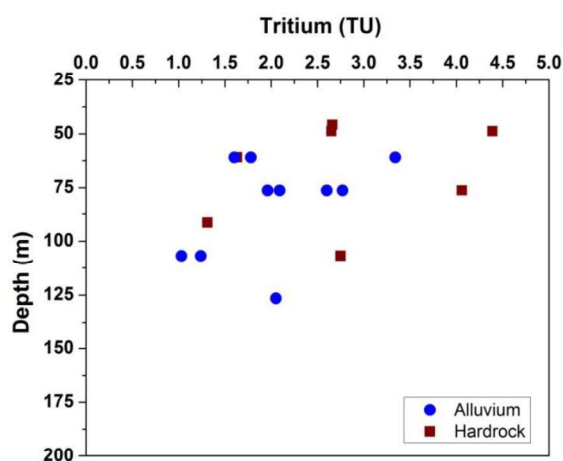


Fig. 4.24 Depth profile for tritium for alluvium and hard rock formation

From the stable isotope and tritium values, the schematic diagram for groundwater flow in the aquifer system can be given as Fig. 4.25

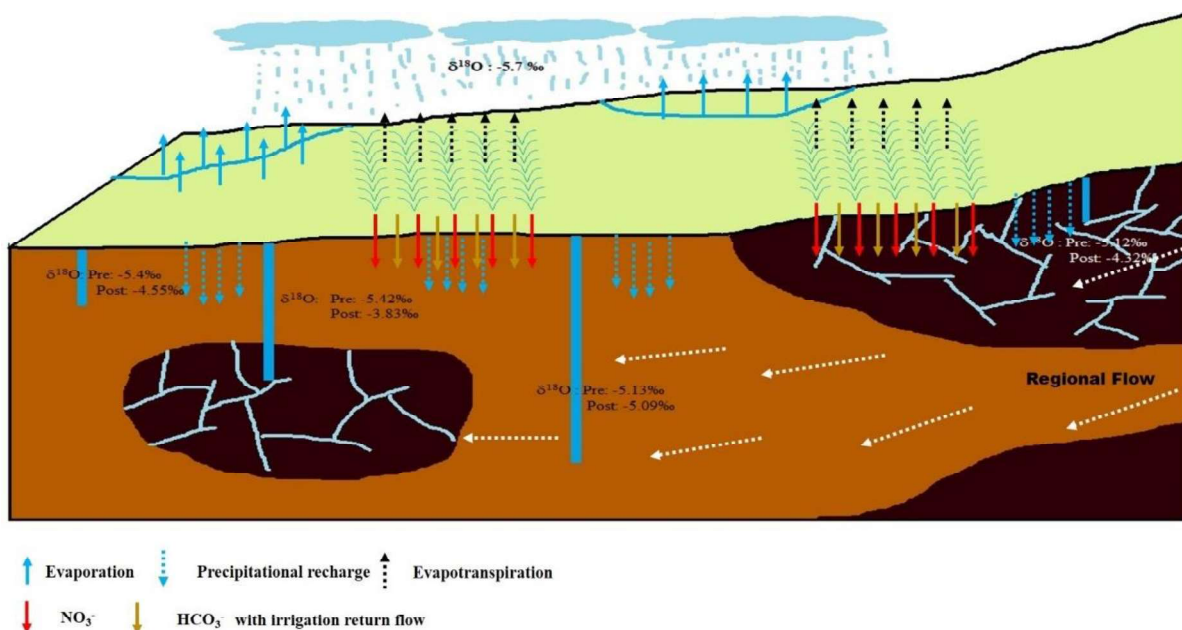


Fig. 4.25 Schematic diagram for groundwater recharge and flow

4.3.5 Factors impacting uranium distribution in groundwater

4.3.5.1 Uranium distribution

A) Uranium distribution: seasonal variation in both formation

The total dissolved uranium ranges from 0.5-177 $\mu\text{g/L}$ with an average value of 25 $\mu\text{g/L}$ for the premonsoon season and 5-142 $\mu\text{g/L}$ with an average value of 47 $\mu\text{g/L}$ for the postmonsoon season for alluvial formation. For hard rock formation, the dissolved uranium concentration ranges from 0.5-115 $\mu\text{g/L}$ with an average of 34 $\mu\text{g/L}$ for the premonsoon season while for postmonsoon the value ranges from 5-145 $\mu\text{g/L}$ with an average value of 51 $\mu\text{g/L}$ (Table. 4.6). The hard rock formation has a higher average concentration of dissolved uranium compared to the alluvial formation in both the seasons (Fig. 4.26). This is attributed to higher concentrations in source rock and long residence time leading to the greater extent of interaction. The concentration also shows an increase in the postmonsoon season which can be attributed to delayed recharge occurring in the study area. This is also corroborated with stable isotope that indicates increased influence of irrigation return flow

during the postmonsoon season i.e. the signature of premonsoon (evaporative enrichment) observed during the postmonsoon season.

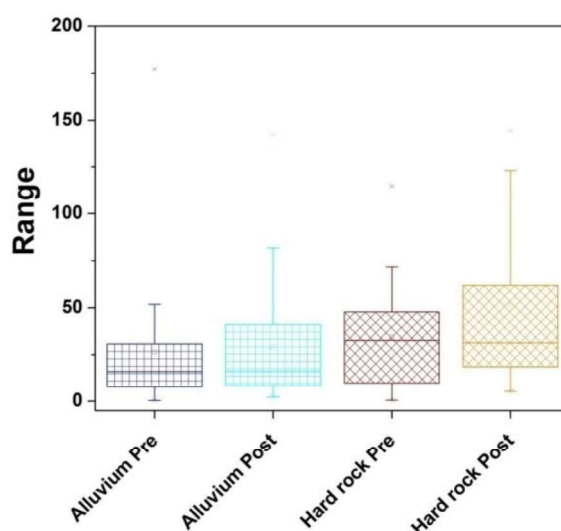


Fig. 4.26 Box plot of uranium in both the formations and both the seasons

The drinking water permissible guidelines as per WHO ^[60] and AERB ^[95] are 30 $\mu\text{g/L}$ and 60 $\mu\text{g/L}$ respectively. 33% and 11% of the samples are above the guidance values of WHO and AERB for the premonsoon season while for postmonsoon season 61% and 36% of the samples are above the guideline values respectively for alluvial formation (Fig. 4.27). In case of hard rock formation, 53% and 13% are above the permissible limit as per WHO and AERB for premonsoon season while for postmonsoon season, 58% and 33% are above the permissible limits respectively. An increase in samples under unsuitable drinking water category is attributed to dissolution of uranium with recharging water.

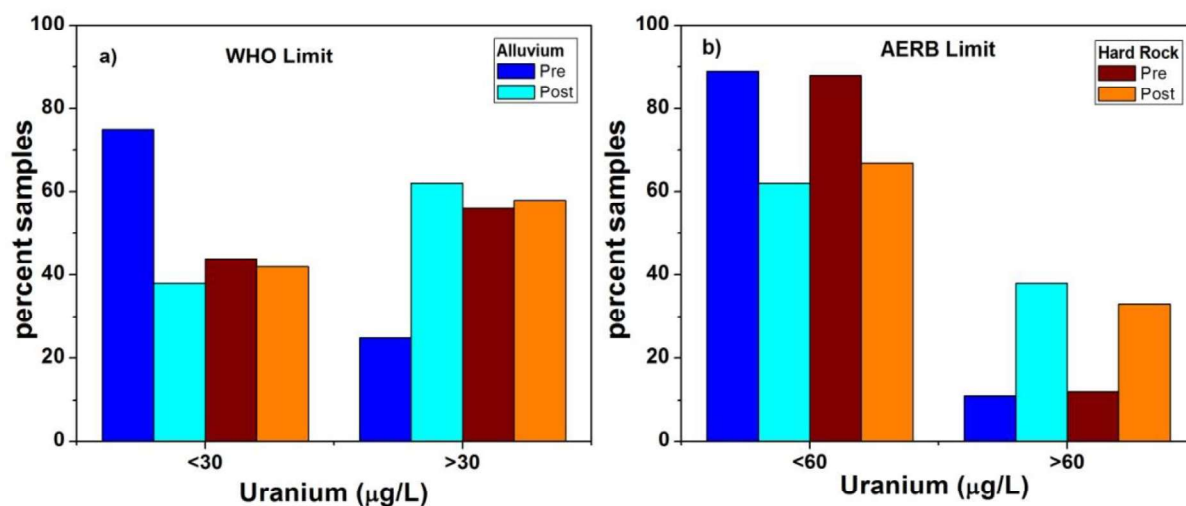


Fig. 4.27 Percent samples above a) WHO and b) AERB limits for both the formations and both the seasons

Similar concentration was reported by researchers in different districts of Rajasthan. Mittal et al. (2017) ^[120] reported dissolved uranium in range of 0.9-167 $\mu\text{g/L}$ with 30% samples above the guidance limit given by AERB. Duggal et al. (2016) ^[121] studied the uranium concentration and found 40%, 40%, 14% and 6% samples above the permissible limits given by AERB respectively. Coyte et al. (2018) ^[122] reported uranium in groundwater in range of 0 to 320 $\mu\text{g/L}$ (n=226) in Rajasthan and 0 to 85 $\mu\text{g/L}$ (n=98) in Gujarat with 33% and 5% samples above the permissible limits given by WHO.

B) Spatial distribution

Spatial distribution of dissolved uranium concentration is shown in Fig. 4.28. During the premonsoon season, the high concentration is observed in the southern part of Jaipur district with few patches in the north-west and central region of the district while Dausa district has compared less contamination (Fig. 4.28 a). During the postmonsoon season, an overall increase in uranium concentrations is observed throughout the study area with high uranium concentration mainly in the south-west portion of the Jaipur district with patches in the central, southern and north-western region while for Dausa district the high concentrations are observed in the central region of the district (Fig. 4.28 b).

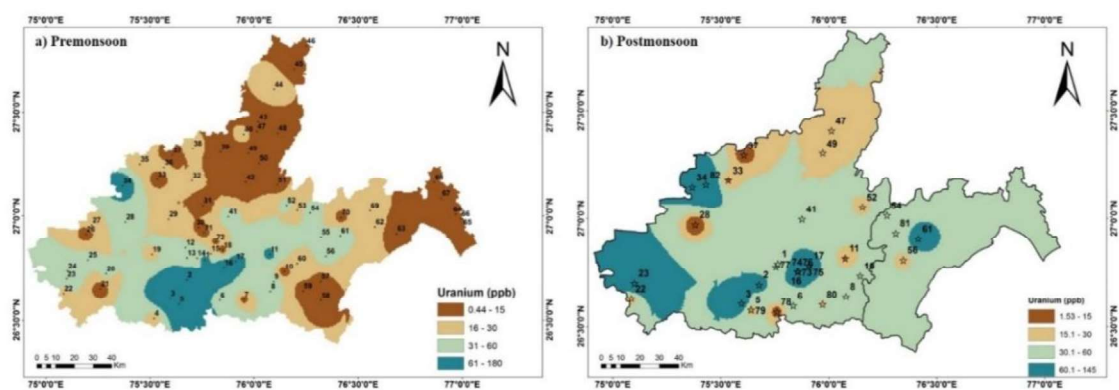


Fig. 4.28 Spatial distribution of dissolved uranium a) premonsoon and b) postmonsoon

From the spatial distribution of HCO_3^- ions (Fig. 4.29), higher concentration is observed in the southern region of Jaipur district with patches in the south-west and north-west regions while in the eastern part with patches in the central region for the Dausa district for the premonsoon. During the postmonsoon season, increased concentrations are observed in southern and western blocks with small patches in the central locations of Jaipur district. For Dausa district central regions show increased concentrations. From the spatial distribution, one can observe an increased concentration of HCO_3^- ions during the postmonsoon season, which can be attributed to the increased irrigation return flow. A clear increase in HCO_3^- is observed in postmonsoon season and a spatial correlation can be observed from the postmonsoon plot of uranium (Fig. 4.28 b) and HCO_3^- (Fig. 4.29 b) mostly in the southern and western part of the study area.

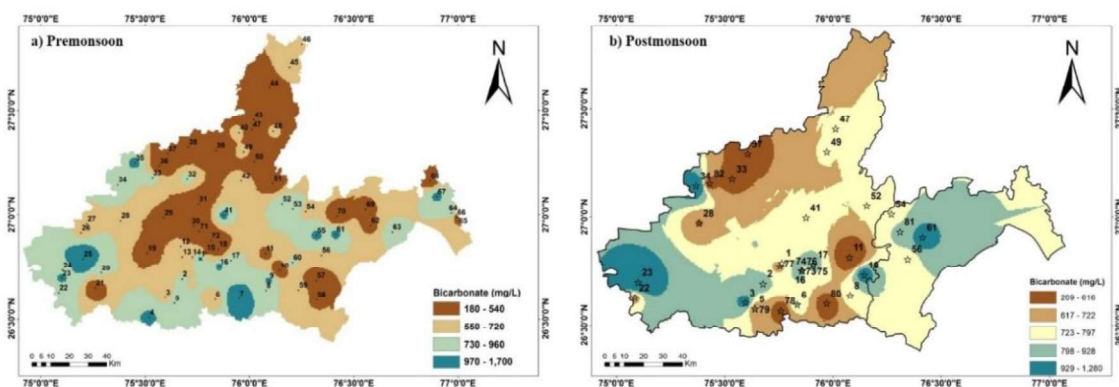


Fig. 4.29 Spatial distribution of HCO_3^- in a) premonsoon and b) postmonsoon seasons

The NO_3^- ion concentrations (Fig. 4.30) are found high in the western region with patches in northern and central regions of Jaipur district while in Dausa district, a small patch in the northern part of the district shows increased concentration during the premonsoon season. During the postmonsoon season, high concentration is observed in the western region with patches in east and southern part of Jaipur district while in Dausa district higher concentrations are observed in the whole area with the highest concentration in the central part of the district. Overall, in postmonsoon season dilution effect is observed at the western location and central location for Jaipur district while increased concentrations are observed in Dausa district and eastern part of Jaipur district.

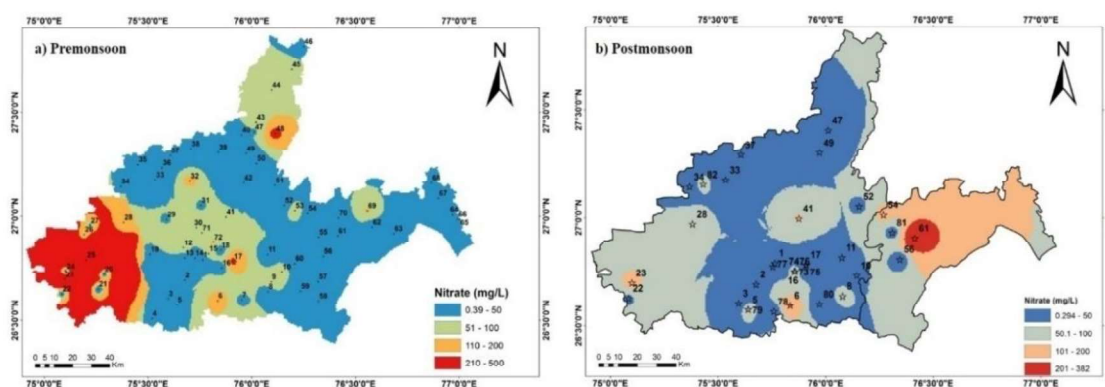


Fig. 4.30 Spatial distribution of NO_3^- in a) premonsoon and b) postmonsoon seasons

The correlation scatters plot of uranium, HCO_3^- ions and NO_3^- ions corroborates the same. From the plot between uranium and HCO_3^- ions, a positive correlation is observed for both the seasons with a dominance in the postmonsoon season (Fig 4.31). From the plot of NO_3^- ions vs. uranium, a strong positive correlation is observed in the postmonsoon season (Fig. 4.32) which is also corroborated from the spatial distribution (Fig. 4.30).

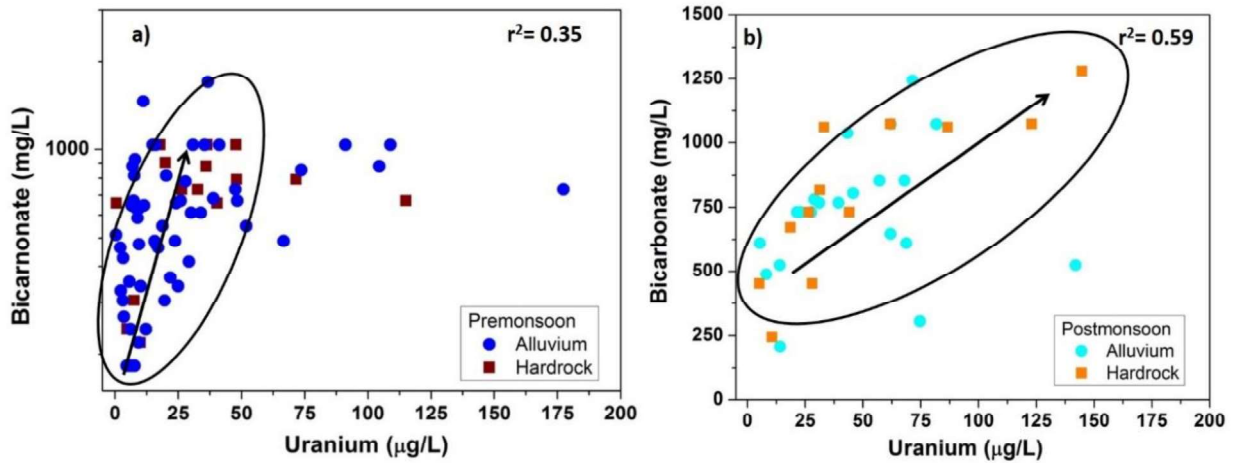


Fig. 4.31 Correlation of uranium with HCO_3^- ions in a) premonsoon and b) postmonsoon seasons

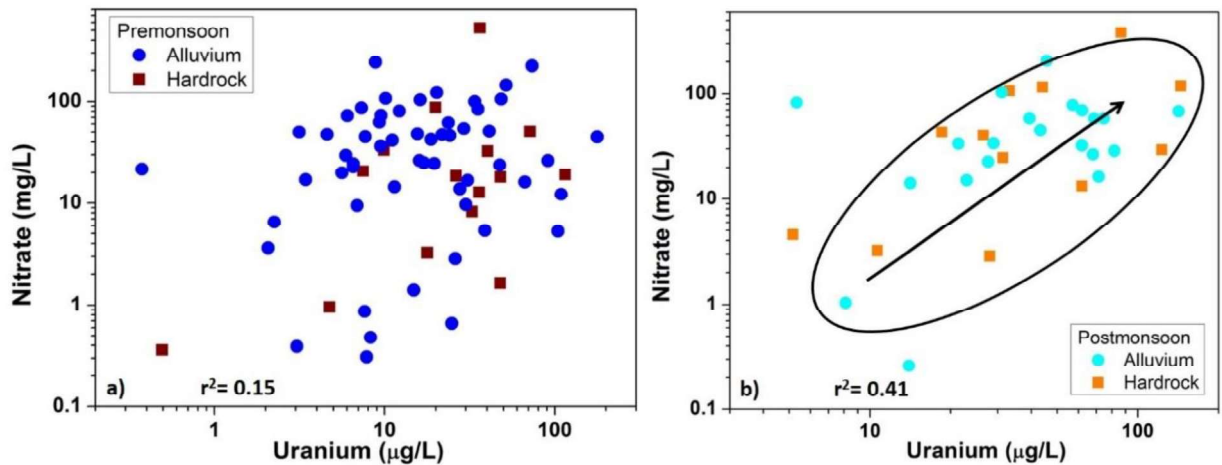


Fig. 4.32 Correlation of uranium with NO_3^- ions in a) premonsoon and b) postmonsoon seasons

Coyte et al. (2019) ^[138] in their study in districts of Rajasthan for various contaminants like F^- ions, NO_3^- ions and uranium concluded that uranium and F^- ions are released due to weathering from rock and their concentration increases due to evapotranspiration, irrigation return flow and ion-exchange. The results of this study infer that all these factors combined led to increased concentration of uranium in groundwater of Rajasthan.

C) Depth profile

The depth profile (Fig. 4.33) of uranium indicates that the spread of contamination in both the formation is equal. The shallower and deep zones both contain contaminated samples. The contamination in deeper zones is less compared to shallower zones. The lower contamination in the deeper zone indicates that contamination is either due to mixing with contaminated samples of shallower zones or the reduction or absence of factors that are leading to the mobilization of uranium from the source rock. This is corroborated with the observed depth profile of NO_3^- ions (Fig. 4.7).

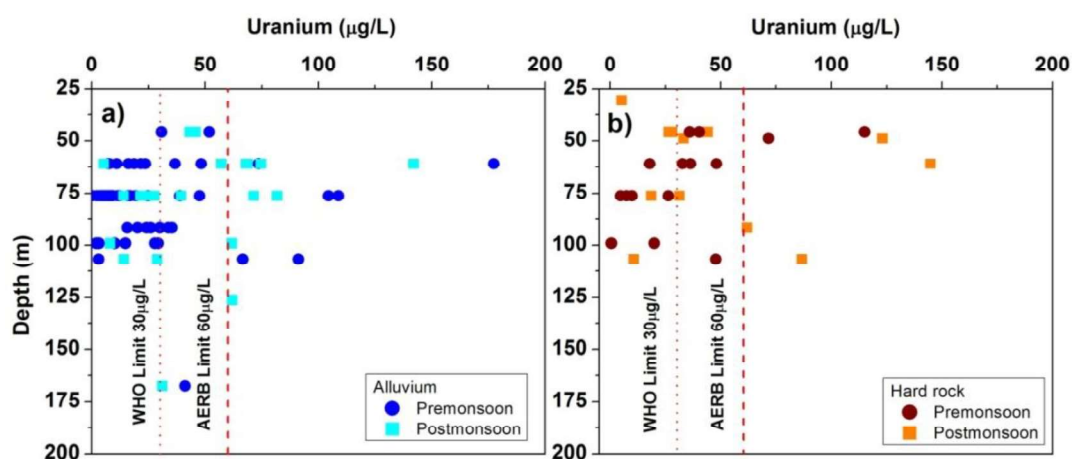


Fig. 4.33 Depth profile of uranium for a) alluvium and b) hard rock formations

The shallower zones have high nitrate which helps in the release of uranium. Thus, more uranium contamination in the shallower zone is observed compared to deeper zone. From the depth profile of $\delta^{18}\text{O}$ (Fig. 4.23), it is observed that shallow zone samples show signatures of irrigation return flow and precipitation recharge. The irrigational return flow mostly has high NO_3^- and HCO_3^- ions and precipitation recharge dissolve along soil CO_2 making water acidic which leaches the uranium from the minerals.

4.3.5.2 Correlations of uranium

The Pearson's correlation of uranium with different physicochemical parameter and major ions are shown in with the help of bar graph (Fig. 4.34). In samples from the alluvial

formation (Fig. 4.34 a), it was observed that uranium shows a positive correlation with almost all parameter except Ca^{2+} ions in premonsoon and pH in both seasons. The correlation is dominant with F^- ions (0.52) followed by Mg^{2+} ions (0.45), EC (0.42) and HCO_3^- ions (0.35) in premonsoon while in postmonsoon, uranium is more correlated with EC (0.8) followed by Na^+ ions (0.78) and Cl^- ions (0.78). Higher correlation of uranium with NO_3^- ions during the postmonsoon season is also observed in alluvial formation i.e. from 0.07 to 0.17. For hard rock formation, uranium shows a positive correlation with all except Ca^{2+} ions in premonsoon and pH in postmonsoon (Fig. 4.34 b). The maximum correlation is observed with F^- ions (0.81) followed by Na^+ ions (0.5), EC (0.36) and HCO_3^- ions (0.32). In the postmonsoon, correlation of uranium is dominant with HCO_3^- ions (0.8), EC (0.78), followed by Na^+ ions (0.75) and Cl^- ions (0.73). The correlation with NO_3^- ion has increased from 0.04 to 0.4 during the postmonsoon season. The above observations also corroborated with correlation plots of uranium, HCO_3^- ions (Fig. 4.31) and NO_3^- ions (Fig. 4.32).

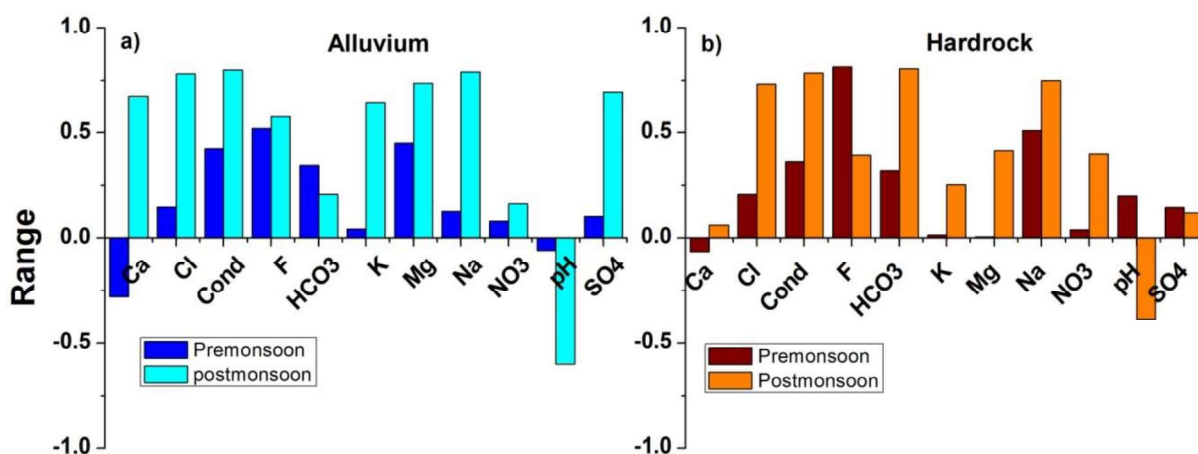


Fig. 4.34 Correlation of physicochemical parameters and major ions with uranium for a) alluvium and b) hard rock formations in both the seasons

Uranium also shows a positive correlation with EC (Fig. 4.35) during both the seasons in both the formations. The correlation increases in postmonsoon season corroborating the increased uranium values in the postmonsoon. Positive correlations of

uranium with EC, TDS were inferred by researchers working in districts of Rajasthan [120, 121].

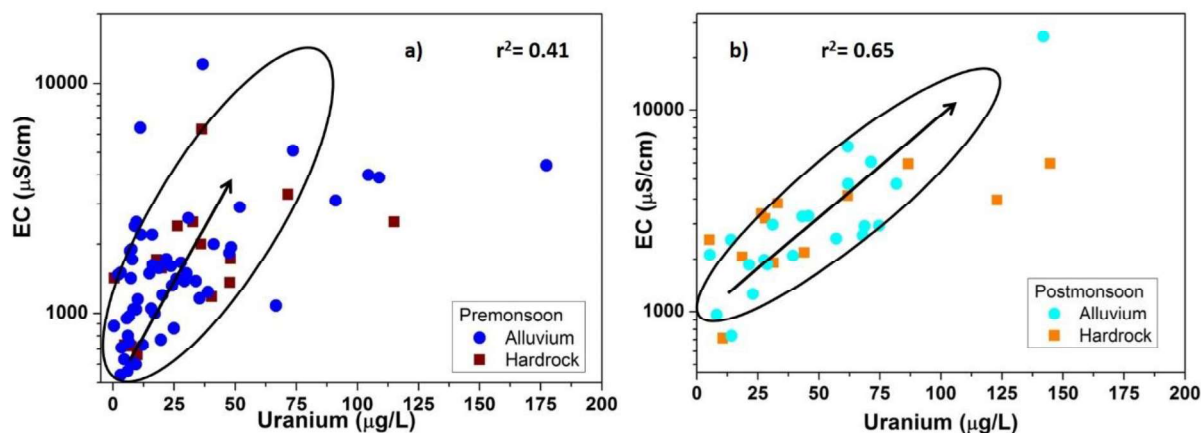


Fig. 4.35 Correlation of uranium with EC in a) premonsoon and b) postmonsoon season

The high uranium concentrations in alluvial formation are associated with Na-HCO₃-Cl (50%) and Na-Cl-HCO₃ (50%) type in premonsoon while for the postmonsoon shift to Na-Cl-HCO₃ water type is observed (Na-HCO₃-Cl: 25% and Na-Cl-HCO₃: 75% of samples). For hard rock formation, all the contaminated samples had Na-HCO₃-Cl water type in premonsoon which shifted to Na-HCO₃-Cl (25%) and Na-Cl-HCO₃ (75%) water type. The highest values of uranium have Na-Cl-HCO₃ water type in both formations and both seasons. Thus, corroborating that EC (Na⁺ and Cl⁻) and HCO₃⁻ ions have a major role in uranium mobilization.

A negative correlation is observed with Ca²⁺ ions in premonsoon season is due to ion-exchange between UO₂²⁺ and Ca²⁺ ions because of similar ionic radii. The dominance of the ion exchange process in the study area is observed in the geochemical process (Chapter 4, Section 4.3.2.2 A). From the correlation data and dominant water type of contaminated water, it can be concluded that factor like EC, NO₃⁻ ions, Ca²⁺ ions and HCO₃⁻ ions plays a major role in the mobilization or solubilization of uranium. The detailed release mechanism is discussed under chapter 5

4.3.5.3 Factor analysis or Principal Component Analysis

After applying PCA to the data set, twelve variables namely EC, pH, Na^+ , K^+ , Ca^{2+} , Mg^{2+} , F^- , Cl^- , NO_3^- , SO_4^{2-} , HCO_3^- and Uranium were considered as they had commonalities more than 0.7 hence all these variables were suitable for loading on the principle components. Kaiser normalization was followed to select the PC covering the maximum variance of the data [241].

A) Alluvial formation

In samples from alluvial formation, three components were found that covers 83% and 85% of the variance for premonsoon and postmonsoon season respectively. For the premonsoon season, PC1 corresponds to 54% of the variance and it shows high correlation with Na^+ , K^+ , Cl^- , SO_4^{2-} and NO_3^- ions. The PC1 indicates ion exchange process as it has a high correlation with Na^+ and K^+ and low correlation with Ca^{2+} and Mg^{2+} ions. The same is corroborated from CAI 1 and CAI 2 values (Section 4.3.3.1). The high correlation of PC1 with NO_3^- ions indicates anthropogenic contamination from fertilizers, septic tanks etc. The PC2 corresponds to 16% of the variance and shows a positive correlation with uranium, F^- and NO_3^- ions while negative correlation with Ca^{2+} ions. The positive correlation of PC2 with NO_3^- ions indicates oxidation of uranium in aquifer matrix. The negative correlation with Ca^{2+} indicates towards ion exchange. This is also corroborated with the dominance of ion exchange reaction in the study area as per PC1 and scatter plot (Fig. 4.17). PC3 corresponds to 14% of the variance and is positively correlated to Ca^{2+} and Mg^{2+} ions, indicates dolomite dissolution in the aquifer system.

For the postmonsoon season, PC1 corresponds to 62% of the variance and shows a strong positive correlation with EC and uranium which indicates leaching of uranium with high ionic strength solution. The positive correlation between uranium and EC is also established using scatter plot (Fig. 4.35). The PC2 component with 14% variance shows a

positive correlation of uranium and NO_3^- ions, hence the dominance of oxidation of uranium with NO_3^- ions can be inferred. This is also supported by the uranium and NO_3^- ion scatter plot which indicated a positive correlation between both (Fig. 4.32). The PC3 component with 9% variance shows a positive correlation of uranium with HCO_3^- ions which points to mobilization/solubilization of uranyl ion as uranyl-carbonate complexes. The same is corroborated with the uranium and HCO_3^- ions correlation plot (Fig. 4.32).

Table 4.11 PCA output Varimax rotated for the alluvial and hard rock formations

Parameters /Components	Alluvium						Hard rock				
	Premonsoon			Postmonsoon			Premonsoon		Postmonsoon		
	PC1	PC2	PC3	PC1	PC2	PC3	PC1	PC2	PC1	PC2	PC3
EC	.799	.532	.216	.965	.205	.138	.849	.496	.864	.439	.164
HCO ₃ ⁻	.546	.600	.002	-.200	.136	.838	.346	.644	.898	.201	-.175
U	-.011	.876	-.067	.716	.299	.462	-.088	.876	.878	.159	-.025
F ⁻	.538	.629	-.336	.361	.032	.722	-.166	.863	.580	-.712	.300
Cl ⁻	.950	.208	.166	.969	.189	.102	.891	.346	.807	.418	.126
NO ₃ ⁻	.710	.007	.316	-.065	.861	.019	.960	.089	.292	.915	.074
SO ₄ ²⁻	.972	.123	.115	.976	.113	.007	.934	.284	.274	.220	.707
Na ⁺	.974	.175	.074	.966	.165	.161	.515	.770	.947	-.134	.241
K ⁺	.977	-.014	.050	.450	.758	.136	.976	.061	.102	.933	.260
Mg ²⁺	.019	.663	.683	.976	.147	.048	.976	.046	.304	.940	.089
Ca ²⁺	.066	-.249	.803	.982	.115	-.069	.980	-.035	-.069	-.083	.866
pH	-.348	-.083	-.753	-.452	-.584	-.204	-.896	.148	-.235	-.812	.463
Eigenvalue	6.46	1.92	1.62	7.47	1.66	1.11	7.82	2.59	5.84	3.12	1.60
% of Variance	53.85	15.97	13.53	62.29	13.85	9.22	65.13	21.56	48.68	25.98	13.35
Cumulative %	53.85	69.82	83.35	62.29	76.14	85.37	65.13	86.68	48.68	74.66	88.01

Table 4.12 The correlation of components with the various variable in both alluvial and hard rock formations

Components	Alluvium		Hard rock	
	Premonsoon	Postmonsoon	Premonsoon	Postmonsoon
PC1	Positively correlated with Na^+ , K^+ , SO_4^{2-} , Cl^- , NO_3^-	Positively correlated with Ca^{2+} , Mg^{2+} , SO_4^{2-} , Cl^- , Na^+ and U	Positively correlated with Ca^{2+} , Mg^{2+} , K^+ , NO_3^- , SO_4^{2-} and Cl^- Negatively with pH	Positively correlated with Na^+ , Cl^- , U and HCO_3^-
PC2	Positively correlated with U, Mg, F^- and HCO_3^- Negatively correlated with pH	Positively correlated with NO_3^- , U and K^+	Positively with HCO_3^- , F^- , U	Positive with Mg^{2+} , K^+ , NO_3^- Negative with pH
PC3	Positively correlated with Ca^{2+} and Mg^{2+} Negatively correlated with pH	Positively with HCO_3^- , F^- , U		Positive with Ca^{2+} and SO_4^{2-}

B) Hard rock formation

For the hard rock formation during premonsoon season two-components were identified with a total variance of 87%. The PC1 corresponds for 65% of the variance. It has a positive correlation with Ca^{2+} , Mg^{2+} SO_4^{2-} ions which can be due to anthropogenic contamination from gypsum-based fertilizer [235]. Similarly, high correlation with K^+ and NO_3^- ions again indicates anthropogenic contamination from excess use of NPK fertilizers [242]. This implies that hard rock formation is highly fractured and getting contribution from irrigation return flow, which is corroborated by the geology of the region (section 4.1). The stable isotope data (section 4.3.4) corroborates that one of the recharge sources to the formations is irrigation return flow. The PC2 correspond to 22% of the variance. It has a positive correlation with uranium and HCO_3^- ions which indicates mobilization of uranyl ion as uranyl carbonates, corroborated by correlation plot (Fig. 4.31).

For the postmonsoon season, the total variance of 88% with three components. The PC1 corresponds for 49% of the variance and has a positive correlation with Na^+ , Cl^- , uranium and HCO_3^- ions and slight negative correlation with Ca^{2+} ions indicating ion exchange reaction leading to increase in Na^+ and uranyl ion. The exchanged uranyl ion is stabilized with HCO_3^- by complexation. The PC2 corresponds to 26% of the variance and has a positive correlation with Mg^{2+} , NO_3^- , K^+ ions that indicates anthropogenic contamination via irrigation return flow. The PC3 corresponds to 13% variance and correlates with Ca^{2+} ions and SO_4^{2-} ions indicting dissolution of gypsum.

Uranium shows a correlation with PC2 during the premonsoon season while it shows a correlation with PC1 during the postmonsoon season which corroborated the increase in concentration during the postmonsoon season in both the formations. PCA also indicates EC, NO_3^- and HCO_3^- ions influence uranium mobilisation.

4.3.5.4 Uranium Speciation

The uranium species were estimated using WATEQ4F and species having a concentration in $\mu\text{g/L}$ (ppb) range were selected and compiled in Table 4.15.

Table 4.13 Various species formed by uranyl ion in groundwater from both the formations

Formation	Season/ Species	$\text{UO}_2(\text{CO}_3)_2^{2-}$ ($\mu\text{g/L}$)			$\text{UO}_2(\text{CO}_3)_3^{4-}$ ($\mu\text{g/L}$)		
		Min .	Ma x	Averag e	Min .	Ma x	Averag e
Alluvium	Pre	0.12	30	4.96	2.8	300	45
	Post	1.2	64	16	6.6	204	70
Hard rock	Pre	0.13	140	13	0.78	202	65
	Post	0.86	46	15	8.3	223	71

The main uranium species found in the groundwater of the study area are $\text{UO}_2(\text{CO}_3)_2^{2-}$ and $\text{UO}_2(\text{CO}_3)_3^{4-}$. The work by researchers in the granitic terrains ascertained similar complexes [246]. The $\text{UO}_2(\text{CO}_3)_3^{4-}$ complex is dominant species in pre and postmonsoon season of both the formations. The concentration of $\text{UO}_2(\text{CO}_3)_2^{2-}$ and $\text{UO}_2(\text{CO}_3)_3^{4-}$ complex is more in the postmonsoon season compared to premonsoon which can be attributed to the availability of uranyl ion and complexing ions. The complexation reactions are discussed under chapter 5 in details.

4.3.5.5 Saturation Index

The generated output for alluvial and hard rock formation is represented in the box plot (Fig. 4.36). The saturation index values indicate that the groundwater is tending to supersaturation with respect to uraninite in pre and postmonsoon seasons of both the formation. The increase in saturation index for uraninite is observed in the postmonsoon season compared to the premonsoon season for both the formation. This is attributed to increased concentration in postmonsoon season. The other uranium minerals are undersaturated out of which Gummite is least saturated and B- $\text{UO}_2(\text{OH})_2$ is more saturated compared to other unsaturated minerals. As the water is undersaturated in uranium, hence

groundwater is more prone to contamination in the study area. The feasible condition can lead to an increase in contamination in both the formation of the study area. Rajasthan is known to contain uraninite as the main mineral of uranium with minor Coffinite, Ilmenite, molybdenite, pyrrhotite, chalcopyrite and Brannerite etc associated with them. They lie in between quartzo-feldspathic or aplitic in Rohil-Ghateshwar-Khandela-Diara and Saladipura area in Sikar district of Rajasthan [261,262].

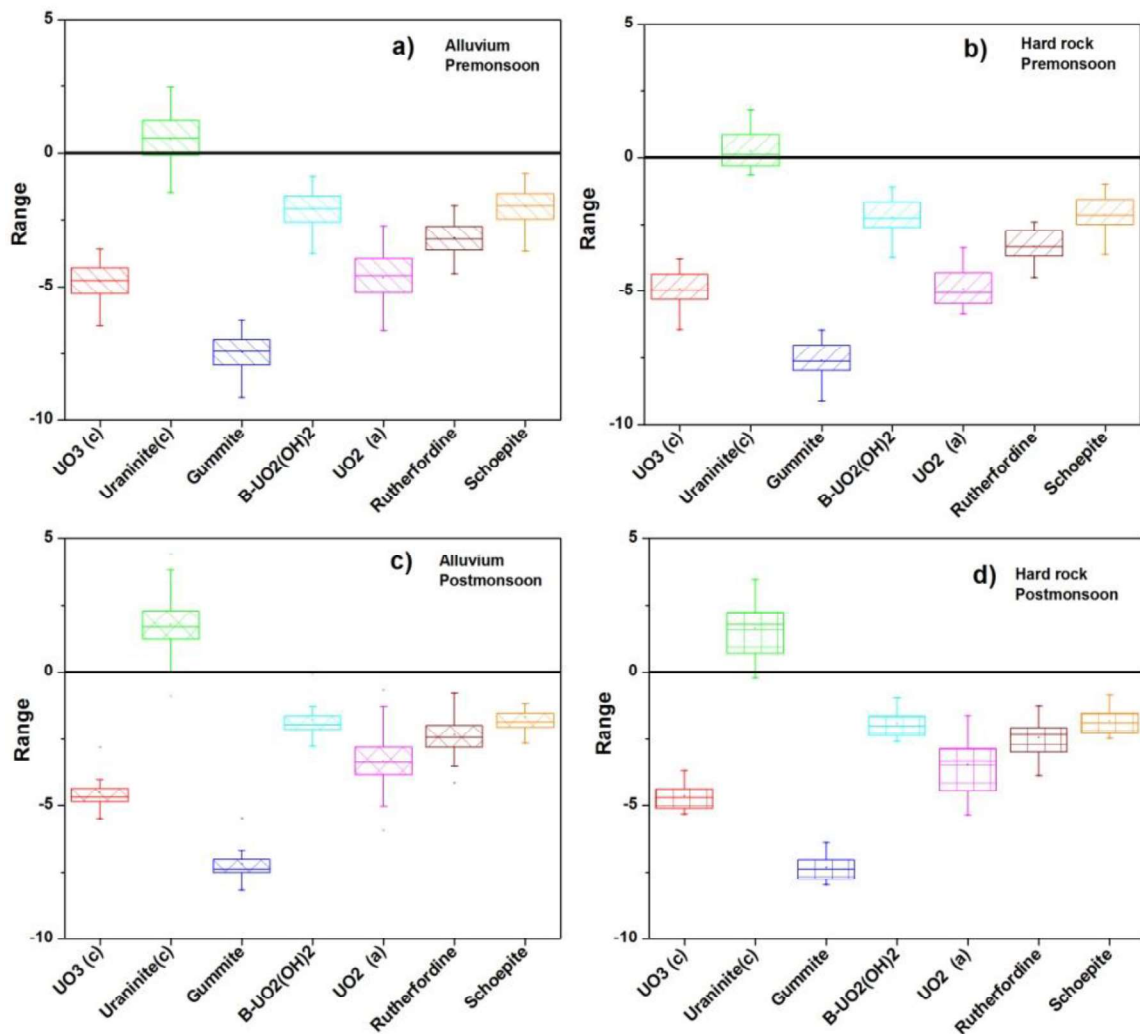


Fig. 4.36 Box plot of saturation indices for common uranium minerals for a) alluvial and b) hard rock formations for both the seasons

4.3.5.6 Uranium isotope

The uranium activity ratio ($^{234}\text{U}/^{238}\text{U}$) ranges from 1.44 to 2.85 with an average value of 2.04 in the alluvial formation and 1.38 to 2.97 with an average value of 2.05 in the hard rock formation. The spread in the activity ratio of both the formations is almost the same. This indicates common geochemical processes leading to uranium mobilization. Activity ratio in the range of 1.5 to 3.5 was estimated by Coyte et al. (2018) ^[125] in Rajasthan. The uranium isotopic data showed disequilibrium condition for $^{234}\text{U}/^{238}\text{U}$, which was attributed to selective leaching of ^{234}U . The process is explained in detail under chapter 5.

From the depth profile (Fig. 4.37), a larger spread was observed in AR in the shallower zones i.e. 1.38 to 2.97 while for the deeper zones the spread is less i.e. 1.69 to 2.38. The less variation is due to longer interaction time leading to uniformity.

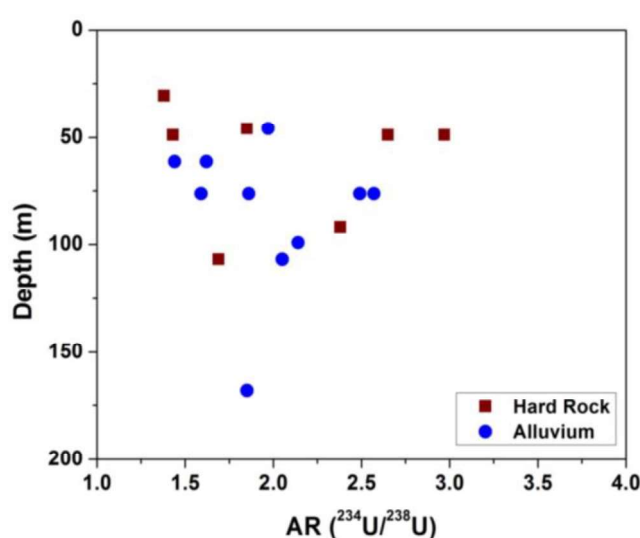


Fig. 4.37 Depth profile for AR ($^{234}\text{U}/^{238}\text{U}$)

Comparing the plot of activity ratio versus inverse uranium concentration with the standard plot by Osmond and Cowart ^[183] (Chapter 2: Fig.2.9), it is observed that leaching of uranium from its mineral is the main process responsible for uranium concentration in the study area (Fig. 4.41). The alpha recoil process is the main reason for the activity ratio greater than 1.

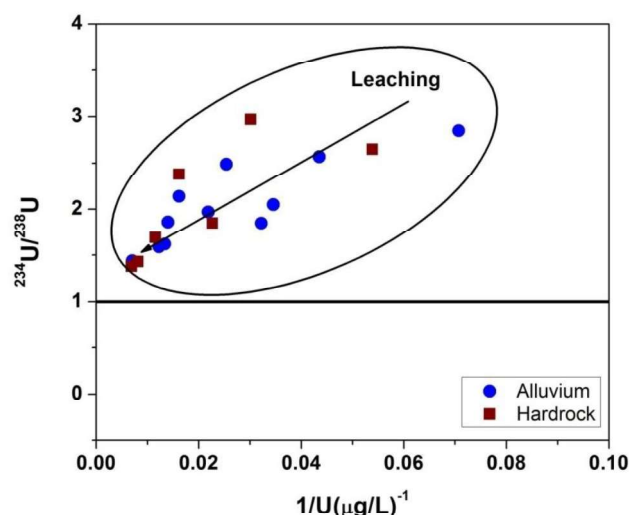


Fig. 4.38 Activity ratio vs. inverse concentration plot to identify the process for uranium mobilization for both the formations

4.4 Conclusions

The water from alluvial and hard rock formation are both unsuitable for the purpose of drinking and irrigation. According to DWQI, 25% of the premonsoon samples are unsuitable which increases to 71% for the postmonsoon season for alluvial formation. For hard rock formation, 60% of the samples are unsuitable for both pre and postmonsoon seasons. According to the IWQI parameter, 100% of the samples from both the seasons and formations are unsuitable for their use. The alluvial formation and hard rock formations seem to be interconnected as the major ions show high concentration in both the formations. The contamination is spread in the deeper zones also which indicate the mixing in shallower and deeper zones. The geochemical process occurring in the study area are i) ion-exchange which is responsible for Na^+ ions in the water, ii) magnesium silicate weathering responsible for Mg^{2+} ions and iii) calcite dissolution leading to Ca^{2+} ions into the aquifer system. The study area has contamination of NO_3^- ions, F^- ions and uranium spread in both the formations and along with the depth. The $\delta^2\text{H}$ values range from -43.44‰ to -8.44‰ for the premonsoon season while the value for the postmonsoon season is -41.49‰ to -15.51‰. The $\delta^{18}\text{O}$ values

are in the range of -7.08‰ to -1.85‰ in the premonsoon season while for the postmonsoon season its range is -6.05‰ to -1.67‰. The source of recharge to groundwater for alluvial formation is i) precipitation and ii) irrigation return flow while the recharge source to hard rock formation is i) irrigation return flow with contribution from the regional flow. The uranium concentration in premonsoon ranges from 0.4-177 µg/L with an average of 28 µg/L. For the postmonsoon season the concentration, ranges are 5-145 µg/L with an average value of 49 µg/L. As per the guidelines laid by WHO for uranium in drinking water, 33% of the samples are above the limit in premonsoon season which increases to 61% in postmonsoon. The increases in concentration are attributed to ions brought along with recharging water that helps uranium mobilization. The spatial distribution of uranium in the study area during the premonsoon period shows higher concentration in southern region of the study area with patches in central and north-western regions. During the postmonsoon season, higher concentrations are observed in south-west and southern regions with patches of high concentration in central and western regions. The spread in the uranium concentration is attributed to the local hydrogeological conditions of the aquifer. The high uranium concentrations are associated with Na-Cl-HCO₃ water type indicating that EC and HCO₃⁻ ions play a major role in uranium mobilization. The depth profile shows a high concentration in shallow as well as the deep zones with an almost similar spread in uranium concentrations. This indicates that there is an interconnection between the two zones with contamination spread throughout and the aquifer behaves like a single unit. The area under study is agriculture intensive with excessive use of fertilisers, which add up to higher levels of NO₃⁻ and HCO₃⁻ in the groundwater through irrigation return flow. From the statistical analysis, factor analysis and speciation study it can be concluded that in the hard rock formations, as the water enters inside of the rock via fractures with limited availability of NO₃⁻ ions it oxidizes uranium from the minerals. As the amount of NO₃⁻ ions is limited whole mineral

dissolution does not take place like in case of alluvial formation from Punjab. The probability of availability of ^{234}U due to alpha recoil phenomenon is more thus the leaching of ^{234}U is more creating disequilibrium condition i.e. the signatures of alpha recoil are retained in case of the study area from Rajasthan. Thus, the higher activity ratio of $^{234}\text{U}/^{238}\text{U}$ was observed. The released uranyl ion in groundwater complexes with HCO_3^- ions under the favourable pH condition forming the major species as $\text{UO}_2(\text{CO}_3)_2^{2-}$ and $\text{UO}_2(\text{CO}_3)_3^{4-}$ for both the alluvial and hard rock formation. The process is more dominant in hard rock formation which can be attributed to the high concentration of uranium mineral in the aquifer matrix. Thus, from the combination of chemical parameters, geochemical processes occurring in the system, isotopic and statistical analysis one can conclude that release of uranium is occurring via three processes i) NO_3^- ions help in oxidizing uranium from the aquifer matrix, ii) ion-exchange also plays the role in uranium release from aquifer matrix and iii) alpha recoil also brings uranium from matrix to water. From the first and second process, uranium is in the oxidized state hence soluble while uranium released via third process may or may not be oxidized. Once the uranium is released, it is oxidized due to the presence of NO_3^- ions in aquifer water. Under the groundwater pH condition, uranyl ions forms carbonate complexes which stabilize the uranyl ion in the aquifer system. The increased rock water interaction corroborated with increased Na^+ , K^+ , F^- ions in the aquifer water in the hard rock formation. The water enters the fracture where the probability of having ^{234}U is more due to alpha recoil and thus the disequilibrium in activity ratio of $^{234}\text{U}/^{238}\text{U}$. The proposed mechanism for uranium release in the formation is given under chapter 5.

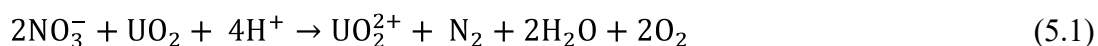
CHAPTER 5 Comparative Analyses

There are many common features between the two study areas, viz., Punjab (Muktsar and Faridkot) and Rajasthan (Jaipur and Dausa), that include semi-arid climate, major rainfall from south-west monsoon, extensively cultivated with cropping intensity more than 150% and excessive use of fertilizers. However, there are some differences in the geological features of groundwater systems in the chosen study areas. Punjab sites are dominated by alluvial formations while Rajasthan sites have both alluvial and hard rock formations. In this chapter, the hydrochemical controls are evaluated considering the diversities and similarities between the study areas and conceptual models are suggested for uranium mobilization.

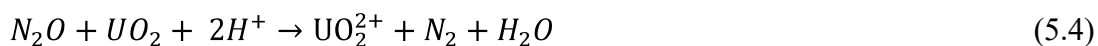
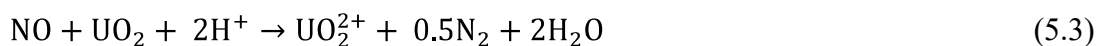
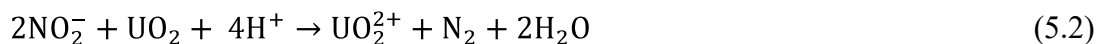
5.1 Hydrochemical drivers

The mobilization of uranium in groundwater is combined effect of multiple governing processes and numerous controlling parameters like geology, aquifer characteristics and physicochemical parameters. Uranium is known to be sparingly soluble/insoluble, mostly found in rocks, sediments etc in its reduced state of +4 while soluble in its oxidized state of +6. The physicochemical parameters also exert control on the uranium mobilization, which include oxidation state of uranium, pH condition of the aquifer, type of ligands (NO_3^- , CO_3^{2-} , HCO_3^- , humic acid, fulvic acid etc) and aquifer condition (oxidative or reductive) etc.

From the interpretation of the results it can be concluded that the HCO_3^- ion and NO_3^- ion are the two important factors that act as hydrochemical drivers for release of uranium from aquifer matrix to water. The NO_3^- ions is known to act as an oxidizing agent that helps convert U(IV) to U(VI) ^[76]. The reaction involved is given in Equ. 5.1

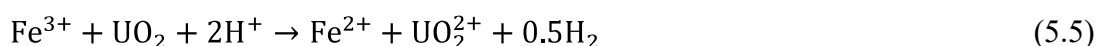


The reactive product like nitrite (Equ. 5.2), nitrogen oxide (Equ5.3) and nitrous oxide (Equ. 5.4) formed as a result of nitrate reduction can additionally oxidize U(IV) to U(VI) and enhance mobilization of uranium [77].

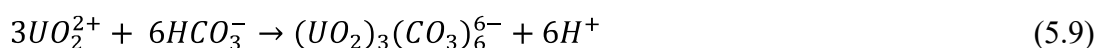
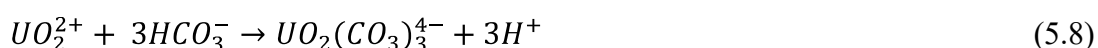
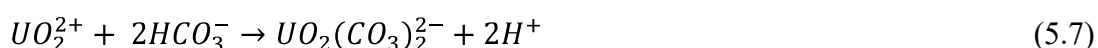


Under anaerobic conditions micro-organisms like *Geobacter metallireducens* and *Thiobacillus denitrificans* coupled with nitrate has known to oxidize U(IV) [78]. Nitrate driven Fe(II) oxidation reaction produces reactive Fe(III) that oxidizes U(IV) to U(VI) [79].

The reaction involved is (Equ.5.5)



Edwards et al. (1995) [76], studies that oxidized uranium is stabilized in groundwater pH condition with the help of bicarbonate ions with the formation of stable complexes like $\text{UO}_2(\text{CO}_3)$, $\text{UO}_2(\text{CO}_3)_2^{2-}$, $\text{UO}_2(\text{CO}_3)_3^{4-}$ and $(\text{UO}_2)_3(\text{CO}_3)_6^{6-}$. The reaction for the formation of complexes is (Equ. 5.6 to 5.9)



The stability constant i.e. log k of the above uranyl carbonate complexes are 9.94, 16.61, 21.84 and 54 respectively [245]. These values suggest that the complexes are stable. The Gibbs free energy of formation of combined reaction i.e. oxidation and complexation were calculated by Nolan and Weber (2015) [76] and were found to be favourable.

The other ion known to play a role in uranium mobilization is calcium ion. The similarity in the size of UO_2^{2+} (~100pm) and Ca^{2+} (~100pm) ions favors their ion-exchange i.e. removal of the Ca^{2+} ions from water in exchange of UO_2^{2+} from aquifer matrix.

The mobilized ion is then stabilized by complexing with ligands like bicarbonate, phosphates etc. Aquifer characteristics like aquifer matrix (i.e. the concentration of uranium mineral, type of mineral etc), pore size, residence time of water are also important factors that help understand the concentration of uranium in the aquifer. All these factors combined are found to play role in uranium mobilization in alluvial formation from Punjab, alluvial formation of Rajasthan and hard rock formation of Rajasthan. The influence of NO_3^- and HCO_3^- ions are discussed in the below sections.

5.2 Uranium distribution

5.2.2 Seasonal variation

A higher uranium concentration was found in Punjab compared to Rajasthan which is contributed to their geology (Table 5.1). Punjab is a uniform formation of sand and silt separated by varied thickness of clay in between, making the zones of the formation as separate units. Rajasthan being a mixed type formation with alluvial and hard rock and no vertical uniformity acts like a single aquifer system that is corroborated with chemical and stable isotope data. The availability of NO_3^- ions are higher in case of Punjab due to its uniform geology for oxidation of U(IV) as compared to Rajasthan where the water takes time to reach the formation as observed from the delayed recharge signatures making the availability of NO_3^- ions limited due to its rapid reduction. This is corroborated with the NO_3^- ion concentration of both Punjab and Rajasthan (Table 5.1).

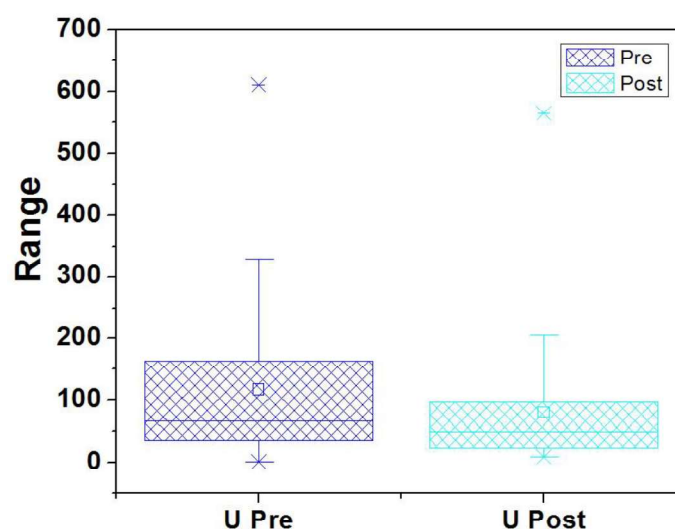


Fig. 5.1 Box plot of uranium in pre and postmonsoon season of Punjab

The decreased concentration in the postmonsoon samples from alluvial formation of Punjab (Fig. 5.1) is attributed to reduced NO_3^- ions available for oxidation (Table 5.1) during the postmonsoon season. The correlation between uranium and NO_3^- ions is also observed to decrease in postmonsoon (Fig. 3.34). The results from factor analysis also corroborates the same i.e. uranium correlates with PC2 in premonsoon while with PC3 in postmonsoon (Table 3.7). By correlating the spatial distribution plot for uranium (Fig. 3.29), NO_3^- (Fig. 3.30) and HCO_3^- ions (Fig. 3.31), it is concluded that locations having high uranium shows a strong correlation with HCO_3^- and NO_3^- ions in premonsoon season while in the postmonsoon season, the correlation is decreased i.e. it is either correlated to HCO_3^- or NO_3^- ions. This leads to decreased uranium concentration of postmonsoon season. The stable isotope also points towards decreased irrigation return flow contribution in the postmonsoon season thus corroborating the decreased concentration (Fig.3.24).

Table 5.1 Comparative table for Punjab and Rajasthan

Parameters	Punjab				Rajasthan			
	Shallow		Deep		Alluvial		Hard rock	
	Pre	Post	Pre	Post	Pre	Post	Pre	Post
Uranium ($\mu\text{g/L}$)	1-610 (120)	10-565 (90)	21-260 (95)	16-135 (43)	0.4-177 (30)	5.3-142 (47)	0.5-115 (34)	5.2-145 (51)
Above WHO	79%	71%	90%	62%	33%	61%	53%	58%
NO_3^- (mg/L)	6.5-710 (124)	8-365 (89)	0.6-77 (27)	0.7-51 (15)	0.3-242 (47)	0.3-205 (50)	0.4-528 (56)	3-382 (74)
HCO_3^- (mg/L)	100-1500 (682)	528-1716 (979)	125-1098 (637)	500-1144 (791)	183-1708 (643)	207-1244 (732)	220-1037 (713)	244-1281 (804)
^3H (TU)	1.5-8.2		1-4		1-3.5		1.3-4.5	
AR ($^{234}\text{U}/^{238}\text{U}$)	0.85-1.05		0.89-0.96		1.69-2.38		1.38-2.97	
Recharge Sources	Canal (-10‰ to -8.8‰) Precipitation (-8‰ to -5‰) irrigation return flow (-4‰ to -2‰)	Canal (-10‰ to -8.8‰) Precipitation (-8‰ to -5‰)	Precipitation (-8‰ to -6‰)	Precipitation (-8‰ to -7.4‰)	Precipitation (-7‰ to -5.5‰) irrigation return flow (-4‰ to -3‰)	Precipitation (-6‰ to -5.5‰) irrigation return flow (-4‰ to -3‰)	Precipitation (-6‰ to -5.5‰) irrigation return flow (-4‰ to -1.8‰)	Precipitation (-6‰ to -5.5‰) irrigation return flow (-4‰ to -1.8‰)
Depth profile	more spread in shallow zone compared to deep zones with dilution in postmonsoon				no depth variation, contamination equally spread in both the formations with increase in postmonsoon			
Uranium mobilization	Oxidative dissolution and mixing process				Oxidative leaching and alpha recoil			

*bracket values are averaged value for uranium, NO_3^- and HCO_3^-

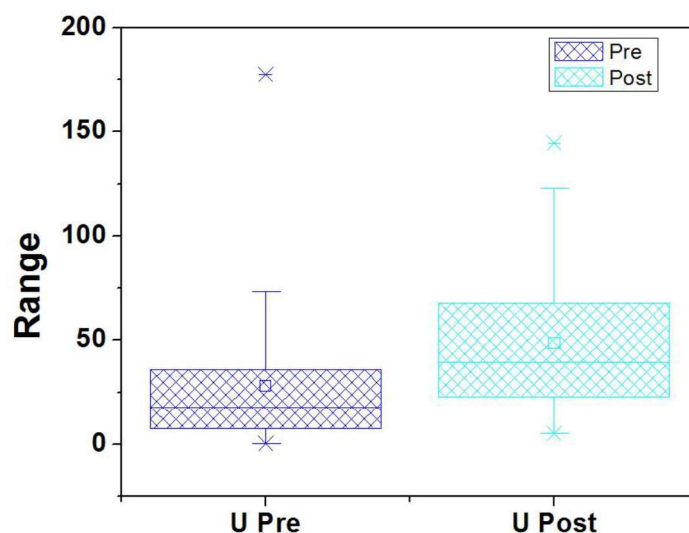


Fig. 5.2 Box plot of uranium in pre and postmonsoon seasons of Rajasthan

The increased concentration in the alluvial and hard rock formation of Rajasthan during the postmonsoon season is again attributed to increased NO_3^- and HCO_3^- ions during the postmonsoon season (Table 5.1). The correlation between uranium and NO_3^- ions is also observed to increase in postmonsoon (Fig. 4.31). The results from factor analysis also corroborates the increased concentration of uranium as during the premonsoon season uranium correlates with PC2 while in postmonsoon it correlates with all the PC in alluvial formation and PC1 in hard rock formation (Table 4.13). The stable isotope also indicates increased irrigation return flow contribution in both alluvial and hard rock formation in the postmonsoon season thus corroborating the increased concentration (Fig. 4.23).

5.2.2 Depth variation

A clear demarcation between the uranium contamination in the shallow and deep zone can be made in the samples from alluvial formation of Muktsar and Faridkot districts of Punjab from the depth profile (Fig. 3.32). A large scatter is observed in the shallow zone for both pre and postmonsoon seasons compared to deep zone. Few pockets of increased concentration of uranium are observed in deep zones during premonsoon which is attributed to mixing i.e. corroborated with signature of irrigation return flow to the deep zone from both stable isotope (Fig. 3.24) and increased nitrate concentration (Fig. 3.7). A decrease

during the postmonsoon season in shallow and deep zone is attributed to decreased irrigation return flow corroborated from decreased nitrate ion concentration (Fig. 3.7) and stable isotope (Fig. 3.24). The same is corroborated from $\delta^{18}\text{O}$ vs nitrate plot (Fig. 5.3), we can see decrease in nitrate concentration in postmonsoon in samples showing irrigation return flow signatures in both shallow and deep zones.

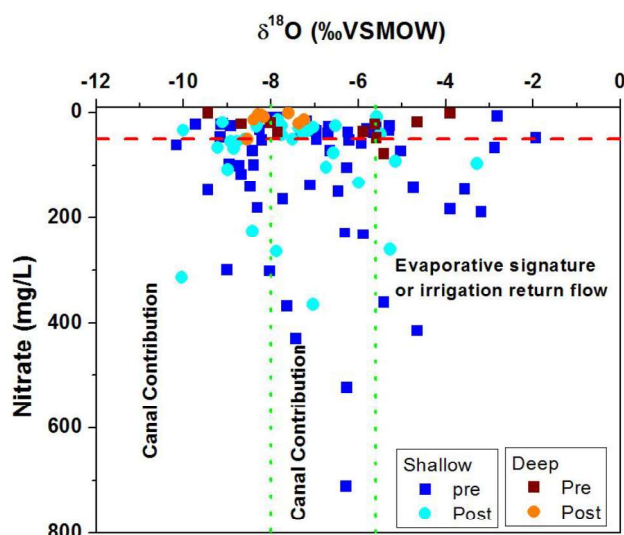


Fig. 5.3 Correlation between nitrate and $\delta^{18}\text{O}$ for samples from study area under Punjab

From the depth profile of uranium for alluvial formation and hard rock of Jaipur and Dausa districts of Rajasthan, no clear depth demarcation can be made. The contamination due to uranium is present throughout (Fig. 4.33) while comparing with the depth profile of NO_3^- ions a similar pattern was observed i.e. no depth demarcation and high concentrations present throughout (Fig. 4.7). The stable isotope also corroborates irrigation return flow signatures. Thus, an overall spread in uranium contamination is observed. The same is corroborated from $\delta^{18}\text{O}$ vs. nitrate plot (Fig. 5.4), we can see increase in nitrate concentration in postmonsoon in samples showing irrigation return flow signatures in both alluvium and hard rock formations.

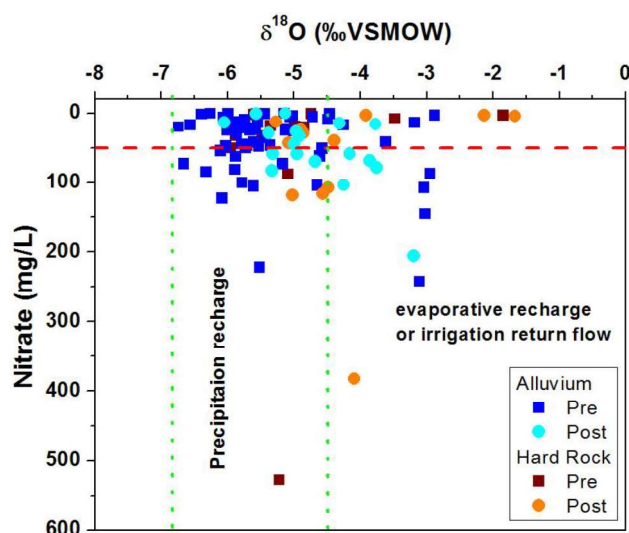


Fig. 5.4 Correlation between nitrate and $\delta^{18}\text{O}$ for samples from study area under Rajasthan

5.3 Groundwater recharge and dynamics

The variation in $\delta^{18}\text{O}$ values and different recharge sources to shallow and deep zone of alluvial formation from Punjab and alluvial and hard rock formation from Rajasthan are given in Table 5.1. It can be observed that the signatures of irrigation return flow contribution in the shallow are diluting during the postmonsoon season. The tritium content of the samples from shallow and deep zones indicate that the formation is getting modern recharge. For the alluvial and hard rock formations from Rajasthan, it is observed that the irrigation return flow is increasing in the postmonsoon season. Thus, a delayed recharge scenario is concluded. The signature of premonsoon season i.e. evaporative signatures due to high summer temperature are observed in the postmonsoon season. The delayed recharge can also be corroborated by the low tritium values compared to the study area under Punjab (Table 5.1). From the distribution of stable isotope of both Punjab and Rajasthan, we can see that samples from Punjab are more depleted compared to Rajasthan (Fig. 5.5). The river water that have its origin in higher altitudes (having depleted $\delta^{18}\text{O}$ values) is contributing to the recharge as they flow through the districts as canals. In Rajasthan, the evaporative effect signatures are observed that enriches $\delta^{18}\text{O}$.

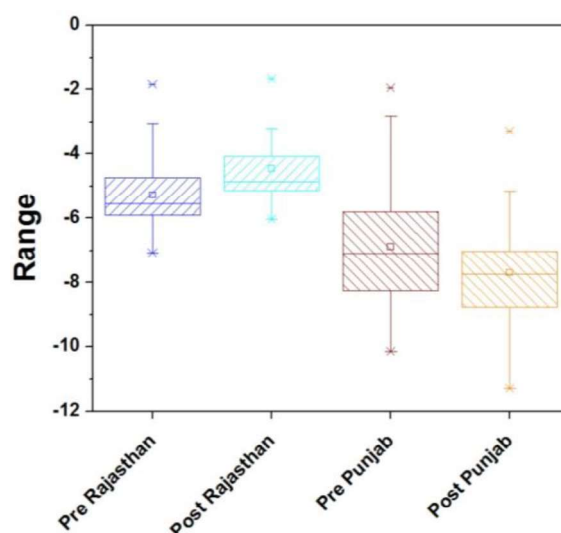


Fig. 5.5 Stable isotope distributions of districts of Punjab and Rajasthan

5.4 Uranium isotope variations

The variation in activity ratio of $^{234}\text{U}/^{238}\text{U}$ is used as tool to understand hydrological condition of an aquifer, its long-term water-rock interactions and geochemical process involved in uranium mobilization. By combining the uranium concentration with its activity ratio, we can predict the redox condition of the aquifer and the stage of aquifer i.e. it's in i) augmenting state i.e. oxidative state of the aquifer where leaching of uranium is favorable thus the concentration of uranium increase and activity ratio indicates equilibrium condition, ii) redox zone i.e. change from oxidative to reducing condition, here the dissolved uranium concentration will decrease and activity ratio will increase i.e. disequilibrium will be attained and iii) decaying state i.e. when aquifer is in reducing state for long time, due to difference in half lives of ^{234}U and ^{238}U the activity ratio will start to fall (Chapter 2, Fig. 2.8).

When there is oxidative leaching or dissolution of uranium mineral wherein whole of the mineral is leached this keeps the activity ratio of $^{234}\text{U}/^{238}\text{U}$ equal to 1 or same as that of the mineral. The activity ratio of $^{234}\text{U}/^{238}\text{U}$ more than 1 is indicative of disequilibrium which can be caused due to alpha recoil, chemical fractionation or oxidative conditions. When ^{238}U decay by releasing an alpha, the daughter nuclide formed (^{234}Th) recoils by 20

nm in any direction. If the daughter nuclide is exposed on the surface of the crystal, the decay product i.e. ^{234}U is easily and more available compared to ^{238}U for leaching leading to disequilibrium situation. Sometimes, the recoil directly releases the daughter nuclide into groundwater and depending on the groundwater conditions the daughter product either mobiles or precipitates. Secondly, the alpha tracks generated in the recoil path also makes the crystal lattice more prone to oxidation and leaching leading to increased concentrations of uranium in the aquifer system. These processes can lead to variable activity ratio ranging from <1 to 20. The recoil process is shown schematically in Fig. 5.6. The plot of activity ratio of $^{234}\text{U}/^{238}\text{U}$ vs. inverse uranium concentration helps in identifying the processes responsible for uranium concentrations like mixing, leaching, decay or dilution (Fig. 2.9). The activity ratio of uranium isotopes ($^{234}\text{U}/^{238}\text{U}$) varies for different process. The ratio increases during leaching and recoil as the ^{234}U available on the surface of mineral leach preferentially or it is released directly into the aquifer due to alpha recoil. In case of radioactive decay due to difference in the half-life of two isotopes, the ratio decreases. In case of dilution the ratio is unaffected as overall both the isotopes are diluted while in case of mixing, the ratio lies between the two end members [172-182].

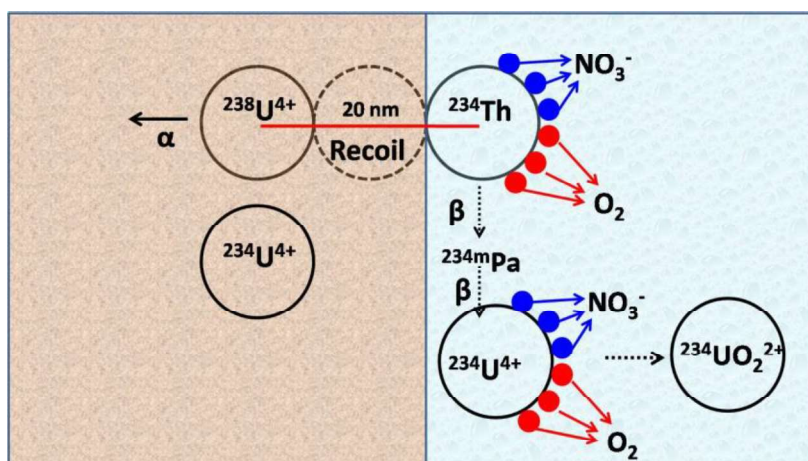


Fig. 5.6 Schematic diagram of alpha recoil phenomenon

In the alluvial formation of Punjab, the activity ratio is in range of 0.85- 1.05 which suggest the equilibrium condition while high uranium condition suggest that aquifer is in augmenting condition i.e. oxidative condition (Fig. 5.7). From the scatter plot of inverse uranium concentration and activity ratio, we observed that shallow zone samples follow the trend line of leaching while the deep zone samples fall on the mixing line. The mixing between deep and shallow zone is corroborated from stable isotope signature (Fig. 3.24) and chemical results.

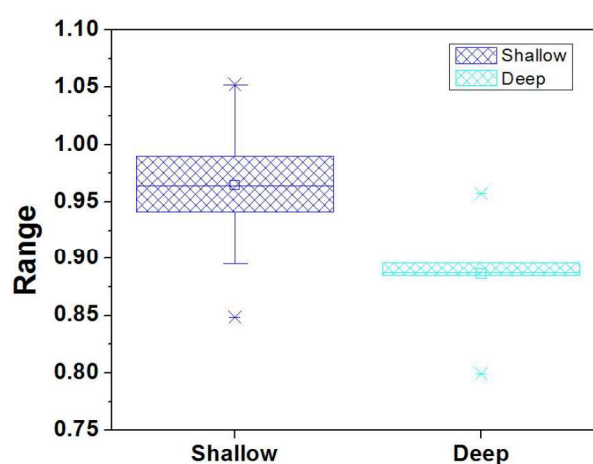


Fig. 5.7 Box plot of AR ($^{234}\text{U}/^{238}\text{U}$) for Punjab

The alluvial aquifer of Rajasthan has the activity ratio in range of 1.69 to 2.38 which is indicative of disequilibrium that is attributed to alpha recoil leading to increased AR (Fig. 5.8). The uranium is also high in the groundwater. Thus, we can conclude that aquifer is in oxidative condition. For the hard rock formation of Rajasthan similar activity ratio were found i.e. 1.38 to 2.97 with a larger spread (Fig. 5.8). Thus, both alluvial and hard rock formations of the aquifer are in similar conditions. The stable isotope signature and chemical results indicates towards the interconnection of both the aquifers.

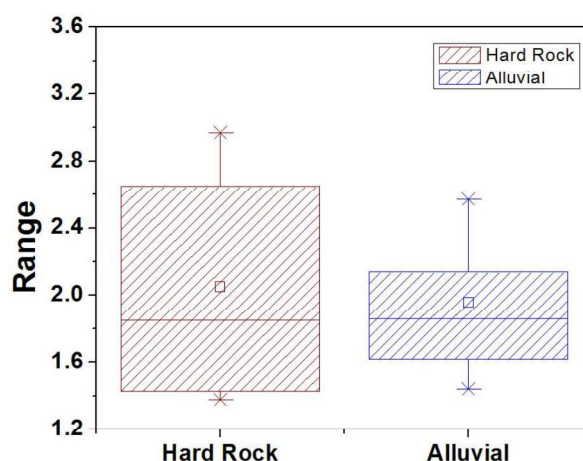


Fig. 5.8 Box plot of AR ($^{234}\text{U}/^{238}\text{U}$) for Rajasthan

By combining the interpretation of chemical data, stable isotopic data, uranium distribution, uranium isotope analysis, statistical and factor analysis the high uranium in the shallow alluvial formation in Punjab is attributed to the aquifer condition i.e. oxidative nature of the aquifer and to the extensive agricultural activity of the area which is increasing NO_3^- ion concentration due to extensive use of fertilizer and HCO_3^- ions due to increased pCO_2 which is result of root respiration and decaying organic matter (again due to agricultural activity). The high uranium pockets in the deep zone of alluvial formation from Punjab are attributed to mixing between the aquifer.

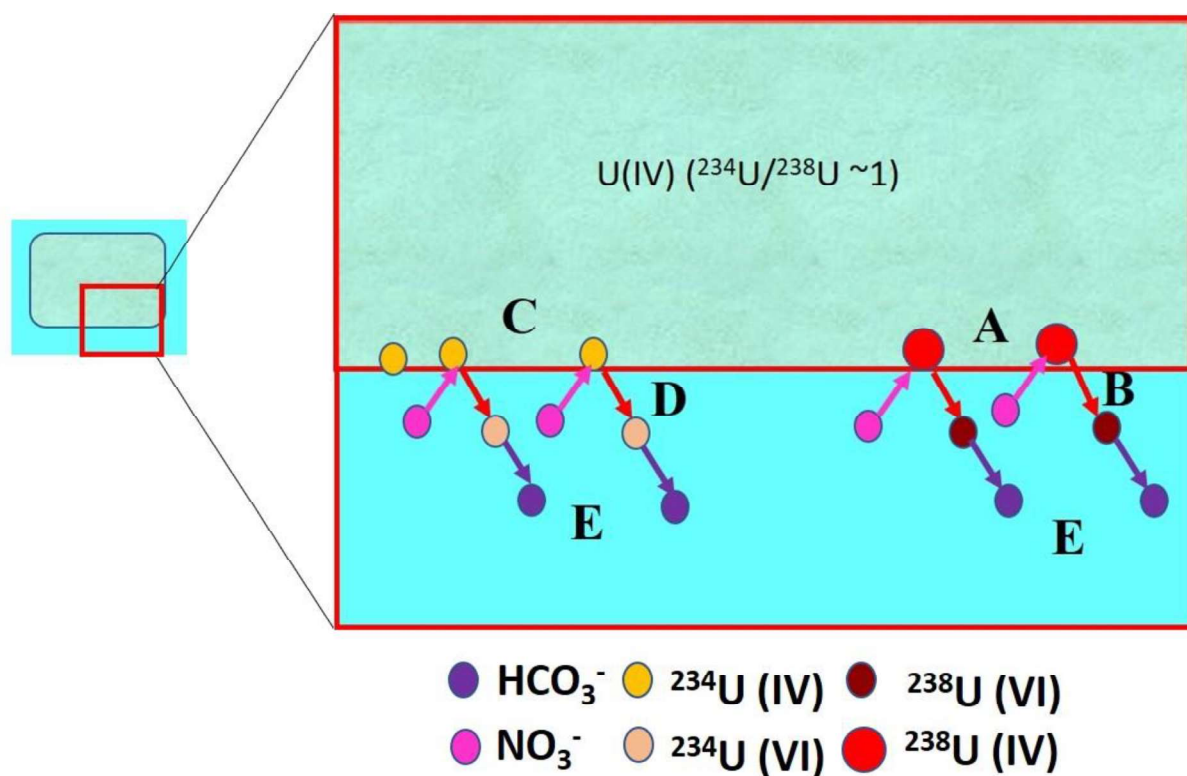
The high uranium in alluvial and hard rock formation of Rajasthan is attributed to the geology and hydrological condition of the aquifer. The aquifer behaves like a single unit which is corroborated with similar concentration of NO_3^- & HCO_3^- ions and similar spread in isotopic values and same recharge sources to both the formation with no variation seasonally. The aquifer receives a delayed recharge making the availability of NO_3^- ions limiting for oxidation. Thus, the main processes responsible for uranium release is leaching from minerals. The high activity ratio ($^{234}\text{U}/^{238}\text{U}$) is attributed to long residence time which increases rock-water interaction. Secondly, the formation is fractured, water moves to interior where the probability of having recoiled nuclide are high. Thus, more of ^{234}U is exposed and available for leaching.

5.5 Conceptual diagram of uranium release in groundwater in alluvial formations

From the above conclusions, a release mechanism for uranium in the groundwater from alluvial formation of Muktsar and Faridkot districts of Punjab is proposed (Fig. 5.9). In the formation, the nitrate present in the groundwater due to increased agricultural activity. The presence of high nitrate in groundwater facilitates oxidation of uranium mineral leading to oxidative dissolution.

- I. Nitrate oxidizes the ^{238}U (IV) and ^{234}U (IV) present and this changes the oxidation state of uranium to ^{238}U (VI) and ^{234}U (VI) (Step A and Step C).
- II. The oxidized species are mobile compared to reduced ones; hence it comes to groundwater (Step B and Step D).
- III. The uranyl ion present in water complexes with the dissolved bicarbonate ion, which is also a major contributor from extensive agricultural activity in the study area.

All these steps combinedly lead to increased concentration of uranium in the groundwater. In the alluvial formation, the oxidation of the mineral is the major factor, hence the signature of alpha recoil is not observed in this formation.



A: NO_3^- acting on ^{238}U (IV)

B: Oxidative Leaching of ^{238}U (IV) to ^{238}U (VI)

C: NO_3^- acting on ^{234}U (IV)

D: Oxidative Leaching of ^{234}U (IV) to ^{234}U (VI)

E: Complexation with HCO_3^-

Fig. 5.9 Uranium release mechanism in alluvial formations of Punjab

5.6 Conceptual diagram of uranium release in groundwater in hard rock formations

From the above conclusions, a release mechanism for uranium in the groundwater from hard rock formation of Rajasthan is proposed (Fig. 5.9). The formation is fractured and is interconnected with the alluvial formation of the region ascertained from the stable isotope signature and chemical analysis. Hence, similar uranium concentration and similar signatures of uranium isotope are seen in both formations. The ^{238}U decays by alpha forming ^{234}Th which intern decays ^{234}Pa and then to ^{234}U . During the alpha decay the daughter nuclide

formed recoil 20nm. This recoil can either expose the nuclide to the surface or release them directly into the water. Both these process increases the activity of ^{234}U compared to ^{238}U i.e. disequilibrium condition. The recoil tracks also make the mineral more prone to oxidation as the lattice is broken. The schematic diagram of alpha recoil is seen in Fig. 5.9 labeled as 3. Water with NO_3^- and HCO_3^- ions enter the fractured zone and oxidizes the available uranium (IV). There are four possibility inside the fractured zone

- I. ^{238}U is available near to the fracture surface which is oxidized by incoming NO_3^- ions (step A)
- II. ^{234}U is exposed to the fractured surface due to alpha recoil and readily available for oxidation by NO_3^- ions (step B)
- III. ^{234}Th is released directly into the water due to alpha recoil, which decays to ^{234}U (IV) (Fig. 5.9 part 3) and is oxidized to $^{234}\text{U(VI)}$ (step C)
- IV. The alpha recoil process is moving the ^{234}U in opposite direction to the fracture making it unavailable for leaching (Step D).

The disequilibrium is enhanced by step B and C. The released uranyl ion is stabilized by the bicarbonate ions (Step E). Thus, $\text{AR} > 1$ is observed in the study area of Rajasthan. As, the formation act like a single aquifer and receives delayed recharge the availability of NO_3^- ions is limited for oxidation due to rapid reduction in the aquifer. The limited quantity and availability of NO_3^- ions is limiting step towards uranium release in case of Rajasthan. Thus, the concentration of uranium is less in case of Rajasthan compared to Punjab.

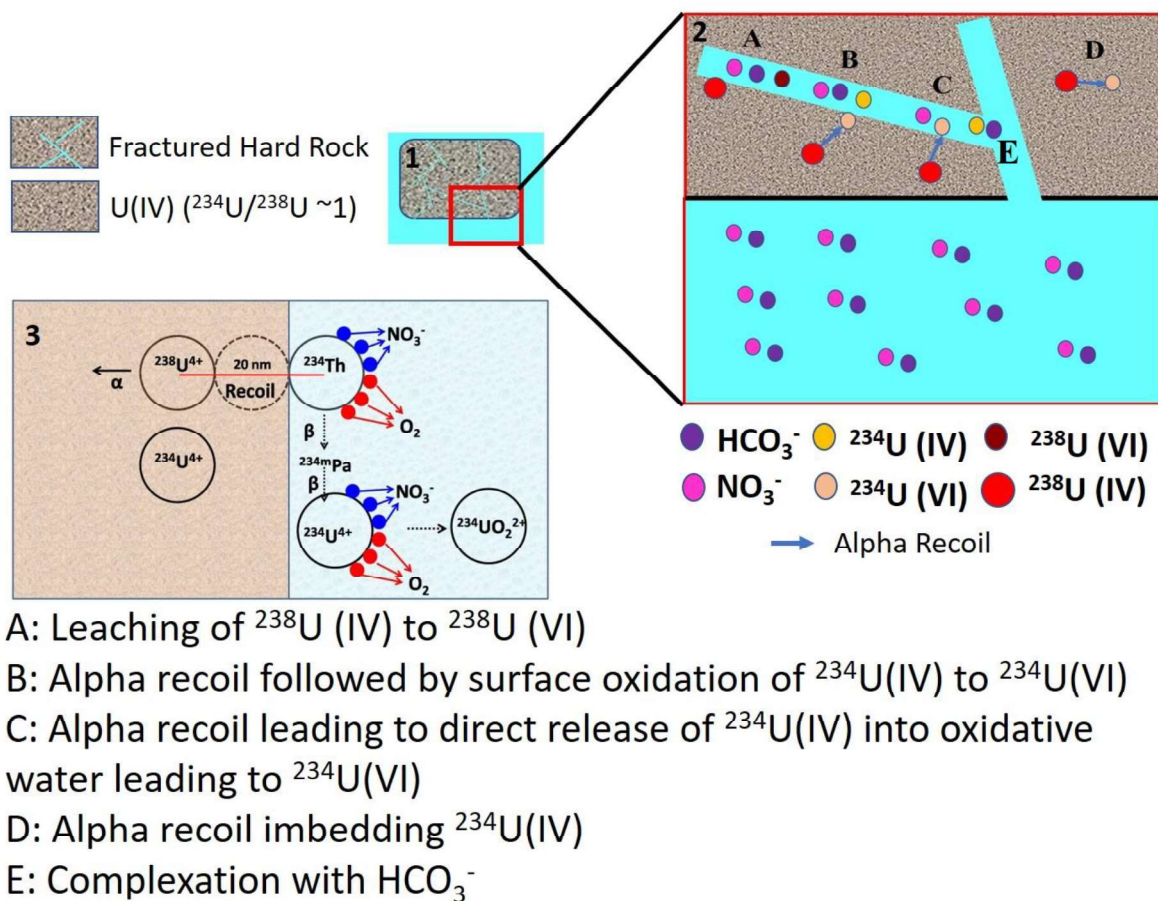


Fig. 5.10 Uranium release mechanism in hard rock formation of Rajasthan

References

1. Mook WG, (2000) Environmental isotope in hydrological cycle: principles and applications, *Technical document in Hydrology* No. 39 **1** UNESCO, Paris
2. Gleeson T, Wada Y, Bierkens MF, van Beek LP (2012) Water balance of global aquifers revealed by groundwater footprint. *Nature*, **488**(7410):197–200doi: 10.1038/nature11295
3. Data by United Nation, World population prospects: the 2019 revision, Department of Economics and Social Affairs, Population Division
4. IWMI (2007) International Water Management Institute (IWMI). Technical reports on Salinity Management in Pakistan: multiple issues, IWMI, Colombo
5. Wada Y, van Beek LPH, van Kempen CM, Reckman JWTM, Vasak S, Bierkens MFP (2010) Global depletion of groundwater resources. *Geophys Res Lett*, **37**(20), L20402. doi: 10.1029/2010gl044571
6. Martinez-Beltran J, Manzur CL (2005) Overview of salinity problems in the world and FAO strategies to address the problem. In: Proceedings of the International Salinity Forum, Riverside, 311–313
7. Konikow LF (2011) Contribution of global groundwater depletion since 1900 to sea-level rise. *Geophys Res Lett*, **38**(17), L17401 doi: 10.1029/2011gl048604
8. Shah, T, Molden D, Sakthivadivel R, Seckler D (2000) The global groundwater situation: Overview of opportunities and challenges. Colombo, Sri Lanka: International Water Management Institute
9. Saha D and Ray RK (2018) Groundwater Resources of India: Potential, Challenges and Management. In: Sikdar P. (eds) Groundwater Development and Management. *Springer, Cham.*, doi: https://doi.org/10.1007/978-3-319-75115-3_2

10. The World Bank (2012) India Groundwater: A Valuable but Diminishing Resource The World Bank. <https://www.worldbank.org/en/news/feature/2012/03/06/india-groundwater-critical-diminishing>
11. Central Ground Water Board (2013) Dynamic Ground Water Resources of India; Department of Water Resources, Ministry of Jal Shakti, Government of India, <http://cgwb.gov.in/Documents/Dynamic%20GWRE-2013.pdf>.
12. Press Information Bureau (PIB 2020) Per Capita Availability of Water by Ministry of Jal Shakti Posted On 02 MAR 2020 5:40 PM by PIB Delhi <https://pib.gov.in/PressReleasePage.aspx?PRID=1604871>.
13. CGWB (2012) Dhiman SC, Aquifer of India, Central Ground Water Board Department of Water Resources, RD & GR Ministry of Jal Shakti Government of India. <http://cgwb.gov.in/AQM/India.pdf>
14. CGWB (2019) Groundwater yearbook 2018-2019, Central Ground Water Board Department of Water Resources, RD & GR Ministry of Jal Shakti Government of India. http://cgwb.gov.in/documents/GW%20Year%20Book_2018-19_JAN%208.pdf
15. CGWB (2017) National Compilation on Dynamic Ground Water Resources of India Central Ground Water Board Department of Water Resources, RD & GR Ministry of Jal Shakti Government of India. <http://cgwb.gov.in/GW-Assessment/GWRA-2017-National-Compilation.pdf>
16. Jurgens, B. C.; Fram, M. S.; Belitz, K.; Burow, K. R.; Landon, M.K. Effects of Groundwater Development on Uranium: Central Valley, California, USA. Ground Water 2010,48, 913–928
17. Morris BL, Lawrence AR, Chilton P, Adams B, Calow RC, Klinck BA (2003) Groundwater and its susceptibility to degradation: a global assessment of the problem

- and options for management. UNEP early warning and assessment vol *Report series* RS. 03–3, Nairobi
18. Gupta S (2012) Drinking Water Quality: A Major Concern in Rural India (Some strategies towards cleaner water and the draft water policy-2012). *Bartolini-An Interdisciplinary Journal* **1**: 2249-2666.
 19. Duttagupta S, Bhattacharya A, Mukherjee A, Chattopadhyay S, Bhanja S N, Sarkar S, Malakar P and Bhattacharya J (2019) Groundwater fecal pollution observation in parts of Indo-Ganges–Brahmaputra river basin from in-situ measurements and satellite-based observations; *J. Earth Syst. Sci.*, **128**(3)44
 20. Foster S, Hirata R, Gomes D, Delia M, Paris M (2002) Groundwater quality protection: a guide for water utilities, municipal authorities, and environment agencies. World Bank, Washington, DC
 21. Chowdary VM, Rao NH, Sarma PBS (2005) Decision support framework for assessment of non-point-source pollution of groundwater in large irrigation projects. *Agric Water Manag.*, **75**(3):194–225 doi: 10.1016/j.agwat.2004.12.013
 22. Smith AH, Lingas EO, Rahman M (2000) Contamination of drinking-water by arsenic in Bangladesh: a public health emergency. *Bull World Health Organ*, **78**(9):1093–1103
 23. Hoque R (2013) A Study of Awareness about Arsenic Pollution in Rural West Bengal. *International Journal of Humanities and Social Science Invention*, **2**: 43-46.
 24. Höhn R, Isenbeck-Schröter M, Kent DB, Davis JA, Jakobsen R, Jann S, Niedan V, Scholz C, Stadler S, Tretner A (2006) Tracer test with As(V) under variable redox conditions controlling arsenic transport in the presence of elevated ferrous iron concentrations. *J Contam. Hydrol*, **88**(1–2):36–54 doi: 10.1016/j.jconhyd.2006.06.001
 25. Mukherjee A, Sengupta MK, Hossain MA, Ahamed S, Das B, Nayak B, Lodh D, Rahman MM, Chakrabarti D (2006) Arsenic contamination in groundwater: a global

- perspective with emphasis on the Asian scenario. *J Health Popul Nutr.*, **24**(2):142-63
PMID: 17195556.
26. WHO (World Health Organization) (2011) Guidelines for drinking water quality
Geneva: WHO
 27. Singh S, Mahipal R (2018). Fluoride Contamination of Water in India and its Impact
on Public Health. **3**:10-15 doi: 10.20431/2456-0049.0302002.
 28. Dissanayake C (1991) The fluoride problem in the ground water of Sri Lanka
environmental management and health. *International Journal of Environmental
Studies*, **38**(2-3):137–155
 29. Singh A, Patel AK, Kumar M (2020) Mitigating the Risk of Arsenic and Fluoride
Contamination of Groundwater through a Multi-model Framework of Statistical
Assessment and Natural Remediation Techniques. *Springer Transactions in Civil and
Environmental Engineering*, 15:285-300 doi: <https://doi.org/10.1007/978-981-32-9771-5>
 30. Ray, S. K., Ghosh, S., Nagchaudhuri, J., Tiwari, I. C. and Kaur, P. (1981) Prevalence of
fluorosis in rural community near Varanasi. *Fluoride*, **14**: 86–90
 31. Ayoob S, and Gupta AK (2006) Fluoride in drinking water. A review on the status and
stress effects. *Crit. Rev. Environ. Sci. Technol.*, **36**:433–487
 32. Tripathi SD, Aravindakshan PK, Ayyappan S, Jena JK, Muduli HK, Suresh C, Pani KC
(2000) New high in crop production in India through intensive polyculture. *J Aqua
Trop*, **15**:119–128
 33. David MD, Gentry LE (2000) Anthropogenic inputs of nitrogen and phosphorus and
riverine export for Illinois, USA. *J Environ Qual*, **29**:494–508
 34. Forman D, Al-Dabbagh S, Doll R. (1985) Nitrates, nitrites and gastric cancer in Great
Britain. *Nature* **27**, 313(6004):620-62 doi: 10.1038/313620a0.

35. Ward MH, Heineman EF, Mc Comb RD, Weisenburger DD (2005) Drinking water and dietary sources of nitrate and nitrite and risk of glioma. *J Occup Environ Med.*, **47**:1260–1267
36. Shomar B, Osenbrück K, Yahya A (2008) Elevated nitrate levels in the groundwater of the Gaza Strip: distribution and sources. *Sci Total Environ*, **398**:164–174
37. Janjevic D (2017) Nitrate threatens groundwater in Germany doi: <http://p.dw.com/p/2VBY0>
38. Beutel MW, Duvel R, Cubas FJ, Grizzard TJ (2017) Effects of nitrate addition on water column methyl mercury in Occoquan Reservoir, Virginia, USA. *Water Res*, **110**:288–296
39. CGWB (2010) Groundwater quality scenario in India, Central Ground Water Board (CGWB), Ministry of Jal Shakti, Department of Water Resources, River Development and Ganga Rejuvenation Government of India <http://cgwb.gov.in/wqoverview.html>
40. Chowdary M, Chandran V, Neeti, Bothale R, Srivastava Y, Ingle P, Ramakrishnan D, Dutta D, Jeyaram, A, Sharma J, Singh R (2008) Assessment of surface and sub-surface waterlogged areas in irrigation command areas of Bihar state using remote sensing and GIS. *Agricultural Water Management*, **95**:754-766 doi: 10.1016/j.agwat.2008.02.009.
41. Werner AD, Bakker M, Post VEA, Vandenbohede A, Lu C, Ataie-Ashtiani B, Simmons CT, Barry DA (2013) Seawater intrusion processes, investigation and management: recent advances and future challenges. *Adv Water Resour*, **51**:3–26 doi: 10.1016/j.advwatres.2012.03.004
42. Siegel MD and Bryan CR (2004) Environmental geochemistry of radioactive contamination. Treatise on geochemistry, *Environmental Geochemistry*, **9**, 205 – 250.
43. Ivanovich M, & Harmon RS (Eds.) (1992) Uranium-series disequilibrium: applications to earth, marine, and environmental sciences 2 ed. United Kingdom: *Clarendon Press*.

44. Chau N, Dulinski M, Jodlowski P, Nowak J, Rozanski K, Sleziak M, Wachniew P, (2011) Natural radioactivity in groundwater - a review. *Isotopes in environmental and health studies*, **47**:415-37 doi: 10.1080/10256016.2011.628123.
45. ATSDR (1999) U.S. Agency for Toxic Substances and Disease Registry Toxicological Profile for Uranium
46. Squibb KS, Mc Diarmid MA (2006) Depleted uranium exposure and health effects in Gulf War veterans. *Philos Trans R Soc Lond B Biol Sci.* **361**(1468):639-648 doi: 10.1098/rstb.2006.1823
47. Milvy P. and Cothorn CR (1990) Radon, Radium and Uranium in Drinking Water. 1-16 *Lewis Publishers, Inc., Chelsea, MI*
48. Saini K, Singh P., Bajwa BS (2016) Comparative Statistical Analysis of Carcinogenic and Non-Carcinogenic Effects of Uranium in Groundwater Samples from Different Regions of Punjab, India. *Appl. Radiat. Isot. Data Instrum. Methods Use Agric. Ind. Med.*, **118**:196–202 doi: 10.1177/1420326x17699978
49. International Atomic Energy Agency. (2011) Radiation protection and safety of radiation sources: international basic safety standards. Interim Edition, General Safety Requirements Part 3, No. GSR Part 3 (Interim) Vienna
50. Sharma DA, Keesari T, Rishi MS, Thakur N, Pant D, Sangwan P, Kishore N. (2020) Distribution and correlation of radon and uranium and associated hydrogeochemical processes in alluvial aquifers of northwest India. *Environmental Science and Pollution Research*, doi: 10.1007/s11356-020-10015-8
51. WHO (2003) World Health Organization, Guidelines for drinking water quality 3rd ed. Geneva, Switzerland

52. Simon O, Garnier-Laplace J (2005) Laboratory and field assessment of uranium trophic transfer efficiency in the crayfish *Orconectes limosus* fed the bivalve *C. fluminea*. *Aquatic Toxicology*, **74**(4);372–383 doi:10.1016/j.aquatox.2005.06.010
53. UNSCEAR. Sources and Effects of Ionizing Radiation. Volume II: Effects. UNSCEAR (2000) Report. United Nations Scientific Committee on the Effects of Atomic Radiation, Report to the General Assembly, with scientific annexes. United Nations sales publication E.00.IX.4. United Nations, New York, 2000
54. Muller M and Anke M and H (1997) Illing-Gunther Aluminium in wild mushrooms and cultivated *Agaricus bisporus*. *Z. Lebensm Unters Forsch. A*, **205**:242-247
55. Bergmann M, Graça, MAS (2019) Bioaccumulation and Dispersion of Uranium by Freshwater Organisms. *Archives of Environmental Contamination and Toxicology*, doi: 10.1007/s00244-019-00677-y
56. ATSDR (2013) Toxicological profile for uranium. Agency for Toxic Substances and Disease Registry, *Atlanta*, Georgia.
57. Fisenne I.M, Perry PM, Decker KM (1987) The daily intake of $^{234,235,238}\text{U}$, $^{228,230,232}\text{Th}$ and $^{226,228}\text{Ra}$ by New York City residents. *Health Phys*, **53**(4):357-363.
58. Fisenne IM, Perry PM, Harley NH (1988) Uranium in humans. *Radiat Prot Dosim*, **24** (1-4):127-131
59. Golchert NW, Duffy TL, Sedlet J (1985) Environmental monitoring at Argonne National Laboratory. ANL-85-17. Argonne National Laboratory, Illinois, USA.
60. WHO (2003) Uranium in drinking-water Background document for development of WHO guidelines for drinking-water quality. WHO/SDE/WSH/03.04/118/Rev/1 (updated 2012) World Health Organization, Geneva, 2003.

61. Thorne MC, Wilson J. (2015) Generally applicable limits on intakes of uranium based on its chemical toxicity and the radiological significance of intakes at those limits. *J Radiol Prot.*, **35**(4):743-762.
62. Stradling N, Hodgson A, Ansoborlo E (2003) Anomalies between radiological and chemical limits for uranium after inhalation by workers and the public. *Radiat Prot Dosim.*, **105**(1-4):175-178.
63. Wrenn ME, Durbin PW, Howard B (1985) Metabolism of ingested U and Ra. *Health Phys*, **48**(5):601-633.
64. Maynard EA, Hodge HC (1949) Studies of the toxicity of various uranium compounds when fed to experimental animals. in: The Pharmacology and Toxicology of Uranium Compounds, First edition (C. Voegtlin and H.C. Hodge, eds.). McGraw-Hill, New York, 309-376
65. Leggett RW (1989) The behavior and chemical toxicity of U in the kidney: A reassessment. *Health Phys*, **57**(3):365-383
66. Ubios AM, Guglielmotti MB, Steimetz T (1991) Uranium inhibits bone formation in physiologic alveolar bone modeling and remodeling. *Environ Res*, **54**(1):17-23
67. Milgram S, Carriere M, Thiebault C (2008) Cytotoxic and phenotypic effects of uranium and lead on osteoblastic cells are highly dependent on metal speciation. *Toxicology*, **250**(1):62-69
68. Kurttio P, Komulainen H, Leino A (2005) Bone as a possible target of chemical toxicity of natural uranium in drinking water. *Environ Health Perspect*, **113**(1):68-72
69. Monleau M, De Meo, Paquet F (2006) Genotoxic and inflammatory effects of depleted uranium particles inhaled by rats. *Toxicol Sci*, **89**(1):287-295
70. Gueguen YC, Rouas A, Monin A (2014) Molecular, cellular, and tissue impact of depleted uranium on xenobiotic-metabolizing enzymes. *Arch Toxicol*, **88**(2):227-239

71. Bensoussan H, Grancolas L, Dhieux-Lestaevél B (2009) Heavy metal uranium affects the braincholinergic system in rat following sub-chronic and chronic exposure. *Toxicology*, **261**(1-2):59-67
72. Mollegaard NE, Murchie AI, Lilley DM (1994) Uranyl photo probing of a four-way DNA junction: evidence for specific metal ion binding. *EMBO J*, **13**(7):1508-1513.
73. Fox PM, Davis JA, Zachara JM (2006) The effect of calcium on aqueous uranium(VI) speciation and adsorption to ferrihydrite and quartz. *Geochimica et Cosmochimica Acta*, **70**(6):1379–1387 doi: 10.1016/j.gca.2005.11.027
74. Burns PC, Finch RJ, eds., (2018) Uranium: mineralogy, geochemistry, and the environment **38** Walter de Gruyter GmbH & Co KG
75. Edwards R, Lepp NW, Jones KC (1995) Antimony and vanadium B.J. Alloway (Ed.), Heavy metals in soils (seconded), Blackie Academic & Professional, Glasgow, 346-352
76. Nolan and weber (2015) Natural uranium contamination in major U.S. aquifers linked to nitrate. *Environ. Sci. Technol. Lett.*, **2**:215-220 doi: 10.1021/acs.estlett.5b00174
77. Senko J M, Suflita J, Krumholz L R (2005) Geochemical controls on microbial nitrate-dependent U(IV) oxidation. *Geomicrobiol. J.*, **22**(7-8) 371-378
78. Weber KA, Thrash JC, Trump JIV, Achenbach LA, Coates JD (2011) Environmental and taxonomic bacterial diversity of anaerobic uranium (IV) bio-oxidation. *Applied and environmental microbiology*, 4693-4696 doi: 10.1128/AEM.02539-10
79. Senko JM, Mohamed Y, Dewers TA, Krumholz LR (2005) Role of Fe(III) minerals in nitrate-dependent microbial U(IV) oxidation. *Enviro. Sci. Technol.*, **39**:2529-2536
80. Lopez A M, Wells A, Fendorf S (2020) Soil and Aquifer Properties Combine as Predictors of Groundwater Uranium Concentrations within the Central Valley, California. *Environmental Science & Technology*. doi:10.1021/acs.est.0c05591

81. Riedel T and Kübeck C (2018). Uranium in groundwater – A synopsis based on a large hydrogeochemical data set. *Water Research*, **129**, 29–38. doi:10.1016/j.watres.2017.11.001
82. Turtiainen T, Muikku M, Vesterbacka P (2011) Uranium and ^{226}Ra in drinking water supplied by Finnish waterworks. *Radioprotection*, **46**(06):255-263
83. Prat OT, Vercouter E, Ansoborlo (2009) Uranium speciation in drinking water from drilled wells in southern Finland and its potential links to health effects. *Environ Sci Technol*, **43**(10):3941-3946
84. Salih I, Pettersson HBL, Lund E. (2002) Uranium and thorium series radionuclides in drinking water from drilled bedrock wells: Correlation to geology and bedrock radioactivity and dose estimation. *RadiatProtDosim*, **102**(3):249-258
85. Banks D, Royset O, Strand T, Skarphagen H (1995) Radioelement (U, Th, Rn) concentrations in Norwegian bedrock groundwaters. *Environmental Geology*, **25**:165-180
86. P. Gómez, A. Garralón, B. Buil, Ma.J. Turrero, L. Sánchez, B. de la Cruz (2006) Modeling of geochemical processes related to uranium mobilization in the groundwater of a uranium mine, *Science of The Total Environment*, **366**(1):295-309 doi: <https://doi.org/10.1016/j.scitotenv.2005.06.024>.
87. Stalder E, Blanc A, Haldimann M (2012) Occurrence of uranium in Swiss drinking water. *Chemosphere*, **86**(6):672-679
88. Larivière D, Tolmachev V, Kochermin (2013) Uranium bone content as an indicator of chronic environmental exposure from drinking water. *J Environ Radioact*, **121**:98-103.
89. Betcher RN, Gascoyne M, Brown D (1988) Uranium in groundwaters of southeastern Manitoba, Canada. *J Earth Sci*, **25**(12): 2089-2103.

90. Magdo HS, Forman J, Graber N (2007) Grand rounds: nephrotoxicity in a young child exposed to uranium from contaminated well water. *Environ Health Perspect*, **115**(8):1237-1241.
91. Cothorn CR and Lappenbusch WL (1983) Occurrence of uranium in drinking water in the U.S. *Health Phys*, **45**(1): 89-99
92. Dawood YH, Abd El-Naby HH, Sharafeldin AA (2004) Influence of the alteration processes on the origin of uranium and europium anomalies in trachyte, central Eastern Desert, Egypt. *Journal of Geochemical Exploration*, **81**(1-3):15–27 doi: 10.1016/s0375-6742(03)00210-3
93. Akram M Khattak NU, Qureshi AA, Iqbal A, Tufail M, Qureshi IE (2004) Fission track estimation of uranium concentrations in drinking water from Azad Kashmir, Pakistan, *Health Physics*, **86**(3) 296-302
94. Khatun R, Saadat AH, Ahasan MM, Akter S (2007) Assessment of natural radioactivity and radiation hazard in soil samples of Rajbari district of Bangladesh. Jahangirnagar University *Environmental Bulletin.*, **5**(2) 1-8.
95. AERB Drinking water specifications in India (2004) Department of Atomic Energy, Govt. of India.
96. CGWB (2020), uranium occurrences in shallow aquifer of India, Central Ground Water Board (CGWB), Ministry of Jal Shakti, Department of Water Resources, River Development and Ganga Rejuvenation Government of India http://cgwb.gov.in/WQ/URANIUM_REPORT_2019-20.pdf
97. Singh J, Singh L, Singh S (1995) High U-contents observed in some drinking waters of Punjab, India. *Journal of Environmental Radioactivity*, **26**(3):217-222.

98. Singh S, Rani A, Mahajan RK, Walia TPS (2003) Analysis of Uranium and Its Correlation with Some Physico-Chemical Properties of Drinking Water Samples from Amritsar, Punjab. *J. Environ. Monit.*, **5**:917–921.
99. Kumar A, Rout D, Narayanan U, Mishra M, Tripathi R., Singh J, Kumar S, Kushwaha H, (2011) Geochemical Modeling of Uranium Speciation in the Subsurface Aquatic Environment of Punjab State in India. *J. Geol. Min. Res.*, **3**:137-146
100. Bhalla A, Singh G, Kumar S, Shahi JS, Mehta D (2011) Elemental Analysis of Ground Water from Different Regions of Punjab State (India) Using EDXRF Technique and the Sources of Water Contamination. *Int. Conf. Environ. Comput. Sci.* **19**:156–164
101. Alrakabi M, Singh G, Bhalla A, Kumar S, Srivastava A, Rai B, Singh N, Shahi N, Mehta D (2012) Study of Uranium Contamination of Ground Water in Punjab State in India Using X-Ray Fluorescence Technique. *J. Radioanal. Nucl. Chem.*, **294**:221–227.
102. Tripathi RM, Sahoo SK, Mohapatra S, Lenka P, Dubey JS, Puranik VD, (2013) Study of Uranium Isotopic Composition in Groundwater and Deviation from Secular Equilibrium Condition. *J. Radioanal. Nucl. Chem.*, **295**:1195–1200.
103. Singh L, Kumar R, Kumar S, Bajwa BS, Singh S (2013) Health Risk Assessments Due to Uranium Contamination of Drinking Water in Bathinda Region, Punjab State, India. *Radioprotection*, **48**:191–202.
104. Krishan G, Lapworth D, Someshwar Rao M, Kumar CP, Smilovic M, Semwal P (2014) Natural (Baseline) Groundwater Quality in The Bist-Doab Catchment, Punjab, India: A Pilot Study Comparing Shallow and Deep Aquifers. *Int. J. Earth Sci. Eng.*, **7**:16–26.
105. Sharma N and Singh J (2016) Radiological and Chemical Risk Assessment Due to High Uranium Contents Observed in the Ground Waters of Mansa District (Malwa Region) of Punjab State, India: An Area of High Cancer Incidence. *Expo. Health*, **8**, 513– 525.

106. Virk H, Jakhu R, Bangotra P (2016) Natural Uranium Content in Ground Waters of Mohali and Fatehgarh Districts of North Punjab (India) for the Assessment of Excess Cancer Risk. *Glob. J. Hum.- Soc. Sci. B Geogr. Geo-Sci. Environ. Sci. Disaster Manag.*, **16**:12–17.
107. Virk H (2017) Uranium Content Anomalies in Groundwaters of Fazilka District of Punjab (India) for the Assessment of Excess Cancer Risk. *Res. Rev. J. Oncol. Hematol.*, **6**:21–26.
108. Saini K and Bajwa BS (2016) Uranium Distribution Study in the Drinking Water Samples of SW Punjab, India. *Adv. Appl. Sci. Res.* **7**:103–108
109. Bajwa BS, Kumar S, Singh S, Sahoo SK, Tripathi RM (2016) Uranium and Other Heavy Toxic Elements Distribution in the Drinking Water Samples of SW-Punjab, India. *J. Radiat. Res. Appl. Sci.*, **10**:13–19
110. Rishi MS, Keesari T, Sharma DA, Pant D, Sinha UK, (2017) Spatial Trends in Uranium Distribution in Groundwaters of Southwest Punjab, India - A Hydrochemical Perspective. *J. Radioanal. Nucl. Chem.*, **311**:1937–1945.
111. Sharma DA, Rishi MS, Keesari T, Pant D, Singh R, Thakur N, Sinha UK (2017) Distribution of Uranium in Groundwaters of Bathinda and Mansa Districts of Punjab, India: Inferences from an Isotope Hydrochemical Study. *J. Radioanal. Nucl. Chem.*, **313**, 625–633.
112. Saini K, Duggal V, Bajwa BS (2017) Assessment of Radiation Dose Due to Intake of Uranium through Groundwater and Its Carcinogenic and Non-Carcinogenic Risks in Southwest and Northeast Punjab, India. *Indoor Built Environ.* doi: 1420326X17699978.

113. Sharma S, Kumar A, Mehra R, Mishra R (2017) Ingestion Doses and Hazard Quotients Due to Intake of Uranium in Drinking Water from Udhampur District of Jammu and Kashmir State, India. *Radioprotection*, **52**:109–118.
114. Virk H (2017) Uranium Anomalies in Groundwater of Sangrur District of Punjab (India) for Cancer Risk Assessment. *Curr. Sci.*, **113**:1661–1663.
115. Singh KP, Kishore N, Tuli N, Loyal RS, Kaur M, Taak JK (2018) Uranium Contamination of Groundwater in Southwest Parts of Punjab State, India, with Special Reference to Role of Basement Granite. In Clean and Sustainable Groundwater in India. *Springer Hydrogeology; Springer, Singapore* 95–106.
116. Kumar M, Kaushal A, Sahoo BK (2019) Measurement of uranium and radon concentration in drinking water samples and assessment of ingestion dose to local population in Jalandhar district of Punjab, India. *Indoor and Built Environment*, **28**(5):611-618 doi: 10.1177/1420326X17703773
117. Kumar A, Manpreet K, Rohit M, Sumit S, Rosaline M, Singh KP, Bajwa BS (2017) Quantification and Assessment of Health Risk Due to Ingestion of Uranium in Groundwater of Jammu District, Jammu & Kashmir, India. *J. Radioanal. Nucl. Chem.*, **310**:793–804.
118. Singh P, Singh P, Sahoo BK, Bajwa BS (2016) A Study on Uranium and Radon Levels in Drinking Water Sources of a Mineralized Zone of Himachal Pradesh, India. *J. Radioanal. Nucl. Chem.*, **309**:541–549.
119. Sharma S, Kumar A, Mehra R, Mishra R (2017) Ingestion Doses and Hazard Quotients Due to Intake of Uranium in Drinking Water from Udhampur District of Jammu and Kashmir State, India. *Radioprotection*, **52**:109–118.

120. Mittal S, Rani A, Mehra R, Balaram V, Satyanarayanan M, Sawant SS (2017) Assessment of Uranium in Correlation with Physico-Chemical Properties of Drinking Water of Northern Rajasthan. *J. Geol. Soc. India*, **90**:233–238.
121. Duggal V, Rani A; Mehra R, Saini K, Bajwa BS (2017) Assessment of Age-Dependent Radiation Dose and Toxicity Risk Due to Intake of Uranium through the Ingestion of Groundwater from Northern Rajasthan, India. *Toxicol. Environ. Chem.*, **99**:516–524.
122. Coyte RM, Jain RC, Srivastava SK, Sharma KC, Khalil A, Ma L, Vengosh (2018) A Large-scale uranium contamination of groundwater resources in India. *Environmental Science & Technology Letters*, **5**(6):341-347.
123. Kansal S, Mehra RP, Singh N (2011) Uranium Concentration in Ground Water Samples Belonging to Some Areas of Western Haryana, India Using Fission Track Registration Technique. *J Public Health Epidemiol*, **3**:352-357.
124. Singh B, Garg VK, Yadav P, Kishore N, Pulhani V (2014) Uranium in Groundwater from Western Haryana, India. *J. Radioanal. Nucl. Chem.*, **301**:427–433.
125. Duggal V and Sharma S (2017) Chemotoxicity and Radiotoxicity Risk Assessment from Exposure to Uranium in Groundwater from Western Haryana, India. *Int. J. Pure Appl. Phys.*, **13**:107–112.
126. Singh RV, Sinha RM, Bisht BS, Banerjee DC (2002) Hydrogeochemical Exploration for Unconformity-Related Uranium Mineralization: Example from Palnadu Sub-Basin, Cuddapah Basin, Andhra Pradesh, India. *J. Geochem. Explor.*, **76**:71– 92.
127. Gupta S, Banerjee R, Vimal R, Achar KK, Umamaheswar K, Parihar P (2015) Seasonal Variation in Groundwater Geochemistry around Koppunuru Uranium Deposit, Guntur District, Andhra Pradesh: An Assessment for Potability and Irrigation. *Explor. Res. At. Miner.*, **25**:71–93.

128. Brindha K and Elango L (2013) Occurrence of Uranium in Groundwater of a Shallow Granitic Aquifer and Its Suitability for Domestic Use in Southern India. *J. Radioanal. Nucl. Chem.*, **295**:357–367.
129. Keesari T, Mohokar HV, Sahoo BK, Mallesh G (2014) Assessment of Environmental Radioactive Elements in Groundwater in Parts of Nalgonda District, Andhra Pradesh, South India Using Scintillation Detection Methods. *J. Radioanal. Nucl. Chem.*, **302**:1391–1398.
130. Raghavendra T, Srilatha K, Mahender C, Elander M, Vijayalakshmi T, Himabindu V, Prasad V, Padma Savithri P, Datta D, Arunachalam J (2014) Distribution of Uranium Concentration in Groundwater Samples from the Peddagattu/Nambapur and Seripally Regions Using Laser Fluorimetry. *Radiat. Prot. Dosimetry*, **158**:325–330.
131. Babu MNS, Somashekar RK, Kumar SA, Shivanna K, Krishnamurthy V, Eappen KP (2008) Concentration of Uranium Levels in Groundwater. *Int. J. Environ. Sci. Technol.*, **5**:263–266.
132. Mathews G, Nagaiah N, Karthik Kumar MB, Ambika MR (2015) Radiological and Chemical Toxicity Due to Ingestion of Uranium through Drinking Water in the Environment of Bangalore, India. *J. Radiol. Prot. Off. J. Soc. Radiol. Prot.*, **35**:447–455.
133. Adithya VS, Chidambaram S, Tirumalesh K, Thivya C, Thilagavathi R, Prasanna MV (2016) Assessment of Sources for Higher Uranium Concentration in Ground Waters of the Central Tamil Nadu, India. *IOP Conf. Ser. Mater. Sci. Eng.*, **121**, 012009.
134. Thivya C, Chidambaram S, Tirumalesh K, Prasanna MV, Thilagavathi R, Nepolian M (2014) Occurrence of the Radionuclides in Groundwater of Crystalline Hard Rock Regions of Central Tamil Nadu, India. *J. Radioanal. Nucl. Chem.*, **302**:1349–1355.

135. Patnaik R, Lahiri S, Chahar V, Naskar N, Sharma PK, Avhad DK, Srivastava A (2015) Study of uranium mobilization from Himalayan Siwaliks to the Malwa region of Punjab state in India. *Journal of Radioanalytical and Nuclear Chemistry*, **308**(3):913–918 doi: 10.1007/s10967-015-4578-3
136. Krishan G and Chopra RPS (2015) Assessment of Water Logging in South - western (SW) Parts of Punjab, India – A case study from Muktsar district. *NDC-WWC journal*. **4**:7-10.
137. Sharma P, Rishi MS, Thakur T (2017) Temporal Variations in Groundwater Quality with Special Reference to Irrigation in Faridkot and Muktsar Areas of Southwest Punjab, India. *International Journal of Science and Research (IJSR)*, **6**(1):577 – 584
138. Coyte R, Singh A, Furst KE, Mitch W, Vengosh A (2019) Co-occurrence of geogenic and anthropogenic contaminants in groundwater from Rajasthan, India. *Science of The Total Environment*, doi: 10.1016/j.scitotenv.2019.06.334
139. Rahman A, Tiwari KK, Mondal NC (2020) Hydrochemical Characterization for Groundwater Suitability in a Semi-Arid Area in Sanganer Block, Jaipur District, Rajasthan. *Journal of the Geological Society of India*, **96**(4):399–409 doi: 10.1007/s12594-020-1569-y
140. Mondal NC, Tiwari KK, Sharma KC, Ahmed S, (2016) A diagnosis of groundwater quality from a semiarid region in Rajasthan, India. *Arabian Journal of Geosciences*, **9**(12) doi:10.1007/s12517-016-2619-z
141. Agarwal R (2016) Nitrate Contamination in Ground Water of Jaipur District, Rajasthan, India: It's Impact on Human Health: A Review. *International Journal of Scientific Engineering and Research (IJSER)*, **4**(11):111-114
142. CGWB (2013) Saigal SK Groundwater information booklet of Faridkot district, Punjab. Government of India, Ministry of Water Resources, River Development & Ganga

143. CGWB (2013) Behera SC Groundwater resources and development potentials of Muktsar district, Punjab. Government of India, Ministry of Water Resources, River Development & Ganga Rejuvenation, Central Ground Water Board http://cgwb.gov.in/district_profile/punjab/muktsar.pdf
144. BIS (Bureau of Indian Standards) (2012) Indian standards specification for drinking water. IS 10500. New Delhi, India: BIS.
145. Saraswat SS (2017) Aquifer Mapping and groundwater management, Jaipur District, Rajasthan, Government of India, Ministry of Water Resources, River Development & Ganga Rejuvenation, Central Ground Water Board (WR) Western Region Jaipur http://cgwb.gov.in/AQM/NAQUIM_REPORT/Rajasthan/Jaipur.pdf
146. Saraswat SS (2017) Aquifer Mapping and groundwater management, Dausa District, Rajasthan. Government of India, Ministry of Water Resources, River Development & Ganga Rejuvenation, Central Ground Water Board (WR) Western Region Jaipur http://cgwb.gov.in/AQM/NAQUIM_REPORT/Rajasthan/Dausa1.pdf
147. American Public Health Association (APHA) (2017) Standard methods for examination of water and wastewater, 23rd edn. APHA, AWWA, WPCF, Washington
148. Hounslow AW (1995) Water quality data analysis and interpretation. Boca Raton, FL: CRC Press.
149. Hem JD (1985) Study and interpretation of the chemical characteristics of natural water. USGS, *Water Supply Paper*, 2254-2264
150. Gibbs RJ (1970) Mechanisms controlling world water chemistry. *Science*, **17**:1088–1090

151. Kumar M, Kumari K, Ramanathan AL, Saxena R (2007) A comparative evaluation of groundwater suitability for irrigation and drinking purposes in two agriculture dominated districts of Punjab, India. *J Environ Geol*, **53**:553–574
152. Keesari T, Shivanna K, Sriraman AK, Tyagi AK (2008) Assessment of quality and geochemical processes occurring in groundwaters near central air conditioning plant site in Trombay, Maharashtra. India *Environ Monit Assess*, doi: 10.1007/s10661-009-0825-9
153. Keesari T, Kulkarni UP, Deodhar A, Ramanjaneyulu PS, Sanjukta AK, Saravana Kumar U (2014) Geochemical characterization of groundwater from an arid region in India. *Environ Earth Sci*, **71** (11): 4869-4888
154. Sharma D, Rishi M, Keesari T (2016) Evaluation of groundwater quality and suitability for irrigation and drinking purposes in southwest Punjab, India using hydrochemical approach. *Applied Water Science* doi: 10.1007/s13201-016-0456-6.
155. Roy A., Keesari T, Mohokar H (2018) Assessment of groundwater quality in hard rock aquifer of central Telangana state for drinking and agriculture purposes. *Appl Water Sci* **8**:124 doi: <https://doi.org/10.1007/s13201-018-0761-3>
156. Richards LA (1954) Diagnosis and improvement of saline and alkali soils. Washington, DC: US Dept. of Agriculture.
157. Wilcox LV (1948) The quality of water for irrigation use: Tech Bull 962. Washington, DC: USDA.
158. Ragunath HM (1987) Groundwater. New Delhi: Wiley Eastern.
159. Doneen LD (1964) Notes on water quality in Agriculture: Published as a water *science and engineering*, paper 4001. Davis, CA: Dept. of Water Sciences and Engineering, Univ. of California, Davis.

160. Szabolcs I, and Darab C. (1964) The Influence of Irrigation Water of High Sodium Carbonate Content of Soils. *Proceedings of 8th International Congress of ISSS, Trans II*, 803-812.
161. Kelley WP (1963) Use of saline irrigation. *Water Soil Sci*, **95**(4):355–391
162. Balasubramanian A (1986) Hydrogeological investigation of Tambraparani River Basin, Tamil Nadu. Unpublished PhD thesis, University of Mysore, 349
163. Brown RM, McClelland NI, Deininger RA, Tozer RG (1970) Water quality index-do we dare *Water Sew Works*, **117**(10):339–343
164. Stoner JD (1978) Water-quality indices for specific water uses. Department of the Interior, Geological Survey.
165. Bhardwaj V, Singh DS, Singh AK (2010) Hydro geochemistry of groundwater and anthropogenic control over dolomitization reactions in alluvial sediments of the Deoria district: Ganga plain, India. *Environ Earth Sci*, **59**(5):1099–1109
166. Veselsky JC, Wicinska BK, Wehrstein E, Suschny O (1988) *Analyst*, **113**: 451
167. Raja Ramanna Centre for Advanced Technology. Manuals for Fluorimeter. Raja Ramanna Centre for Advanced Technology, DAE, India (2001).
168. Piper AM (1944) A graphical procedure in the geochemical interpretation of water analysis. *Trans Am Geophys Union*, **25**:914–928
169. Hallastadius L (1984) A method for the electrodeposition of actinides. *Nucl. Instrum. Methods Phys Res*, **223**:266–267
170. Knoll GF, Radiation detection and measurement (4th edition) 2010 ISBN: 978-0-470-13148-0

171. Rosholt JN, Harshman EN, Shields WR and Garner EL (1963) Isotopic fractionation of uranium related to roll features in sandstone, Shirley Basin, Wyoming. *Econ. Geol.*, **59**:570–585.
172. Cherdyntsev VV (1971) Uranium 234. Israel Program for Scientific Translations, Jerusalem.
173. Cherdyntsev VV, Chalov PI Khasdarov GZ (1955) On isotopic composition of radioelements in natural objects, and problems of geochronology. *Izv. Acad. Nauk. SSR*, a75.
174. Thurber DL (1962) Anomalous $^{234}\text{U}/^{238}\text{U}$ in nature. *J. Geophys. Res.*, **67**:4518–4523.
175. Osmond JK, Rydell HS, Kaufman MI (1968) Uranium disequilibrium in groundwater: an isotope dilution approach in hydrologic investigations. *Science*, **162**:997–999.
176. Suksi J and Rasilainen K (2002) Isotopic fractionation of U reflecting redox conditions around a groundwater flow route. *Mater. Res. Soc. Symp. Proc.*, **663**:961–969.
177. Suksi J, Rasilainen K, Pitkänen P (2006) Variations in $^{234}\text{U}/^{238}\text{U}$ activity ratios in groundwater—A key to flow system characterization? *Physics and Chemistry of the Earth, Parts A/B/C*, **31**(10-14):556–571 doi: 10.1016/j.pce.2006.04.007
178. Hussain N and Krishnaswami S (1980) U-238 series radioactive disequilibrium in groundwaters: implications to the origin of excess U-234 and fate of reactive pollutants. *Geochim. Cosmochim. Acta*, **44**:1287–91.
179. Petersen JO, Deschamps P, Hamelin B, Goncalves J, Michelot J-L, Zouari K (2013) Water-Rock Interaction and Residence Time of Groundwater Inferred by $^{234}\text{U}/^{238}\text{U}$ Disequilibria in the Tunisian Continental Intercalaire Aquifer System. *Procedia Earth and Planetary Science*, **7**:685–688 doi: 10.1016/j.proeps.2013.03.206

180. Hostettler PB and Garrels RM (1962) Transportation and precipitation of uranium and vanadium at low temperatures, with special reference to sandstone-type deposits. *Econ. Geol.*, **57**:137–167.
181. Osmond JK and Cowart JB (1982) Groundwater in Uranium Series Disequilibrium, eds. M. Ivanovich and R.S. Harmon, 202–245 Oxford Univ. Press.
182. IAEA (2006) Reference sheet for international measurement standards https://nucleus.iaea.org/rpst/documents/vsmow_slap.pdf
183. Craig M (1961) *Science***133**:1702–1703
184. Dansgaard W (1964) Stable isotopes in precipitation. *Tellus*, **16**(4), 436–468 doi: 10.1111/j.2153-3490.1964.tb00181.x
185. Yurtsever Y (1975) Worldwide survey of stable isotopes in precipitation Rep. Isotope Hydrol. Sect. *Int. At. Energy Agency, Vienna*40
186. Bahadur J (2000) Water resources management in the Himalayan region. Proceedings of the Internal Conference on Managing Natural Resources for Sustainable Agricultural Production in the 21st Century, New Delhi, 14–18 February 2000, 459–461.
187. Horita J, Ueda A, Mizukami K, Takatori I (1989) Automatic δD and $\delta^{18}O$ analyses of multi-water samples using H_2 and CO_2 -water equilibration methods with a common equilibration set-up. *Int J Radiat Appl Instrum*, **40**:801–805
188. Clark ID and Fritz P (1997) Environmental isotopes in hydrogeology. Lewis Publishers, Boca Raton, 328.
189. Taylor CB (1981) Present status and trends in electrolytical enrichment of low level 3H in water. In: Methods of Low-level Counting and Spectrometry, *Proceedings of IAEA Symposium, Berlin*, 303–323.
190. Nair AR, Joseph TB, Rao SM (1990) Measurement of low-level tritium in water by electrolytic enrichment and liquid scintillation counting. *Bulletin of Radiation*

191. Morgenstern U, Taylor CB (2009) Ultra low-level tritium measurement using electrolytic enrichment and LSC. *Isotopes Environ Health Stud.*, **45**(2):96-117 doi: 10.1080/10256010902931194.
192. Tweed S, Leblanc, Marc, Cartwright I, Bass A, Travi Y, Marc V, Bach Thao N, Duc N, N, Massuel S, Kumar U, (2020) Stable Isotopes of Water in Hydrogeology. doi: 10.1002/9781119300762.wsts0154.
193. Ali KK and Ajeena AR (2016) Assessment of interconnection between surface water and groundwater in Sawa Lake area, southern Iraq, using stable isotope technique. *Arab J Geosci* **9**:648 doi: <https://doi.org/10.1007/s12517-016-2673-6>
194. Ala-aho P, Soulsby C, Pokrovsky OS, Kirpotin SN, Karlsson J, Serikova S, Vorobyev SN, Manasypov RM, Loiko S, Tetzlaff D (2018) Using stable isotopes to assess surface water source dynamics and hydrological connectivity in a high-latitude wetland and permafrost influenced landscape. *Journal of Hydrology*, **556**:279-293
195. Price RM, and Swart PK (2006) Geochemical indicators of groundwater recharge in the surficial aquifer system, Everglades National Park, Florida, USA. *Special Paper of the Geological Society of America*, **404**:251-266 doi: [https://doi.org/10.1130/2006.2404\(21\)](https://doi.org/10.1130/2006.2404(21))
196. Yeh HF, Lee CH, Kuo-Chin, Chang, Po-Hsun, Wang CH (2009) Using stable isotopes for assessing the hydrologic characteristics and sources of groundwater recharge. *J Environ Eng Manage.*,19
197. Shivanna K, Tirumalesh K, Noble J, Joseph TB, Singh G, Joshi AP, Khati VS. Isotope Techniques to Identify Recharge Areas of springs for Rainwater Harvesting in the Mountainous Region of Gaucher Area, Chamoli District, Uttarakhand. *Current Science*, **94**(8):1003-011 doi: <http://www.jstor.org/stable/24100794>

198. Edwards TWD and Fritz P (1986) Assessing meteoric water composition and relative humidity from ^{18}O and ^2H in wood cellulose; paleoclimatic implications for southern Ontario, Canada. *Appl. Geochem.*, **1**(6), 715–723 doi: 10.1016/0883-2927(86)90093-4.
199. Hoffmann G, Jouzel J, Masson V (2000) Stable water isotopes in atmospheric general circulation models. *Hydrol. Processes*, **14**(8):1385–1406 doi: 10.1002/1099-1085(20000615)14(8)1385
200. Miljevi N, Globoanin D (2007) Potential use of environmental isotopes in pollutant migration studies. *Arh Hig Rada Toksikol*, **58**:251-262 doi: 10.2478/v10004-007-0015-5
201. McGuire, K. J., McDonnell, J. J., Weiler, M., Kendall, C., McGlynn, B. L., Welker, J. M., & Seibert, J. (2005) The role of topography on catchment-scale water residence time. *Water Resources Research*, **41**(5) doi: 10.1029/2004wr003657
202. Rodgers, P., C. Soulsby, and S. Waldron (2005), Stable isotope tracers as diagnostic tools in upscaling flow path understanding and residence time estimates in a mountainous mesoscale catchment. *Hydrol. Processes*, in press.
203. McConville C, Kalin, R. M., Johnston, H., & McNeill, G. W. (2001) Evaluation of Recharge in a Small Temperate Catchment Using Natural and Applied $\delta^{18}\text{O}$ Profiles in the Unsaturated Zone. *Groundwater*, **39**(4):616–623 doi: 10.1111/j.1745-6584.2001.tb02349.x
204. Abbott MD, Lini A, Bierman PR (2000) $\delta^{18}\text{O}$, δD and ^3H measurements constrain groundwater recharge patterns in an upland fractured bedrock aquifer, Vermont, USA. *Journal of Hydrology*, **228**(1-2):101–112 doi: 10.1016/s0022-1694(00)00149-9
205. Blasch KW and Bryson JR (2007) Distinguishing Sources of Ground Water Recharge by Using ^2H and ^{18}O . *Ground Water*, **45**(3):294–308 doi: 10.1111/j.1745-6584.2006.00289.x

206. Jeelani G, Bhat NA, Shivanna K, (2010) Use of ^{18}O tracer to identify stream and spring origins of a mountainous catchment; A case study from Liddar watershed, Western Himalaya, India. *J. Hydrol.*, **393**: 257-264
207. Fetter CW (1988) *Applied Hydrogeology*, Second Edition, Macmillan Publishing Company, New York, 592
208. Wigley TML (1967) Non-steady flow through a porous medium and cave breathing. *Journal of Geophysical Research*, **72**(12):3199–3205 doi: 10.1029/jz072i012p03199
209. Davies CW (1962) Ion Association. London: Butterworths, 190
210. Pearson's Correlation Coefficient. In: Kirch W. (eds) Encyclopedia of Public Health. Springer, doi: https://doi.org/10.1007/978-1-4020-5614-7_2569
211. Davis JC (1986) Statistics and Data Analysis in Geology. John Wiley & Sons, New York.
212. Alberto WD, María del Pilar D, María Valeria A, Fabiana PS, Cecilia HA, María de los Ángeles B (2001) Pattern Recognition Techniques for the Evaluation of Spatial and Temporal Variations in Water Quality. A Case Study. *Water Research*, **35**(12):2881–2894 doi: 10.1016/s0043-1354(00)00592-3
213. Richman MB (1986) Rotation of principal components. *Journal of Climatology*, **6**(3):293–335 doi: 10.1002/joc.3370060305
214. Meta. (2019) Rainfall data for Jaipur and Dausa Districts of Rajasthan Indian Meteorological Dept., Ministry of Earth Science, Government of India. https://www.indiawaterportal.org/met_data/
215. Census (2011) <https://www.census2011.co.in/states.php>
216. Rocca CD, Belgiorno V, Meriç S (2007) Overview of in-situ applicable nitrate removal processes. *Desalination*, **204**(1-3):46–62

217. Suthara S, Bishnoib P, Singh S, Mutiyara PK, Nema AK, Patil NS (2009) Nitrate contamination in groundwater of some rural areas of Rajasthan, India *Journal of Hazardous Materials*, **171**:189–199
218. Saxena U and Saxena S. (2014) Groundwater quality evaluation with special reference to Fluoride and Nitrate contamination in Bassi Tehsil of district Jaipur, Rajasthan, India. *International Journal of Environmental Sciences*, **5**(1)
219. Mondal NC, Prasad RK, Saxena VK, Singh Y, Singh VS (2009) Appraisal of highly fluoride zones in groundwater of Kurmapalli watershed, Nalgonda district, Andhra Pradesh (India). *Environ Earth Sci*, **59**:63–73 doi: 10.1007/s12665-009-0004-x
220. Vikas C. (2009) Occurrence and distribution of fluoride in groundwaters of central Rajasthan, India. *J Environ Sci Eng*, **51**(3):169-74
221. Todd DK (1980) Ground water hydrology. Wiley, New York
222. Durfor CN and Becker E (1964) Public water supplies of the 100 largest cities in the United States; Water Supply. **1812**: 343–346.
223. USSL (US Salinity Laboratory). (1954) Diagnosis and improvement of saline and alkaline soils. Washington, DC: USDA.
224. Keesari T, Roy A, Pant D, Sinha UK, Kumar PVN, Rao LV (2020) Major ion, trace metal and environmental isotope characterization of groundwater in selected parts of Uddanam coastal region, Andhra Pradesh, India. *Journal of Earth System Science*, **129**(1) doi: 10.1007/s12040-020-01467-0
225. Drever JI (1988) The geochemistry of natural waters, 2nd edn. Prentice Hall, Englewood Cliffs, 437

226. Maya AL and Loucks MD (1995) Solute and isotopic geochemistry and groundwater flow in the Central Wasatch Range, Utah. *J Hydrol*, **172**:31–59
227. Katz BG, Coplen TB, Bullen TD, Davis JH (1998) Use of chemical and isotopic tracers to characterize the interaction between groundwater and surface water in mantled Karst. *Groundwater*, **35**:1014–1028
228. Schoeller H (1977) Geochemistry of groundwater. In: Brown RH et al (eds) Groundwater studies-an international guide for research and practice. UNESCO, Paris, 1–18
229. Singh K, Hundal HS, Singh D (2011) Geochemistry and assessment of hydrogeochemical processes in groundwater in the southern part of Bathinda district of Punjab, northwest India. *Environ Earth Sci*, **64**:1823–1833 doi: 10.1007/s12665-011-0989-9
230. Fisher RS and Mulican WF III (1997) Hydrochemical evolution of sodium-sulfate and sodium-chloride groundwater beneath the Northern Chihuahuan desert, Trans-Pecos, Rexas, USA. *Hydrogeol J*, **10**:455–474
231. Datta P and Tyagi S (1996) Major ion chemistry of groundwater in Delhi area: Chemical weathering processes and groundwater flow regime. *Journal of the Geological Society of India*, **47**:179-188.
232. Elango L, Kannan R, Senthil Kumar M (2003) Major ion chemistry and identification of hydrogeochemical processes of groundwater in part of Kancheepuram district, Tamil Nadu. *Journal of Environmental Geoscience*, **10**(4):157–166
233. Vengosh A, Gill J, Davisson ML, Hudson GB (2002) A multi isotope (B, Sr, O, H, and C) and age dating (^3H - ^3He and ^{14}C) study of groundwater from Salinas Valley,

- California: hydrochemistry, dynamics, and contamination processes. *Water Resources Research*, **38**(9):9-17.
234. Rozanski KL, Araguas-Araguas, Gonfiantini R (1993) Isotopic patterns in modern global precipitation, in Climate Change in Continental Isotopic Records. *Geophys. Monogr. Ser.*, **78**:1–36
 235. Kumar B, Rai SP, Kumar US, Verma SK, Garg P, Kumar SVV, Pande NG (2010) Isotopic characteristics of Indian precipitation. *Water Resources Research*, **46**(12) doi: 10.1029/2009wr008532
 236. Gupta SK, Deshpande RD, Bhattacharya SK, Jani RA (2005) Groundwater $\delta^{18}\text{O}$ and δD from central Indian Peninsula: influence of the Arabian Sea and the Bay of Bengal branches of the summer monsoon. *Journal of Hydrology*, **303**(1-4):38–55 doi: 10.1016/j.jhydrol.2004.08.016
 237. Keesari T, Sharma DA, Rishi MS, Pant D, Mohokar HV, Jaryal AK, Sinha UK (2017) Isotope investigation on groundwater recharge and dynamics in shallow and deep alluvial aquifers of southwest Punjab. *Applied Radiation and Isotopes*, **129**:163–170 doi: 10.1016/j.apradiso.2017.07.022
 238. Sharma DA, Rishi MS, Keesari T (2017) Evaluation of groundwater quality and suitability for irrigation and drinking purposes in southwest Punjab, India using hydrochemical approach. *Appl Water Sci*, **7**:3137–3150 doi: <https://doi.org/10.1007/s13201-016-0456-6>
 239. Kaiser HF (1958) The varimax criterion for analytic rotation in factor analysis *Psychometrika*, **23**:187–200 doi: <https://doi.org/10.1007/BF02289233>
 240. Kundu MC, Mandal B, Sarkar D (2008) Assessment of the potential hazardous of nitrate contamination in surface and groundwater in a heavily fertilized and intensively cultivated district of India. *Environ. Monit. Assess.*, **146**:183-189

241. Langmuir DL (1997) Aqueous environmental geochemistry. Prentice Hall, New Jersey, 168
242. Murphy WM and Shock EL (1999) Mineralogical Society of America. In: Burns PC, Finch R (eds) Environmental aqueous geochemistry of actinides. *Uranium: mineralogy, geochemistry and the environment*, **38**:221–254
243. HYDRA Database <http://www.speciation.net/Database/Links/HydraMedusa-;i3474>
244. Thivya C, Chidambaram S, Keesari T, Prasanna MV, Thilagavathi R, Adithya VS, Singaraja C (2015) Lithological and hydrochemical controls on distribution and speciation of uranium in groundwaters of hard-rock granitic aquifers of Madurai District, Tamil Nadu (India). *J of Environ Geochem Health*, doi:10.1007/s10653-015-9735-7
245. Zielinski RA, Simmons KR, Orem WH (2000) Use of ^{234}U and ^{238}U isotopes to identify fertilizer-derived uranium in the Florida Everglades. *Applied Geochemistry*, **15**(3):369–383 doi: 10.1016/s0883-2927(99)00053-0
246. Yamaguchi N, Kawasaki A, Iiyama I (2009) Distribution of uranium in soil components of agricultural fields after long-term application of phosphate fertilizers. *Science of The Total Environment*, **407**(4):383–1390 doi:10.1016/j.scitotenv.2008.10.011
247. Sharma DA (2017) Investigations of source of uranium and its geochemical pathways in aquifer systems in parts of southwest Punjab using environmental isotope techniques. Unpublished Ph.D. thesis Faculty of Science, Panjab University, Chandigarh
248. Rainfall Data (2019) Monsoon reports for district-wise annual rainfall, Water Resources Department, Government of Rajasthan, India. <http://www.water.rajasthan.gov.in/content/water/en/waterresourcesdepartment/WaterManagement/IWRM/annualrainfall.html#>

249. PHED (2013) Hydrogeological Atlas of Rajasthan Sabi River Basin 2013
https://phedwater.rajasthan.gov.in/content/dam/doitassets/water/Ground%20Water/Pd/f/PublicReports/Groundwater_Atlas/Basinwise/Sabi%20River%20Basin.pdf
250. PHED (2013) Hydrogeological Atlas of Rajasthan Banganga River Basin 2013
https://phedwater.rajasthan.gov.in/content/dam/doitassets/water/Ground%20Water/Pd/f/PublicReports/Groundwater_Atlas/Basinwise/Banganga%20River%20Basin.pdf
251. CP-2012 (2012), Agriculture Contingency Plan for district Jaipur report, Indian Council of Agricultural Research Ministry of Agriculture and Farmers Welfare and Central Research Institute for Dryland Agriculture (CRIDA), [http://www.crida.in/CP-2012/statewiseplans/Rajasthan%20\(Pdf\)/RAU,%20Bikaner/RAJ1-Jaipur%203.2.2011.pdf](http://www.crida.in/CP-2012/statewiseplans/Rajasthan%20(Pdf)/RAU,%20Bikaner/RAJ1-Jaipur%203.2.2011.pdf)
252. PHED (2013) Hydrogeological atlas of Rajasthan Jaipur district 2013
https://phedwater.rajasthan.gov.in/content/dam/doitassets/water/Ground%20Water/Pd/f/PublicReports/Groundwater_Atlas/Districts/Districtwise%20Atlas%20-%20Jaipur.pdf
253. CP-2012 (2012), Agriculture Contingency Plan for district Dausa report, Indian Council of Agricultural Research Ministry of Agriculture and Farmers Welfare and Central Research Institute for Dryland Agriculture (CRIDA) [http://www.crida.in/CP-2012/statewiseplans/Rajasthan%20\(Pdf\)/RAU,%20Bikaner/RAJ13-Dausa-9.3.2012.pdf](http://www.crida.in/CP-2012/statewiseplans/Rajasthan%20(Pdf)/RAU,%20Bikaner/RAJ13-Dausa-9.3.2012.pdf)
254. PHED (2013) Hydrogeological atlas of Rajasthan Dausa district 2013
https://phedwater.rajasthan.gov.in/content/dam/doitassets/water/Ground%20Water/Pd/f/PublicReports/Groundwater_Atlas/Districts/Districtwise%20Atlas%20-%20Dausa.pdf

255. Gram Chetna Kendra, Sambhar Lake Area Overview & Issues <https://www.gck.org.in/aboutus/sambharlake.html>
256. Reddy AGS and Rao PN (2006) Occurrence, behavior and genesis of fluoride in groundwater of Wailpalli watershed in Nalgonda District, Andhra Pradesh, India. *J Appl Geochem*, **8**(2a):618–630
257. Mines and Minerals of Rajasthan (2016) <https://www.rajras.in/rajasthan-mines-minerals/>
258. Adimalla N and Venkatayogi S (2016) Mechanism of fluoride enrichment in groundwater of hard rock aquifers in Medak, Telangana State, South India. *Environmental Earth Sciences*, **76**(1) doi:10.1007/s12665-016-6362-2
259. Tatawat, Rakesh and CHANDEL, C. (2008). Quality of ground water of Jaipur-city, Rajasthan, (India) and its suitability for domestic and irrigation purpose. *Applied Ecology and Environmental Research*. 6. 10.15666/aer/0602_079088.
260. Sinha UK and Navada SV (2008) Application of isotope techniques in groundwater recharge studies in arid western Rajasthan, India: some case studies. *Geological Society, London, Special Publications*, **288**(1):121–135 doi:10.1144/sp288.10
261. Narayan GRD, Sharma DK, Singh G, Singh R (1980), Uranium Mineralization in Sikar District, Rajasthan. *Journal of Geological society of India*, **21**(9)
262. Padhi A, Khandelwal MK, Jain RC, Dash S, Nanda LK (2010). Geological characteristics of Rohil uranium deposits, District Sikar, Rajasthan. *Geological Society of India*, **76**:75-85
263. Li J and Zhang Y (2012) Remediation technology for the uranium contaminated environment: a review. *Procedia Environmental Sciences*, 13, 1609–1615. doi:10.1016/j.proenv.2012.01.153

264. Pentyala VB and Eapen S (2020). High efficiency phytoextraction of uranium using *Vetiveria zizanioides* L. Nash. International Journal of Phytoremediation, 1–10.
doi:10.1080/15226514.2020.1741506

Thesis Highlight

Name of the Student: Mrs. Diksha Pant

Name of the CI/OCC: Bhabha Atomic Research Centre **Enrolment No.:** CHEM01201404022

Thesis Title: Isotope and hydrochemical investigation on uranium in groundwater of south west Punjab and central Rajasthan

Discipline: Chemical Sciences

Sub-Area of Discipline: Isotope hydrology

Date of viva voce: 13/03/2021

High uranium concentrations are reported in groundwater of Punjab, Rajasthan, Madhya Pradesh, Andhra Pradesh, Chhattisgarh and Haryana by researchers. These high concentrations are not limited to one kind of geological formation and are spread across the diverse geological setups in India. Hence, it is very important to understand the role played by aquifer geology, geochemistry and dynamics towards the mobilization of uranium into groundwater. In this connection, two areas with diverse geological setup were chosen to study the role of geology, hydrogeology, geochemistry and aquifer dynamics on uranium mobilization. Environmental isotopes ($\delta^2\text{H}$, $\delta^{18}\text{O}$, ^3H), hydrochemistry (Cl^- , NO_3^- , SO_4^{2-} , F^- , HCO_3^- , Na^+ , K^+ , Mg^{2+} , Ca^{2+}), total uranium and its isotope activity ratio ($^{234}\text{U}/^{238}\text{U}$), geochemical and statistical modeling approaches were applied to address the stated objectives. The uranium concentration in the groundwater from alluvial formation of Punjab was in range of 1 to 610 $\mu\text{g/L}$ with 78% of the samples showing contamination ($>\text{WHO}$ permissible limit of 30 $\mu\text{g/L}$). The uranium concentration in the alluvial formation from Rajasthan was in range of 0.5 to 177 $\mu\text{g/L}$ with 33% of the samples contaminated by uranium while in the hard rock formation it ranges from 0.5 to 115 $\mu\text{g/L}$ with 53% of the samples contaminated. In case of Punjab, a decrease in uranium concentration is observed in the postmonsoon season while for Rajasthan samples it is increased. The environmental isotopes suggest that the shallow zones of Punjab area have three recharge sources viz. precipitation, irrigation return flow canal, while the deeper zones are recharged from regional groundwater flows. The alluvial and hard rock formation of Rajasthan behave like a single aquifer system with precipitation and irrigation return flow as the main recharge sources. Oxidative dissolution is the main mechanism for uranium mobilization in shallow zones of Punjab, which is due to presence of excessive nitrate ions as a result of extensive agricultural activity while for the deeper zone, mixing with uranium contaminated shallow groundwater is the reason for higher concentrations. However, both alpha recoil and oxidative leaching are the main processes leading to high uranium in alluvial and hard rock formations of Rajasthan. Optimal use of fertilizers and using surface sources or deep groundwater for drinking can help mitigate uranium contamination in Punjab while removal of uranium through membranes or ultrafiltration techniques can be applied to in the case Rajasthan.

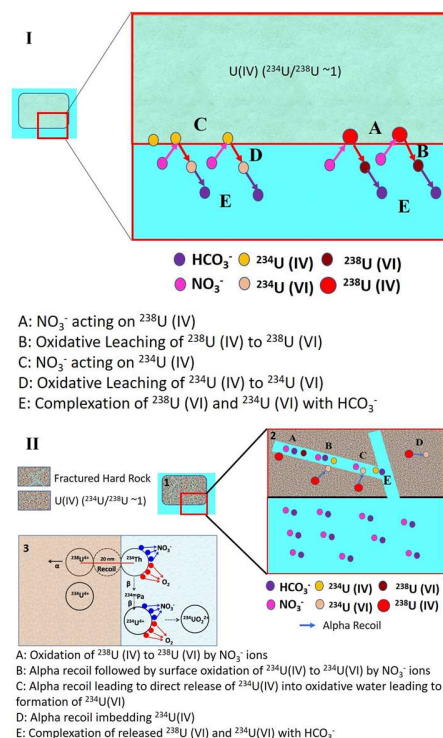


Figure 1. Conceptual model of uranium release in i) alluvial formation of Punjab and ii) hard rock formation of Rajasthan